To the Graduate Council:

I am submitting herewith a dissertation written by Michael Tyrone Harris entitled "Ultrafine Ceramic Precursor Powders by Homogeneous Precipitation and Electrodispersion." I have examined the final copy of this dissertation for form and content and recommend that it be accepted in partial fulfillment of the requirements for the degree of Doctor of Philosophy, with a major in Chemical Engineering.

Charles H. Byers, Major Professor

We have read this dissertation
and recommend its acceptance:

Accepted for the Council:

Associate Vice Chancellor
and Dean of The Graduate School

# ULTRAFINE CERAMIC PRECURSOR POWDERS BY HOMOGENEOUS PRECIPITATION AND ELECTRODISPERSION

A Dissertation

Presented for the

Doctor of Philosophy

Degree

University of Tennessee, Knoxville

Michael Tyrone Harris

May 1992

## ACKNOWLEDGEMENTS

I would like to thank my major advisor and section head Dr. Charles H. Byers, for encouragement and helpful suggestions. The interest and support of my committee, Dr. Osman A. Basaran, Dr. Joseph J. Perona, and Dr. Thomas Meek are also greatly appreciated. I would like to thank Ron R. Brunson, Edward D. Wilkes, Michael Burgess, Colin Mattingly, Lymarie Maldonada-Baez, Lois M. Hamm and Patricia G. McNabb for their invaluable assistance. I would like to give special recognition to Dr. Timothy C. Scott, co-inventor of the electric dispersion reactor, for his expertise in electrodispersion. The author also wishes to acknowledge the services provided by the Oak Ridge National Laboratory, managed by Martin Marietta Energy Systems, Inc., for the Department of Energy. The work was supported by the Office of Basic Energy Sciences, U.S. Department of Energy under contract DE-AC05-84OR21400. Finally, I would like to give a special thanks to my wife, Terry Harris, for her patience and encouragement.

# ABSTRACT

A fundamental study was undertaken of the early stages of particle formation and growth in the production of ultrafine precursor powders for advanced ceramic materials. More specifically, the formation of ultrafine hydrous oxide particles by the hydrolysis of metal alkoxides was investigated. Initially, the growth of Stober silica spheres was studied experimentally and modeled by solving the hydrolysis and condensation kinetic expressions and applying the method of moments to expedite the solution of the governing population balance equation. The model was applied over a wide range of TEOS, water, and ammonia concentrations. A comparison of the experimental and theoretical results indicated that the particles grew by controlled aggregation at high water concentrations and ammonia concentrations. At low water and ammonia concentrations, the particles appeared to grow by the addition of soluble, or ramified, species to the particle surface.

A qualitative evaluation of titania, zirconia, titania-zirconia and titania-alumina systems shows that, like silica, the formation of roughly spherical particles involved four steps: (a) formation of soluble polymers, (b) precipitation and collapse of polymers, and (c) particle growth by controlled aggregation. However, contrary to silica where spherical particles were formed in all low molecular weight alcohols, solvent greatly affected the morphology of these particles. Spherical particles were easily formed by the hydrolysis of titanium, zirconium, and mixed titanium-zirconium alkoxides in primary alcohols. Irregular shaped gelatinous precipitates were formed in *tert*-butyl alcohol. Steric effects played an important role in particle morphology when hydrolysis rates were very fast. The

hydrolysis of titanium-aluminum alkoxides resulted in gelatinous precipitate for high aluminum content to roughly spherical particles for low aluminum concentrations. Theory suggested that partially hydrolyzed aluminum alkoxides have a greater tendency to form linear polymers that yield gelatinous precipitates.

As an outgrowth of the homogeneous precipitation studies, a new reactor, the electric dispersion reactor (EDR), was invented to produce ultrafine powders by electrodispersion and the subsequent reaction of aqueous drops emanating from a nozzle. By varying reactant concentrations and by strategically locating reactants in the proper phase, porous and dense silica particles have been made as well as the composite material of 1:2:3 yttrium, barium and copper. Finally, extensive electrohydrostatic computations elucidate the effect of reactor geometry and drop size on the stability of pendant drops hanging from a conducting pipe.

TABLE OF CONTENTS


SECTION ..... PAGE

1. INTRODUCTION ..... 1

1.1. Background and Origin of Research ..... 3
1.2. Thesis Scope ..... 7
1.2.1. Homogeneous Precipitation Experiments ..... 7
1.2.2. Electric Dispersion Reactor ..... 9
1.3. Thesis Synopsis ..... 10
1.3.1. Silica Synthesis by TEOS Hydrolysis ..... 10
1.3.2. Hydrous Metal Oxide Powder Synthesis by Metal Alkoxide Hydrolysis ..... 11
1.3.3. Electric Dispersion Reactor ..... 12
1.3.4. Electrohydrostatics of Axisymmetric Pendant Drop Problem ..... 12
1.4 Retrospective and Outlook ..... 14

2. SILICA POWDER SYNTHESIS BY TEOS HYDROLYSIS ..... 17

2.1. Introduction ..... 17
2.2. Literature Survey ..... 18
2.2.1 Hydrolysis and Condensation of Silicon Alkoxides ..... 18
2.2.2 Mechanisms for Particle Formation and Growth ..... 24
2.2.3 Experimental Methods ..... 28
2.3. Experimental ..... 33
2.3.1. Chemicals ..... 33
2.3.2. Instrumentation ..... 34
2.3.3. Experimental Procedure ..... 37
2.4. Theory ..... 40
2.4.1. Reaction Model ..... 40
2.4.2. Particle Growth Model and Colloidal Stability ..... 42
2.4.3. Solving the Population Balance Equation ..... 47
2.4.3.1. Continuous method ..... 48
2.4.3.2. Moment method ..... 49
2.4.4. Estimating Chemical Reaction Parameters ..... 50
2.4.5. Estimating the Stern Potential, $\psi_d$ ..... 51
2.4.6. Computing Zeta Potential from Electrophoretic Mobilities 51
2.4.7. Classical Light Scattering - Particle Number Concentration 55
2.4.8. QELS - Particle Size and Size Distribution ..... 57
2.5. Results and Discussion ..... 61
2.5.1. Hydrolysis Reaction ..... 61
2.5.1.1. Hydrolysis reaction-dilute TEOS solutions ..... 61
2.5.1.2. Hydrolysis reaction-concentrated TEOS solutions ... 62
2.5.1.3. Hydrolysis reaction-solvent effects ..... 67
2.5.2. Condensation Reaction ..... 76

2.5.3. Silicic Acid, Conductivity and pH ..... 76
2.5.4. Particle Growth and Particle Size Distribution ..... 92
2.5.5. Estimating Condensation, Nucleation Kinetic Parameters. 99
2.5.6. Colloidal Stability Parameters ..... 105
2.5.7. Predicting Particle Growth Kinetic and Final Particle Size Distributions ..... 108
2.6. Conclusions ..... 124

3. HYDROUS METAL OXIDE POWDER SYNTHESIS BY METAL ALKOXIDE HYDROLYSIS ..... 131

3.1. Introduction ..... 131
3.2. Literature Survey ..... 131
3.2.1. Titania Synthesis by Titanium Alkoxide Hydrolysis ..... 131
3.2.2. Zirconia Powders by Alkoxide Reactions ..... 134
3.2.3. Alumina Powders by Alkoxide Reactions ..... 135
3.2.4. Alumina-Titania, Titania-Zirconia Powders by Alkoxide reactions ..... 136
3.2.5. Surface Charge of Titania, Alumina and Zirconia Particles 139
3.2.6. Chemical Analyses ..... 140
3.3. Experimental ..... 140
3.4. Theory ..... 142
3.4.1. Chemistry ..... 142
3.4.2. Evaluating Chemical Reactivity by Partial Charge Analysis ..... 144
3.5. Results and Discussion ..... 146
3.5.1. Alcoholysis and Hydrolysis Reactions ..... 146
3.5.1.1. Titanium alkoxides ..... 146
3.5.1.2. Zirconium, titanium-zirconium and titanium-aluminum alkoxides ..... 150
3.5.2. Condensation and Particle Growth Kinetics ..... 151
3.5.2.1. Titanium hydrous oxide ..... 151
3.5.2.2. Zirconium, titanium-zirconium and titanium-Aluminum hydrous oxides ..... 165
3.6. Conclusions ..... 177

4. ELECTRIC DISPERSION REACTOR ..... 182

4.1. Introduction ..... 182
4.1.1. Physicochemical Synthesis of Ceramic Precursor Powders 183
4.1.2. Potential Benefits of the Electric Dispersion Reactor (EDR) ..... 187
4.1.3. EDR Process Description ..... 188
4.2. Chemical Methods for Particle Formation in the EDR ..... 193
4.2.1. External gelation ..... 194
4.2.2. Internal gelation ..... 198
4.3. Results and Discussion ..... 198
4.4. Conclusions ..... 202

5. ELECTROHYDROSTATICS OF AXISYMMETRIC PENDANT DROPS ..... 205

5.1. Introduction ..... 205
5.2. Liquid Dispersion by an Electric Field ..... 206
5.3. Effect of Field Strength on Dispersion ..... 207
5.4. Use of Transient Fields for Dispersion ..... 210
5.5. Solving the Electrohydrostatic problem ..... 214
5.5.1. Finite Element Solution to the Augmented Young-Laplace Equation ..... 215
5.5.2. Boundary Element Solution to the Laplace Equation ..... 219
5.5.3. Solution of Nonlinear Equation by Newton's Method ..... 224
5.6. Results: Theoretical Analysis of Axisymmetric Electrohydrostatics Problem ..... 228
5.7. Conclusions ..... 269

6. SUMMARY AND RECOMMENDATIONS ..... 274

BIBLIOGRAPHY ..... 279

APPENDIXES ..... 289

A.1 Computer Programs ..... 290
A.1.1. popcon.f - Population Balance Model - Continuous Method ..... 291
A.1.2. popsol.f - Population Balance Model - Method of Moments 307
A.1.3. bemfem.f - Algorithm for Solving Electrohydrostatic Problem by Hybrid Finite Element - Boundary Element Method ..... 320
A.2. Discretization of Boundary for Solving Electrohydrostatic Problem by Hybrid Finite Element-Boundary Element ..... 395

VITA ..... 397

## LIST OF TABLES


| TABLE | | PAGE |
|---|---|---|
| 2.1. | Assignment of Raman bands of $Si(OCH_3)_{4-x}(OH)_x$ | 31 |
| 2.2. | Hydrolysis rate constant for TEOS hydrolysis in various alcohols | 71 |
| 2.3. | The effect of the activity of water on the hydrolysis rate constant | 74 |
| 2.4. | $pK_S$, $pK_A$ and $pK_B$ | 75 |
| 2.5. | Fitted parameter values | 106 |
| 2.6. | Experimentally determined zeta potentials | 109 |
| 3.1. | Effect of initial titanium ethoxide and water concentration on the induction period | 149 |
| 3.2. | Partial Charge Distributions for aluminum Ethoxide and aluminum butoxide hydrolysis products | 171 |
| 5.1. | Governing Dimensionless groups | 229 |
| 5.2. | Effect of number of elements on the turning point | 231 |
| 5.3. | Effect of plate diameter on the turning point: $N_{Drop}$=30, $N_{Nozzle}$=30, $N_{Top}$=20, $N_{Side}$=10, $N_{Bottom}$=20 | 232 |
| 5.4. | Effect of plate diameter on the turning point: $N_{Drop}$=40, $N_{Nozzle}$=40, $N_{Top}$=40, $N_{Side}$=40, $N_{Bottom}$=40 | 233 |

## LIST OF FIGURES


| FIGURE | | PAGE |
|---|---|---|
| 2.1. | Typical silica particles produced by Stober process | 18 |
| 2.2. | Homogeneous nucleation (La Mer theory) | 25 |
| 2.3. | Schematic diagram of homogeneous nucleation, controlled aggregation and gel formation in colloidal suspensions | 27 |
| 2.4. | Schematic diagram of silica formation by base catalyzed TEOS hydrolysis | 29 |
| 2.5. | Schematic diagram of the dynamic light scattering spectrometer | 36 |
| 2.6. | Comparison of optical density for reaction of molybdate with sodium metasilicate and TEOS standards | 39 |
| 2.7. | Schematic depicting Stern potential, $\psi_d$, zeta potential, $\varsigma$, and surface potential, $\psi_o$ (Shaw 1990) | 52 |
| 2.8. | Hydrolysis of 0. 014M TEOS in various alcohols | 63 |
| 2.9. | Effect of temperature on the rate of TEOS (0.014M) hydrolysis in tert-butyl alcohol | 64 |
| 2.10. | Arrhenius plot of TEOS hydrolysis rate constant for reaction in various alcohols | 65 |
| 2.11. | Typical Raman spectra for the hydrolysis of 1.0M TEOS with 11.0M $H_2O$ and 0.7M $NH_3$ in ethanol | 66 |
| 2.12. | Hydrolysis of concentrated TEOS solution in ethanol (1M TEOS, 11M $H_2O$, and 0.7M $NH_3$) | 68 |
| 2.13. | Activity of water in water-aliphatic alcohol mixtures | 69 |
| 2.14. | Total soluble silica: TEOS hydrolysis in various alcohols (0.014M TEOS, 6M $H_2O$ and 0.7M $NH_3$) | 77 |
| 2.15. | Total soluble silica: TEOS hydrolysis in various alcohols (0.05M TEOS, 6M $H_2O$ and 0.7M $NH_3$) | 78 |

FIGURE PAGE

2.16. Total soluble silica: TEOS hydrolysis in various alcohols (1.0M TEOS, 6M $H_2O$ and 0.7M $NH_3$) ..... 79

2.17. TEOS and total soluble silica: TEOS hydrolysis in 2-propanol at high temperature (0.014M TEOS, 6M $H_2O$ and 0.7M $NH_3$, 50°C) ..... 80

2.18. Total soluble silica and silicic acid: TEOS hydrolysis in 2-butanol (0.014M TEOS, 6M $H_2O$ and 0.7M $NH_3$, 22°C) ..... 82

2.19. Total soluble silica and silicic acid: TEOS hydrolysis in methanol (0.05M TEOS, 6M $H_2O$ and 0.7M $NH_3$, 22°C) ..... 83

2.20. Total soluble silica and silicic acid: TEOS hydrolysis in ethanol (0.05M TEOS, 6M $H_2O$, and 0.7M $NH_3$, 22°C) ..... 84

2.21. Total soluble silica and silicic acid: TEOS hydrolysis in 1-butanol (0.05M TEOS, 6M $H_2O$ and 0.7M $NH_3$, 22°C) ..... 85

2.22. Total soluble silica and silicic acid: TEOS hydrolysis in ethanol (0.1M TEOS, 11.8M $H_2O$ and 0.7M $NH_3$, 22°C) ..... 86

2.23. Total soluble silica and silicic acid: TEOS hydrolysis in ethanol (0.3M TEOS, 11.8M $H_2O$ and 1.4M $NH_3$, 22°C) ..... 87

2.24. Effect of TEOS concentration, and high and low water and ammonia concentrations: (a) silicic acid, (b) conductivity, (c) pH (0.3M TEOS, 22°C) ..... 88

2.25. Effect of ammonia concentration: (a) silicic acid, (b) conductivity, (c) pH (0.3M TEOS, 11.8M $H_2O$, 22°C) ..... 89

2.26. Effect of ammonia concentration: (a) silicic acid, (b) conductivity, (c) pH (0.1M TEOS, 11.8M $H_2O$, 1.4M $NH_3$, 22°C) ..... 90

2.27. Effect of water concentration: conductivity (0.1M TEOS, 0.7M $NH_3$) ..... 91

FIGURE PAGE

2.28. TEOS hydrolysis in ethanol: particle growth kinetics (6.0M $H_2$, 0.7M $NH_3$, 22°C) ..... 93

2.29. TEOS hydrolysis in ethanol: particle growth kinetics-high and low reactant concentrations ..... 94

2.30. TEM of silica particles synthesized during the hydrolysis of TEOS in ethanol (22°C): (a) 0.3M TEOS, 2.9M $H_2O$, 0.7M $NH_3$, (b) 1.0M TEOS, 2.9M $H_2O$, 0.7M $NH_3$, (c) 1.0M TEOS, 2.9M $H_2O$, 0.175M $NH_3$, (d) 1.0M TEOS, 2.9M $H_2$), 0.057M $NH_3$ ..... 96

2.31. TEM of silica particles synthesized during the hydrolysis of TEOS in ethanol (6M $H_2O$ and 0.7M $NH_3$): (a) 0.014M TEOS, (b) 0.05M TEOS, (c) 0.1M TEOS, (d) 0.3M TEOS ..... 97

2.32. TEM of silica particle synthesized during the hydrolysis of TEOS in ethanol (22°C): (a) 0.1M TEOS, 11.8M $H_2O$, 1.4M $NH_3$, (b) 0.3M TEOS, 11.8M $H_2O$, 0.7M $NH_3$, and (c) 0.3M TEOS, 11.8M $H_2O$, 1.4M $NH_3$ ..... 98

2.33. Ultimate size distribution of silica particles formed during the hydrolysis of TEOS in ethanol: 2.9M $H_2O$, 22°C ..... 100

2.34. Ultimate size distribution of silica particles formed during the hydrolysis of TEOS in ethanol: (0.014-0.3M TEOS, 6M $H_2O$, 0.7M $NH_3$, 22°C) ..... 101

2.35. Ultimate size distribution of silica particles formed during the hydrolysis of TEOS in ethanol: (0.014-1.0M TEOS, 6M $H_2O$, 0.7M $NH_3$, 22°C) ..... 102

2.36. Ultimate size distribution of silica particles formed during the hydrolysis of TEOS in ethanol: (11.8M $H_2O$, 22°C) ..... 103

2.37. Typical fit of silicic acid data to Eq. 2.10: TEOS hydrolysis in ethanol (0.014 and 0.05M TEOS, 6.0M $H_2O$, 0.7M $NH_3$, 22°C) ..... 104

2.38. Dielectric constant of water-ethanol mixtures ..... 107

FIGURE PAGE

2.39. Potential energy curves for Bogush and Zukoski (1991) zeta potential data ($A_J = 0.48 \times 10^{-20}$, $\varsigma = -13$mV, $\kappa = 3.48 \times 10^8$ cm$^{-1}$ and $A_S = 1.5 \times 10^{-3}$) ..... 110

2.40. Potential energy curves for zeta potential data determined during this study ($A_J = 0.48 \times 10^{-20}$, $\varsigma = -40$mV, $\kappa = 3.48 \times 10^8$ cm$^{-1}$ and $A_S = 1.5 \times 10^{-3}$) .. 111

2.41. Typical fit of silicic acid data by detail population balance-chemical kinetic model: TEOS hydrolysis in ethanol-[TS] data (0.014M and 0.05M TEOS, 6.0M $H_2O$, 0.7M $NH_3$, 22°C) ..... 113

2.42. Typical fit of silicic acid data by detail population balance-chemical kinetic model: TEOS hydrolysis in ethanol (a) [TS] data, (b) conductivity data (0.1 and 0.3M TEOS, 6.0M $H_2O$, 0.7M $NH_3$, 22°C) ..... 114

2.43. Predicted and experimental particle growth data: TEOS hydrolysis in ethanol (0.014M and 0.05M TEOS, 6.0M $H_2O$, 0.7M $NH_3$, 22°C) ..... 115

2.44. Predicted and experimental particle growth data: TEOS hydrolysis in ethanol (0.1 and 0.3M TEOS, 11.8M $H_2O$, 1.4M $NH_3$, 22°C) ..... 116

2.45. Predicted primary particle number concentration: TEOS hydrolysis in ethanol (0.014, 0.05, and 0.3M TEOS, 6M $H_2O$, 0.7M $NH_3$, 22°C) ..... 118

2.46. Predicted and experimental aggregate number concentration: TEOS hydrolysis in ethanol (0.014, 0.05 and 0.3M TEOS, 6M $H_2O$, 0.7M $NH_3$, 22°C) ..... 119

2.47. Predicted primary particle number concentration: TEOS hydrolysis in ethanol (0.1 and 0.3M TEOS, 11.8M $H_2O$, 1.4M $NH_3$, 22°C) ..... 121

2.48. Predicted aggregate number concentration: TEOS hydrolysis in ethanol (0.1 and 0.3M TEOS, 11.8M $H_2O$, 1.4M $NH_3$, 22°C) ..... 122

2.49. Collision efficiency factor (0.1, 11.8M $H_2O$, 1.4M $NH_3$, 22°C) ..... 123

FIGURE PAGE


2.50. Experimental and predicted particle size distribution (0.014, 0.05, and 0.3M TEOS, 6M $H_2O$, 0.7M $NH_3$, 22$o$C) ..... 125

2.51. Experimental and predicted particle size distribution (0.1 and 0.3M TEOS, 11.8M $H_2O$, 1.4M $NH_3$, 22°C) ..... 126

2.52. Experimental and predicted polydispersity factor (0.014, 0.05, and 0.3M TEOS, 6M $H_2O$, 0.7M $NH_3$, 22°C) ..... 127

2.53. Experimental and predicted polydispersity factor (0.1 and 0.3M TEOS, 11.8M $H_2O$, 1.4M $NH_3$, 22°C) ..... 128

3.1. Soluble titania condensation kinetics: Hydrolysis of titanium ethoxide in ethanol ..... 153

3.2. Soluble titania condensation kinetics: Hydrolysis of titanium ethoxide in 1-butanol ..... 154

3.3. Soluble titania condensation kinetics: comparison of titanium ethoxide hydrolysis in ethanol and 1-butanol .... 155

3.4. Titania growth kinetics: Hydrolysis of titanium ethoxide in ethanol ..... 157

3.5. Titania growth kinetics: Hydrolysis of titanium ethoxide in 1-butanol ..... 159

3.6. Scanning electron micrographs of titania particles synthesized in ethanol and 1-butanol ..... 160

3.7. Transmission electron micrograph of titania particles synthesized in ethanol ..... 161

3.8. Transmission electron micrograph of titania particles synthesized in 1-butanol ..... 162

3.9. Titania growth kinetics in t-butyl alcohol ..... 164

3.10. Transmission electron micrograph of titania particles synthesized in t-butyl alcohol ..... 166

3.11. The growth of "zirconia"-"titania" particles in 1-butanol and t-butyl alcohol: Hydrolysis of mixed titanium- zirconium alkoxides ..... 167

FIGURE PAGE


3.12. Transmission electron micrographs of titania and zirconia-titania particles synthesized in ethanol and 2- butanol ..... 168

3.13. TEM of alumina-titania particles produced in ethanol effect of the initial molar ratio of [ASB]:[TIE]; 0.8M $H_2O$: (a) 0.015M TIE, 0.023M ASB; (b) 0.023M TIE, 0.019M ASB; (c) 0.031M TIE, 0.012M ASB; (d) 0.02M TIE ..... 173

3.14. Particle growth kinetics in 1-butanol: Effect of the initial molar ratio of ASB:TIE ..... 175

3.15. Transmission electron micrographs of alumina-titania particles produced in ethanol (effect of initial water concentration: 0.023M TIE, 0.019M ASB): (a) 1.6M $H_2O$; (b) 0.4M $H_2O$ ..... 178

3.16. Transmission electron micrographs of alumina-titania particles (effect of solvent: 0.56M $H_2O$, 0.025M TIE, 0.05M ASB): (a) ethanol; (b) 1-propanol; (c) 1-butanol ... 179

3.17. Differential thermal analysis for alumina-titania powder .. 180

4.1. Electric Dispersion Reactor ..... 189

4.2. Continuous EDR Process ..... 191

4.3. External gelation technique for metal salt solutions ..... 195

4.4. External gelation technique for silica formation from sodium metasilicate ..... 196

4.5. Silica particles produced in the EDR [0.7M $NH_3$ (disperse phase) and TEOS (continuous phase) ..... 200

4.6. Silica particles produced in the EDR [sodium metasilicate in water (disperse phase) and acetic acid in 2-ethyl-1- hexanol (continuous phase) ..... 201

4.7. Particles produced in the EDR containing hydrous oxides of Y-Ba-Cu (approx. 1:2:3 molar ratio) ... 203

FIGURE PAGE


5.1. Effect of electric field on fluid drop ..... 208

5.2. Problem statement: Conducting drop hanging for a conducting nozzle in insulating fluid between two parallel plates ..... 216

5.3. Effect of pipe length on drop shape and stability ..... 217

5.4. Initial drop shape: Pendant/sessile drop in absence of external forces ..... 227

5.5. Typical axisymmetric drop profiles in an electric field ..... 234

5.6. Solution families in parameter space: effect of pipe on length on aspect ratio ..... 235

5.7. Effect of pipe length on drop stability when distance between tip of pipe and bottom plate is held fixed ($H_1$=10, D=0, G=0) ..... 236

5.8. Distribution of surface charge on supported drops when (electrical/surface charge forces=0) ($H_1$=10, D=0, G=0) ..... 237

5.9. Distribution of surface charge on supported drops at turning point (stability limit) ($H_1$=10, D=0, G=0) ..... 238

5.10. Distribution of surface charge on pendant/sessile drops near contact line ..... 240

5.11. Effect of pipe length on total surface charge and electrical force on supported drops ($H_1$=10, D=0, G=0) ..... 241

5.12. Effect of moving bottom plate away from drop and tip of pipe ..... 242

5.13. Effect of increasing plate spacing on drop stability: case of no pipe ($H_2$=0, D=0, G=0) ..... 243

5.14. Effect of increasing plate spacing on drop stability: case of short pipe ($H_2$=5, D=0, G=0) ..... 244

5.15. Effect of increasing plate spacing on drop stability: case of long pipe ($H_2$=75. D=0, G=0) ..... 245

FIGURE PAGE

5.16. Distribution of surface charge along the plates: no pipe and moderate plate spacing ($H_1$=10, $H_2$=0, D=0, G=0) .. 247

5.17. Distribution of surface charge along the plates: case of short pipe ($H_1$=10, $H_2$=5, D=0, G=0) ..... 248

5.18. Distribution of surface charge along the plates: case of long pipe ($H_1$=10, $H_2$=75, D=0, G=0) ..... 249

5.19. Distribution of surface charge along the pipe: case of short pipe ($H_1$=10, $H_2$=5, D=0, G=0) ..... 250

5.20. Distribution of surface charge along pipe: case of short pipe ($H_1$=10, $H_2$=75, D=0, G=0) ..... 251

5.21. Locus of singular points as a function of drop size ($H_1$=10, G=0) ..... 252

5.22. Effect of drop size on distribution of surface charge: case of no pipe ($\mathcal{E}$=$P$=0, $H_1$=10, $H_2$=0, G=0) ..... 253

5.23. Effect of drop size on distribution of surface charge: case of no pipe ($\mathcal{E}$=$\mathcal{E}_{TP}$, $H_1$=10, $H_2$=0, G=0) ..... 254

5.24. Effect of drop size on distribution of surface charge: case with a pipe ($\mathcal{E}$=$P$=0, $H_1$=10, $H_2$=5, G=0) ..... 255

5.25. Effect of drop size on distribution of surface charge: case with a pipe ($\mathcal{E}$=$\mathcal{E}_{TP}$, $H_1$=15, $H_2$=5, G=0) ..... 256

5.26. Effect of pipe on distribution of surface charge on small drops ($\mathcal{E}$=$\mathcal{E}_{TP}$, $H_1$=15, $H_2$=5, G=0) ..... 257

5.27. Effect of drop size on distribution of surface charge: case with a pipe ($\mathcal{E}$=$P$=$\mathcal{E}_{TP}$, $H_1$=15, $H_2$=5, G=0) ..... 258

5.28. Evolution of drop shapes with field strength: case without a pipe ($H_1$=10, $H_2$=0, G=0) ..... 260

5.29. Evolution of drop shapes with field strength: case with pipe ($H_1$=10, $H_2$=5, G=0) ..... 261

5.30. Evolution of drop shapes with field strength: case with pipe ($H_1$=10, $H_2$=5, G=0) ..... 262

FIGURE PAGE

5.31. Evolution of drop shapes with field strength: case with pipe ($\mathcal{E}=\mathcal{E}_{TP}$, $H_1=10$, $H_2=0$, G=0) ..... 263

5.32. Solution families in parameter space: effect of mesh refinement on (mean curvature)$^{-1}$ ($H_1=10$, $H_2=0$, D=0, G=0) ..... 264

5.33. Solution families in parameter space: effect of mesh refinement on drop aspect ratio ($H_1=10$, $H_2=0$, D=0, G=0) ..... 265

5.34. Solution families in parameter space: effect of mesh refinement on reference pressure ($H_1=10$, $H_2=0$, D=0, G=0) ..... 266

5.35. Effect of mesh refinement on drop shape at termination of run ($H_1=10$, $H_2=0$, D=0, G=0) ..... 267

5.36. Effect of mesh refinement on cone angle at termination of run ($H_1=10$, $H_2=0$, D=0, G=0) ..... 268

5.37. Effect of pipe on cone angle at termination of run ($H_1=10$, D=0, G=0) ..... 270

5.38. Effect of pipe on cone angle at termination of run: Expanded region near tip of drop ($H_1=10$, D=0, G=0) ... 271

5.39. Solution families in parameter space: effect of side boundary condition on aspect ratio ($H_2=5$, $R_2=5$, D=0, G=0) ..... 273

A.1. Discretization of boundary for solving electro-hydrostatic problem by hydrid finite element-boundary element method ..... 396

## LIST OF SYMBOLS

| | |
|---|---|
| $a^i$ | activity coefficient |
| $a_i$ | constants in equation 2.67 |
| $a$ | particle radius |
| $A_H$ | Hamaker constant |
| $A_{ij}$ | coefficient of Margules equation |
| $A_s$ | solvation force constant |
| $A_s^*$ | normalized autocorrelation function |
| $\overline{A}$ | fluctuating influence of molecular collision process |
| $d$ | diameter of ions |
| $d_p$ | diameter of particle |
| $D$ | drop size parameter |
| $D_s$ | diffusion coefficient |
| $e$ | charge of an electron |
| $f_n(v)$ | nuclei particle size distribution |
| $f_a(v)$ | aggregate size distribution |
| $\mathbf{E}$ | electric field strength |
| $\mathbf{E}_n$ | normal electric field strength |
| $F_i$ | interparticle forces |
| $g$ | gravitation constant |
| $g(c)$ | linear growth rate |
| $G$ | gravitational bond number |
| $h$ | distance between plates |
| $H$ | dimensionless distance between plates |

| | |
|---|---|
| $J$ | rate of nucleation, ions/(cm$^3$ s) |
| $J^*$ | rate of nucleation, particles/(cm$^4$ s) |
| $k$ | Botzmann constant |
| $k_0$ | conductivity of bulk electrolyte solution |
| $k_1$ | conductivity of particles |
| $K$ | reference pressure |
| $K_B$ | collision kernel |
| $K_C$ | condensation rate constant |
| $K_D$ | dissolution rate constant |
| $K_H$ | hydrolysis rate constant |
| $K_o$ | constant, Eq. 2.23 |
| $K_{Si}$ | acid-base equilibrium constant for the ammonia- silicic reaction |
| $l$ | path length of cell |
| $l_M$ | mode number |
| $m$ | ratio of particle and solvent refractive indices |
| $m_p$ | mass of particle |
| $n$ | ionic concentration |
| $n_m$ | refractive index of medium |
| $n_p$ | refractive index of particle |
| $n_s$ | refractive index of solvent |
| $N$ | particle number density |
| $N_1$ | number of carbon atoms |
| $N_2$ | number of carbon atoms |
| $N_e$ | electric bond number |
| $N_T$ | total number of particles per unit volume |

| | |
|---|---|
| $n(r,t)$ | particle size distribution |
| $P$ | intensity of light |
| $P(q,r)$ | Mie scattering factor |
| $pK_S$ | autoprotolysis constants |
| $pK_A$ | Acidity constant |
| $pK_B$ | Basicity constant |
| $P_o$ | intensity of incident light |
| $q$ | magnitude of scattering vector difference |
| $Q_E$ | net charge on the particle |
| $Q_{sca}$ | scattering efficiency |
| $r$ | particle size |
| $R$ | drop radius |
| $S$ | supersaturation ratio |
| $S(G)$ | softness |
| $S_p$ | total surface area of particles |
| $t$ | time |
| $\overline{u}$ | particle velocity |
| $u_E$ | electrophoretic mobility |
| $u_o$ | electric potential |
| $U$ | dimensionless potential |
| $v_\gamma$ | lognormal average volume of primary particles |
| $v_\lambda$ | lognormal average volume of aggregate particles |
| $V_A$ | Van der Waals attractive potential |
| $V_o$ | drop volume |
| $V_R$ | repulsive electrostatic potential |

| | |
|---|---|
| $V_S$ | solvation potential |
| $V_T$ | total potential |
| $w$ | experimental order of hydrolysis reaction for water |
| $W_P$ | polydispersity factor |
| $x$ | dimensionless distance |
| $x_i$ | mole fraction of component i |
| $y$ | ratio of particle radii |
| $z$ | ionic charge number |
| $Z_C$ | total charge |
| $\alpha$ | constant |
| $\alpha_m$ | constant, Eq. 2.63 |
| $\beta$ | coefficient of dynamic friction |
| $\beta_E$ | collision efficiency factor |
| $\overline{\beta}_{\gamma\gamma}$ | average nuclei-nuclei collision efficiency factor |
| $\overline{\beta}_{\gamma\lambda}$ | average nuclei-aggregate collision efficiency factor |
| $\overline{\beta}_{\lambda\lambda}$ | average aggregate- aggregate collision efficiency factor |
| $\delta$ | partial charge distribution |
| $\gamma_i$ | activity coefficient of component i |
| $\gamma_n$ | n-th order moment for nuclei |
| $\gamma_S$ | solvation decay length |
| $\overline{\Gamma}$ | average linewidth |
| $\epsilon$ | dielectric constant |
| $\epsilon_m$ | constant Eq. 2.63 |
| $\epsilon_o$ | permittivity of a vacuum |
| $\zeta$ | zeta potential |

| | |
|---|---|
| $\varsigma_m$ | constant Eq. 2.63 |
| $\eta$ | viscosity |
| $\eta_i$ | hardness |
| $rho^*$ | natural frequency of drops |
| $\sigma_S$ | surface tension |
| $\kappa$ | inverse Debye length |
| $\theta$ | scattering angle |
| $\lambda$ | wavelength of light |
| $\lambda_C$ | conductivity |
| $\lambda_n$ | n-th order moment for aggregates |
| $\Lambda$ | equivalent conductance |
| $\mu_i$ | viscosity of droplet |
| $\mu_o$ | viscosity of continuous phase |
| $\nu_E$ | particle velocity |
| $\rho$ | particle size |
| $\rho'$ | particle size |
| $\rho_s$ | $2x\|m-1\|$ |
| $\rho_o$ | density of continuous phase |
| $\rho_i$ | density of droplet |
| $\chi_i$ | electronegativity |
| $\overline{\chi_i}$ | mean electronegativity of a molecule |
| $\psi_d$ | Stern potential |
| $\psi_o$ | surface potential |
| $\sigma_B$ | bulk conductivity of the liquid |
| $\sigma_\gamma$ | standard deviation of nuclei distribution |

| | |
|---|---|
| $\sigma_\lambda$ | standard deviation of aggregate distribution |
| $\phi$ | volume fraction of particles |
| $\tau$ | dimensionless time |
| $\tau_c$ | characteristic decay time |
| $\tau_E$ | extinction coefficient, $cm^{-1}$ |
| $\tau_i$ | decay time for particle of size $r_i$ |
| $\aleph$ | mean curvature |
| $\mathcal{F}$ | Faraday constant |
| $J$ | Jacobian |

# 1. INTRODUCTION

Hydrous metal oxide powders consisting of unagglomerated monosized-submicron particles are important in the fabrication of better ceramic materials. The synthesis of such powders by metal alkoxide precipitation reactions in liquids are of particular interest because of purity of the starting material, the low temperatures at which synthesis occurs, and the rapidity of the reactions. The ability to form mixed metal alkoxides is also attractive for the synthesis of mixed hydrous oxide powders with uniform composition.

The first phase of this research focuses on elucidating the chemistry and physics that govern the formation and growth of monosized ultrafine particles by the hydrolysis of metal alkoxides. This is greatly needed in developing chemical schemes for the host of materials that are required in the development and production of advanced ceramics. Furthermore, the limitations of powder synthesis by metal alkoxides are better defined by a fundamental understanding of the precipitation process.

Encouraging results have been noted for the synthesis of some single- and multi-component spherical particles by the homogeneous precipitation of alkoxides (Fegley and Barringer 1984). However, spherical particles are not formed from metals alkoxides such as aluminum alkoxides which tend to form linear polymers during condensation. In multi-component systems, each metal alkoxide hydrolyzes at a different rate, polymerizes differently (i.e. forming either linear or highly crosslinked polymers) and precipitates at different rates with varied morphologies. Thus, it has proven to be difficult to achieve stoichiometric homogeneity and/or particle sphericity when single- or multi-component metal

oxide particles are produced using homogeneous precipitation methods. With this in mind, several techniques have been developed recently to produce ultrafine single- and multi-component hydrous metal oxide powders by the creation of microreactor environments that confine precipitation to very small regimes in a continuum. These techniques include coprecipitation in vesicles (Bhandardar and Bose 1990), aerosol reactions (Ingebrethsen, Matijevic and Partch 1981), spray pyrolysis (Martin et al. 1990, Zhang and Messing 1990, Pratsinis 1990) coprecipitation in emulsions (Minehan and Messing 1990), and the electrostatic atomization of liquid droplets into air (Slamovich and Lange 1988). Each method has advantages and major disadvantages.

To overcome the disadvantages, a new approach, particle formation by electrodispersion, is investigated in the second part of this research. This method is a direct result of the fundamental work explored in this thesis. The technique of concern in the current research involves the use of high-intensity-pulsed electric fields for droplet size control in dispersed liquid systems. Unlike the electrostatic atomization of liquid droplets into air, this method involves the dispersion of liquid drops into another liquid, which reduces the amount of energy required to produce ultrafine powders. Furthermore, particle agglomerates are usually soft (i.e., easily broken up) in comparison to the aerosol reactor methods and electrostatic atomization of liquid drops into air. This leads to an increase in the green-body density and consequently improves the microstructure of the ceramic.

## 1.1. Background and Origin of Research

The synthesis of well defined powders that consist of monodisperse high-purity metal oxide particles is of primary interest in the development of existing ceramics. Furthermore, the shape, size and, in the case of composite powders, the composition of these particles are found to significantly affect the microstructure of the final ceramic material (Rhodes 1981). The push for controlled synthesis of precursor ceramic particles has lead to numerous techniques for powder synthesis (Akinc and Richardson 1986). These techniques include chemical methods such as homogeneous precipitation of aqueous salts solutions or metal alkoxides; and physicochemical techniques such as spray pyrolysis and water-oil emulsions (Johnson 1981). This research focuses on the ultrafine particle synthesis from the homogeneous precipitation of metal alkoxide solutions and by electrodispersion.

Metal alkoxides have been used to form monosized particles of silica, titania, zirconia, yttria, yttria-zirconia, zirconia-alumina and others (Fegley and Barringer 1984). The formation of monodisperse-spherical silica particles from the base-catalyzed hydrolysis of tetraethylorthosilicate in various alcohol solvents was first studied by Stober, Fink and Bohn (1968). The kinetics of the hydrolysis and condensation reactions were given first reported by Aeolin (1950) and Stober, Fink and Bohn (1968). Titanium ethoxide, an analog of tetraethylorthosilicate (TEOS), hydrolyses to form titania. Barringer and Bowen (1982, 1985) reported the formation of monodisperse titania powders by the hydrolysis of titanium tetraethoxide in ethanol and have discussed their chemical and

physical properties. The delay time for the initial observation of turbidity as a function of the initial water and titanium ethoxide concentration was used to establish hydrolysis and condensation reaction kinetics.

The synthesis of submicron-mixed oxide particles of titania- alumina, yttria-zirconia, and titania-zirconia from mixed alkoxides has been reported (Harris et al. 1988). Composite particles that were formed by mixed alkoxides sintered at lower temperature than those that were formed by the mixing of separate powders.

Although monodisperse particles have been formed from several alkoxide and alkoxide mixtures, the development of recipes for synthesis of monodisperse powders is primarily an ad hoc technique that is sometimes hindered by a poor understanding of the physics and chemistry of forming the starting powders (Bowen 1980). The phenomena which control the formation, nucleation, and growth, of monodisperse powders occur in a size range of 0.005 to 1 micron. In the past, there were limitations in methods of observing submicron particles; therefore, particle growth was usually observed in the size range above 1 $\mu$m. Invariably, populations of particles with a wide size distribution were studied, requiring a number of assumptions about population dynamics before any analysis could be made. A better understanding of the fundamentals of nucleation and particle growth may be obtained if nucleation and growth were followed from the 0.005- to 1-$\mu$m range, and if the growth of monodisperse particles could be observed.

The most significant contribution to particle sizing in the past decade has been the development of dynamic laser-light scattering, and its applications to the observation of submicron particles in liquids (Dahneke 1982). Laser-

light scattering provides an excellent in situ method of nonintrusively observing particles in the size range of interest. Computer algorithms have also been developed to deconvolute laser light scattering data for particle size distribution analysis (Provencher 1979 and 1982).

Metal alkoxide precipitation reactions in liquids are of particular interest in the development of new ceramic materials (Bowen 1980) and are ideal for homogeneous precipitation studies by dynamic laser light scattering. The formation of submicron monodisperse silica particles from the hydrolysis of TEOS in various alcohol solvents has been followed by dynamic laser-light scattering and chemical analysis (Byers et al. 1987). This work was an offshoot of an earlier investigation by Williams, Byers and Watson (1986) and Williams and Byers (1986).

Williams et al. (1986) used dynamic light scattering to determine high-temperature fluid viscosities. The technique involved the growth of organophobic silica particles by the Stober-Fink-Bohn method, the synthesis of organophilic silica particles by esterification of the particle surface and seeding the organic fluid with a trace amount of the organophilic particles. The viscosity of the fluid was obtained by measuring the particle mobility or self diffusion and applying the Stokes-Einstein relation. During the course of these studies, it became apparent that a more fundamental understanding of the growth of well defined particles was desperately needed and that dynamic light scattering could be used to monitor the early stages of particle growth.

This study is an extension of the work of Williams, Byers and Watson (1986) and Byers (1987). More specifically, the research is directed at evaluating the formation of silica, titania, titania-zirconia and titania-alumina by the hydrol-

ysis of tetraethylorthosilicate (TEOS) and metal alkoxides in various alcohol solvents. The silicon and titanium alkoxide systems were chosen because they represent systems where the hydrolysis reaction, in comparison to the condensation reaction, is slow and fast, respectively. The mixed titanium-zirconium and titanium-aluminum alkoxide systems were chosen because of the different chemical kinetics and surface charge properties.

The main objectives of the homogeneous precipitation studies are to (1) experimentally determine the hydrolysis, condensation and particle growth kinetics, (2) estimate Stern potential by electrophoretic mobility measurements and to (3) determine the effect of reaction kinetics and colloidal stability on the formation of monodisperse particles, (4) develop scientifically sound predictive models for particle growth in the homogeneous precipitation of alkoxide systems.

During the investigation of homogeneous precipitation of metal alkoxide solutions, it became apparent that physicochemical techniques were needed to synthesize well defined particles that could not be made by homogeneous precipitation. A new device the Electric Dispersion Reactor (EDR) was invented to prepare 0.1 to 5$\mu$ particles by the use of intense electric fields to create aqueous-organic emulsions.

The EDR is an outgrowth of two research programs: (a) powder synthesis by homogeneous precipitation and (b) the effects of electric fields on multiphase systems. Part (a) was discussed above. Of particular interest in Part (b) is the development of a device know as the Emulsion Phase Contactor (EPC) (Scott 1989, Byers and Scott 1989 and Scott and Wham 1989). This device uses pulsing d.c. fields to enhance mass transport by dispersing aqueous drops into a relatively nonconducting continuous organic phase. The dispersion consists of

micron size droplets (Scott 1987 and Scott and Sisson 1988); thus, the surface area is very large for interfacial mass transport. In addition to dispersing the drop, this device also promotes coalescence of the aqueous droplets (Byers and Scott 1989); hence, there is good separation of the aqueous and organic phases.

The connection between the EPC and EDR involves the generation of micron size droplets for fast interfacial mass transport. In contrast, the droplets formed in the EDR serve as microreactors in which precipitation and/or gelation occurs. Furthermore, unlike the EPC, the EDR requires the minimization of coalescence to control particle size distribution.

The main objectives of the electrodispersion research are to (1) use intense electric fields to synthesize ultrafine particles, (2) vary particle morphology, (3) solve electrostatic problem to determine the effect of reactor geometry on drop stability.

Ultimately, the goal of the homogeneous precipitation and electrodispersion studies is the controlled and reproducible production of ultrafine precursor ceramic powders. The results of this research allow the development of recipes for powder synthesis with minimal experimentation.

## 1.2. Thesis Scope

### 1.2.1. Homogeneous Precipitation Experiments

An understanding of the chemistry and physics of homogeneous precipitation from metal alkoxide solutions is essential to the production of good powders and to the development of theoretical models that describe this process. Numerous studies have been done on both silicon alkoxides and titanium alkoxide

systems. Hydrolysis and condensation kinetics have been studied and major reaction species have been identified. The formation and growth of submicron particles have also been studied. As a result of the hydrolysis and condensation kinetic data and particle growth studies, it has been proposed that the formation of monodisperse particles is governed by either homogeneous nucleation [(reaction kinetics); Matsoukas and Gulari (1988)] or controlled aggregation [(colloidal stability); Bogush and Zukoski (1991)].

The objective of this project is to evaluate the effects of precipitation kinetics and colloidal stability on the synthesis of submicron-monodisperse particles by metal alkoxide hydrolysis. Silica and Titania syntheses from TEOS and titanium alkoxides, respectively, are used as model systems for situations where the hydrolysis reaction is easily controlled while condensation is fast and where the hydrolysis reaction is facile, while condensation is slow [Bradley, Mehrotra and Gaur (1978)]. Mixed alkoxides systems will also be investigated to determine the possibility of synthesizing mixed titania-zirconia and titania- alumina hydrous oxides.

This work primarily involves three phases: (1) experimental studies of the hydrolysis, condensation and particle growth kinetics by available techniques; (2) electrophoretic mobility studies to determine surface potential of particles; (3) theoretical analysis of data by coupled chemical kinetic-detailed population balance models (Santacesaria et al. 1986 and Bogush and Zukoski 1991).

In phase one, hydrolysis and condensation rate constants will be determined from experimental kinetic data. The initial concentration of alkoxide, water, and ammonia (TEOS hydrolysis only) will be varied to determine the effect of reaction kinetics on the final characteristics of the particles and to test the

validity of theoretical models.

The zeta potentials that are determined in phase two are used to evaluate the effect of colloidal stability on particle morphology, growth and size distribution. This is also an important parameter for determining the collision efficiency factor of particle in solution.

The final and most important phase of this research entails incorporating the fitted parameter values that are determined in phase one and the zeta potentials obtained in phase two into the coupled chemical kinetic-detailed population balance model. This model is be used to theoretically determine the effect of reaction kinetics and colloidal stability on the evolution of particle size, size distribution, and particle number concentration. To test the validity of the above model, the computed data will be compared to experimental data.

### 1.2.2. Electric Dispersion Reactor

This research focuses on an innovative new concept, the Electric Dispersion Reactor (EDR), which accomplishes formation of ultrafine particles in dispersed liquid-liquid systems. The EDR utilizes transient electric fields to create dispersions of micron-sized aqueous-based drops in organic media. After formation, reaction and precipitation occur in the aqueous drops to create chemically homogeneous particulates. This thrust is the result of a collaborative effort between research on enhanced solvent extraction by the emulsion-phase contractor (EPC) (Scott and Wham 1989) and research in the area of homogeneous precipitation of ceramic precursor powders.

This new technology is evaluated for its application to the production of

mixed ceramic precursor powders and for the synthesis of ultrafine spherical shells. The experiments are used to establish the varied nature of the products that can be produced but have not addressed capacity, energy efficiency, or optimization of the technology. Additionally, theoretical analysis of various axisymmetric reactor designs is done to determine the optimal geometry. The theoretical analysis involved using finite element and boundary element analyses to solve the augmented Young-Laplace equation and Laplace's equation which govern the drop shape and electrostatics (Pelekasis, Tsamopoulos and Manolis 1990 and Tsukada et al. 1986).

## 1.3. Thesis Synopsis

### 1.3.1. Silica Synthesis by TEOS Hydrolysis

Chapter two discusses the formation of silica particles by the hydrolysis of TEOS in ethanol over a wide range of reactant and catalyst concentrations. Initially, the base-catalyzed hydrolysis and condensation reactions were conducted in various low molecular weight alcohols with dilute TEOS solutions. It was observed that the hydrolysis reaction was affected by the alcohol. These effects were explained in terms of hydrogen bonding and the degree of basicity of ammonia in each alcohol. The reaction was fastest when hydrogen bonding was less and the basicity was greatest. The activation energies for the hydrolysis reaction ranged from 3.5 to 6.9 cal/mol.

A more extensive experimental investigation of the hydrolysis and condensation reaction of dilute and concentrated TEOS solutions in ethanol was used to test models for silica particle formation and growth from ammonia catalyzed

TEOS hydrolysis. The computations were based on solving the hydrolysis and condensation kinetic expressions and applying the method of moments to expedite the solution of the governing population balance equation. The model semi-quantitatively predicted particle growth kinetics, size and size distribution and the effect of reactant concentrations on these parameters. These data also indicated that the aggregative growth model is applicable at high water and ammonia concentrations. However, particles grew by the addition of monomer, soluble polysilicates and small ramified precipitates to the particle surface at low water and ammonia concentrations. Thus, it was implied from the current studies that the dominant mechanism varies for the growth of silica particles with respect to reactant and catalyst concentrations.

1.3.2. Hydrous Metal Oxide Powder Synthesis by Metal Alkoxide Hydrolysis

Chapter three extends the work in chapter two to "true" metal alkoxides. Unlike the silica system, the reaction between the alcohol solvent and the metal alkoxide has a profound effect on the nature of metal hydrous oxide precipitates that are synthesized by the hydrolysis of titanium ethoxide, titanium-zirconium alkoxides and titanium- aluminum alkoxides in ethanol, 1-butanol, and tert-butyl alcohol. Monodisperse and spherical "titania", and "titania"-"zirconia" particles grow at constant rates when produced in ethanol and 1-butanol. However, the rate of growth in tert-butyl alcohol increases with time. The particles that are formed in tert-butyl alcohol are agglomerated and have irregular shapes. Although not monodisperse or spherical, the precipitate that is produced in tert-butyl alcohol could possibly form a sol-gel system. This system could subsequently be used to produce ceramic powders.

This investigation has shown that the "alumina" content affects the type polymers formed, the rate of precipitation and the colloidal stability which ultimately affects particle morphology. A procedure is proposed for the synthesis of 100- to 300-nm spherical particles of 2:1 "alumina"-"titania" by the controlled hydrolysis/condensation of a homogeneous mixture of aluminum and titanium alkoxides in low-molecular-weight alcohols. However, the aggregation of these spherical particles in solution lowers the green-body density of the final powder. To produce a more ideal powder for ceramic applications, future studies should investigate the use of surfactants to minimize aggregation of these spherical particles in solution.

### 1.3.3. Electric Dispersion Reactor

Experiments have shown that the synthesis of submicron- to micron-size metal hydrous oxide ceramic particles can be formed by imposing intense, pulsing, dc electric fields on a conducting liquid drop suspended in a nonconducting liquid. The characteristics of the particles can be changed by strategically locating the reactants in the proper phase. The ability to distribute reactants in either phase makes the EDR an attractive process for synthesizing specialty powders and for improving the synthesis of complexed mixed oxide powders. Future experimental work should involve large-scale synthesis of powders in the EDR and comparing the sinterability, composition, and the ability of these powders to produce improved ceramics to precursors produced by other methods.

### 1.3.4. Electrohydrostatics of Axisymmetric Pendant Drop Problem

Theoretical evaluation was completed of the electrostatics of shapes and stability of drops hanging from a pipe in an electric field. The important results obtained from this work are: (1) the presence of a pipe enhances electrodispersion by increasing the surface charge on the drop; (2) drops greater than $D = D^*$ jet from a conical tip, while annular jetting occurs for skinny drops $D < D^*$; (3) beyond the stability limit, the families of solutions terminated when the radius of curvature approached infinity, (4) for initially hemispherical drop, $D = 0$, the cone angle at the tip of the final drop increases monotonically with pipe length and is greater that 40 degrees and is bounded by the Taylor limit of 49.3. Future theoretical work should include (a) determining the effect of gravity on instability of the axisymmetric electrostatics problem, (b) the development of a three dimensional hybrid boundary element-finite element algorithm to analyze drops hanging from a nozzle; (c) developing methods to solve the electrodynamics and hydrodynamics problem of drops flowing or oscillating from a pipe in an electric field. Another problem that is more easily solved is the effect of the "cup" electrodes configuration on drop stability. In this configuration the potential on the side and bottom boundaries are set equal unity and the top boundary is such that $\frac{\partial V}{\partial n} = 0$. For comparable dimensions, the "cup" electrode configuration causes instability to occur faster than the pipe-two parallel configuration. Future work should involve detail modeling of the "cup" electrode configuration for both process optimization and for providing an in-depth fundamental behavior of drop deformation in this configuration.

## 1.4 Retrospective and Outlook

An understanding of the physical and chemical phenomena that control the formation and growth of monodisperse particles is greatly needed to develop recipes and reactor schemes that can be applied to a host of materials. A review of the literature has shown that three primary mechanisms [i.e., (1) homogeneous precipitation (LaMer and Dinegar 1950; Matijevic 1976 and Matsoukas and Gulari 1988), (2) controlled aggregation (Iler 1979; Feeney, et al. 1984 and Bogush and Zukoski 1991) and (3) collapse of ramified precipitates and their deposition on particle surface (Bailey and McCartney 1990) have been proposed for the synthesis of monodisperse particles. All three mechanisms have been recently proposed for the formation of submicron monodisperse silica particles by the base-catalyzed hydrolysis of TEOS (Matsoukas and Gulari 1988; Bogush and Zukoski 1991 and Bailey and McCartney 1990). To resolve this mechanistic dilemma, the present research focused on investigating the hydrolysis and condensation kinetics of solutions containing dilute to concentrated TEOS, water and ammonia concentrations. A detailed chemical kinetic-population balance model was used to evaluate the data. The results show that mechanisms (2) or (3) dominate depending on the reactant concentrations.

The overall aim of research in this area is to develop models that predict particle formation based on the chemistry and colloidal stability of any given system. As a result of the present work, it is recommended that additional research is needed to put the rate expressions for the condensation and nucleation kinetics on a more fundamental level. Futhermore, the effect of cation binding to ionic silicate species is not incorporated in the hydrolysis and condensation rate

expression. Recently, Sanchez and McCormick (1991) used NMR spectroscopy and a bond orbital electronegativity equalization model (Bergaman, and Hinze 1987) to show that alkaline cations interact with charged silicate fragments during the base-catalyzed hydrolysis of TEOS. This work needs to be extended to show the effect of cations on hydrolysis and condensation kinetics and the utilization of these data in detailed chemical kinetic-population balance models.

The model used in this research assumes a unimodal distribution for ultimate silica particles. As is shown in chapter two, this is clearly not the case for high TEOS, water and ammonia concentrations. Therefore, it is suggested that additional research is needed to develop computationally efficient and accurate methods to predict the formation of multi-modal distributions of silica particles during the hydrolysis of concentrated TEOS solutions with high water and ammonia concentrations.

The extension of the knowledge gained from the silica work is applied to the growth of titania, zirconia and mixed titania- zirconia and titania-alumina particles. It has been shown that hydrolysis and alcoholysis is facile for these systems (Bradley, Mehrotra and Gaur (1978). The research that is reported in this thesis focuses on the effect of solvent and colloidal stability on powder synthesis and a qualitative description of the hydrolysis and condensation reaction of these alkoxide systems. Additional research is required to determine hydrolysis and condensation rate expressions of these very fast reactions that can be used in predictive models.

The formation of ultrafine particles by electrodispersion (i.e., in the EDR) is discussed in chapter four. The main emphasis of this chapter is the creation of ultrafine droplets that serve as microreactors for precipitation and/or gelation.

Controlling particle morphology by reactant concentration and by strategically locating reactants in the proper phase has been shown in this work. Extensive work is required, however, to determine the effect of surfactant concentration, disperse phase concentration and electric field strength on the ultimate particle size and size distribution. The commercialization of this device requires process optimization and detailed economic analysis.

Process optimization requires an understanding of the effect of electric field strength and reactor configuration (i.e., nozzle- electrode configuration) on drops emanating from a nozzle. This can be done by solving the equations that govern the electrohydrostatics and electrohydrodynamics of such systems. A complete analysis of the electrohydrostatics of axisymmetric pendant drops hanging from a nozzle is reported in this thesis. The data clearly show that nozzle-electrode configuration has a profound effect on drop stability.

A complete analysis of the EDR entails solving the governing electrohydrodynamic equations. These equations must be solved numerically by techniques such as the finite element method or a hybrid finite element-boundary element method. This work is currently being done by researchers at the Oak Ridge National Laboratory.

# 2. SILICA POWDER SYNTHESIS BY TEOS HYDROLYSIS

## 2.1 Introduction

Stober, Fink, and Bohn (1968) developed a method of producing monodisperse silica particles by the base-catalyzed hydrolysis of tetraethylorthosilicate (TEOS) and the subsequent condensation of silicic acid in various alcohol solvents. By using a number of different solvents and varying the concentration of the morphological catalyst (NH3) and water, particles were formed with diameters ranging from less than 0.05 to 2 $\mu$m. Fig. 2.1 shows typical silica particles that are synthesized by the Stober-Fink-Bohn (SFB) process.

The most attractive feature of the SFB process for the production of advanced ceramics is that the formation of spherical particles of a particular size is extremely reproducible. Since the properties of the ultimate ceramic part depends, to a large extent, on the reproducibility of precursor powder synthesis, the SFB technique is a model process for precusor powder synthesis. Thus, it is advantageous to determine the phenomena that govern the formation of silica particles by ammonia catalyzed hydrolysis. Such fundamental studies will inevitably lead to the development of predictive models for particle formation and growth that may be used in the controlled synthesis of a hosts of well defined precursor ceramic particles by metal alkoxide hydrolysis. Furthermore, chemical kinetic and particle population dynamics data and models are needed for the optimal design of industrial-scale reactors for powder production.

The purpose of this chapter is to investigate the effect of reactant concentrations (e.g. $[H_2O]$, $[NH_3]$ and $[TEOS]$), solvent, and temperature on TEOS

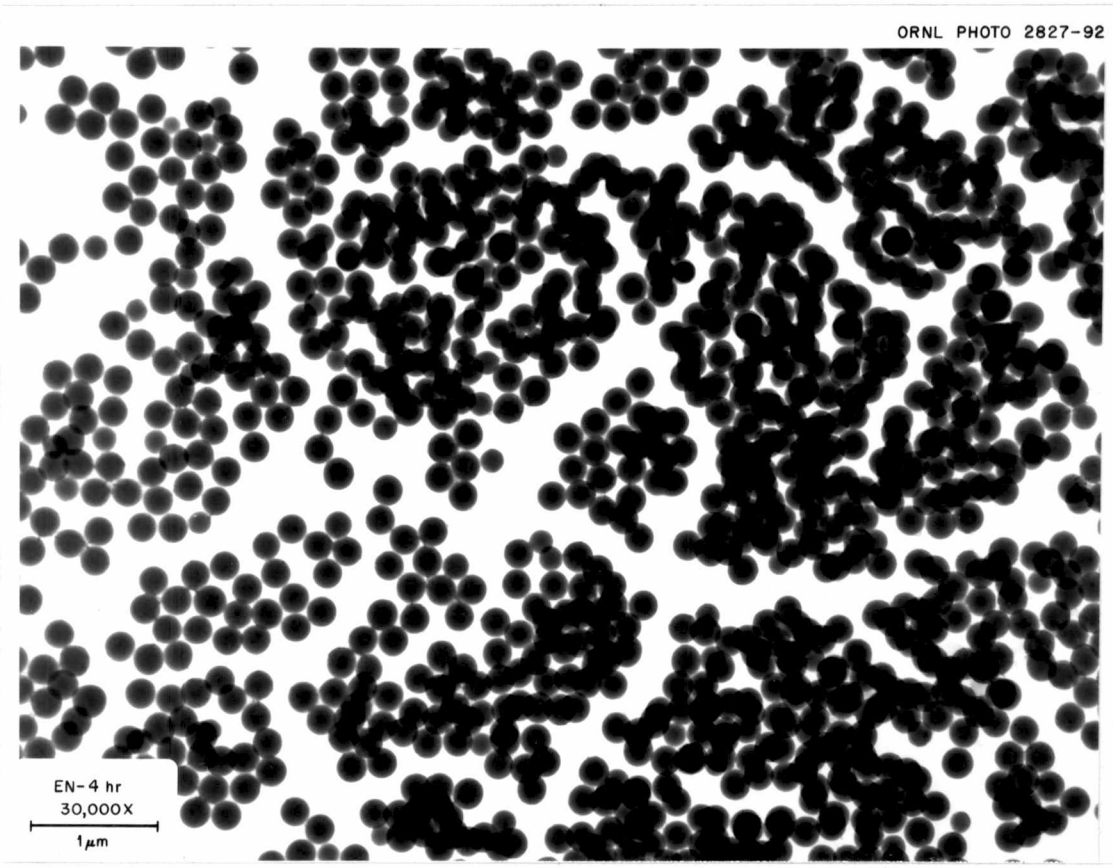



Fig. 2.1. Typical silica particle produced by the Stober process (0.25 $\mu$m diameter, 0.014M TEOS, 6M $H_2O$ and 0.7M $NH_3$).

hydrolysis and condensation kinetics, and particle growth kinetics. A detailed chemical kinetic-population balance model is developed to evaluate the relative effects nucleation kinetics and colloidal stability.

## 2.2. Literature Survey

### 2.2.1. Hydrolysis and Condensation of Silicon Alkoxides

Understanding the mechanisms which control the formation of monodisperse silica by the Stober process requires an initial investigation of the chemical behavior of the hydrolysis and condensation reactions. The overall hydrolysis reaction for TEOS is given as follows:

$$Si(OC_2H_5)_4 + 4H_2O \xrightarrow{OH^-} Si(OH)_4 + 4C_2H_5OH \ , \tag{2.1}$$

and the subsequent overall condensation reaction is given as

$$Si(OH)_4 \overset{OH^-}{\rightleftharpoons} SiO_2 \downarrow + 2H_2O. \tag{2.2}$$

It should be noted that if partial hydrolysis occurs, the following condensation will result:

$$(H_5C_2O)_3Si - OH + Si(OC_2H_5)_4 \longrightarrow$$

$$(H_5C_2O)_3Si - O - Si(OC_2H_5)_3 + C_2H_5OH. \tag{2.3}$$

To further complicate the reaction scheme, the following ester exchange reactions may also occur if the reaction of TEOS is conducted in solvents other than ethanol:

$$(RO)_nSi(OC_2H_5)_{4-n-p}(OH)_p + mROH \longrightarrow$$

$$(H_5C_2O)_{4-n-m-p}Si(OR)_{n+m}(OH)_p + (n+m)C_2H_5OH. \qquad (2.4)$$

With such a variety of possible mechanisms for the hydrolysis and condensation reaction, a number of studies have been conducted to characterize the reaction products and the kinetics for hydrolysis and condensation.

In earlier studies, Aeolin, Loebel, and Eirich (1950) performed a series of wet chemistry tests to provide quantitative information on the rate of hydrolysis of TEOS in acidic and basic media. These studies revealed that the rate of acid-catalyzed TEOS hydrolysis was first order with respect to TEOS, water, and acid concentrations. From these data, it was proposed that the acid hydrolysis involved a mechanism intermediate between general acid and oxonium ion catalysis. The rate of the basic hydrolysis of TEOS was first order with respect to TEOS and the concentration of base; however, the reaction rate was independent of the amount of water present. Therefore, it was proposed that the base catalysis involved a nucleophilic displacement of the alkoxy group by the hydroxyl ion. Aeolin, Loebel, and Eirich (1950) also found that the condensation reaction was faster in base–catalyzed reactions, and the nature of the final product was different for acid and base catalysis.

More recent studies have used methods such as gas chromatography, Raman spectroscopy, and $^{1}H$ and $^{29}Si$ nuclear magnetic resonance spectroscopy to study the products from TEOS hydrolysis. Peace, Mayhan, and Montle (1973) employed gas chromatography and nuclear magnetic resonance spectroscopy to study the acid–catalyzed hydrolysis of TEOS under various solvent and temperature conditions. This research was conducted to determine the structure of polymers obtained from the hydrolysis of TEOS and to evaluate the rate of both of the hydrolysis and the ester exchange reactions. Of particular interest

to the present study is the finding that the ester exchange reaction does not occur until after hydrolysis is complete (i.e., all of the water has been reacted). With respect to the exchange process, primary alcohols are more reactive than secondary alcohols, while tertiary alcohols do not undergo ester exchange. It can, therefore, be postulated that Eq. 2.4 does not occur to any appreciable extent in the presence of excess water.

Pouxviel, Boilot, Beloeil, and Lallemand (1987) have used $^{29}$Si nuclear magnetic resonance to study the acid–catalyzed hydrolysis and condensation of TEOS in ethanol and propanol. It was concluded from their study that with excess water, acid–catalyzed hydrolysis reaction is complete (i.e., all ethoxy groups are removed from the silicon atom) before condensation begins. With an excess molar water/alkoxide ratio of 10, Artaki, Sinka, Irwin, and Jonas (1985) also studied the acid–catalyzed hydrolysis of tetramethylorthosilicate (TMOS) by $^{29}$Si NMR and concluded that monomeric silicic acid was the only species initially present in solution. Thus, the hydrolysis of TMOS in acid solutions is fast and complete to form monomeric silicic acid as represented by the hydrolysis of TEOS (Eq. 2.1). This was also confirmed by the multinuclear ( $^{1}$H, $^{29}$Si, $^{17}$O) NMR study by Turner and Franklin (1986).

Artaki, Bradley, Zerda, and Jonas (1985) employed $^{29}$Si NMR and Raman spectroscopy to study the noncatalyzed hydrolysis of TMOS in formamide and methanol. The water/alkoxide ratio was 10. Their studies showed that the species during the hydrolysis of TMOS in methanol were monomeric, primarily TMOS, and, to a lesser extent, the monosubstituted species, $Si(OCH_3)_3OH$ and possibly the dimer $(CH_3O)_3Si - O - Si(OCH_3)_3$. The other partially hydrolyzed species were not present in any appreciable quantity. Furthermore,

the hydrolyzed product contains mainly monomeric silicic acid, $Si(OH)_4$, and, to a lesser extent, the dimeric species, $(OH)_3Si^{\alpha}-O-Si^{\beta}$. Another interesting feature of their study is the explanation that the impact of solvent on the rate of hydrolysis is possibly a function of viscosity and hydrogen bonding effects. Byers and Harris (1987) have also proposed that hydrogen bonding and steric effects influence the rate of TEOS hydrolysis in different alcohol solvents.

Kelts, Effinger, and S. M. Melpolder (1986) have shown by $^{1}H$ and $^{29}Si$ NMR that increasing the water/alkoxide ratio results in more complete hydrolysis before condensation. By theoretical analyses, Schmidt, Kaiser, Rudolph, and Lentz (1986) have suggested that, due to a decrease in the stabilizing effect of alkyl groups in the transition state, the hydrolysis rate increases with an increasing number of hydrolyzed $OR$ groups of the reacting silane. From these observations, it is suggested that, in the case of a large excess of water, the removal of the first alkoxy group is the controlling step in the hydrolysis of TEOS in alkaline–alcoholic solutions and the subsequent alkoxy groups are removed at a much faster rate due to a decrease in stabilization of the transition state. This will result in the subsequent condensation of the completely hydrolyzed monomeric and possibly dimeric silicic acid. It should be noted at this point that, although the hydrolysis reaction is slower than condensation in the base–catalyzed hydrolysis of TEOS, in the case of a large excess of water ensures complete hydrolysis of each TEOS molecule occurs before it participates in condensation.

Schmidt, Scholze, and Kaiser (1982), and Byers, Harris, and Williams (1987) have proposed a mechanism for the base–catalyzed hydrolysis of TEOS where TEOS reacts with hydroxide ions and water to form a transition state

complex which decomposes to form monosubstituted silane, alcohol, and hydroxide ions. Initially, the $OH^-$ ion attacks the TEOS molecule by a nucleophilic reaction mechanism. Since nucleophilic attack is sensitive to the steric effects of the substitutes and the electron density around the silicon atom, the fewer bulky and highly basic alkoxy groups surrounding the silicon atom, the more rapid the attack by the $OH^-$ ion. Thus, TEOS will hydrolyze at a slower rate and monomeric partially hydrolyzed products will hydrolyze at a faster rate, tending to produce monomeric silicic acid (Keefer 1984). The resulting rate of hydrolysis is, therefore, expressed as a function of the following variables:

$$\frac{\mathrm{d}[TEOS]}{\mathrm{d}t} = f([H_2O], [NH_4OH], [TEOS]). \tag{2.5}$$

Iler (1979) has proposed a mechanism for the condensation of silicic acid which also involves a nucleophilic attack on the silicon by the hydroxide ion. Thus, the rate of condensation should be proportional to the concentration of base catalyst.

In the case of TEOS hydrolysis in other alcohol solvents and noting that Eq. 2.1 applies for the base–catalyzed hydrolysis of TEOS in the presence of a large excess of water, it is possible to monitor the rate of TEOS hydrolysis by following the production of ethanol (Byers, Harris, and Williams 1987). This is assuming, however, that ester exchange reactions do not occur to any appreciable degree, which is the case when the solution contains a large excess of water. Matsoukas and Gulari (1988) studied the ammonia-catalyzed synthesis of colloidal silica particles from TEOS in methanol and ethanol by quasi-elastic light scattering and Raman spectroscopy. The latter method was used to obtain information

about the rate of particle growth by making use of Rayleigh scattering of the plasma lines.

### 2.2.2. Mechanisms for Particle Formation and Growth

It has been postulated that the synthesis of monodisperse sols requires conditions in which nucleation occurs in a very short period at the start of the sol formation (homogeneous precipitation) or by seeding a supersaturated solution with small particles (heterogeneous precipitation) (Shaw 1980). During the past 20 years, Matijevic and his co-workers (1976) have used homogeneous precipitation to produce a number of monodisperse metal oxide particles by carefully heating aqueous solutions of metal salts. These salts will hydrolyze and as the temperature rises a critical concentration of hydrated metal ions will be deprotonated to form the "complex" precursors of nuclei. Nucleation occurs in a short period to relieve the system of this critical concentration; and according to La Mer's hypothesis (La Mer and Dinegar 1950), a subsequent growth of monodisperse particles occurs (See Fig. 2.2).

The process of homogeneous precipitation, as described above, is a proposed mechanism for synthesizing monodisperse silica particles by the controlled hydrolysis of TEOS in alkaline-alcoholic solutions (i.e., Stober method) (Byers, Harris, and Williams 1987) and for synthesizing monodisperse titania particles by titanium alkoxides (Barringer and Bowen 1985). Since the hydrolysis is slower than the condensation reaction for TEOS, it is postulated that, as the TEOS hydrolyzes to form silicic acid, a critical concentration of silicic acid, which is the

ORNL DWG 85-1076R

- SOLUTION TEMPERATURE RISES, HYDRATED METAL IONS ($M^{z+}$) HYDROLYZE:

$$M^{z+}(aq) + z(OH)^{-}(aq) \rightarrow M(OH)_z(s)$$

- A SINGLE "BURST" OF NUCLEI IS FORMED
- SUBSEQUENT GROWTH UNIFORM-MONODISPERSE PRODUCT

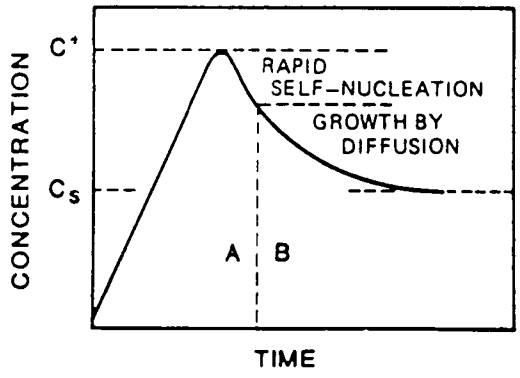



Fig. 2.2 Homogeneous nucleation (La Mer Theory).

precursor material for nuclei formation, is obtained and nucleation ensues. As with Matijevic's method, nucleation relieves the system of the critical concentration of silicic acid, and the result is the growth of monodisperse silica particles (Byers, Harris, and Williams 1987). A similar mechanism has been proposed for the titanium ethoxide system (Barringer and Bowen 1985, Jean and Ring 1986).

Recent papers by Bogush and Zukoski (1987 and 1991) have suggested that the synthesis of monodisperse silica particles by the Stober process is probably due to controlled aggregation. This mechanism has also been proposed by Santacesaria et al. (1986) for synthesis of titanium dioxide from titanium chloride and by Feeney, Napper and Gilbert (1984) for the formation of latex sphere by emulsion polymerization. It is proposed in their studies that nucleation occurs during a significant part of hydrolysis–condensation reaction. Initially, very small particles, $\approx$5 nm, which are unstable colloids, aggregate under the influence of Brownian motion to form larger more stable colloids. Once this size is achieved, these particles pass through the suspension, picking up freshly formed nuclei and smaller aggregates. It is concluded that monodispersity of the final particles is achieved through size-dependent aggregation. Fig. 2.3 shows a schematic of the formation of stable colloids by homogeneous nucleation and controlled aggregation, and also the formation of gels by the uncontrolled aggregation of particles.

Bailey and Mecartney (1990) used cryo-transmission electron microscopy (TEM) to study the precipitation of silica by the base-catalyzed hydrolysis of TEOS. It was concluded that particle formation involved the formation of ramified species which subsequently collapsed after reaching a certain size. Subsequently, these particles grew by the deposition of soluble silicates.

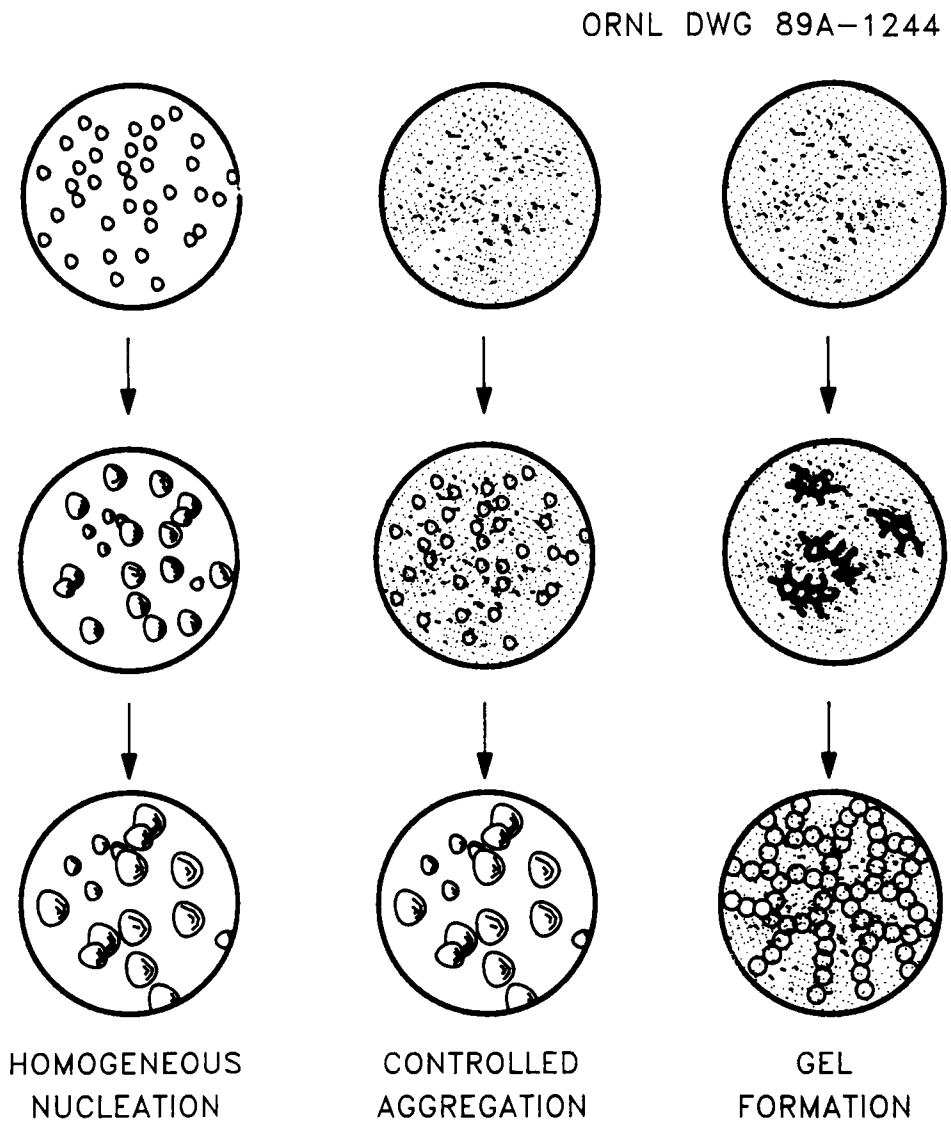



Fig. 2.3 Schematic diagram of homogeneous nucleation, controlled aggregation, and gel formation in colloidal suspensions.

In view of the work by Bailey and McCartney (1990), the model shown in Fig. 2.4 is proposed for the formation of silica particles during the hydrolysis of TEOS.

The figure shows the reaction of monomers (silicic acid or silicate ions), polysilicates-ramified structures, primary dense particles and aggregates of dense particles.

### 2.2.3. Experimental Methods

The experimental methods that have been used to monitor chemical species during the hydrolysis and condensation of TEOS and tetramethylorthosilicate (TMOS) include gas chromatography, ($^{1}H$, $^{17}O$, $^{29}Si$) NMR and Raman spectroscopy, Fourier transform infrared spectroscopy (FTIR), colorimetric molybdate method or combinations of these techniques. Peace, Mayhan and Montle (1973) used gas chromatography, NMR and osmometry to determine the structure of polysilicates during the acid-catalysed hydrolysis of TEOS. The gas chromatograph was a employed a 2m x 3mm Porapack Q column and a thermal conductivity cell. This technique yielded information regarding the relative ratios of silicon to alcohols. While, NMR spectra was used to determine the silicon to hydroxy ratio. The peak assignments for the NMR included methyl groups appearing at $\tau$ =9.17, methylene groups and the secondary proton of isopropanol appearing at $\tau$ =6.34, and the hydroxy proton appearing as a broad peak at $\tau$ =5.34. By comparing the area under the hydroxyl proton peaks to that under the alkyl peak, sufficient information was obtained to generate an empirical formula. Brinker et al. (1984), and Blum and Ryan (1986) also

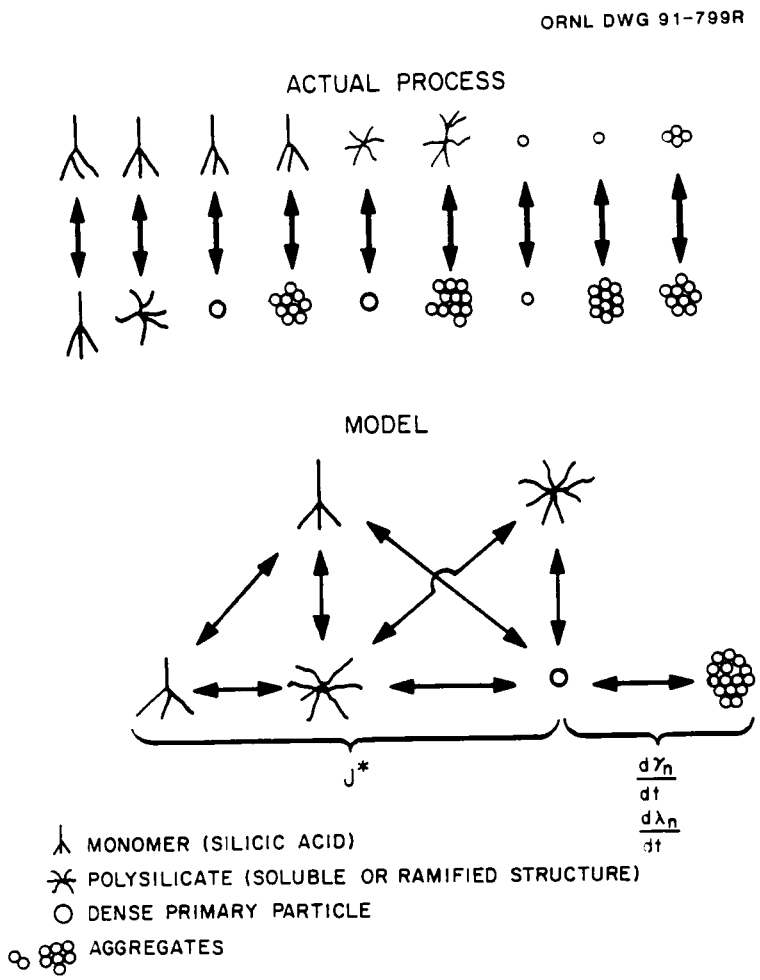



Fig. 2.4 Schematic diagram of silica formation by base- catalyzed TEOS hydrolysis.

used a gas chromatography techniques that were similar to that of Peace et al. (1973) to study the acid-catalyzed hydrolysis of TEOS. Byers, Harris, and Williams (1987) and Byers and Harris (1988) used gas chromatography and the colorimetric molybdate method to study the effect of solvent on hydrolysis and condensation kinetics during the base-catalysed hydrolysis of TEOS.

Yamane, Inoue and Yasumori (1984) used gas chromatography to study the hydrolysis of silicon methoxide in acidic, basic and neutral pH. The chromatograph included a 2m Porapack Q column and a TCD detector. The amounts of methanol, TMOS and water were obtained from the chromatogram.

($^{1}H$, $^{17}O$, $^{29}Si$) NMR has been primarily used to study the chemical species during the acid-catalyzed hydrolysis of TEOS [Brinker et al. (1984), Turner and Franklin (1986), Kelts et al. (1986), Yoldas (1986), Pouxviel et al. (1987), Turner and Franklin (1987)] and TMOS [Artaki et al. (1985 a & b), Kelts et al. (1986) and Zerda et al. (1986)]. This method has been less successful in studying base-catalyzed systems. Raman spectroscopy of TMOS systems has been studied by Artaki et al (1985a). The characteristic peaks are defined in Table 2.1.

Artaki et al. (1985a) showed that Raman spectroscopy and NMR gave the same results for the concentration of $Si(OCH_3)_4$ and $Si(OCH_3)_3(OH)$. Similar work was done by Lippert et al. (1988). However, the number of intermediates was extended to eight and the pH ranged from 2.5-12. Sakka et al. (1988) used Raman spectroscopy to study the effect of catalyst (acid or base) and pH on the hydrolysis of TMOS. The 645 $cm^{-1}$ was used to follow the concentration of $Si(OCH_3)_4$. Matsoukas and Gulari (1987) used Raman spectroscopy to study the ammonia-catalyzed hydrolysis of TEOS in methanol. The 664 and 807

Table 2.1. Assignment of Raman Bands of $Si(OCH_3)_{4-x}(OH)_x$

| $\nu$, $cm^{-1}$ | Specie | Assignment |
|---|---|---|
| 645 | $Si(OCH_3)_4$ | Si-O-C |
| 675 | $Si(OCH_3)_3(OH)$ | Si-O-C |
| 695 | $Si(OCH_3)_2(OH)_2$ | Si-O-C |
| 720 | $Si(OCH_3)(OH)_3$ | Si-O-C |
| 795 | silica dimers | Si-O-Si |
| 830 | silica network | Si-O-Si |

$cm^{-1}$ peaks were used to monitor the concentration of TEOS and the 880 $cm^{-1}$ was used to determine the ethanol concentration. Furthermore, the Rayleigh scattering of the plasma lines at 740, 563 and 531 $cm^{-1}$ were used to determine the extent of the condensation reaction.

Che et al. (1988) used Raman and FTIR spectroscopy to study the rapid synthesis of sol-gels by the HF-catalyzed hydrolysis of TEOS. The Raman spectrometer was equipped with a multichannel linear diode detector which allowed considerably faster spectra acquisition than the conventional moving grating spectrometers that were used in previous studies. Raman spectroscopy was used to monitor the TEOS (644 $cm^{-1}$) and ethanol (880 $cm^{-1}$). The water and ethanol concentrations were obtained from the 1650 $cm^{-1}$ and 880 $cm^{-1}$, respectively, of the FTIR spectra. Dutta and Shieh (1985) used Raman spectroscopy to determine the distribution of silicate species in aqueous solutions at varying hydroxide ion concentrations. The total silicate concentration in these solutions was 1M. In the base-catalyzed hydrolysis of TEOS, however, the concentration of silicates is usually less that 0.1 mol/L. Therefore, a method for detecting the concentration of silicate, especially monomeric and dimeric species, is needed for this system.

Dilute silicic acid concentrations have been measured by the colorimetric method based on the $\beta$-complex of silicic acid with molybdate (Makrides et al. 1980). The optical density at 400 nm of the $\beta$-complex produced from a $3 \times 10^{-4}$ mol (equivalent $SiO_2$) is approximately 0.75. Molybdate-reactive silica includes monosilicic and disilicic acids. Higher condensed species do not contribute significantly to the total amount of soluble silica.

Recently, Bogush and Zukoski (1991) have used $^{29}Si$ NMR to measure the

concentration of TEOS, atomic absorption to measure total soluble silica and conductivity to detect the presence of hydrolyzed TEOS. Conductivity was found to be an excellent method of determining the behavior of the silicic acid concentration.

## 2.3. Experimental

The previous section reported the techniques that have been used to determine the reaction intermediates and products during the hydrolysis and condensation of silicon alkoxides (TMOS and TEOS).

Techniques such as NMR and Raman spectroscopy are excellent for chemical analyses. But can be time consuming when solids are present in solution. In base catalyzed TEOS systems of interest in this research, it is sufficient to assume that each TEOS molecule undergoes complete hydrolysis before condensation. Therefore, a measure of the total soluble silica and TEOS concentration are sufficient to evaluate the hydrolysis and condensation kinetics. This section discusses the chemicals and methods used in this study.

### 2.3.1. Chemicals

Ethanol, 1-propanol, 2-propanol, 1-butanol, 2-butanol, *tert*–butyl alcohol, and *tert*–amyl alcohol were used as solvents and were of analytical reagent quality. The TEOS (Fisher Scientific Co.) was the purified grade. Titanium ethoxide from Alfa Products was used without further purification. Triple-distilled

water was used in all studies. The ammonia (Mallinckrodt, Inc.) was of analytical grade.

### 2.3.2. Instrumentation

A Tracor 550 Gas Chromatograph equipped with a flame–ionization unit was used to follow the production of ethanol. The chromatograph was operated with a column temperature of 130°C and a detector temperature of 175°C. A glass column packed with 1% SP1000 on 80/100 Carbopac C was used to separate the species involved in the reactions. Absorbance readings for the spectrophotometric method of determining monomeric silicic acid were obtained with a Perkin–Elmer Model 200 Spectrometer. The spectrometer was equipped with a dual holder for standard 1-cm quartz reference and sample cells. Absorbance measurements were taken at a wavelength of 400 nm. Fourier transform infrared spectroscopy analyses were done with a BOWEN–Michelson 100 FTIR that was interfaced to an IBM PC–AT for data manipulation. Raman spectra were obtained in a standard quartz spectrophotometer cell with the use of a Spex 1404 spectrometer that was controlled by a compudrive microprocessor. The sample was excited with a 488-nm line of a Spectra-Physics 165-06 argon ion laser and a power setting of 400mW. The scattered light was collected at 90° without a polarizer analyzer. A photomultiplier/photon counter (EMI No. 9863B350) was the detection device. The photomultiplier/photon counter was connected to an IBM PC-AT computer which housed a multichannel analyzer board for data acquisition and display.

Classical-light scattering (CLS) measurements were obtained by the spectrometer at 420-nm to measure the transmittance of the light source passing through the solution containing the growing particles. These data were coupled with dynamic laser-light-scattering data to obtain the concentration of particles in solution.

The dynamic light–scattering (DLS) spectrometer (Fig. 2.5) consisted of a 2–W argon–ion laser (Spectra Physics model 165-06) which focused a 488-nm beam onto the center of a quartz sample cell containing the colloidal particles.

Light scattered at 90° was collected in an end–window photomultiplier (EMI No. 9863B350), amplified, and transmitted to a digital correlator. The autocorrelator (Langley Ford, Model 1096) is a digital signal processor which can accurately approximate the ideal autocorrelation function of the scattered light signal. This autocorrelation function is related to the mobility of particles undergoing Brownian motion in solution. A detailed theoretical analysis which relates the diffusivity of the particles to the scattered light signal is given elsewhere (Berne and Pecora 1976; Dahneke 1983). The major parameter that is obtained from the autocorrelator is the self-diffusion coefficient, which in the case of a dilute solution of particles much larger than the size of the solvent molecules, is related to the diameter of the particle by the Stokes–Einstein equation:

$$D = \frac{kT}{3\pi d\eta} , \tag{2.6}$$

where $D$ = self-diffusion coefficient, $k$ = Boltzmann constant, $T$ = absolute temperature, $d$ = diameter of particle, and $\eta$ = viscosity.

Zeta potential will be determined by electrophoretic mobility measurement in a Zeta-Meter (Zeta-Meter, Inc.; Model ZM-77). This instrument is equipped

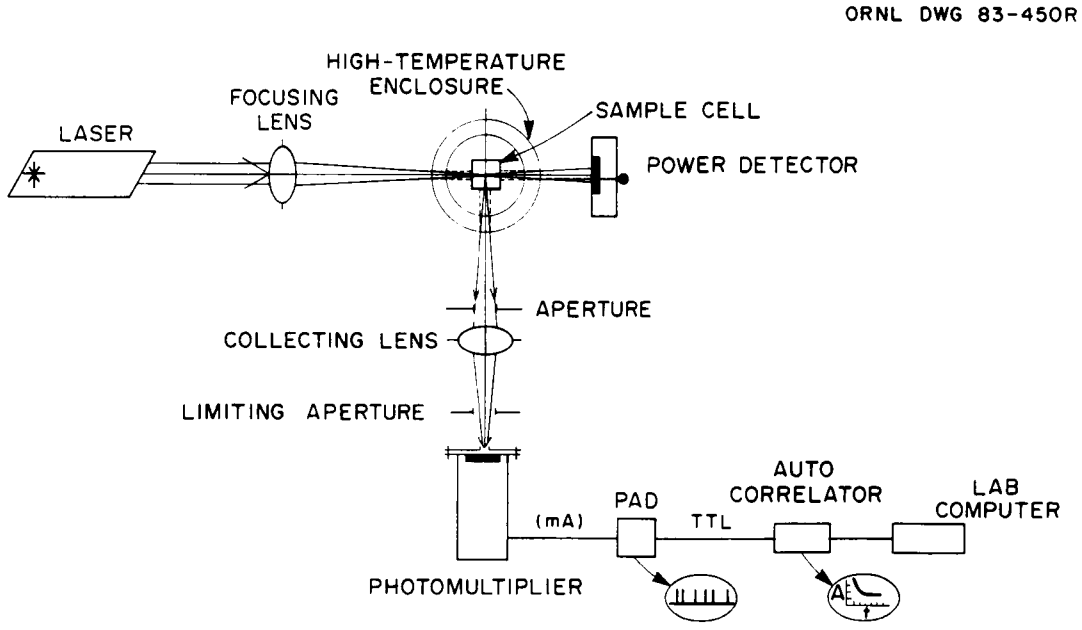



Fig. 2.5 Schematic diagram of the dynamic light scattering Spectrometer.

with a power booster for determining electrophoretic mobility in nonaqueous media.

### 2.3.3. Experimental Procedure

Distilled water and ammonia were mixed with enough alcohol solvent to dissolve the water. TEOS was dissolved in a separate portion of the alcohol solvent. After the two solutions had been vigorously mixed for approximately 5 s, the mixture was poured into a clean temperature controlled quartz spectrophotometer cell in the DLS facility. Gas chromatographic analysis of the TEOS–alcohol portions showed that ester exchange reactions did not occur within the brief period (<2 minutes) before the two solutions were mixed.

Part of the reaction solution was extracted and poured into a clean temperature controlled quartz spectrophotometer cell in the DLS facility. The DLS data were acquired at intervals as small as 1 minute for the period during which particle growth occurred (usually several hours). Some of the sample was poured into another temperature-controlled quartz cell for transmittance measurements in the Perkin–Elmer Model 200 Spectrometer.

A portion of the mixture was analyzed for ethanol using the Tracor GC. The ethanol eluted in approximately 1 min; however, the solvent peaks required as along as 6 min to return to baseline. Samples were taken on an average of every 6 to 10 min.

Another portion of the mixture was analyzed for "soluble silica". The term "soluble silica" refers to the amount of unreacted TEOS and monomeric and, to a lesser degree, dimeric silicic acid in solution. The amount of soluble silica

was determined by a modified version of the molybdate method that is given by Makrides, Turner, and Slaughter (1980). This method determines the amount of monomeric silicic acid and, to a lesser extent, dimeric silicic acid in solution. The procedure can be outlined as follows:

1. The acidic dilution solution (0.1N $H_2SO_4$) was prepared by adding 100 mL of 1N $H_2SO_4$ to 900 mL of distilled water.
2. The 0.4 % Molybdate Solution was prepared by adding 20 mL of 10 % Molybdate Solution to 380 ml of distilled water and 100 mL of 1N $H_2SO_4$.
3. For an initial [TEOS] of 0.1 mol/L, 0.1 mL of sample was added to 5 mL of the acidic dilution solution and 0.5 mL of this solution was quickly added to 5mL 0.4 % Molybdate Solution.
4. For an initial [TEOS] of 0.3 mol/L, 0.1 mL of sample was added to 5 mL of the acidic dilution solution and 0.2 mL of this solution was quickly added to 10mL of the 0.4 % Molybdate Solution. The solution was allowed to react for 20 minutes.
5. The absorbance was measured at 400 nm.

Standards were made from TEOS and were taken throughout the procedures listed above. A comparison of the optical densities of the TEOS standards to sodium metasilicate standards [Marsha, Klein and Vermeulen (1975)] is shown in Fig. 2.6. There is good agreement between absorbances for the TEOS and metasilicate standards.

Conductance and pH were measured continuously on a YSI conductivity meter (Model 34) and a Extech pH meter (microcomputer pH version 246071),

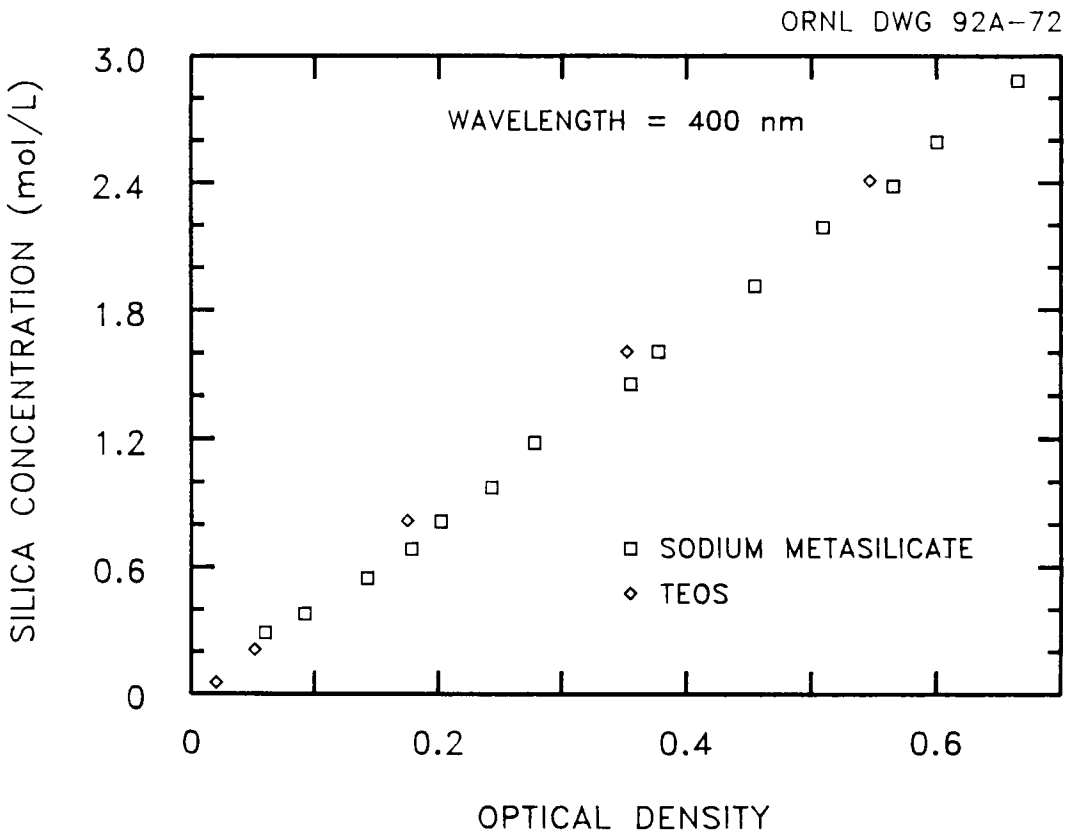



Fig. 2.6 Comparison of optical density for reaction of molybdate with sodium metasilicate and TEOS standards.

respectively. The pH and conductivity meters were interfaced to an IBM PC-AT Computer through a Data Translation DT707 screw terminal panel and a Data Translation 2801 analog to digital board.

## 2.4. Theory

### 2.4.1. Reaction Model

A model for the formation of monodisperse silica by the base-catalyzed hydrolysis of TEOS must include consideration of both the hydrolysis and condensation reactions, which are written as follows:

$$Si(OC_2H_5)_4 + 4H_2O \xrightarrow[OH^-]{K_H} Si(OH)_4 + 4C_2H_5OH\ , \tag{2.7}$$

$$Si(OH)_4 \underset{K_D}{\overset{K_C}{\rightleftharpoons}} SiO_2 \downarrow + \ 2H_2O. \tag{2.8}$$

TEOS is hypothesized to react with hydroxide ions and water to form a transition state complex which decomposes to form monosubstituted silane, alcohol, and hydroxide ions. The removal of the first alkoxy group and generation of the monomeric partially hydrolyzed product, the rate controlling step, are followed by completion of hydrolysis at a faster rate, producing monomeric silicic acid (Schmidt et al. 1984 and Keefer 1984). If ammonia is the catalyst, the rate expression for the hydrolysis reaction for dilute TEOS solutions is (Byers, Williams and Harris 1987):

$$\frac{\mathrm{d}[TEOS]}{\mathrm{d}t} = -K_H[H_2O]^{1.5}[NH_3]^{0.9}[TEOS]. \tag{2.9}$$

As suggested by Iler (1979) a reversible reaction occurs in the condensation-dissolution reaction shown in Eq. 2.2. The following rate expression for this

complex reaction includes a term that represents the loss of silicic acid by the formation of nuclei:

$$\frac{\mathrm{d}\,[Si(OH)_4]}{\mathrm{d}t} = -K_C S_p([Si(OH)_4] - [Si(OH)_4]_e) - J - \frac{\mathrm{d}\,[TEOS]}{\mathrm{d}t}. \quad (2.10)$$

In terms of the measurable total soluble silica, [TS], and [TEOS], the rate expression is of the form

$$\frac{\mathrm{d}[TS]}{\mathrm{d}t} = -K_C S_p \{[TS] - [TEOS] - [Si(OH)_4]_e\} - J. \quad (2.11)$$

The rate of nucleation, $J$, is based on classical nucleation theory and is computed from the expression given by Nielsen (1964):

$$J \doteq \left(\frac{2D}{d^5}\ln(S)\right) \exp\left(\frac{-A_J}{\ln^2(S)}\right), \quad (2.12)$$

where $A_J$ is the nucleation constant, $D$ is the diffusion coefficient, $d$ is the diameter of $SiO_2$ molecules, $S$ is the supersaturation ratio, and $S_p$ is the total surface area of the particles per volume of solution.

In addition to the hydrolysis and condensation reactions, the following solvent dissociation and acid-base reactions are also occurring:

$$2HS \rightleftharpoons H_2S^+ + S^-, \quad (2.13)$$

$$NH_4^+ + HS \rightleftharpoons NH_3 + H_2S^+, \quad (2.14)$$

$$NH_3 + H_2SiO_2(OH)_2 \rightleftharpoons NH_4^+ + HSIO_2(OH)_2^{-1}, \quad (2.15)$$

where $HS$ represents the treatment of ethanol plus water as one solvent (ethanol + water) (Tremillon 1974).

The mathematical expressions for these equilibrium reactions are

$$\frac{([NH_3]-[NH_4^+])[H_2S^+]}{[NH_4^+]} = 10^{-8.5}, \tag{2.16}$$

$$[H_2S^+][S^-] = 10^{-16}, \tag{2.17}$$

$$\frac{[NH_4^+][HSiO(OH)_2^-]}{([NH_3]-[NH_4^+])([TSi]-[HSiO(OH)_2^-])} = K_{Si}, \tag{2.18}$$

where $K_{Si}$ is the acid-base equilibrium constant for the ammonia-silicic acid reaction (Eq. 2.15).

The ions in solution must obey the law of electroneutrality; therefore, a fourth equation is written which gives four independent equations to compute the four unknown quantities $[NH_4^+]$, $[H_2S^+]$, $[S^-]$, and $[HSiO_2(OH)_2^-]$ to be computed,

$$[NH_4^+]+[H_2S^+]-[S^-]-[HSiO_2(OH)_2^-] = 0. \tag{2.19}$$

Of primary importance is the computation of $[NH_4^+]$ which is the major cation that controls the DeBye length. Solving for $[NH_4^+]$, the following expression is obtained

$$[NH_4^+]^3+[NH_3]K_{Si}[NH_4^+]^2-(K_{Si}[NH_3][TSi]+10^{-7.5}[NH_3])[NH_4^+] - 10^{-7.5}[NH_3]^2K_{Si} = 0. \tag{2.20}$$

### 2.4.2. Particle Growth Model and Colloidal Stability

The plethora of possible reaction combinations shown in Fig. 2.4 makes the full solution to the silica synthesis problem untractable. However, if several of

the reaction combinations are lumped into one expression, such as a nucleation rate expression, the problem becomes more tractable. Thus nucleation is defined as the rate at which dense primary particles are formed. These are called nuclei.

Once these nuclei are formed, it was postulated that growth occurs by monomer addition to the solid surface and/or by controlled aggregation. These postulates are tested by a detailed model which simultaneously solves the hydrolysis and condensation rate expressions (Eqs. 2.9 and 2.10 for silica), the population balance equations that govern the coagulation of Brownian particles with electrostatic repulsive forces (Bogush and Zukoski 1988, Feeney et al. 1984, and Santacesaria et al. 1986) and particle growth by monomer addition (Santacesaria et al. 1986). The population balance equations in terms of particle volume and particle radius are:

$$\frac{\partial f(v,t)}{\partial t} + \frac{\partial (f(v,t)g(c)v^{2/3})}{\partial v} = J^*\delta(v-v^*) + \frac{1}{2}\int_0^v K_B(v-v',v')f(v-v',t) \\ f(v')\mathrm{d}v' - f(v)\int_o^\infty K_b(v,v')f(v')\mathrm{d}v', \tag{2.21}$$

and

$$\frac{\partial n(r,t)}{\partial t} = \int_{\rho=0}^{\rho=\rho_{max)}} K_B(\rho,\rho')n(\rho,t)n(\rho',t)\left(\frac{r}{(r^3-\rho^3)^{1/3}}\right)^2 \mathrm{d}\rho + J^*(r,t) \\ - \int_{\rho=0}^{\rho=\infty} K_B(r,\rho)n(r,t)n(\rho,t)\mathrm{d}\rho \\ - g(c)\left(\frac{1}{36\pi}\right)^{1/3}\frac{\partial n(r,t)}{\partial r}, \text{ respectively.} \tag{2.22}$$

where $n(v,t)$ = particle size distribution in terms of particle volume, $n(r,t)$ = particle size distribution in terms of particle radius, $K_B$ = coagulation kernel,

$g(c)$ = linear growth rate, $J^* = J$/number of molecules in critical nucleus, $\rho =$ particle radius, $\rho' = (r^3 - \rho^3)^{1/3}$, $v$ and $v'$ = particle volume.

The coagulation kernel, $K_B$, is given by

$$K_B = K_o \frac{(r+\rho)^2}{r\rho} \beta_E \tag{2.23}$$

with

$$K_o = \frac{2kT}{3\eta} \tag{2.24}$$

The term $\beta_E$ is the collision efficiency factor and accounts for the effect of inter-particle forces on the Brownian coagulation rate (Fuchs 1964). It is computed by the following equation:

$$\beta_E = \frac{1}{2\int_2^\infty \exp\left(\frac{V_T}{kT}\right) \frac{ds}{s^2}}. \tag{2.25}$$

where $V_T$ is the sum of the repulsive electrostatic potential, $V_R$, and the Van der Waals attractive potential, $V_A$. The attractive potential is computed by the following equation first derived by Hamaker (1937):

$$V_A = -\frac{A}{12}\left[\frac{y}{x^2+xy+x} + \frac{y}{x^2+xy+x+y} + 2\ln\left(\frac{x^2+xy+x}{x^2+xy+x+y}\right)\right], \tag{2.26}$$

where,

$$x = \frac{H}{a_1 + a_2} \text{ and}$$
$$y = a_1/a_2$$

If the DeBye length is small compared to the particles radii and the surface potential is less than 50 mV, the following equation can be used to compute the

repulsive potentials (Hogg et al., 1966 constant surface potential):

$$V_R = \frac{\pi\epsilon a_1 a_2}{(a_1 + a_2)} 2\psi_{d1}\psi_{d2} \cdot \ln\left(\frac{1 + \exp[-\kappa H]}{1 - \exp[-\kappa H]}\right) + \frac{\pi\epsilon a_1 a_2(\psi_{d1}^2 + \psi_{d2}^2)}{(a_1 + a_2)} \ln(1 - \exp[-2\kappa H]). \quad (2.27)$$

Another approximate expression for $V_R$ has been given Reerink and Overbeek (1970). The low-potential approximation is not assumed, but the inter-particle distance is considered to be sufficiently large (i.e. exp[-$\kappa$H]$\ll$ 1) for the potential at any point between the particles to be given by the sum of the individual potentials at that point for each particle in the absence of the other. The equation for unequal size spheres is

$$V_R = \frac{64\pi\epsilon a_1 a_2 (kT)^2 \gamma_1 \gamma_2}{(a_1 + a_2) e^2 z^2} \exp[-\kappa H], \quad (2.28)$$

where,

$$\gamma_i = \frac{\exp[ze\psi_{di}/2kT] - 1}{\exp[ze\psi_{di}/ekT] + 1} \quad (2.29)$$

Analytical expressions for unequal spheres have also been developed by Bell et al. (1970), and Barouch and Matijevic (1985a & b).

The reciprocal double layer thickness or inverse Debye length,$\kappa$, is calculated using the expression

$$\kappa = \left(\frac{2e^2 n}{\epsilon\epsilon_o kT}\right)^{0.5} \quad (2.30)$$

where, the ionic concentration, $n$, is obtained as

$$n = \frac{\sigma_B \Im}{e\Lambda_o}, \quad (2.31)$$

where, $\sigma_B$ is the bulk conductivity of the liquid (measured in the electrophoresis cell) and $\Lambda_O$ is the equilvalent conductance.

In addition to the electric double layer and the Van der Waals attractive forces, solvation forces are also present in colloidal suspensions [Israelachvili and Adams (1977), Horn and Israelachvili (1981), Pashley (1981), Peschel et al. (1982), Christenson and Horn (1983), Christenson (1984), Christenson and Horn (1984), and Pashley and Israelachvili (1984)]. These forces become important at surface separations less than approximately 5 nm. It was initially believed that these forces decayed monotonically ($\gamma_s$, decay length $\approx 1nm$) with surface separation [Israelachvili (1977) and Pashley (1981) and Peschel et al. (1982)]. However, studies have show that the solvation force is an oscillatory function of distance [Horn and Israelachvili (1981), Christenson and Horn (1983), Christenson (1984), and Christenson and Horn (1984) and Pashley and Israelachvili (1984)]. Assuming monotonic decay, Bogush and Zukoski (1991) derived the following equation for the solvation interaction potential for two spheres:

$$V_S = \pi A_S \gamma_s \frac{2r_i r_j}{r_i + r + j} \exp\left[-\frac{(H - r_i - r_j)}{\gamma_s}\right] \tag{2.32}$$

Based on the value of $\beta_E$, Brownian coagulation has been classified as: $\beta_E = 1$ for rapid coagulation, $\beta_E < 1$ slow coagulation, and $\beta \rightarrow 0$ for no coagulation or colloidal stability. It is easily seen from Eqs. 28-32 that $\beta_E$ =f($a_1$, $a_2$, $A$, $\kappa$, $\psi_1$, $\psi_2$, $z$, $\epsilon$). However, for systems where everything is constant except for the particle sizes, it has been shown theoretically by the Derjaguin- Landau-Verwey-Overbeek (D.L.V.O) theory and observed experimentally by Verwey and Overbeek (1948) that smaller particles coagulate faster than larger particles. This is the basic philosophy behind the controlled aggregation for particle synthesis by metal alkoxide hydrolysis (See section 2.3). It was also observed by Ottewill and Shaw (1966) that smaller particles coagulated faster than larger particles

to a certain size regime (approximately 0.1$\mu$m) at which a transition occurs where further increase in particle size causes an increase in the rate of coagulation. This phenomenon, as explained by Wiese and Healy (1970), was due to a secondary minimum in the potential energy curve.

### 2.4.3. Solving the population balance equation

The mathematical description of the population balance model is a simple integrodifferential equation. However, this equation has no analytical solution and straightforward numerical solutions involve excessive computer time on even the fastest supercomputer (Frenklach and Harris 1987). For this reason, several methods providing approximate solutions to this problem have been developed in the literature. These methods can be classified as being either moment, sectional, or continuous, depending on their treatment of the particle size distribution (Landgrebe and Pratsinis 1990).

Moment methods describe the evolution of the moments of the size distribution by approximating its shape as monodisperse, lognormal, or self-perserving. Moment methods are orders of magnitude faster than the discrete method and provide information on average properties of the particle size distribution such as total particle concentration, average diameter, and polydispersity. The accuracy of the moment methods, however, depends on the validity of the assumed distribution shape. Therefore, it should not be expected that these solutions provide high accuracy during the early stages of particle formation, when particle mass is being formed by chemical reaction (Landgrebe and Pratsinis 1990).

Sectional models approximate the continuous size distribution by a finite number of sections within which the particle size distribution function is assumed

to be constant. The accuracy and the computational speed of these models depends on the number of sections employed, on the selection of the numerically conserved integral property of the distribution, and on the treatment of the lower end of the size distribution (Langrebe and Pratsinis 1990).

Continuous models solve the detailed population balance equations and therefore most accurately describe the evolution of the particle size distribution. These models, however, require enormous amounts of computer time and memory. Thus, continuous models are mostly used for validation of other approximate particle dynamic models or for investigation of the attainment of asymptotic self-preserving size distribution.

The moment and continuous methods are used in this research to solve the population balance equation. Discrete methods are used to follow the particle size distribution during the early stages of particle formation.

2.4.3.1. Continuous method

In the continuous method, the particle size range $1.0\times10^{-10}$ to $1.0\times10^{-6}$m is divided into M-intervals. Eq. 2.32 is solved for each interval by the Euler method for differentiation and Simpson's method for integration. Each time step is determined by the equation

$$\Delta t = f_t \frac{\left(-N_{PT} + \sqrt{N_{PT}^2 + 1.5\times10^{11} t_{cog} J^*}\right)}{2J^*}. \qquad (2.33)$$

The discretization of the particle size range and the value of $f_t$ are chosen to minimize the loss of mass during the integration.

2.4.3.2. Moment method

The moment method is used to convert the population balance equation which is an integro-partial-differential equation into a set of ordinary differential equations (Randolph and Larson 1971). Furthermore, to apply the method of moments to the homogeneous precipitation problem where nucleation and controlled aggregation are occurring simultaneously, sets of moment equations are required for the nuclei and aggregates (Santacesaria et al. 1986). The moments equations for the nuclei and aggregates are

$$\frac{d\gamma_n}{dt} = ng(c)\gamma_{2/3+n-1} + J^* v^{*n} - \overline{\beta}_{\gamma\gamma}(\gamma_{1/3}\gamma_{n-1/3} + 2\gamma_o\gamma_n + \gamma_{-1/3}\gamma_{n+1/3}) - \overline{\beta}_{\gamma\lambda}(\lambda_{1/3}\gamma_{n-1/3} + 2\lambda_o\gamma_n + \lambda_{-1/3}\gamma_{n+1/3}), \quad (2.34)$$

$$\begin{aligned}\frac{d\lambda_n}{dt} =& ng(c)\lambda_{(2/3+n-1)} \\ &+ \frac{\overline{\beta}_{\lambda\lambda}}{2} \times \sum_{k=0}^{n}\left[\binom{n}{k}(\lambda_{n-k-1/3}\lambda_{k+1/3} + 2\lambda_{n-k}\lambda_k + \lambda_{n-k+1/3}\lambda_{k-1/3})\right] \\ &+ \frac{\overline{\beta}_{\gamma\gamma}}{2} \times \sum_{k=0}^{n}\left[\binom{n}{k}(\lambda_{n-k-1/3}\gamma_{k+1/3} + 2\gamma_{n-k}\gamma_k + \gamma_{n-k+1/3}\gamma_{k-1/3})\right] \\ &- \overline{\beta}_{\gamma\lambda}(\gamma_{1/3}\lambda_{n-1/3} + 2\gamma_o\lambda_n + \gamma_{-1/3}\lambda_{n+1/3}) \\ &- \overline{\beta}_{\lambda\lambda}(\lambda_{1/3}\lambda_{n-1/3} + 2\lambda_o\lambda_n + \lambda_{-1/3}\lambda_{n+1/3}), \text{respectively.} \quad (2.35)\end{aligned}$$

The n-th order moment for the nuclei and aggregates are defined as

$$\gamma_n = \int_0^\infty f_n(v)v^n dv \text{and} \quad (2.36)$$

$$\lambda_n = \int_0^\infty f_a(v)v^n dv. \quad (2.37)$$

To economically solve the moment equations, Eqs 2.34 and 2.35 are written for the 0,1 and 2 moments. Relationships are, therefore, needed to compute all moments from the zeroth, first and second moments. The zeroth and first order moments give the particle number concentration and total particle volume, respectively. The secondth moment is the volume squared or allows an easy method of approximating $r^6$. This quantity is important in computing the intensity of light scattered by colloidal particles.

Assuming a lognormal distribution for the nuclei and aggregates, the moments with order n different form 0, 1, and 2 can be determined by the relations:

$$\gamma_n = (\overline{v}_\gamma)^n \exp(1/2n^2 \log^2 \sigma'_\gamma), \tag{2.38}$$

$$\lambda_n = (\overline{v}_\lambda)^n \exp(1/2n^2 \log^2 \sigma'_\lambda), \tag{2.39}$$

where,

$$\overline{v}_\gamma = \frac{\gamma_1}{\sigma_\gamma^{0.5} \gamma_0}, \tag{2.40}$$

$$\sigma_\gamma = \frac{\gamma_2 \gamma_0}{\gamma_1^2}, \tag{2.41}$$

$$\overline{v}_\lambda = \frac{\lambda_1}{\sigma_\lambda^{0.5} \lambda_0}, \tag{2.42}$$

$$\sigma_\lambda = \frac{\lambda_2 \lambda_0}{\lambda_1^2}. \tag{2.43}$$

2.4.4. Estimating Chemical Reaction Parameters

Nonlinear parameter estimation was used to fit the chemical rate expressions for the hydrolysis and condensation of TEOS (Eqs. 2.9 and 2.10), particle growth and particle concentration data to determine values for $K_H$, $K_C$, and

$A_J$. Numerical methods (e.q., Runge Kutta or Euler) were used to integrate the chemical rate expressions.

The equilibrium constant, $K_{Si}$, is estimated from pH and silicic acid data. The pH data are used to estimate $[H_2S^+]$ and applying Eq. 2.16, $[NH_4^+]$ is computed. Equation 2.20 is then used to compute an estimate for $[K_{Si}]$.

2.4.5. Estimating the Stern Potential, $\psi_d$

The Stern potential, $\psi_d$, can be estimated by zeta potential, $\varsigma$, measurements (Shaw 1980). A schematic depicting the relationship between $\psi_d$, $\varsigma$ and the surface potential, $\psi_o$ is shown in Fig. 2.7.

Zeta potentials are measured using the electrokinetic phenomena that arise from the mutual effect of an electric field and of tangential motion of two phases with respect to each other. If an applied field is directed along the phase boundary, one phase moves relative to the other phase; and conversely, motion along the charge phase boundary creates an electric potential. Small Charged particles suspended in a medium move (electrophoresis) when a potential gradient is applied; or if the solid is stationary, the effect of moving the medium past the interface is to generate a potential difference (streaming potential) (Shaw 1980, Ross and Morrison 1988).

2.4.6. Computing Zeta Potential from Electrophoretic Mobilities

Three basic equations are largely used to compute zeta potentials from electrokinetic measurements:

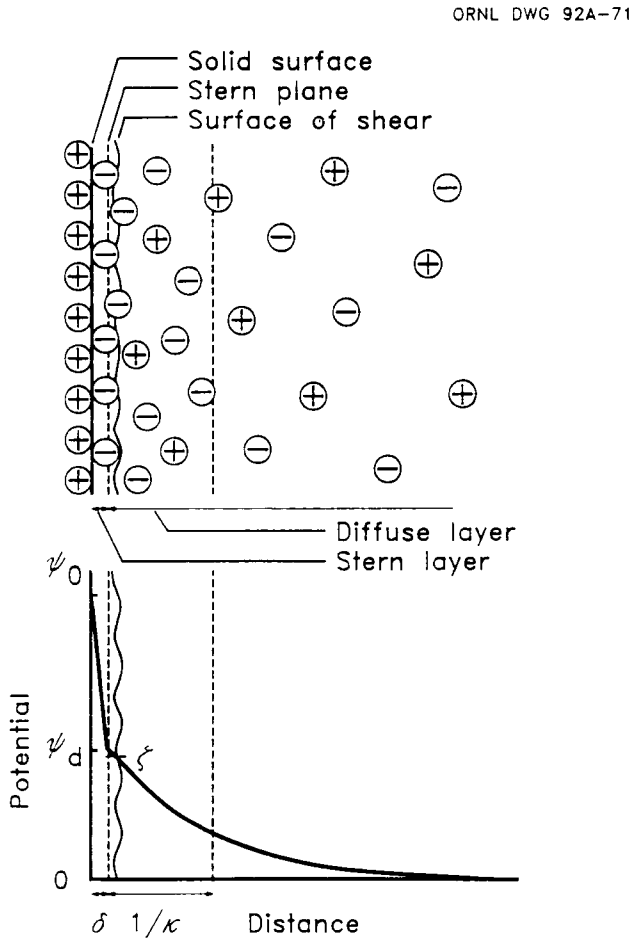



Fig. 2.7 Schematic depicting Stern potential, $\psi_d$, zeta potential, $\zeta$, and surface potential, $\psi_o$ (Shaw 1980).

1. Huckel Equation (small $\kappa$a) - The derivation of equation assumes that a spherical particle is small enough to be treated as a point charge ($\kappa a \ll 1$; but large enough to obey Stokes law. Electrical forces are then equated to the frictional resistance of the medium;

$$Q_E \mathbf{E} = 6\pi\eta\nu_E, \tag{2.44}$$

or

$$u_E = \frac{Q_E}{6\pi\eta a}. \tag{2.45}$$

where

$$\begin{aligned} u_E &= \frac{\nu_E}{\mathbf{E}} - \text{electrophoretic mobility,} \\ Q_E &= \text{net charge on the particle,} \\ \eta &= \text{viscosity of the fluid and} \\ a &= \text{radius of the particle.} \end{aligned}$$

By definition, the zeta potential is the resultant potential at the surface of shear due to the charges $+Q_E$ of the electrokinetic unit and $-Q_E$ of the mobile part of the double layer. The resulting equation is

$$\varsigma = \frac{Q_E}{4\pi\epsilon a(1+\kappa a)}. \tag{2.46}$$

Substituting Eq. 2.45 into Eq. 2.46 and considering $\kappa a \ll 1$, the resulting equation relates zeta potential to the electrophoretic mobility,

$$u_E = \frac{\zeta \epsilon}{1.5\eta}. \tag{2.47}$$

As stated by Shaw (1980), the Huckel equation is probably not applicable to particle electrophoresis in aqueous media; however, it does have possible applicability to electrophoresis in non-aqueous media of low conductance.

2. Smoluchowski equation (large $\kappa a$) – If, when an electric field is applied, liquid is moving in the diffuse part of the double layer relative to that of a non-conducting flat surface, each layer of liquid will rapidly attain a uniform velocity relative and parallel to the surface, with electrical and viscous forces balanced. Thus, Smoluchowski derives an equation which

shows that the electrophoretic mobility is related to the zeta potential by the following equation:

$$u_E = \frac{\zeta \epsilon}{\eta}. \tag{2.48}$$

It is interesting to note that this equation shows that the size of a nonconducting particle has no effect on the electrophoretic mobility.

3. Henry equation – In deriving Henry's equation, the following assumptions were made: (a) Debye-Huckel approximation is made. (b) Applied electric field and the field of the electric double layer are assumed to be simply superimposed. (c) $\epsilon$ and $\eta$ are assumed to be constant throughout the mobile part of the double layer. The following general electrophoretic mobility equation was derived by Henry for conducting and nonconducting spheres:

$$u_E = \frac{\zeta\epsilon}{1.5\eta}[1 + \mathrm{F}(\kappa a)] \tag{2.49}$$

where F($\kappa$a) varies between zero for small values of $\kappa a$ and 1.0 for large values of $\kappa a$, and $\lambda = \dfrac{(k_o - k_1)}{(2k_o + k_1)}$, where $k_o$ is the conductivity of the bulk electrolyte solution and $k_1$ is the conductivity of the particles.

### 2.4.7. Classical Light Scattering - Particle Number Concentration

Another important quantity that is useful in analyzing controlled homogeneous precipitation is the particle number concentration as a function of time. The particle number concentration, $N$, is the number of particles per unit volume of solution. In the case of controlled homogeneous precipitation, this quantity would be expected to remain constant after the initial stage of nuclei formation.

Both classical light scattering (CLS) and DLS were applied to monitor $N$ as a function of time. With CLS, the extinction coefficient is measured by observing the power, $P$, of a light source as seen through a container with scattering particles. If $P_o$ is the intensity of the same light source seen through

the same container without scattering particles, the ratio of $P/P_o$ is given by

$$\frac{P}{P_o} = \exp(-\tau_E l) \ , \tag{2.50}$$

where

$\tau_E = NQ_{sca}\pi r^2 =$ extinction coefficient, $cm^{-1}$;

$N =$ particle density, particles/cm$^3$;

$Q_{sca} =$ scattering efficiency;

$r =$ particle radius, cm; and

$l =$ path length through the particulate medium, cm.

The scattering efficiency, $Q_{sca}$, is a function of $x$ and $m$, which are defined as:

$$x = \frac{2\pi r}{\lambda} \tag{2.51}$$

and

$$m = \frac{n_p}{n_s} \ , \tag{2.52}$$

where

$\lambda =$ wavelength of light, cm;

$n_p =$ refractive index of particle; and

$n_s =$ refractive index of solvent.

The following equation for nonabsorbing spheres is derived from Mie theory (Van de Hulst 1957) for $m$ close to one and $x$ ranging from 0 to 200:

$$Q_{sca} = 2 - \frac{4}{\rho_s} \sin \rho_s + \frac{4}{\rho_s^2}(1 - \cos \rho_s) \ , \tag{2.53}$$

where $\rho_s = 2x|m-1|$.

If it is assumed that the refractive index of the particles remains constant during growth, $Q_{sca}$ is easily calculated by Eq. 2.53 and the average particle sizes that are obtained by DLS. After $Q_{sca}$ has been determined, the particle concentration, $N$, is computed by Eq. 2.50. Since large particles scatter considerably more than smaller particles, $N$ will be weighted more toward the concentration of the larger particles.

### 2.4.8. QELS - Particle Size and Size Distribution

The scattered light from a dilute colloidal suspension in a transparent liquid is related to the physical properties that cause the fluctuations of the solution and the scattering disposition. The physical phenomenon governing the behavior of dilute colloidal suspensions is Brownian motion. Brownian motion can be observed in particles that are relatively large (diameter = 1 $\mu$m) on the molecular scale (Cosignoni et al. 1974, Chu 1974, and Berne and Pecora 1976).

Brownian motion of a free particle (i.e., no applied force field) is described by the Langevin equation (Chandrasekar 1943):

$$\frac{d\overline{u}}{dt} = -\beta\overline{u} + \overline{A}(t) \ , \tag{2.54}$$

where

$\overline{u}$ = particle velocity vector ,

$t$ = time,

$\beta$ = coefficient of dynamic friction,

$\overline{A}(t)$ = fluctuating influence of molecular collision process.

For a spherical particle, the coefficient of dynamic friction is given by Stokes' Law:

$$\beta = \frac{6\pi a\eta}{m} \ , \tag{2.55}$$

where

$a =$ particle radius,

$\eta =$ fluid viscosity,

$m_p =$ mass of particle.

A detailed theoretical formulation of the solution to the Langevin equation and how it is used in relating the particle motion to light signal fluctuations is given elsewhere Crosignoni et al. 1974). This derivation yields the following equation for the autocorrelation of the random light signal fluctuations that are generated by the Brownian motion of a system of monodispersed colloidal particles:

$$A_s^* \approx \exp(-q^2 Dt) = \exp(-t/\tau_c) \ , \tag{2.56}$$

where

$$A_s^* = \text{ normalized autocorrelation function,}$$

$$q = |\overline{q}| = \frac{4\pi n_m \sin(\theta/2)}{\lambda_i},$$

$$n_m = \text{ refractive index of medium ,}$$

$$\theta = \text{scattering angle ,}$$

$$\lambda = \text{ wavelength of incident light ,}$$

$$D = \text{ diffusion coefficient , } = \frac{kT}{6\pi a\eta},$$

$$k = \text{Boltzmann constant,}$$

$$T = \text{absolute temperature, K ,}$$

$$\tau_c = \text{ characteristic decay time } = (q^2 D)^{-1}.$$

For polydispersed systems, the following equation is given (4):

$$A_s^* = K \int_{r=0}^{r=\infty} \left[ f(r) P(q,r) r^6 \exp(-t/\tau_i) \right] dr \ , \qquad (2.57)$$

where

$$r = \text{ particle radius,}$$

$$f(r) = \text{ normalized distribution of particle size,}$$

$$P(q,r) = \text{ Mie scattering factor, } P \approx 1 \text{ for } r \ll \lambda \ ,$$

$$\tau_i = \text{ decay time for } r = r_i.$$

The exact solution requires inversion of this equation to yield $f(r)$ directly. This is very difficult to do accurately for complex signals; however, significant improvement has been made in the development of computer algorithms to deconvolute this integral (Provencher 1979). The $r^6$ dependence of the scattering

power indicates that large particles are more easily detected than small ones. The cumulants method is a widely used technique for detecting polydispersity (Brown and Pusey 1975, Bargeron 1974 and Koppel 1972). This analysis leads to the following approximation for the autocorrelation function:

$$\begin{aligned} \ln(A_s^*) &= -\overline{\Gamma}t + \frac{\mu_2 t^2}{2!} - \frac{\mu_3 t^3}{3!} + \ \ldots \\ &= -\overline{\Gamma}t + \frac{1}{2!}\frac{\mu_2}{\overline{\Gamma}^2}(\overline{\Gamma}t)^2 - \frac{1}{3!}\frac{\mu_3}{\overline{\Gamma}^3}(\overline{\Gamma}t)^3 + \ \ldots \end{aligned} \tag{2.58}$$

The form of $\ln(A_s^*)$ is a polynomial in $t$ with the coefficients representing different properties of the line-width distribution. The linear and quadratic terms, which are the most significant, are readily measured in most experiments. The linear term is the average line-width, $\overline{\Gamma}$, as defined in Eq. (2.58). Since the scattering power of individual particles is skewed heavily toward large particles [Eq. (2.57)], this "average" $\Gamma$ will result in "average" diameters weighted toward the largest species.

The second moment ($\mu_2$) normalized by the square of the average linewidth ($\mu_2/\overline{\Gamma}^2$) is termed the polydispersity parameter. For a perfect monodisperse suspension, $\mu_2/\overline{\Gamma}^2 = 0$. In practice, values of $\mu_2/\overline{\Gamma}^2$ less than 0.1 are taken as an indication of a narrow distribution.

It is readily apparent that a quadratic regression analysis of $\ln[A_s^*(t)]$ vs $t$ will provide estimates of $\overline{\Gamma}$ and $\mu_2/\overline{\Gamma}^2$. Using the following equation [Eq. (2.59)] which relates the diffusion coefficient to the average line-width and the Stokes-Einstein relation [Eq. (2.6)], we obtain the particle diameter directly:

$$D = \frac{\overline{\Gamma}}{q^2} \tag{2.59}$$

and

$$d_p = \frac{kt}{3\pi\eta D}. \tag{2.60}$$

This relationship, which is widely used, forms the basis for the size analysis in our current work. In particular, it permits measurements of particle size and allows estimation of polydispersity in dilute solutions. Some care must be taken, however, when using QELS to measure the particle size in electrostatically stabilized colloidal dispersions where interparticle forces can greatly reduce the self-diffusion of colloidal particle; thus, resulting in apparent particle sizes that are larger than the actual particle size. The effect of the interparticle forces on the self diffusion coefficient can be evaluated by extensive experimental studies or by Brownian dynamic computer simulations.

## 2.5. Results and Discussion

### 2.5.1. Hydrolysis Reaction

#### 2.5.1.1. Hydrolysis reaction-dilute TEOS solutions

In evaluating chemical kinetics, Eqs. 2.1 and 2.2 are the proposed mechanisms for the synthesis of silica from TEOS. As is shown by Eq. 2.1, the kinetics of the hydrolysis reaction can be obtained by observing the rate of ethanol production (assuming complete hydrolysis and no ester exchange). These assumptions are most probably correct when the base–catalyzed reaction is conducted in the presence of excess water and with dilute TEOS solutions. In the dilute

studies, the molar ratio of excess water to alkoxide ranges from ≈200 to 400. Fig. 2.8 shows a plot of the $[TEOS]$ versus time data for the hydrolysis of TEOS in 1-propanol, 2-propanol, 1-butanol, 2-butanol, tert-butyl alcohol and tert-amyl alcohol. The initial concentrations of $[TEOS]_o$, $[H_2O]_o$ and $[NH_3]_o$ were 0.014, 6.0 and 0.7M, respectively.

The effect of temperature on the rate of TEOS hydrolysis in tert- butyl alcohol is shown in Fig. 2.9.

Similar results were obtained in other alcohols. An Arrenhnius plot of the rate constants is shown in Fig. 2.10.

The activation energies for the hydrolysis reaction ranged from 3.5 kcal/mol to 6.9 kcal/mol. The low activation energies are characteristic of homogeneous-catalytic reactions.

2.5.1.2. Hydrolysis reaction-concentrated TEOS solutions

As stated previously, Matsoukas and Gulari (1988) Raman spectroscopy can be used to study the hydrolysis of TEOS in ethanol. Fig. 2.11 shows typical Raman spectra that are used to determine the rate of TEOS hydrolysis in ethanol.

The initial TEOS concentration was 1.0 M TEOS. The concentration of TEOS was determined by the area under the peak at approximately 790 $cm^{-1}$ which decreases with time during the hydrolysis reaction. Gas chromatography was used to study the hydrolysis of TEOS in alcohols other than ethanol. Fig. 2.12 shows the data for the hydrolysis of 1M TEOS in various alcohols. This log[TEOS] versus time plot curves because the water concentration is reduced

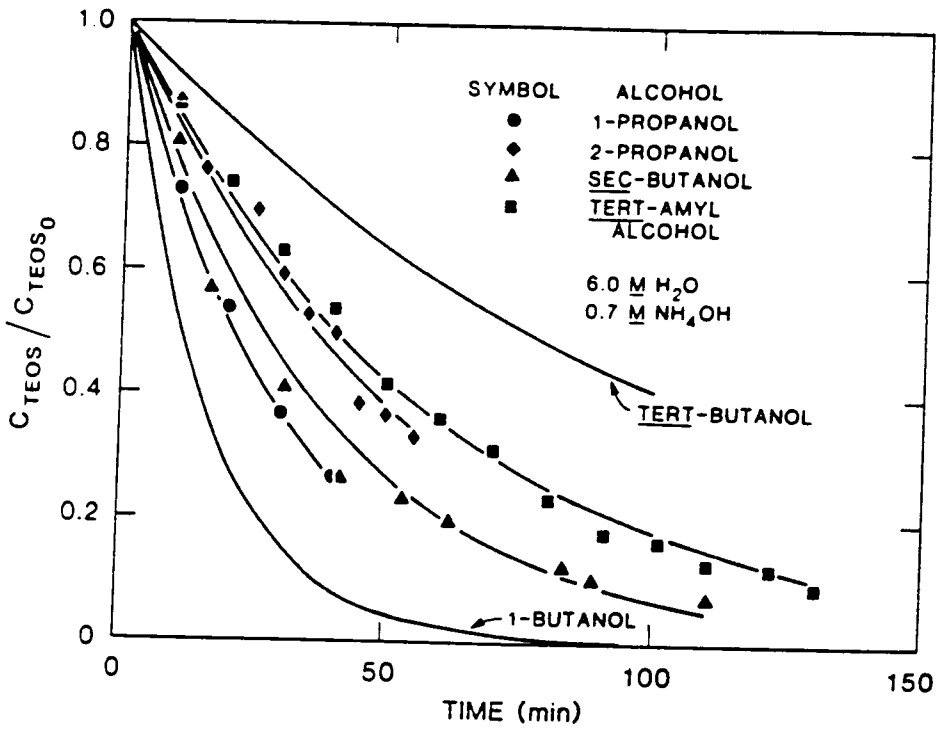



Fig. 2.8 Hydrolysis of 0.014 M TEOS in various alcohols.

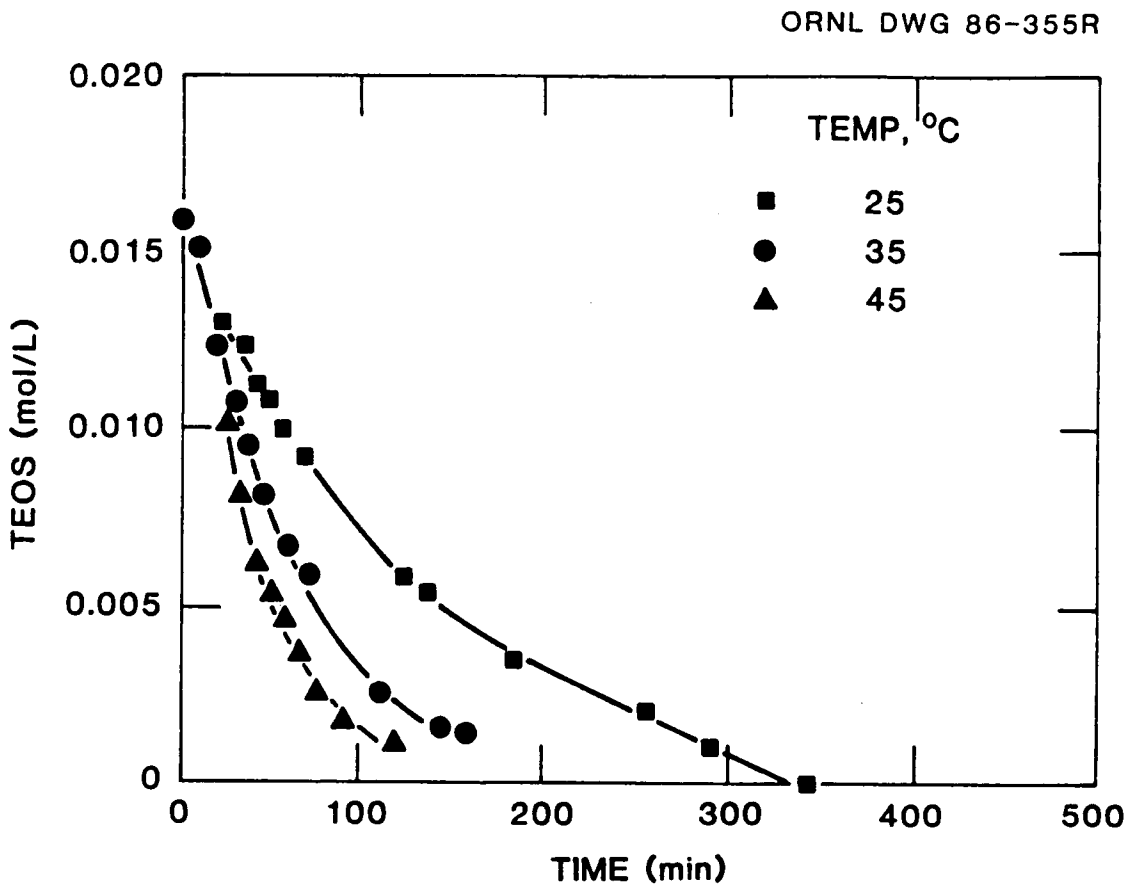



Fig. 2.9 Effect of temperature on the rate of TEOS (0.014M) hydrolysis in tert-butyl alcohol.

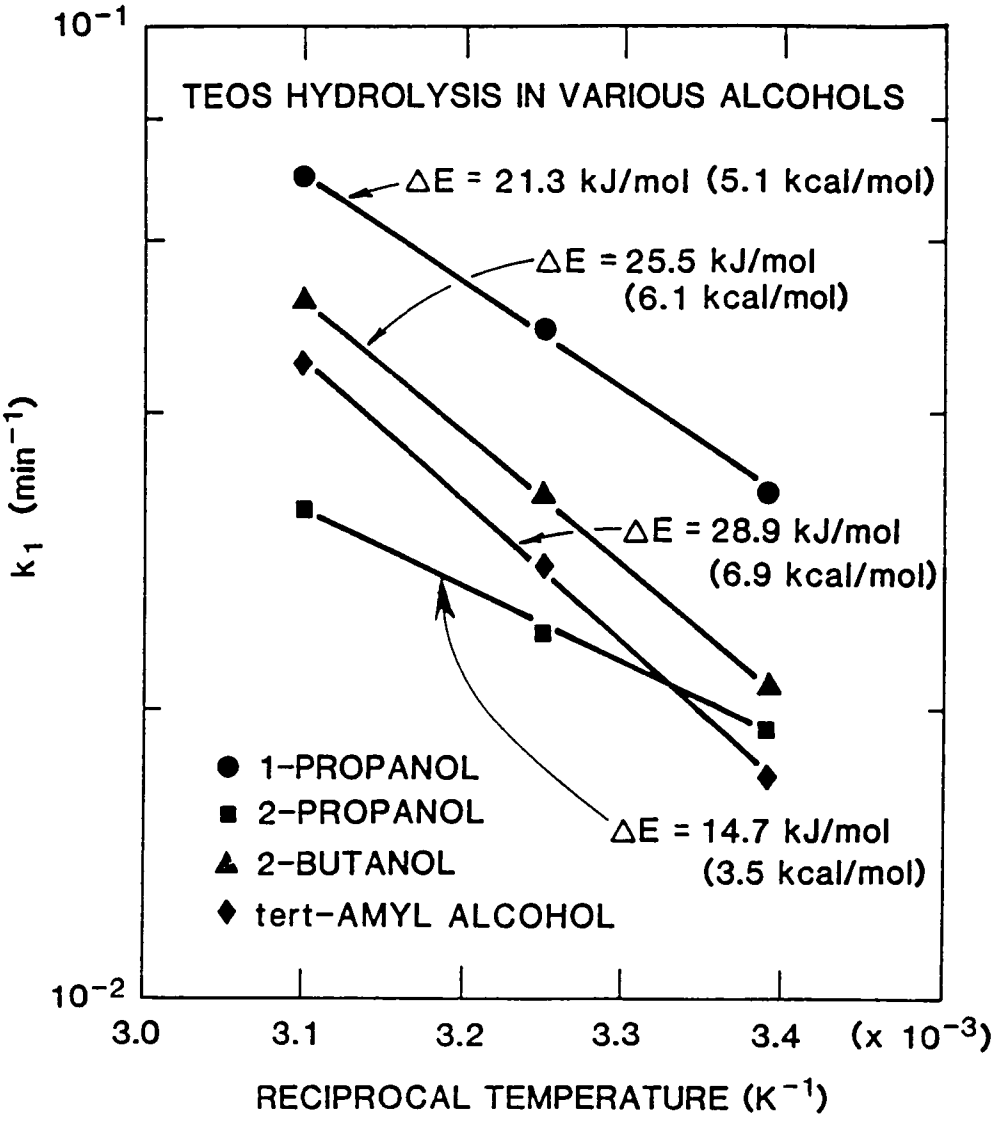



Fig. 2.10 Arrenhnius plot of TEOS hydrolysis rate constant for reaction in various alcohols.

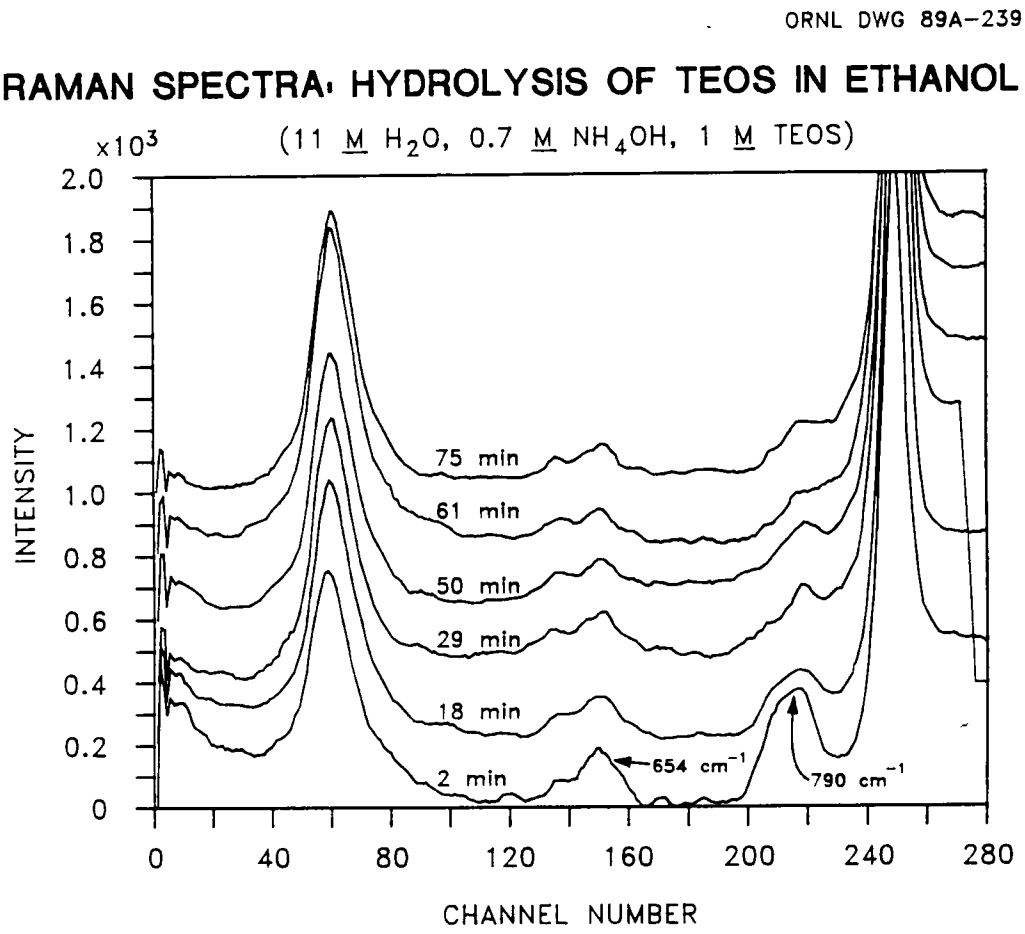



Fig. 2.11 Typical Raman spectra for the hydrolysis of 1.0M TEOS with 11.0M $H_2O$ and 0.7M $NH_3$ in ethanol.

during the hydrolysis reaction. The rate constants that are reported in Table 2.2 are estimated from the initial slope of the curves in Fig. 2.12. These values are in excellent agreement with the values obtained for the dilute studies.

2.5.1.3. Hydrolysis reaction-solvent effects

The solvent effects the rate of hydrolysis in the order 1- butanol > methanol >1-propanol > ethanol ≥ 2-butanol > 2-propanol > tert-amyl alcohol > tert-butyl alcohol (See Table 2.2). Upon further inspection, it is observed from the rate constants in Table 2.2 (Figs. 2.8, 2.9 and 2.12) that, in the case of methanol, ethanol, propanol, and butanol, the rate of hydrolysis initially decreases with an increase in the molecular weight (methanol and ethanol) of the alcohol and subsequently increases with an increase in molecular weight (ethanol, 1-propanol and 1- butanol). This behavior is explained in terms of basicity in alcohols and hydrogen bonding effects. It is known that lower alcohols dissociate in the presence of a base. The degree of dissociation decreases as the molecular weight of the alcohol increases. For a weak base such as ammonia, its basicity follows the order methanol > ethanol > propanol > butanol. Since the hydrolysis reaction is catalyzed by $OH^-$ ions, one would expect the rate of hydrolysis to follow the same order. However, since alcohols form hydrogen bonds, it is likely that the rate of hydrolysis should be inhibited in solvents where hydrogen bonding is greatest. Fig. 2.13 shows the activity of water in various alcohols.

The activity coefficient of water in each solvent may be computed by the following three suffix Margules equations (Reid, Prausnitz, and Sherwood 1977):

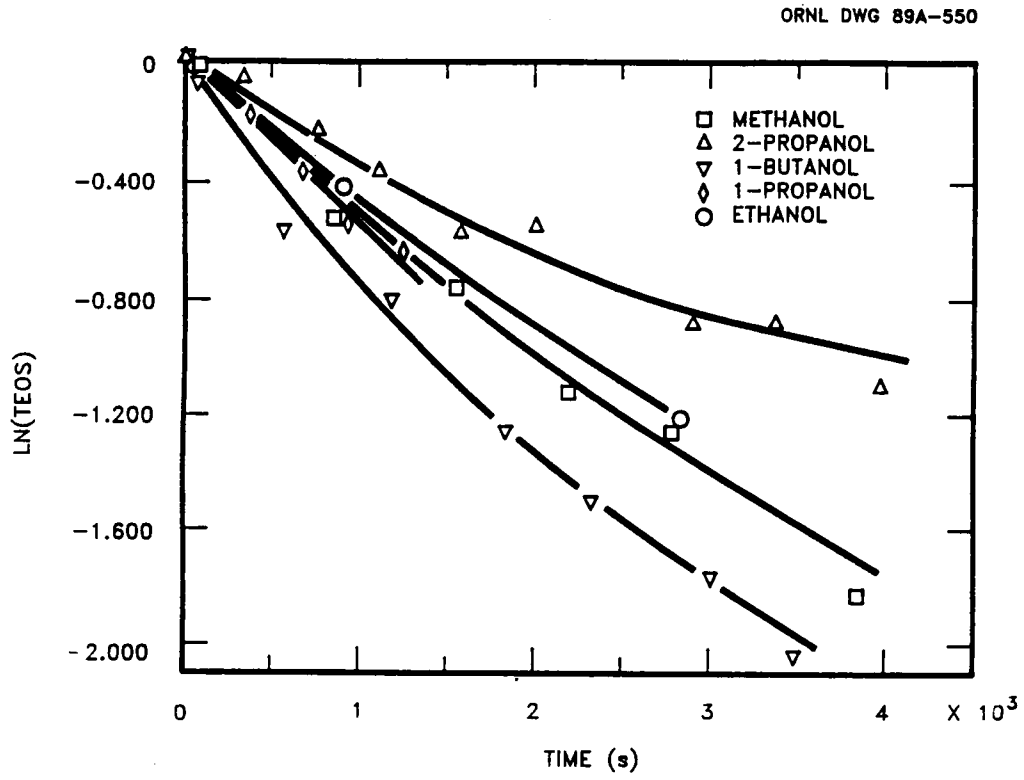



Fig. 2.12 Hydrolysis of concentrated TEOS solution in ethanol (1M TEOS, 11M $H_2O$, and 0.7M $NH_3$).

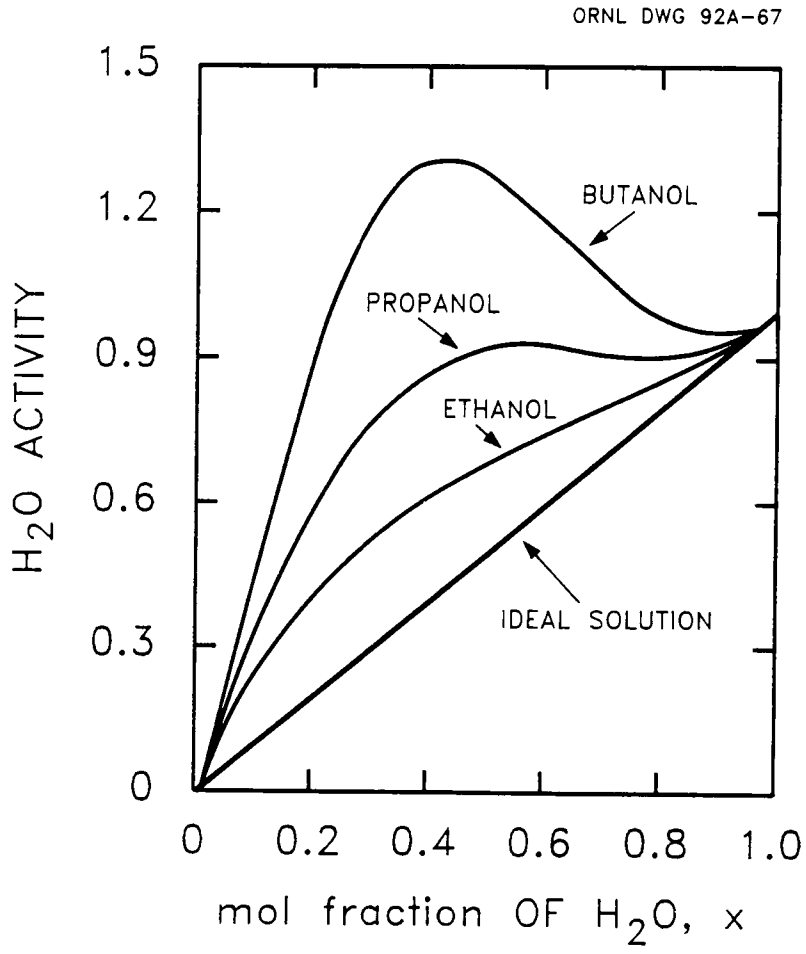



Fig. 2.13 Activity of water in water-aliphatic alcohol mixtures.

$$\ln \gamma_1 = \left[A_{12} + 2\left(A_{21} - A_{12}\right) x_1\right] x_2^2 \,, \tag{2.61}$$

$$\ln \gamma_2 = \left[A_{21} + 2\left(A_{12} - A_{21}\right) x_2\right] x_1^2 \,, \tag{2.62}$$

where

$A_{12} = \ln \gamma_1^{\infty}$,

$A_{21} = \ln \gamma_2^{\infty}$,

$\gamma_i =$ activity coefficient of component i,

$x_i =$ mol fraction of component i, and

$\gamma_i^{\infty} =$ activity coefficient of component i at infinite dilution.

The activity coefficients at infinite dilutions, $\gamma_i^{\infty}$, are estimated by an extensive correlation given by Reid, Prausnitz, and Sherwood (1977). For a homologous series of normal alcohols, the correlation is as follows:

$$\log \gamma_1^{\infty} = \alpha + \epsilon N_1 + \frac{\varsigma}{N_1} + \frac{\theta}{N_2} \,, \tag{2.63}$$

where

$\alpha$, $\epsilon$, $\varsigma$, and $\theta =$ constants,

$N_1 =$ number of carbons in component 1, and

$N_2 =$ number of carbons in component 2.

For water in a homologous series of normal alcohols at 25 °C, this equation reduces to

Table 2.2. Hydrolysis rate constant for TEOS hydrolysis in various alcohols

| Solvent | [TEOS] mol/L | [$H_2O$] mol/L | [$NH_3$] mol/L | $K_H$ $(L/mol)^{2.4}s^{-1}$ | Temp. °C |
|---|---|---|---|---|---|
| methanol | 1.0 | 6.0 | 0.7 | $6.0\times10^{-5}$ | 22 |
| ethanol | 1.0 | 6.0 | 0.7 | $4.2\times10^{-5}$ | 22 |
| ethanol | 1.0 | 11.0 | 0.7 | $4.2\times10^{-5}$ | 22 |
| 1-propanol | 0.014 | 6.0 | 0.7 | $5.2\times10^{-5}$ | 22 |
| 1-propanol | 0.014 | 6.0 | 0.25 | $5.1\times10^{-5}$ | 22 |
| 1-propanol | 0.014 | 3.0 | 0.7 | $4.2\times10^{-5}$ | 22 |
| 1-propanol | 0.014 | 6.0 | 0.7 | $7.3\times10^{-5}$ | 35 |
| 1-propanol | 0.014 | 6.0 | 0.7 | $1.1\times10^{-4}$ | 50 |
| 1-propanol | 0.05 | 6.0 | 0.7 | $5.5\times10^{-5}$ | 22 |
| 1-propanol | 1.0 | 6.0 | 0.7 | $5.0\times10^{-5}$ | 22 |
| 2-propanol | 0.014 | 6.0 | 0.7 | $3.0\times10^{-5}$ | 22 |
| 2-propanol | 0.014 | 6.0 | 0.25 | $2.4\times10^{-5}$ | 22 |
| 2-propanol | 0.014 | 3.0 | 0.7 | $2.4\times10^{-5}$ | 22 |
| 2-propanol | 0.014 | 6.0 | 0.7 | $2.9\times10^{-5}$ | 22 |
| 2-propanol | 0.014 | 6.0 | 0.7 | $3.8\times10^{-5}$ | 35 |
| 2-propanol | 0.014 | 6.0 | 0.7 | $5.0\times10^{-5}$ | 50 |
| 2-propanol | 0.05 | 6.0 | 0.7 | $3.0\times10^{-5}$ | 22 |
| 2-propanol | 1.0 | 6.0 | 0.7 | $3.2\times10^{-5}$ | 22 |

Table 2.2. Hydrolysis rate constant for TEOS hydrolysis in various alcohols (cont.)

| Solvent | [TEOS] mol/L | [$H_2O$] mol/L | [$NH_3$] mol/L | $K_H$ $(L/mol)^{2.4}s^{-1}$ | Temp. $^oC$ |
|---|---|---|---|---|---|
| 1-butanol | 0.014 | 6.0 | 0.7 | $9.7\times10^{-5}$ | 22 |
| 1-butanol | 0.05 | 6.0 | 0.7 | $9.7\times10^{-5}$ | 22 |
| 1-butanol | 1.0 | 6.0 | 0.7 | $9.5\times10^{-5}$ | 22 |
| 2-butanol | 0.014 | 6.0 | 0.7 | $4.1\times10^{-5}$ | 22 |
| 2-butanol | 0.014 | 6.0 | 0.7 | $5.2\times10^{-5}$ | 35 |
| 2-butanol | 0.014 | 6.0 | 0.7 | $8.1\times10^{-5}$ | 50 |
| 2-butanol | 0.014 | 6.0 | 0.25 | $4.3\times10^{-5}$ | 22 |
| 2-butanol | 0.014 | 3.0 | 0.7 | $4.0\times10^{-5}$ | 22 |
| tert-butyl alcohol | 0.014 | 6.0 | 0.7 | $2.0\times10^{-5}$ | 25 |
| tert-amyl alcohol | 0.014 | 6.0 | 0.7 | $2.7\times10^{-5}$ | 22 |
| | 0.014 | 6.0 | 0.7 | $4.4\times10^{-5}$ | 35 |
| tert-amyl alcohol | 0.014 | 6.0 | 0.7 | $7.0\times10^{-5}$ | 50 |

$$\log \gamma_1^{\infty} = 0.760 - \frac{0.630}{N_2} \ . \tag{2.64}$$

Since higher activity coefficients indicate less hydrogen bonding, the hydrolysis reaction is expected to be faster in 1- butanol if hydrogen bonding effects are significant. To test if hydrogen bonding is important, the following equation is used

$$\frac{k_{H \text{ alcohol}}}{k_{H \text{ 1-propanol}}} = \left( \frac{a_{H_2O}^{alcohol}}{a_{H_2O}^{1-propanol}} \right)^{1.5} \tag{2.65}$$

Table 2.3 summarizes the comparison between the ratio of the hydrolysis rate constants and the activity coefficients. Eq. 2.65 holds for butanol; however, it becomes increasingly worse for ethanol and methanol where the rate constants are greater than what would be expected if hydrogen bonding was inhibiting the reaction. The increased rates of hydrolysis in ethanol and methanol is postulated as being due to an increase in the strength of ammonia as a base catalyst in these solvents. Table 2.4 shows the autoprotolysis constants (ionic product: $pK_s$) for water, methanol, ethanol and propanol; and $pK_A$ and $pK_B$ for ammonia (Tremillon 1974). The lower $pK_B$ values indicate a stronger base. Ammonia is slightly more basic in ethanol than in propanol; however, it is considerably more basic in methanol than in propanol. Thus, it is possible, as observed, that the rate of hydrolysis in methanol is faster than the rate in either ethanol or propanol.

The rate of hydrolysis also decreases as the alcohol solvent becomes more branched. This is attributed to steric hindrance of the hydrogen bonded water.

Table 2.3. The effect of the activity of water on the hydrolysis rate constant

| Solvent | $K_H$ $(L/mol)^{2.4}s^{-1}$ | $a_{H_2O}$ | $K_H/K_H^*$ | $(a_{H_2O}/a^*_{H_2O})^{1.5}$ |
|---|---|---|---|---|
| methanol | $6.0\times10^{-5}$ | 0.264 | 1.24 | 0.18 |
| ethanol | $4.2\times10^{-5}$ | 0.502 | 0.86 | 0.48 |
| 1-propanol | $4.8\times10^{-5}$ | 0.816 | 1.0 | 1.0 |
| 1-butanol | $9.7\times10^{-5}$ | 1.287 | 2.0 | 1.98 |

* – denotes propanol as reference solvent.

Table 2.4. $pK_s$, and $pK_A$ and $pK_B$

| Solvent | $pK_s$ | $pK_A$ | $pK_B$ |
|---|---|---|---|
| water | -14 | -9.25 | -4.8 |
| methanol | -16.7 | -10.8 | -5.9 |
| ethanol | -19.1 | -10.3 | -8.7 |
| 1-propanol | -19.4 | -10 | -9 |

### 2.5.2. Condensation Reaction

Figs. 2.14, 2.15, and 2.16 show the depletion of total soluble silica during the hydrolysis of TEOS ($[TEOS]_o$=0.014M, 0.05M and 1.0M, respectively) in various alcohols.

The rate of the condensation reaction follows the sequence 1-butanol > methanol > 1-propanol > ethanol > 2-propanol > tert- butyl alcohol. The similarity between the effect of solvent on the rate of hydrolysis and condensation is because both reactions are catalyzed by $OH^-$ ions.

It has been shown by Makrides, Turner and Slaughter (1980) that the activation energy for the condensation of silicic acid is approximately 17 kcal/mol. This is considerably higher than the activation energy ($\approx$5 kcal/mol) for the hydrolysis rate constant. Therefore, it is expected that the hydrolysis reaction will become the rate limiting step at higher temperatures. Consequently, the independent methods (gas chromatography and molybdate methods) for determining the hydrolysis and condensation kinetics should yield the same kinetic plot. This is shown in Fig. 2.17 for the hydrolysis of TEOS ($[TEOS]_o$=0.014M) in 2-propanol at 50 °C.

The hydrolysis rate constant from the [TEOS] and [TS] data is the same $5.0 \times 10^{-5} s^{-1} (\mathrm{l/mol})^{2.4}$. These data tend to confirm that the gas chromatography and molybdate methods are giving reliable results and assumption of complete hydrolysis before condensation is reasonable.

### 2.5.3. Silicic Acid, Conductivity and pH

One of the main questions in using gas chromatography or Raman spec-

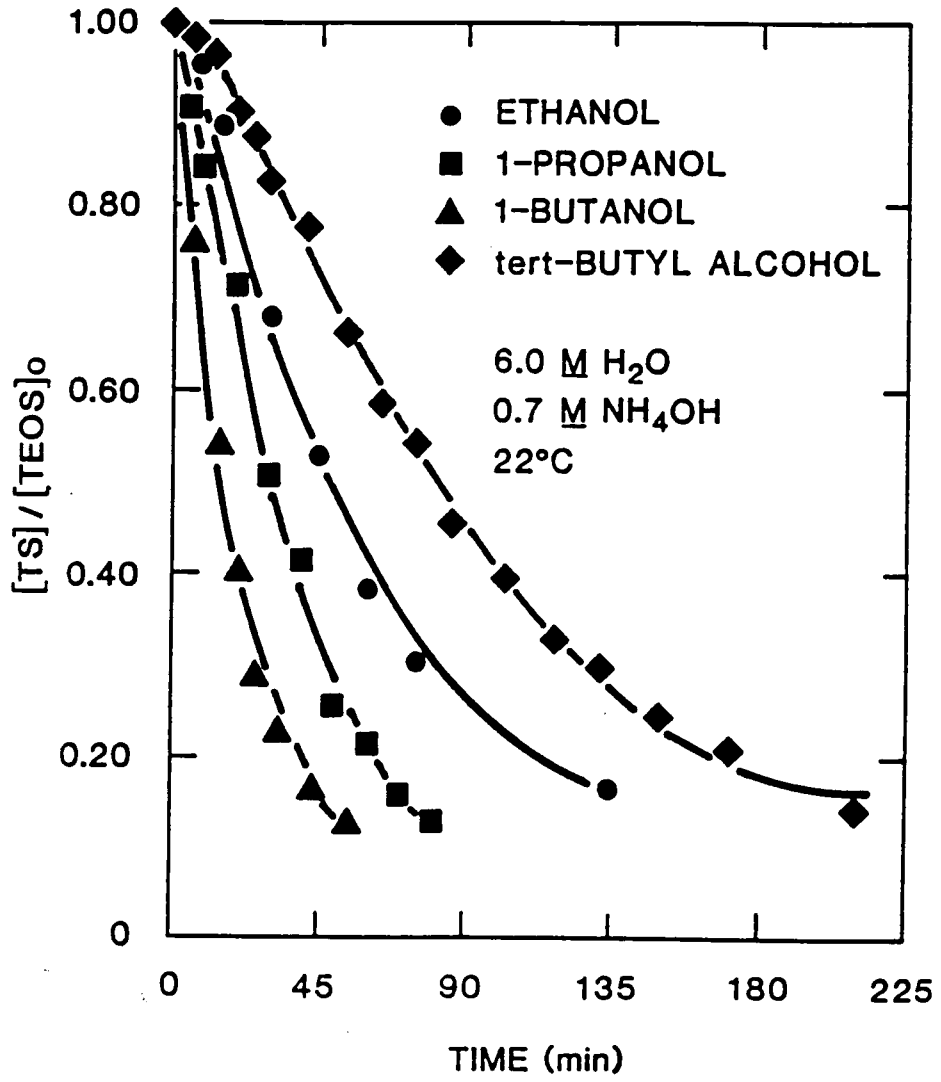



Fig. 2.14 Total soluble silica: TEOS hydrolysis in various alcohols (0.014M TEOS, 6M $H_2O$ and 0.7M $NH_3$).

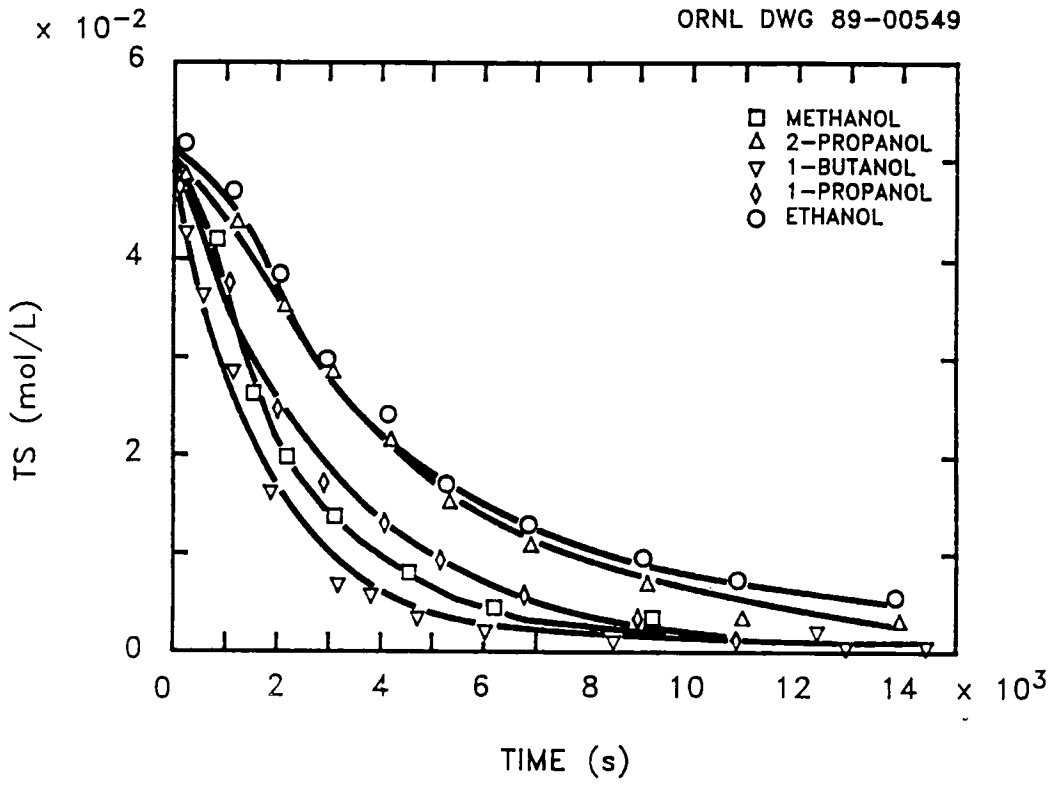



Fig. 2.15 Total soluble silica: TEOS hydrolysis in various alcohols (0.05M TEOS, 6M $H_2O$ and 0.7M $NH_3$).

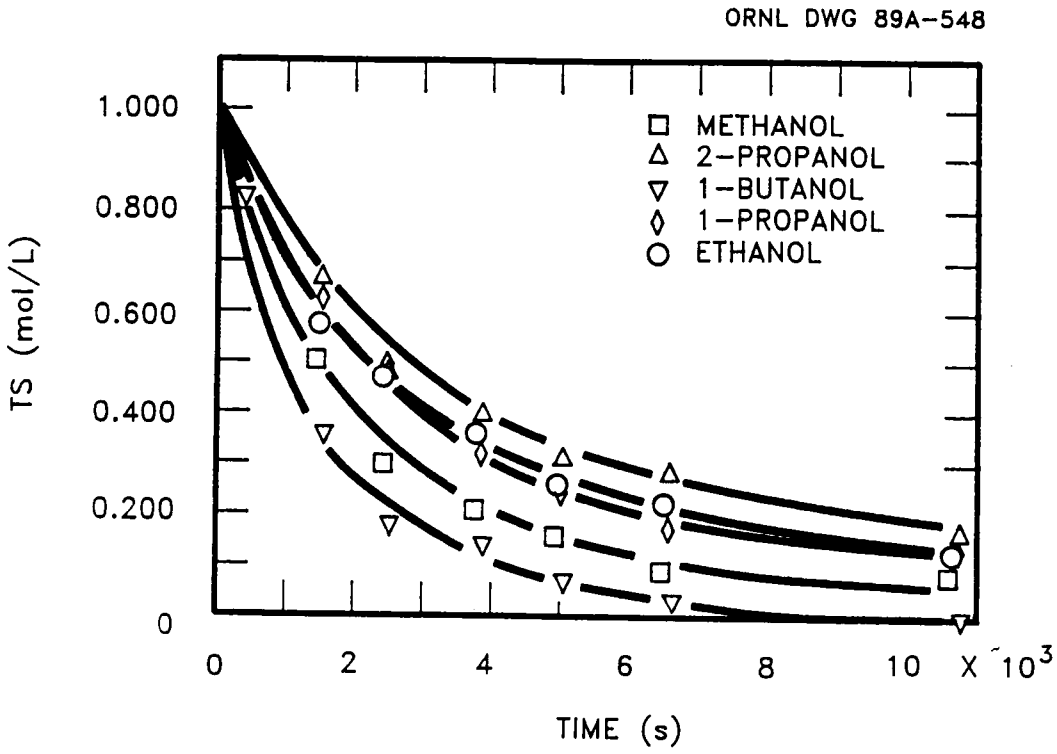



Fig. 2.16 Total soluble silica: TEOS hydrolysis in various alcohols (1.0M TEOS, 6M $H_2O$ and 0.7M $NH_3$).

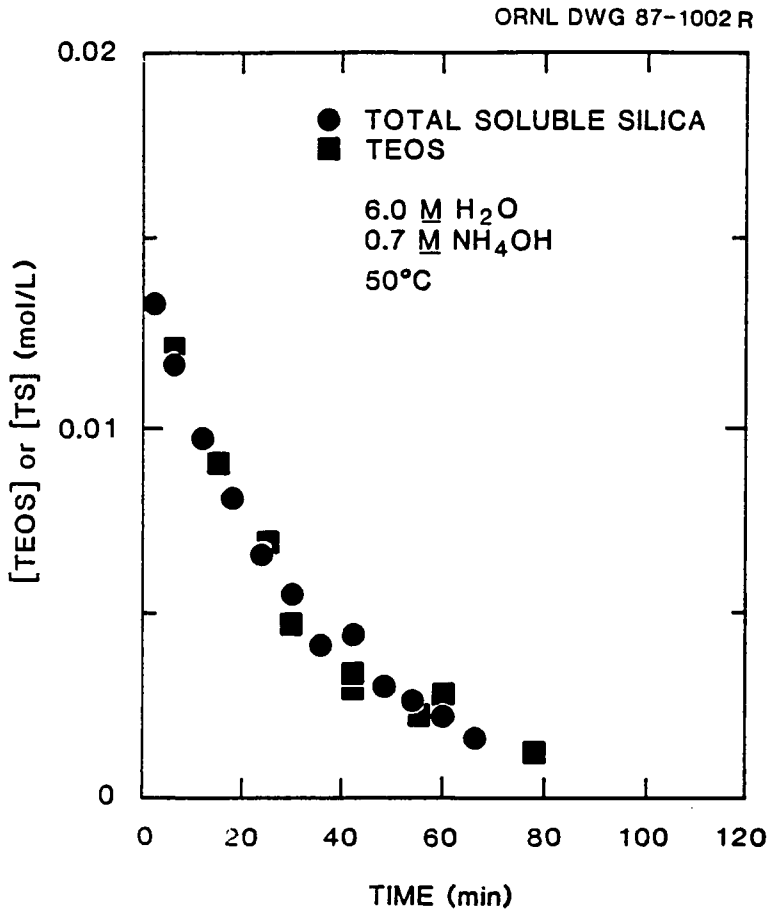



Fig. 2.17 TEOS and Total soluble silica: TEOS hydrolysis in 2-propanol at high temperature (0.014M TEOS, 6M $H_2O$ and 0.7M $NH_3$, 50 °C)

troscopy and the molybdate method to respectively determine the hydrolysis and condensation reaction kinetics is whether the difference between the total soluble silica and TEOS concentrations is large enough to be measurable (Note: $[TS] - [TEOS] = [Si(OH)_4]$). Figs. 2.18 to 2.23 show total soluble silica $[TS]$, and silicic acid concentrations for the hydrolysis of TEOS ($[TEOS]_o$ ranging from 0.014 to 0.3M) in various solvents.

In each plot, the silicic acid qualitatively follows the expected variation of concentration with time. Duplicate runs are shown in Fig. 2.22. There is good agreement between the duplicate runs.

Bogush and Zukoski (1991) have recommended the use of conductivity as an accurate method of determining the presence of $SiOH$ bonds. Therefore, to further check the silicic acid data, the variation in conductivity and pH is compared to the variation in the silicic acid concentration with time. This is shown in Figs. 2.24 to 2.27.

As expected from theory, the silicic acid and conductivity passes through a maximum and subsequently decreases to some equilibrium value. On the other hand, the pH decreases to a minimum value, after which it increases to an equilibrium value.

The behavior of the silicic acid, conductivity data and pH are in accordance with Eqs. 2.7, 2.8, and 2.16. There is an initial build-up of silicic acid as hydrolysis occurs. The silicic acid concentration decreases as condensation occurs. Silicic acid has a neutralization effect (pH decreases) on the ammonia (acid-base reaction) to form ammonium ions and silicate ions. These ions cause the conductivity of the solution to follow the trend of the apparent silicic acid concentration. The dependence of conductivity on silicic acid concentra-

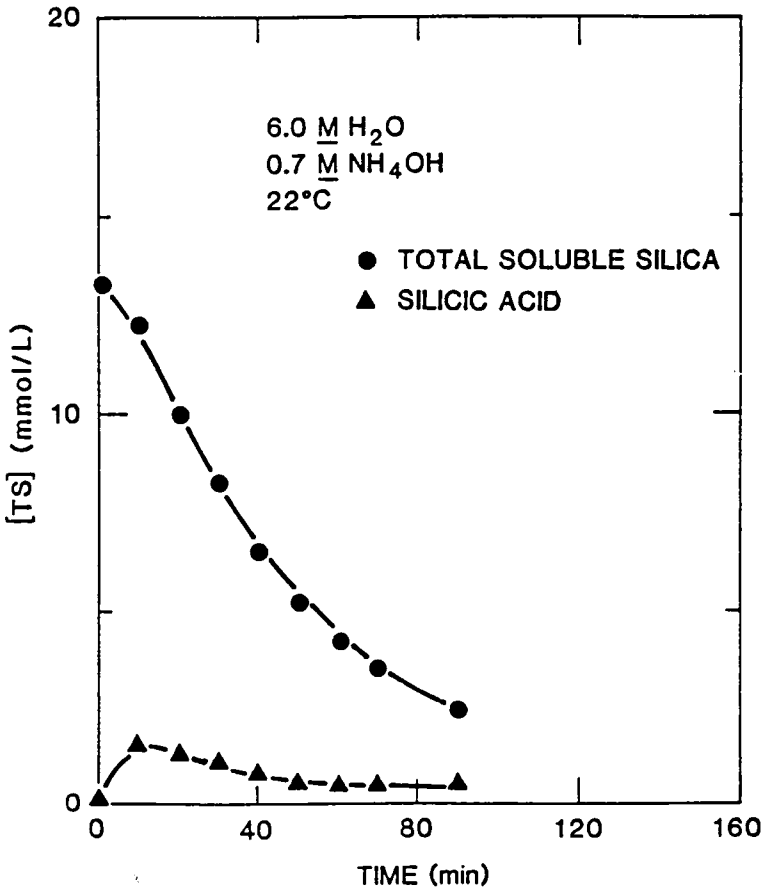



Fig. 2.18 Total soluble silica and silicic acid: TEOS hydrolysis in 2-butanol (0.014M TEOS, 6M $H_2O$, 0.7M $NH_3$, 22 °C).

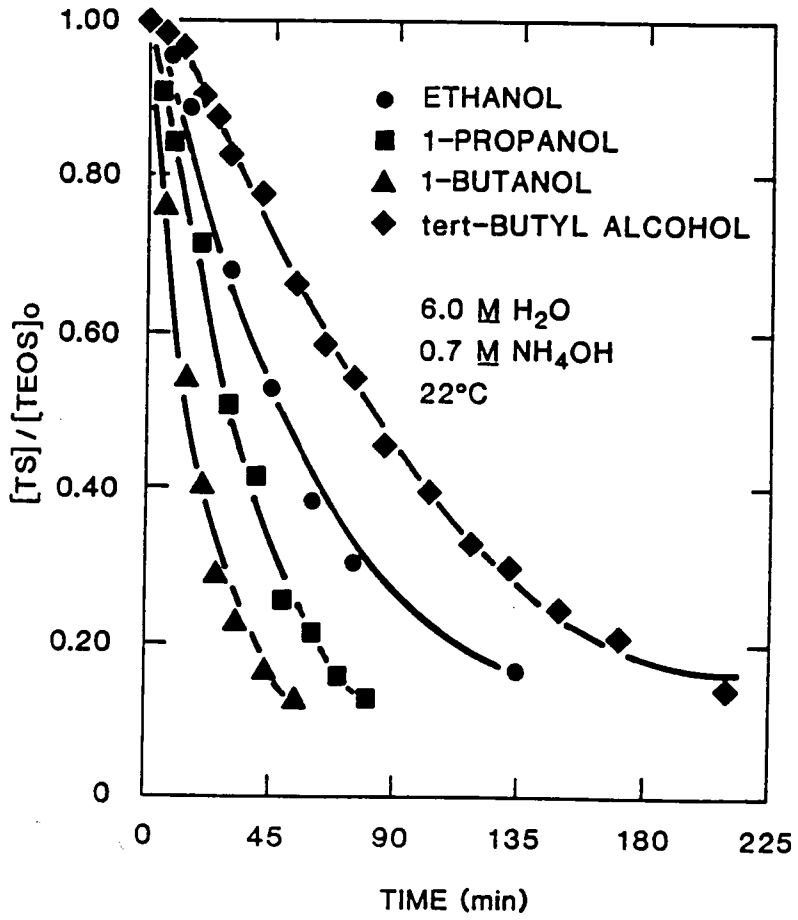



Fig. 2.19 Total soluble silica and silicic acid: TEOS hydrolysis in methanol (0.05M TEOS, 6M $H_2O$, 0.7M $NH_3$, 22 °C).

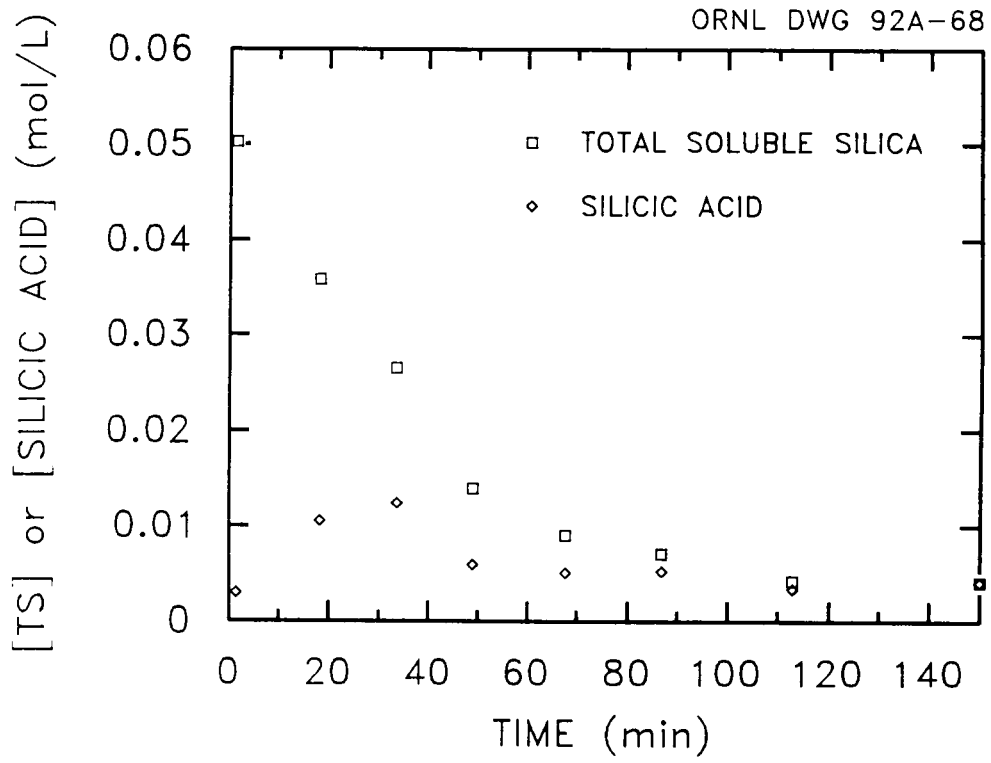



Fig. 2.20 Total soluble silica and silicic acid: TEOS hydrolysis in ethanol (0.05M TEOS, 6M $H_2O$, 0.7M $NH_3$, 22 °C).

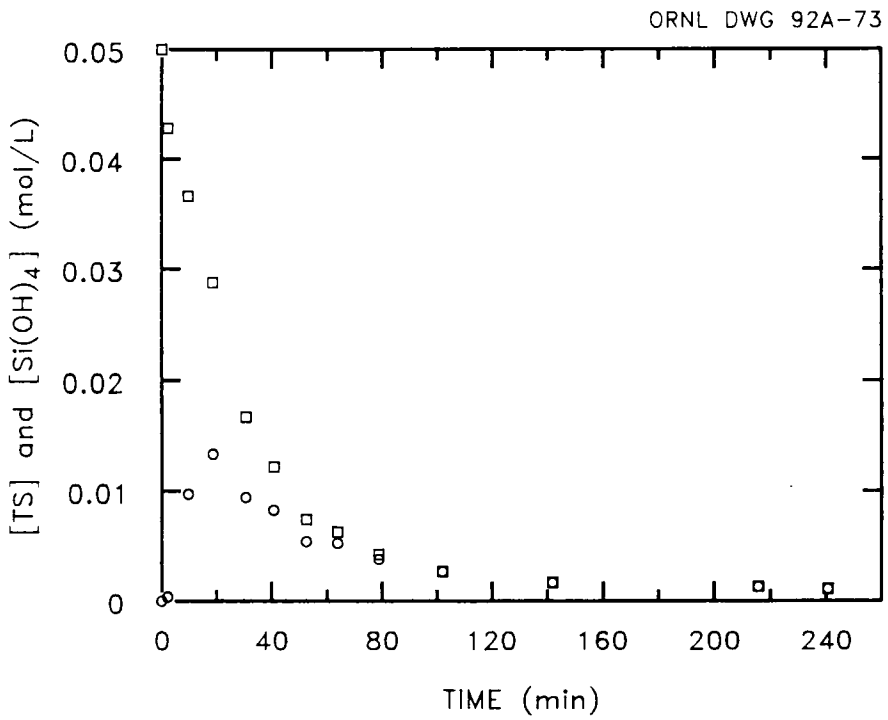



Fig. 2.21 Total soluble silica and silicic acid: TEOS hydrolysis in 1-butanol (0.05M TEOS, 6M $H_2O$, 0.7M $NH_3$, 22 °C).

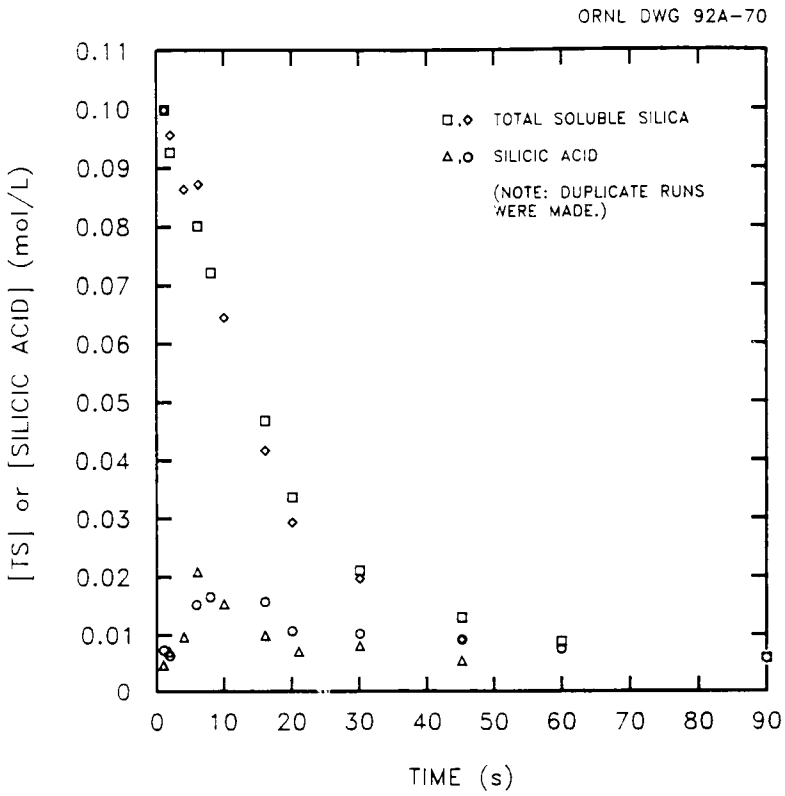



Fig. 2.22 Total soluble silica and silicic acid: TEOS hydrolysis in ethanol (0.1M TEOS, 11.8M $H_2O$, 0.7M $NH_3$, 22 °C).

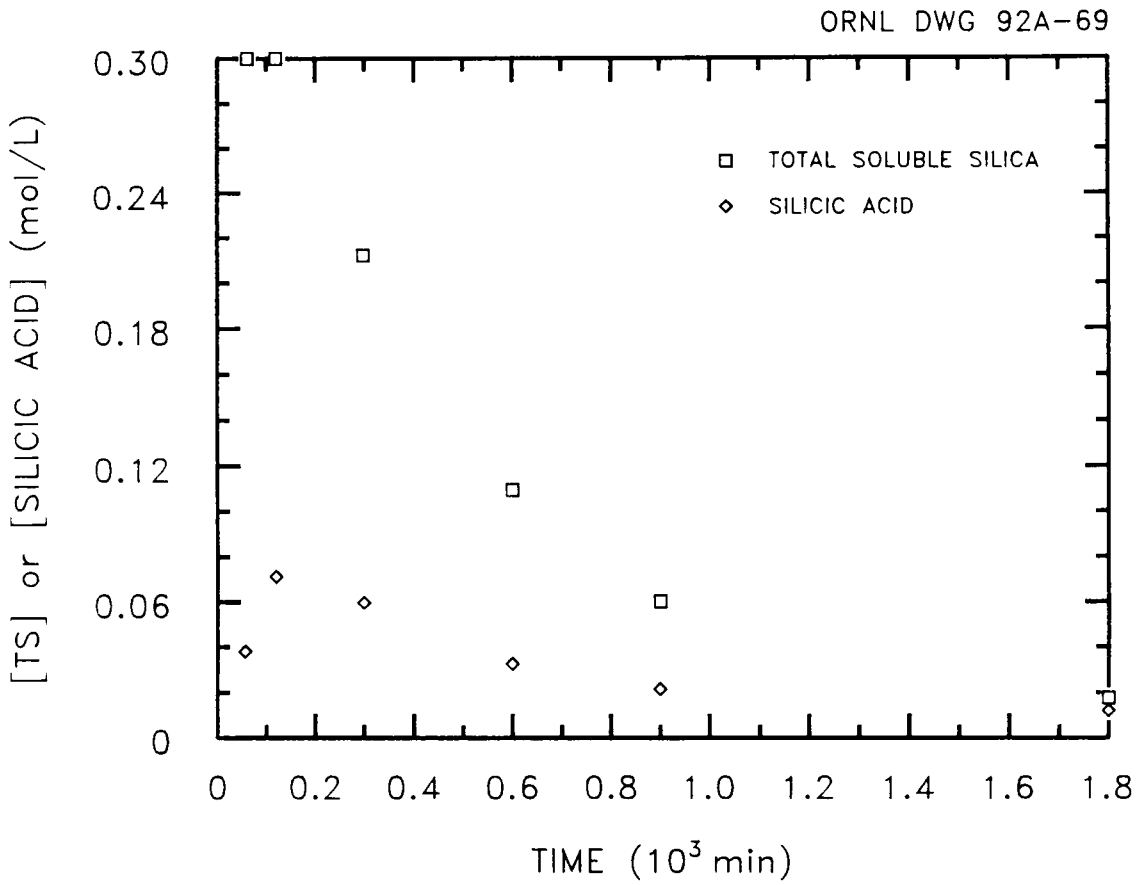



**Fig. 2.23** Total soluble silica and silicic acid: TEOS hydrolysis in ethanol (0.3M TEOS, 11.8M $H_2O$, 1.4M $NH_3$, 22 °C).

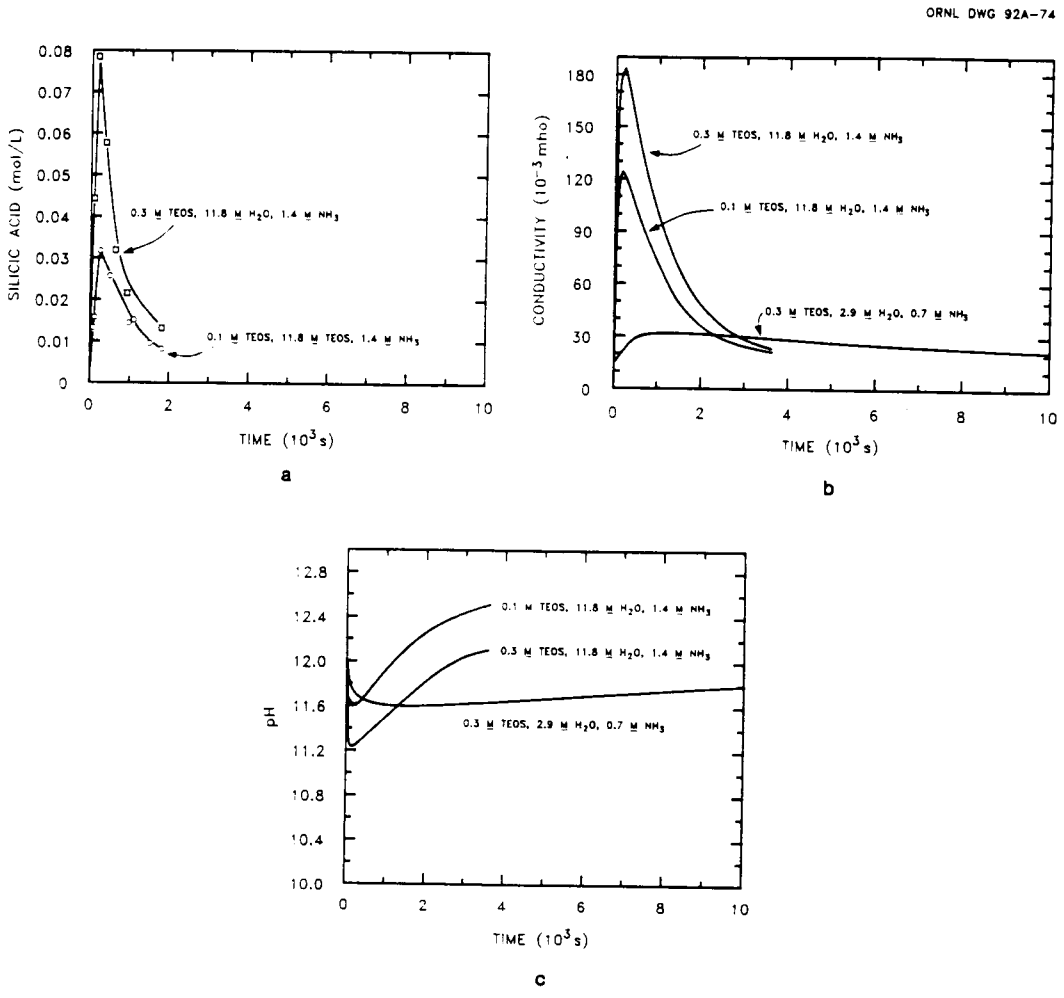



Fig. 2.24 Effect of TEOS concentration, and high and low water and ammonia concentrations: (a) silicic acid, (b) conductivity, (c) pH (0.3M TEOS, 22 °C).

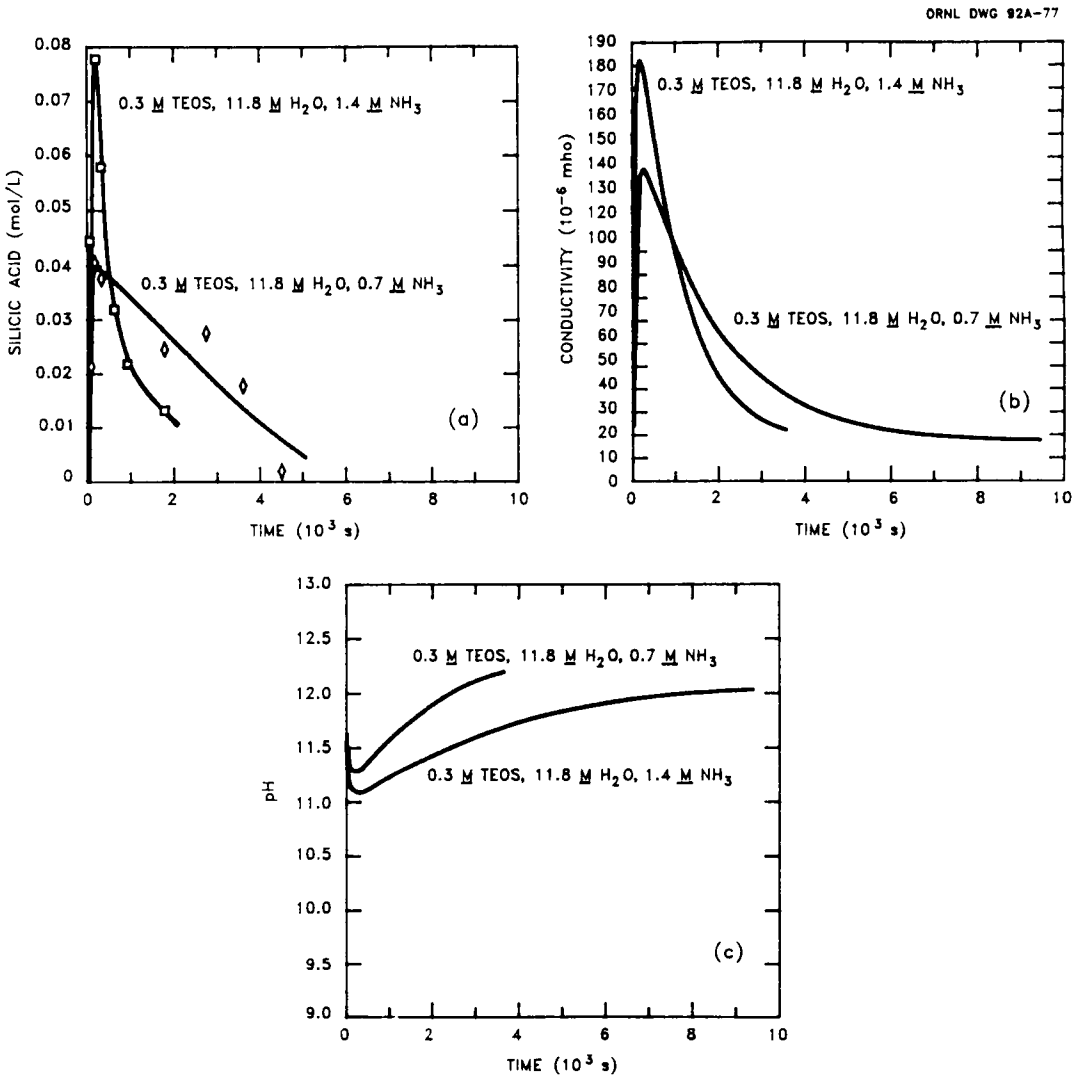



Fig. 2.25 Effect of ammonia concentration: (a) silicic acid, (b) conductivity, (c) pH (0.3M TEOS, 11.8M $H_2O$, 22 °C).

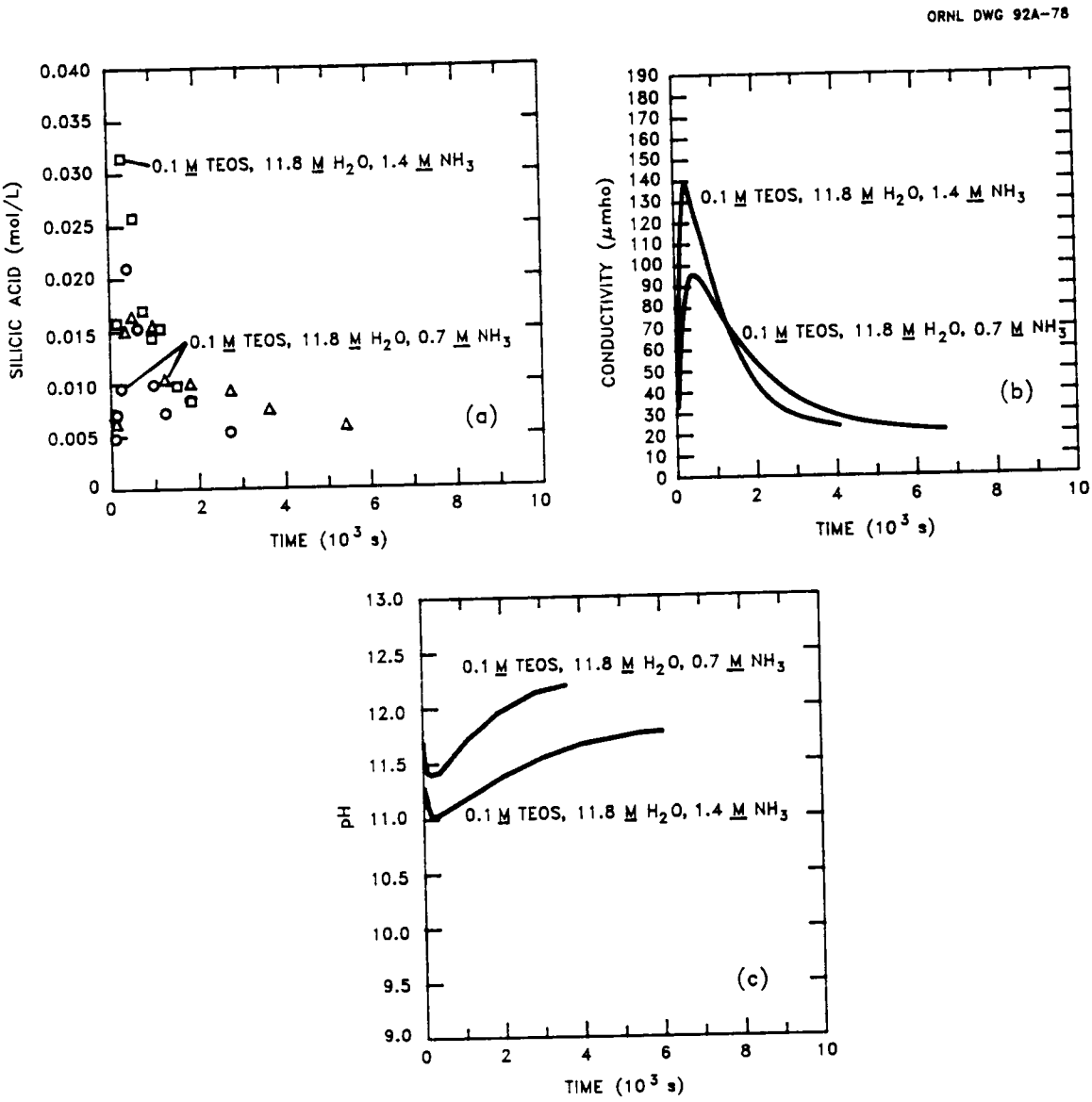



Fig. 2.26 Effect of ammonia concentration: (a) silicic acid, (b) conductivity, (c) pH (0.1M TEOS, 11.8M $H_2O$, 1.4M $NH_3$, 22 °C).

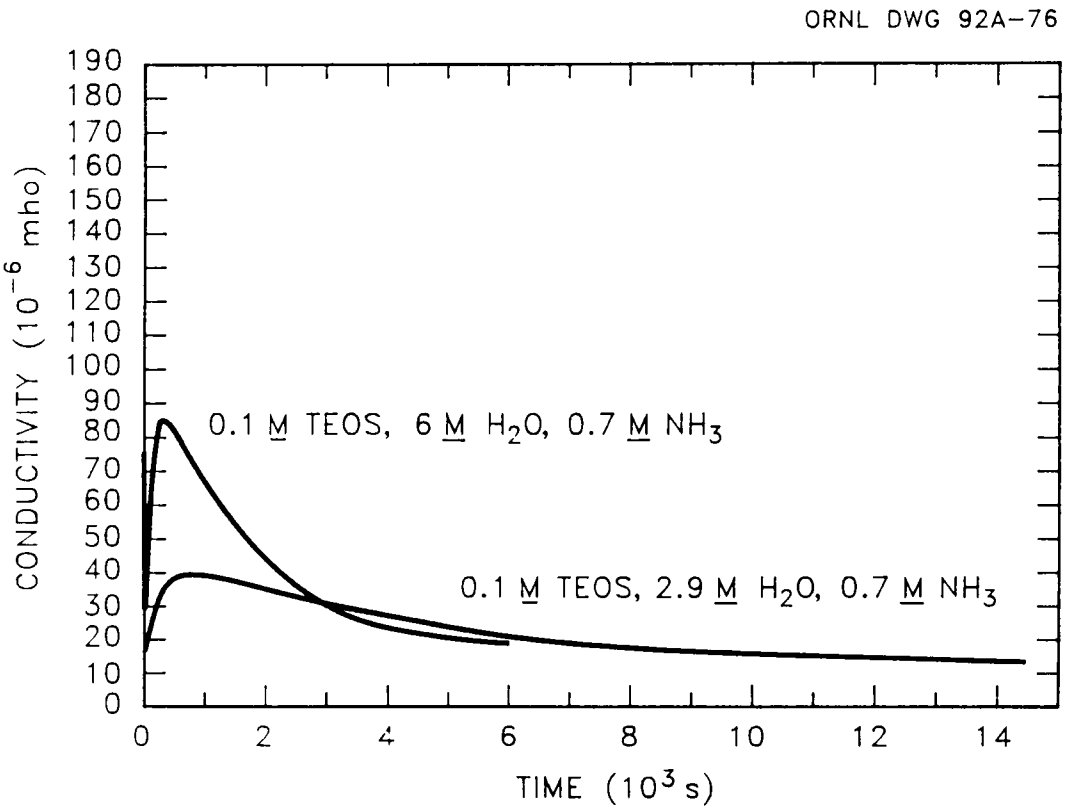



**Fig. 2.27 Effect of water concentration: conductivity, (0.1M TEOS, 0.7M $NH_3$, 22 °C).**

tion lead to the following equation which relates the silicic acid concentration to conductivity

$$[Si(OH)_4] = 0.00018 + 2.2348 \times 10^{-6}\lambda^2, \qquad (2.66)$$

$$r^2 = 0.998.$$

Thus, the conductivity measurements provide an additional technique for obtaining kinetic data and is especially useful when the concentration of silicic acid is too small to be determine by the difference between the total soluble silica and TEOS concentrations.

2.5.4. Particle Growth and Particle Size Distribution

Typical particle growth data are shown in Figs. 2.28 and 2.29. Dynamic light scattering and scanning electron microscopy are used to obtain particle growth data.

Fig. 2.28 shows the growth of silica particles during the hydrolysis of TEOS with 6M $H_2O$ and 0.7M $NH_3$. The data show that the first detectable particle size is ~0.06 $\mu$m. This indicates that either the primary nuclei are very large or that aggregation is very rapid and, therefore, the particles have already grown to this size before detection by light scattering. In each plot, the particles grow to some ultimate size. The rate of growth and final particle size are affected by the initial TEOS concentration, water concentration and ammonia concentration.

Fig. 2.29 shows the growth of silica particles during the hydrolysis of TEOS with high and low water and ammonia concentrations. The plot clearly shows that the final particle size decreases with a decrease in the initial TEOS, water

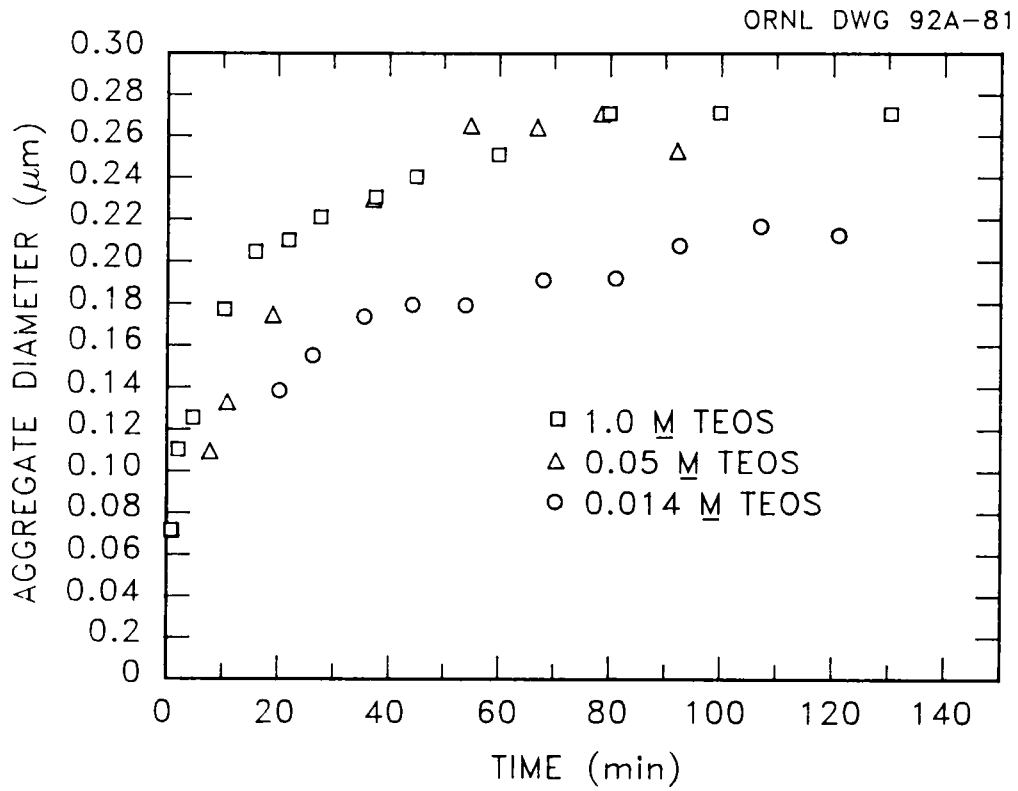



**Fig. 2.28 TEOS hydrolysis in ethanol: Particle growth kinetics (6.0M $H_2O$, 0.7M $NH_3$, 22 °C).**

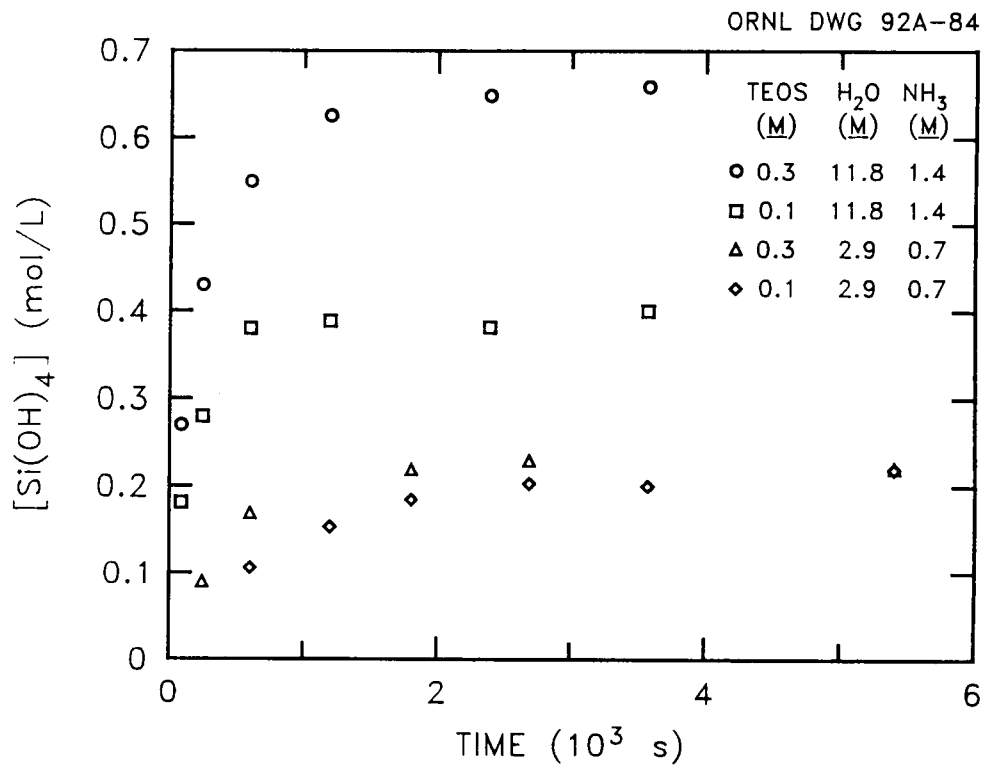



**Fig. 2.29 TEOS hydrolysis in ethanol: Particle growth kinetics-high and low reactant concentrations.**

and ammonia concentrations for the range of reaction conditions studied.

Fig. 2.30 shows transmission electron micrographs of silica particles that are produced in solutions with low water (2.9 M) and low to medium ammonia concentrations (0.057 to 0.7M).

There is an increase in the particle size as the ammonia concentration is increased. Referring to the previous two sections, it is seen that increasing the ammonia concentration increases the hydrolysis and condensation reactions, and raises the time-average conductivity of the solution. It is primarily the latter, the increase in the conductivity, that results in larger particles at higher ammonia concentrations. The increase in the conductivity decreases the electric double layer which causes a decrease in the repulsive electrostatic forces and which enhances agglomeration.

Fig. 2.31 shows TEMs of particles that are synthesized during the hydrolysis of TEOS with 6.0M water, 0.7M ammonia and initial TEOS concentrations of 0.014M, 0.05M and 0.3M.

The particle sizes increase with an increase in the initial TEOS concentration. As stated above, the increase in particle size is due to the decrease in the electric double layer that is caused by the increase in conductivity with an increase in the initial TEOS concentration.

TEMs are shown in Fig. 2.32 of particles that are synthesized by the hydrolysis of solutions containing 0.1M and 0.3M TEOS, 11.8M water and 1.4 M ammonia, and 0.7M ammonia concentration.

The largest particles are synthesized in these solutions. It is also in these solutions where conductivity is highest (Fig. 2.24) and consequently aggregation is enhanced.

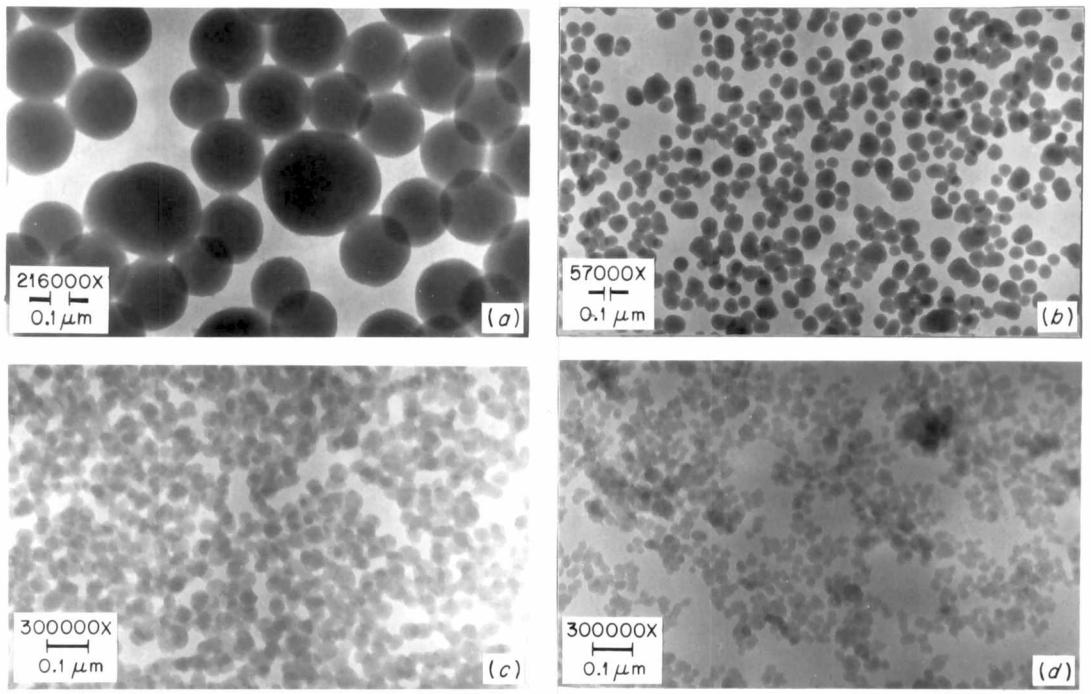



Fig. 2.30 TEM of silica particles synthesized during the hydrolysis of TEOS in ethanol: (a) 0.3M TEOS, 2.9M $H_2O$, 0.7M $NH_3$, 22 °C, (b) 1.0M TEOS, 2.9M $H_2O$, 0.7M $NH_3$, 22°C, (c) 1.0M TEOS, 2.9M $H_2O$, 0.175M $NH_3$, 22°C,(d) 1.0M TEOS, 2.9M $H_2O$, 0.057M $NH_3$, 22°C.

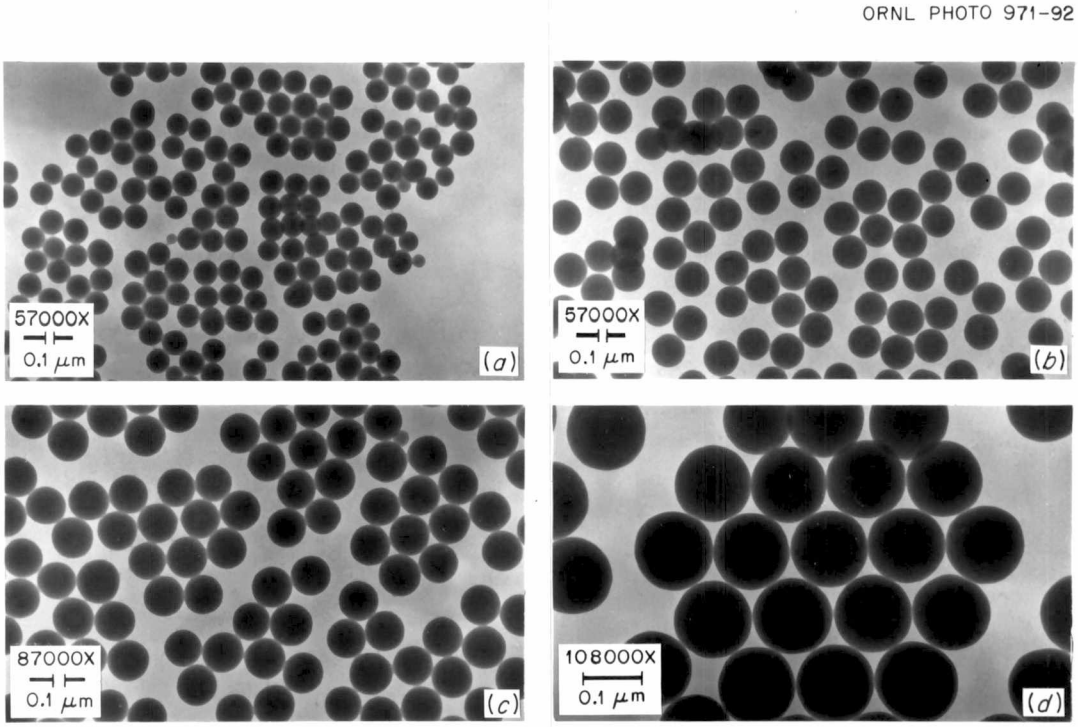



Fig. 2.31 TEM of silica particles synthesized during the hydrolysis of TEOS in ethanol (6.0M $H_2O$, 0.7M $NH_3$, 22°C): (a) 0.014M TEOS, (b) 0.05M TEOS, (c) 0.3M TEOS, (d) 0.3M TEOS.

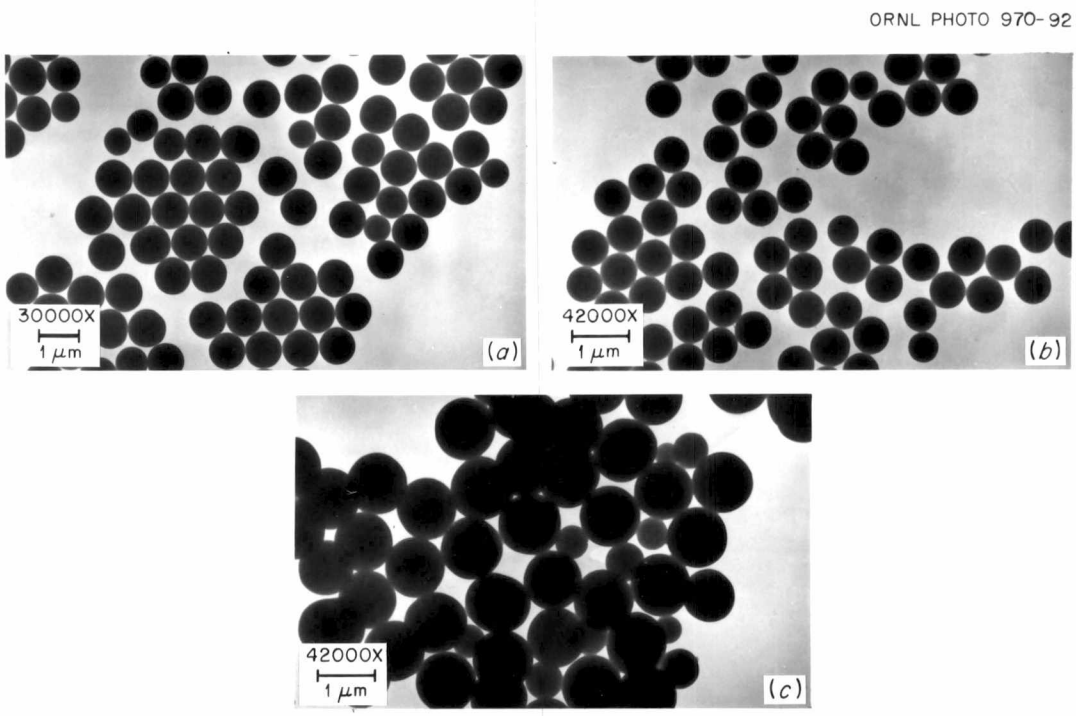



Fig. 2.32 TEM of silica particles synthesized during the hydrolysis of TEOS in ethanol (22 °C): (a) 0.1M TEOS, 11.8M $H_2O$, 1.4M $NH_3$, (b) 0.3M TEOS, 11.8M $H_2O$, 0.7M $NH_3$, (c) 0.3M TEOS, 11.8M $H_2O$, 1.4M $NH_3$.

Particle size distributions are shown in Figs. 2.33 to 2.37. Fig. 2.33 shows the particle size distributions for particles synthesized during the hydrolysis of solutions containing initial water concentrations of 2.9M.

The particle size distribution is unimodal for low ammonia concentrations (0.057M and 0.175); however, at higher ammonia and initial TEOS concentrations, the distribution becomes bimodal.

Figs. 2.34 and 2.35 show the final particle size distribution for particles synthesized from 6.0M water and 0.7M ammonia concentrations. These figures show that the ultimate particle size initially increases with the initial TEOS concentration (0.014M to 0.5M) and the particle size distribution is unimodal. However, the hydrolysis of 0.75M and 1.0M TEOS solutions results in a bimodal distribution with smaller particle sizes.

The final particle size distributions are shown in Fig. 2.36 for the hydrolysis of solutions containing 11.8M water, 0.7 and 1.4M ammonia and initial TEOS concentrations of 0.1 and 0.3M. These particles are larger than those synthesized in the previous runs. However, in all cases, the particle size distributions are wider and are essentially bimodal.

### 2.5.5. Estimating Condensation, Nucleation Kinetic Parameters

The experimentally determined hydrolysis rate constant, condensation (silicic and conductivity) and particle growth kinetic data are used to estimate the condensation rate constant, $K_C$, and the nucleation kinetic parameter, $A_J$. Particle growth data were fitted to a fourth order polynomial of the form:

$$d = a_o + a_1 t + a_2 t^2 + a_3 t^3 + a_4 t^4. \tag{2.67}$$

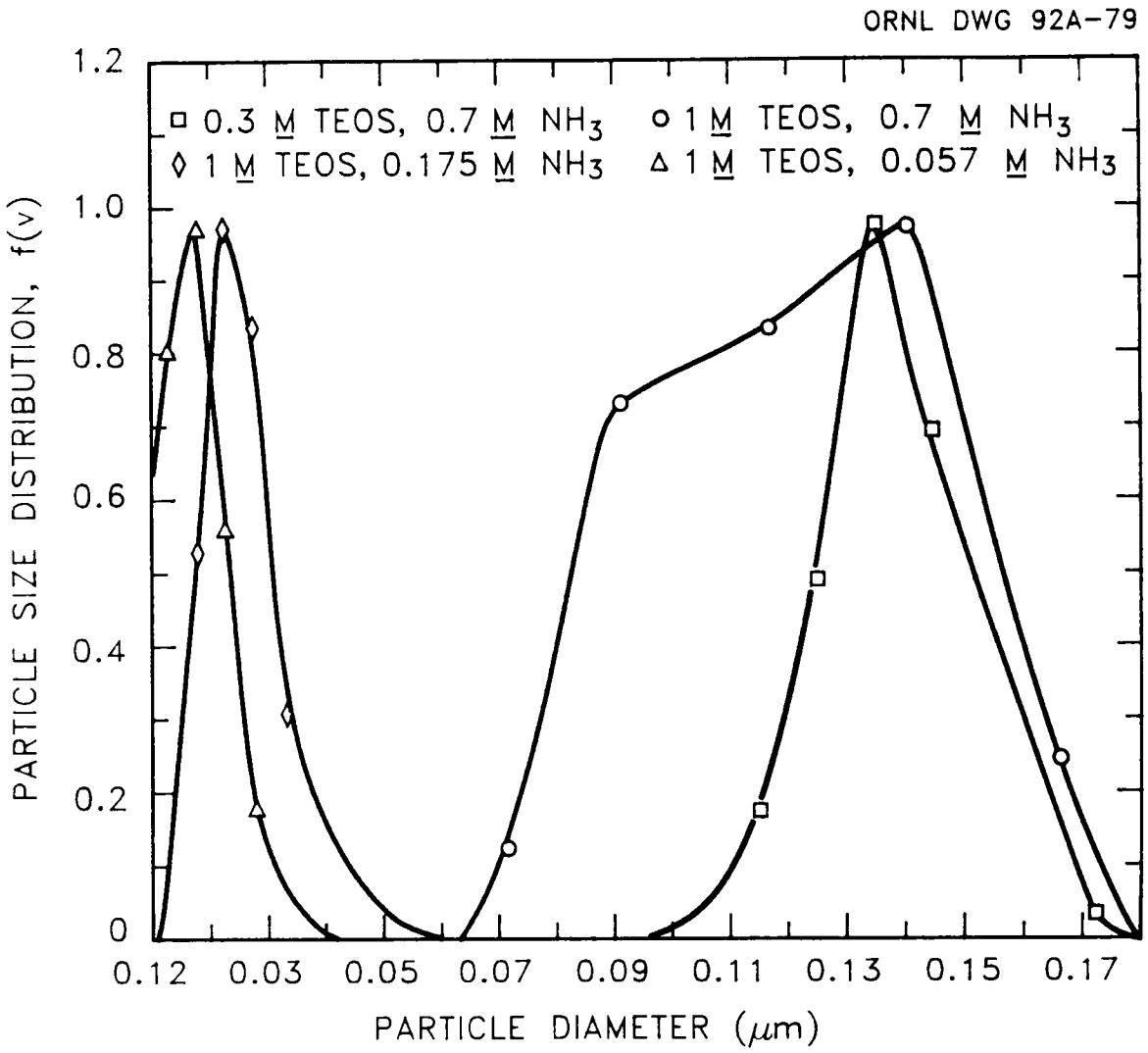



Fig. 2.33 Ultimate size distribution of silica particle formed during the hydrolysis of TEOS in ethanol: 2.9M $H_2O$, 22°C.

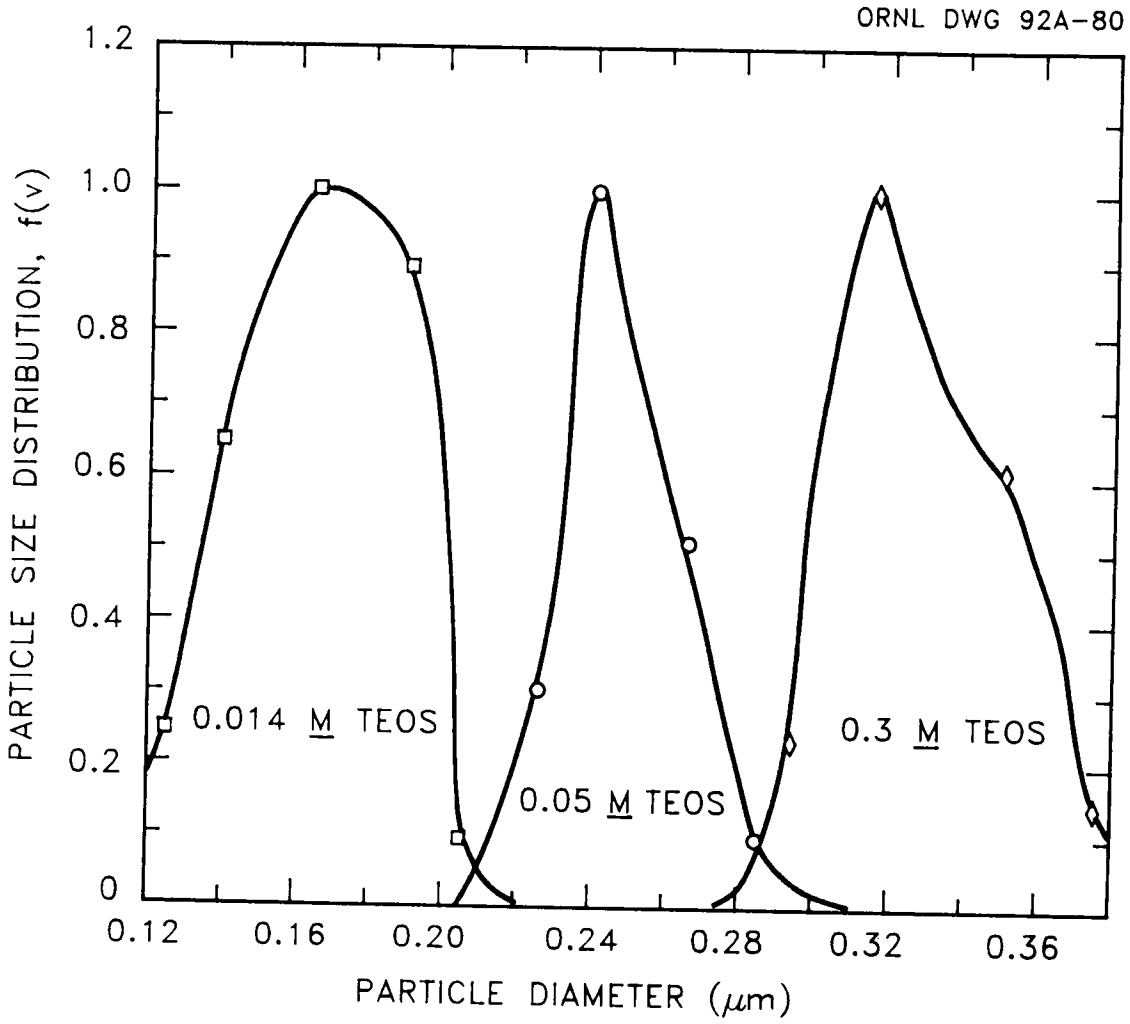



Fig. 2.34 Ultimate size distribution of silica particle formed during the hydrolysis of TEOS in ethanol: (0.014-0.3M TEOS, 6.0M $H_2O$, 0.7M $NH_3$ 22°C).

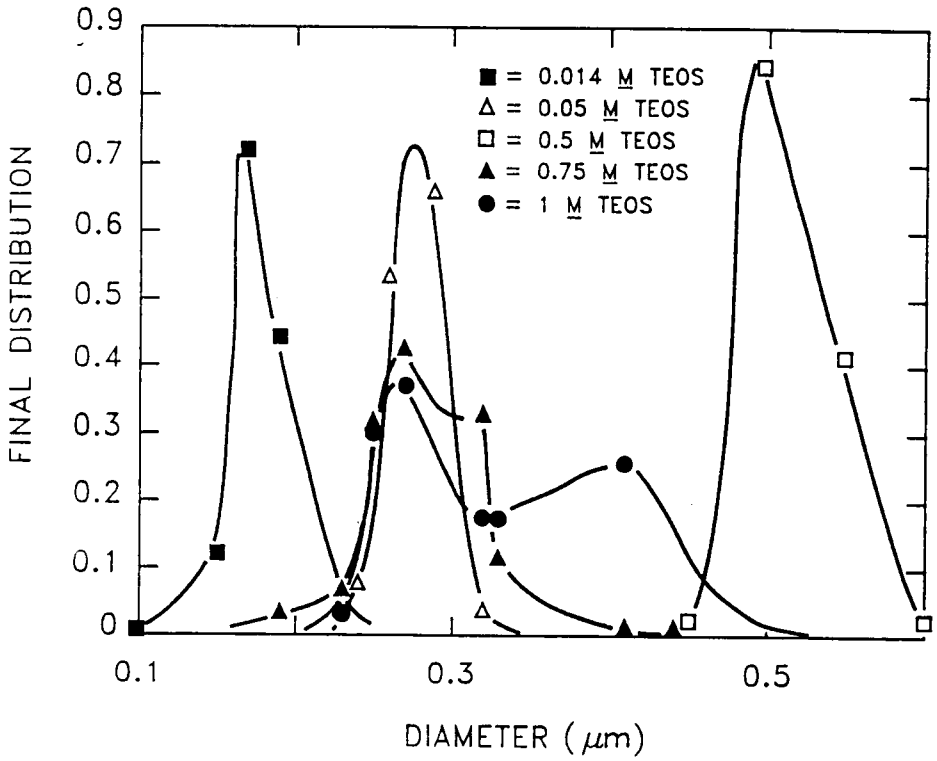



Fig. 2.35 Ultimate size distribution of silica particle formed during the hydrolysis of TEOS in ethanol: (0.014-1.0M TEOS, 6.0M $H_2O$, 0.7M $NH_3$ 22°C).

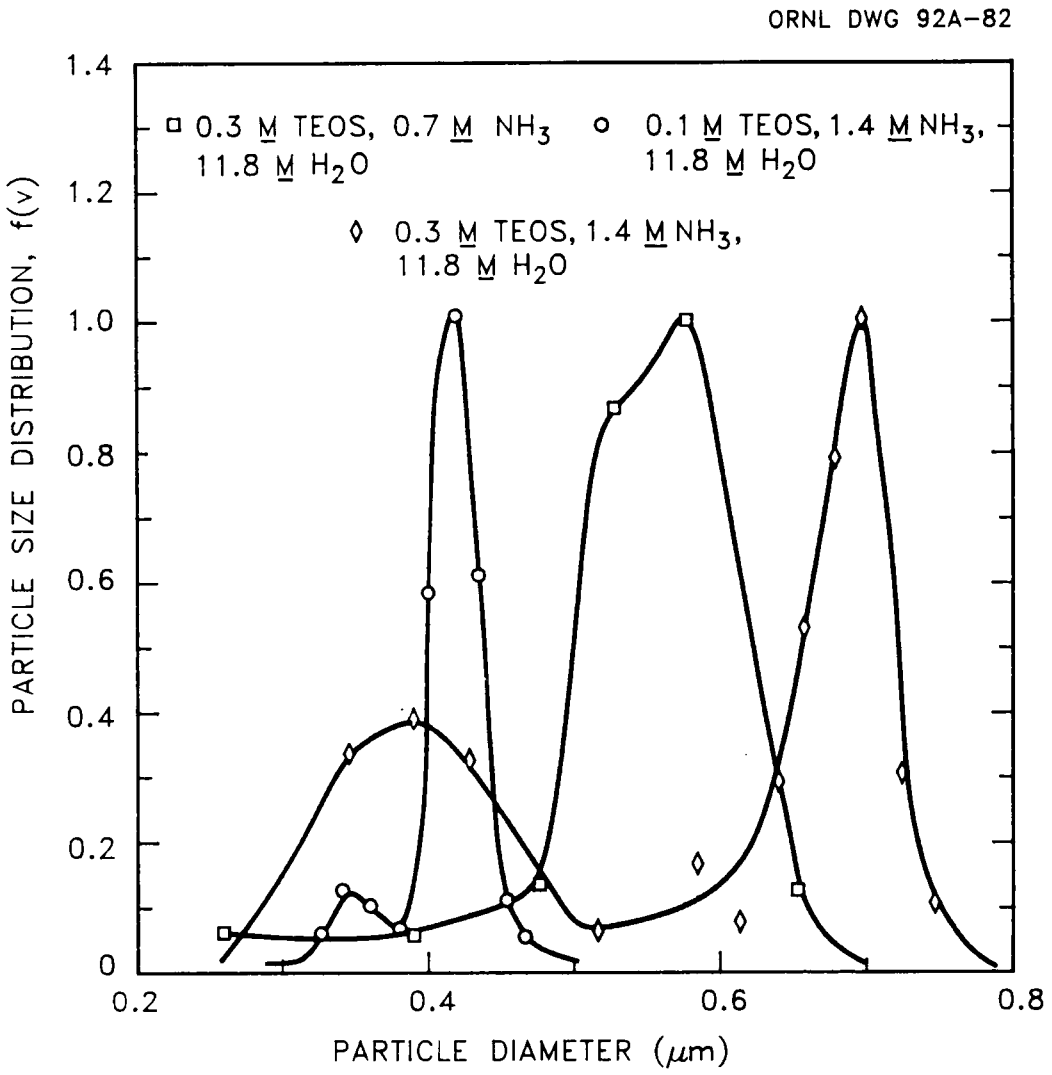



Fig. 2.36 Ultimate size distribution of silica particle formed during the hydrolysis of TEOS in ethanol: (11.8M $H_2O$, 22°C).

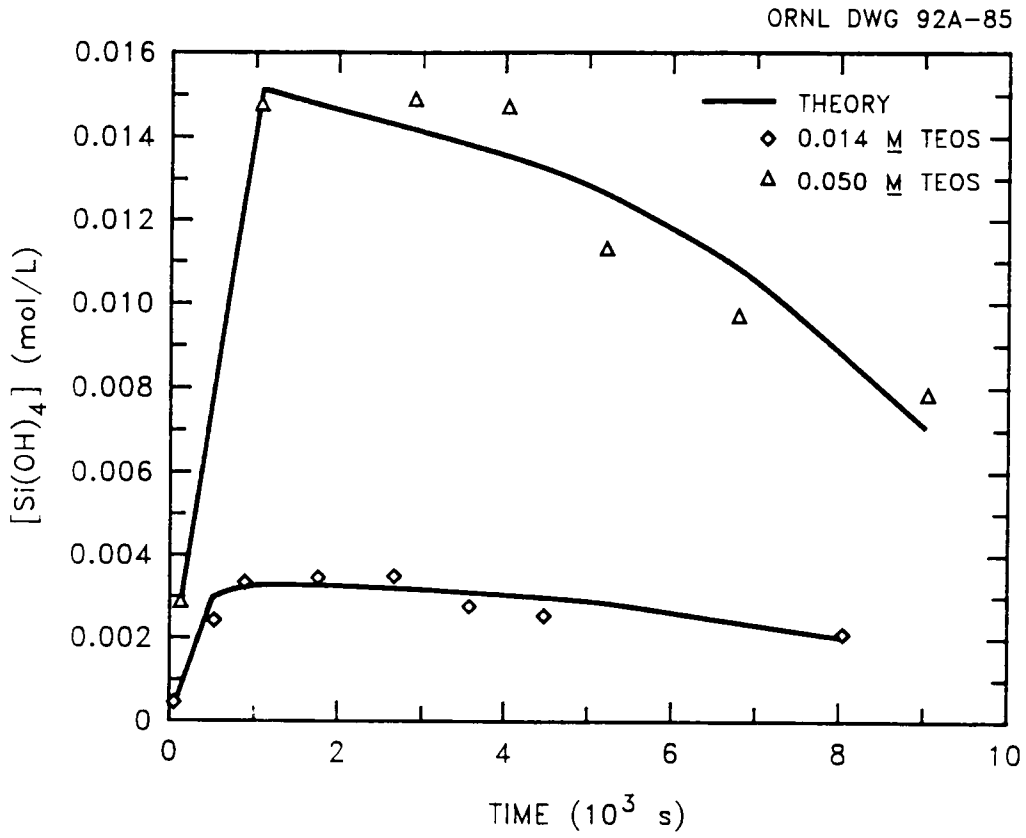



Fig. 2.37 Typical fit of silicic acid data to Eq. 2.10: TEOS hydrolysis in ethanol (0.014 and 0.05M TEOS, 6.0M $H_2O$, 0.7M $NH_3$ 22°C).

Conductivities are converted to silicic acid concentrations by Eq. 2.66.

Fig. 2.37 shows typical regressions of the condensation kinetic data to Eq 2.10. Table 2.5 gives the parameter values that are determined from conductivity and silicic acid data. The model fits the data well; however, as is seen in table 2.5, the nucleation and condensation parameters, $A_J$ and $K_C$, are not constant. Furthermore, these data indicate that the condensation rate constant varies primary with the ammonia concentration. Its variation with the water concentration is anomolous. On the other hand, the nucleation parameter varies primarily with the water concentration.

These parameters along with the colloidal stability parameters [i.e., zeta potential ($\zeta$), dielectric constant ($\epsilon$) and Hamaker constant ($A_H$)] are used in the population balance model which predicts particle growth kinetics. The determination of the colloidal stability parameters are discussed in the next section.

### 2.5.6. Colloidal Stability Parameters

The colloidal stability parameters include the dielectric constant, zeta potential and the Hamaker constant. Fig. 2.38 shows the dielectric constant of water-ethanol mixtures. This plot is used to estimate the dielectric constant all water- ethanol mixtures and reaction solutions.

Table 2.6 lists the zeta potential values that were determined by electrophoretic mobility measurements. Smoluchowski's equation (Eq. 2.45) was used to convert electrophoretic mobilities to zeta potentials. The zeta potentials vary with water concentration and ammonia concentration. This variation

Table 2.5. Fitted parameter values.

| [TEOS] mol/L | [$H_2O$] mol/L | [$NH_3$] mol/L | $K_C$ $(s-cm)^{-1}$ | $A_J$ | Data Type |
|---|---|---|---|---|---|
| 0.014 | 6.0 | 0.7 | $2.5\times10^{-6}$ | 467 | [TS] |
| 0.05 | 6.0 | 0.7 | $7.8\times10^{-7}$ | 977 | [TS] |
| 0.3 | 11.8 | 1.4 | $1.4\times10^{-5}$ | 1499 | [TS] |
| 0.3 | 2.9 | 0.7 | $4.8\times10^{-6}$ | 360 | conductivity |
| 0.1 | 6.0 | 0.7 | $6.2\times10^{-6}$ | 422 | conductivity |
| 0.1 | 11.8 | 0.7 | $3.5\times10^{-6}$ | 1297 | conductivity |
| 0.1 | 11.8 | 1.4 | $1.4\times10^{-5}$ | 1199 | conductivity |
| 0.3 | 11.8 | 1.4 | $1.4\times10^{-5}$ | 1499 | conductivity |

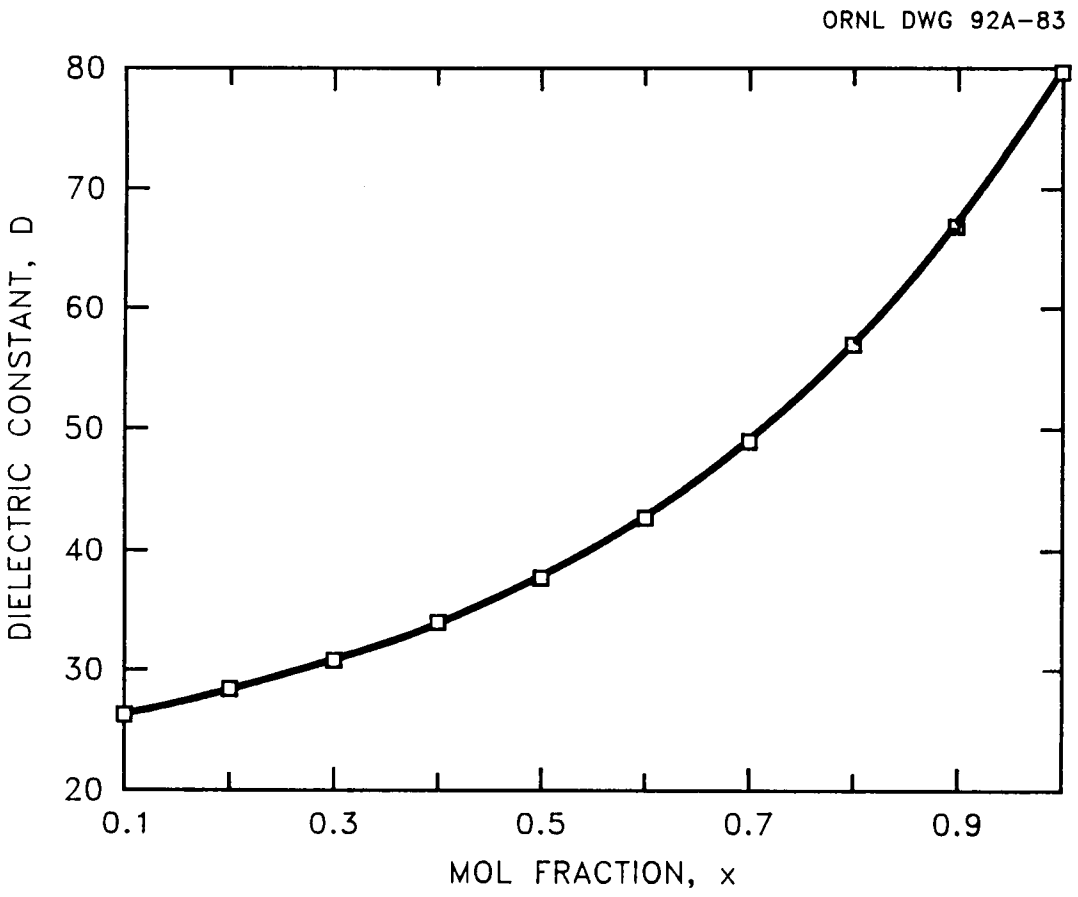



Fig. 2.38 Dielectric constant of water-ethanol mixtures.

was found to be adequately modeled by the expression

$$\varsigma = -58 + 1.56[H_2O] + 4.95[NH_3] \tag{2.68}$$

The Hamaker constant is not measured directly; therefore, it is used as an adjustable parameter in the population model. Typical Hamaker constants are approximately 1.0 $\times 10^{-20}$J.

Bogush and Zukoski (1991) proposed that electric double layer, solvation and Van der Waals attractive forces govern the colloidal stability of silica particles formed by the Stober process. The following colloidal stability parameters are used in their model: $\varsigma = -13mV$, $A_H = 0.48 \times 10^{-20}$J, $A_S = 1.5 \times 10^{-3}J$, and $\lambda_S = 1.0 \times 10^{-9}m$. Figs. 2.39 and 2.40 show plots of the solvation, electric double layer and Van der Waals attractive potentials for $r = 1.0 \times 10^{-8}$, $A_S = 1.5 \times 10^{-3}$J, $A_H = 0.48 \times 10^{-20}$J, $\kappa = 3.48 \times 10^{8}m^{-1}$, $\varsigma = -13mV$ (Bogush and Zukoski 1991) and -40 mV (this work), respectively. It is clearly seen that the solvation forces dominate the repulsive forces if $\varsigma = -13mV$; however, for $\varsigma = -40mV$, electrostatic forces dominate the repulsive forces.

### 2.5.7. Predicting Particle Growth Kinetics and Final Particle Size Distributions

As is stated in section 2.4.3, particle growth is predicted by simultaneously solving the hydrolysis, condensation, solvent dissociation and acid-base reactions (Eqs. 2.9, 2.10 or 2.11, 2.18); and the population balance equations (Eqs. 2.32 and 2.33).

Tables 2.5 and 2.6 list the parameter values that are used in the computer simulations. Except for the Hamaker constant, $A_H$, parameter values for the

Table 2.6. Experimentally determined zeta potentials.

| $[H_2O]$ mol/L | $[NH_3]$ mol/L | $\epsilon$ | $\zeta$ mV |
|---|---|---|---|
| 11.8 | 1.4 | 37 | -32.7 |
| 6.0 | 0.7 | 29 | -45.2 |
| 11.8 | 1.4 | 37 | -37.9 |
| 2.9 | 0.7 | 26 | -47.8 |

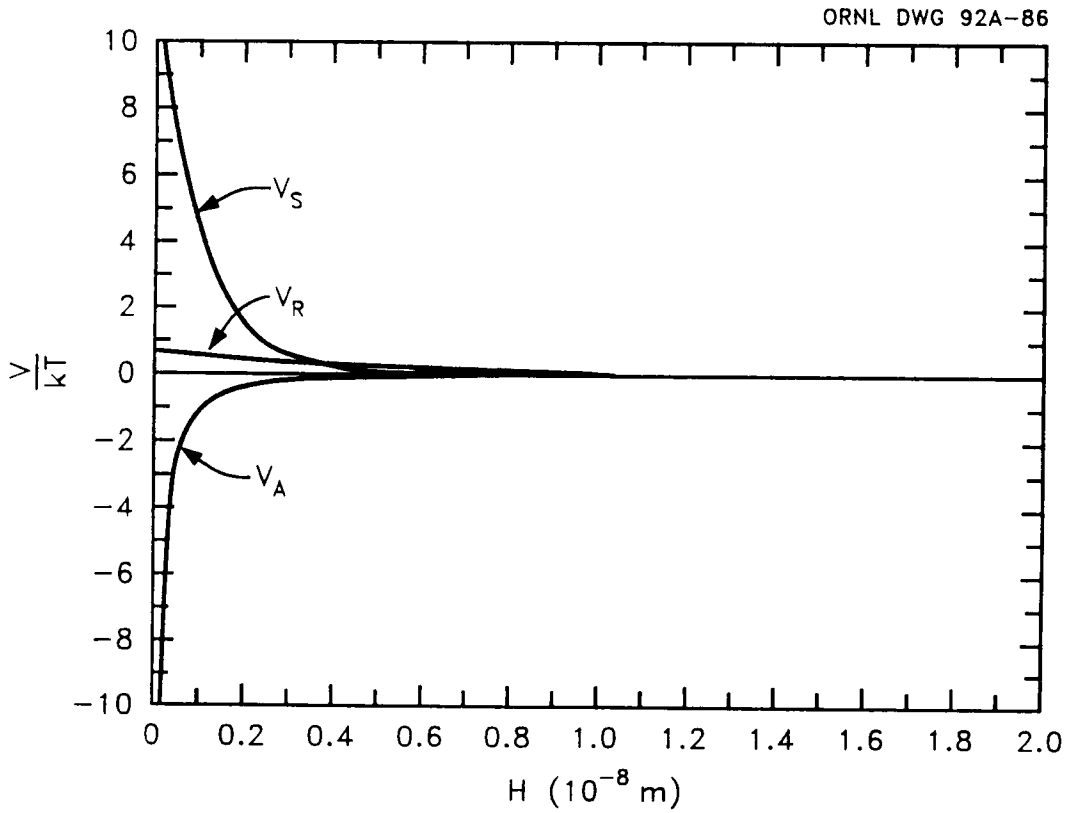



Fig. 2.39 Potential energy curves for Bogush and Zukoski (1991) zeta potential data ($A_J = 0.48\times10^{-20}$, $\varsigma = -13$ mV, $\kappa = 3.48\times10^{8}$ cm$^{-1}$ and $A_S = 1.5\times10^{-3}$.

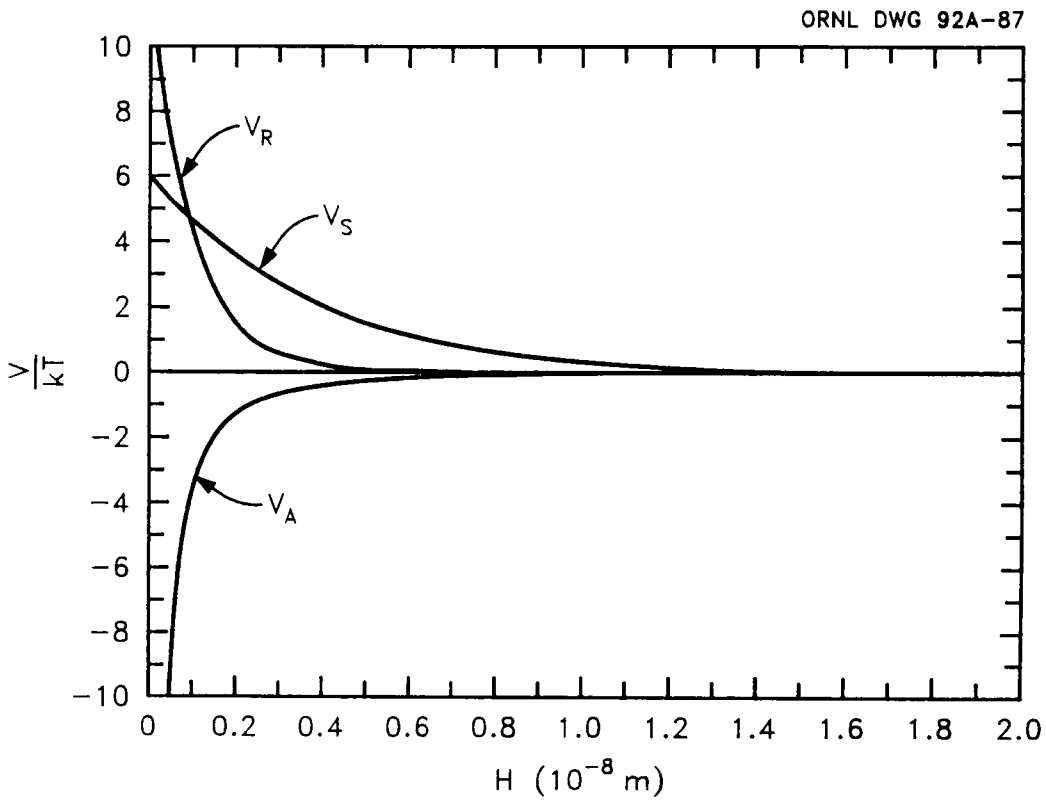



Fig. 2.40 Potential energy curves for zeta potential data determined during this study ($A_J = 0.48 \times 10^{-20}$, $\zeta = -40$ mV, $\kappa = 3.48 \times 10^8$ cm$^{-1}$ and $A_S = 1.5 \times 10^{-3}$.

other equations have been determined from experimental data or obtained from literature. The Hamaker constant is determined by adjusting its value until the theoretical final particle size matches that of the 0.05M TEOS, 6.0M $H_2O$ and 0.7M $NH_3$ run. A Hamaker constant, $A_H$, of $0.7 \times 10^{-20}$J is used for all computer simulations.

Before studying the simulation of particles growth, it is necessary to determine if the kinetics of the apparent silicic acid concentration is adequately modeled by the coupled population balance-chemical kinetics model. Fig. 2.41 shows the theoretical and experimental silicic acid concentrations for the hydrolysis of 0.014M and 0.05M TEOS with 6M $H_2O$ and 0.7M $NH_3$ in ethanol.

There is very good correlation between the theoretical model and the experimental data. Fig. 2.42a illustrates the experimental and theoretical silicic acid concentrations for the hydrolysis of 0.1M and 0.3M TEOS with 11.8M $H_2O$ and 1.4M $NH_3$ in ethanol. The experimental silicic acid data are obtained from the total soluble silica and ethanol measurements. The model agrees reasonably well with the experimental data. Fig. 2.42b is similar to Fig. 2.42a except the experimental silicic acid data are obtained from conductivity data. Again there is good agreement between experimental data and the model.

Particle growth kinetics are shown in Figs. 2.43 and 2.44.

Fig. 2.43 shows the predicted and experimental particle growth data for the hydrolysis of 0.014 and 0.05M TEOS with 6.0M $H_2O$ and 0.7M $NH_3$. The model underestimates particle growth; however, the model does show the qualitative behavior of the particle growth. These qualitative features include: (a) the increase in the final particle size with an increase in the initial TEOS concentration and (b) capturing the general trend of the particle growth kinetics.

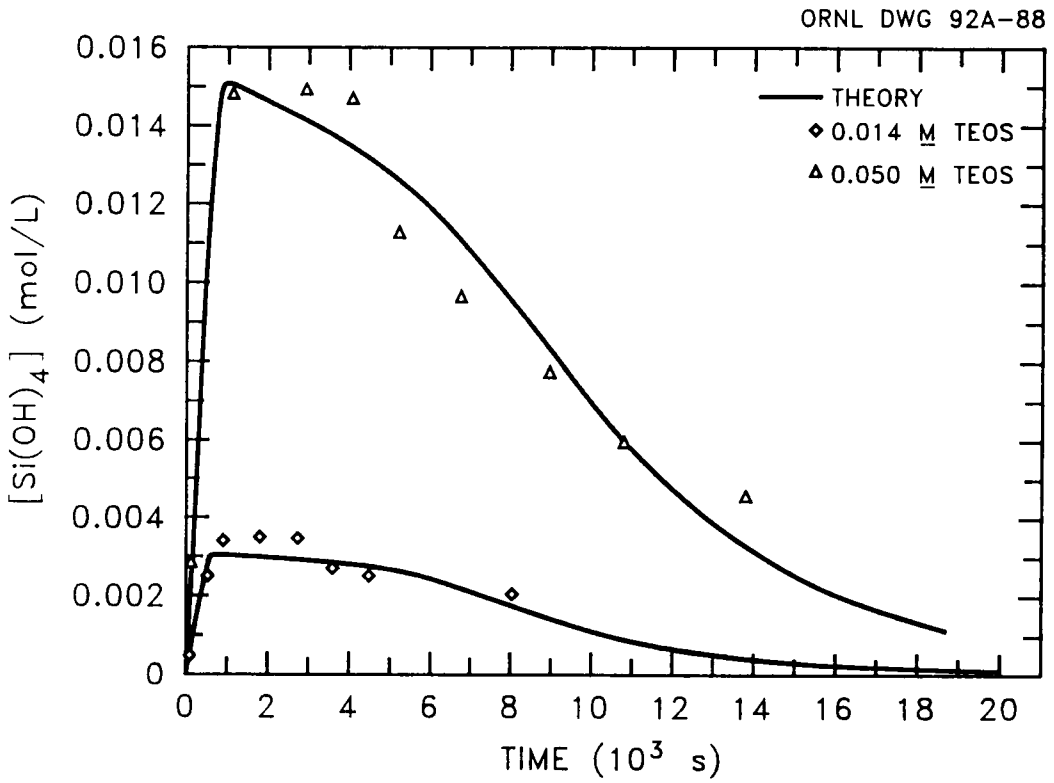



Fig. 2.41 Typical fit of silicic acid data by detail population balance-chemical kinetic model: TEOS hydrolysis in ethanol-[TS] data (0.014 and 0.05M TEOS, 6.0M $H_2O$, 0.7M $NH_3$ 22°C).

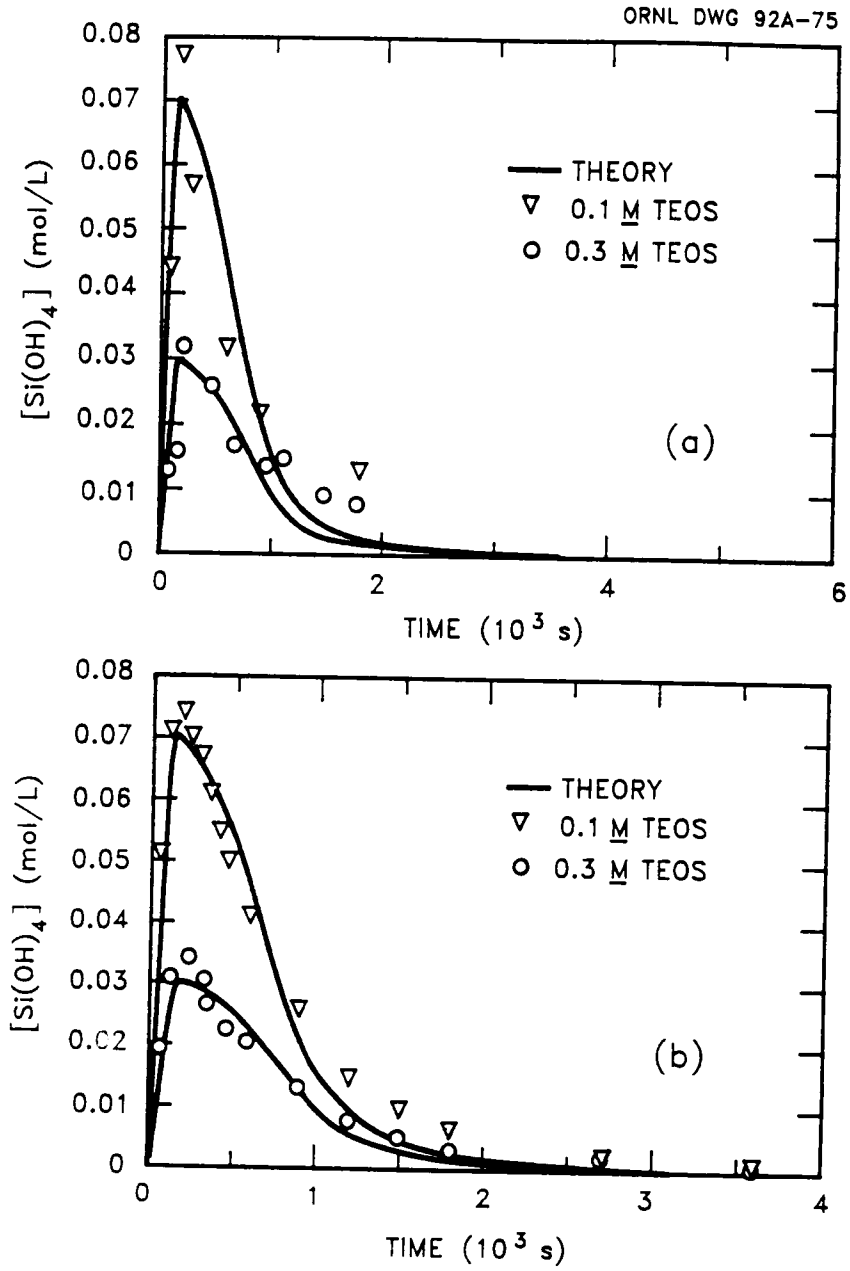



Fig. 2.42. Typical fit of silicic acid data by detail population balance-chemical kinetic model: TEOS hydrolysis in ethanol (a) [TS] data, (b) conductivity data (0.1 and 0.3M TEOS, 6.0M $H_2O$, 0.7M $NH_3$, 22°C).

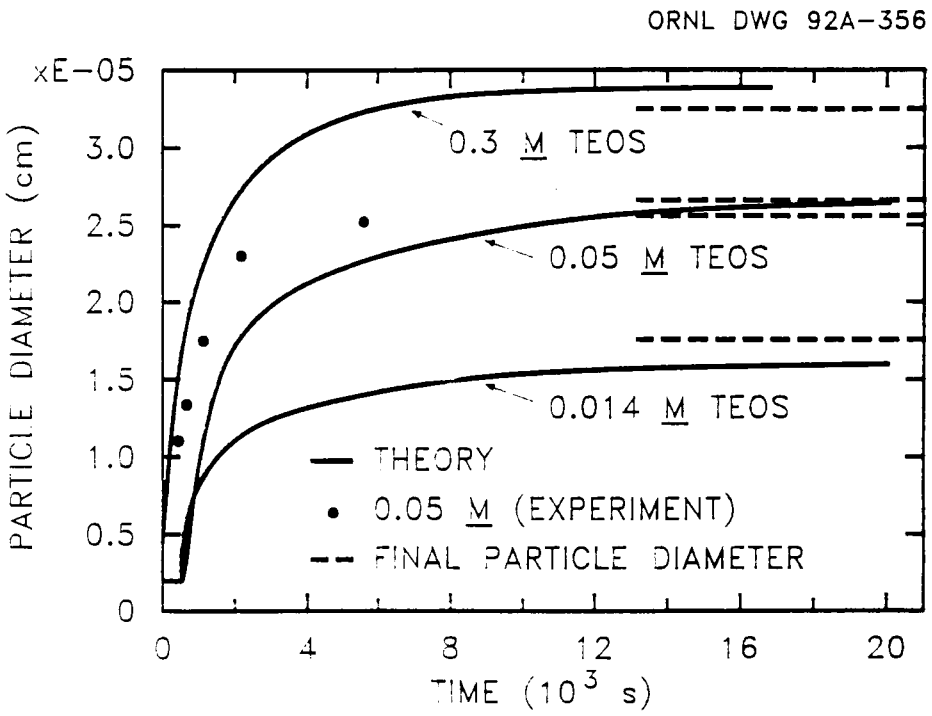



Fig. 2.43 Predicted and experimental particle growth data: TEOS hydrolysis in ethanol (0.014 and 0.05M TEOS, 6.0M $H_2O$, 0.7M $NH_3$ 22°C).

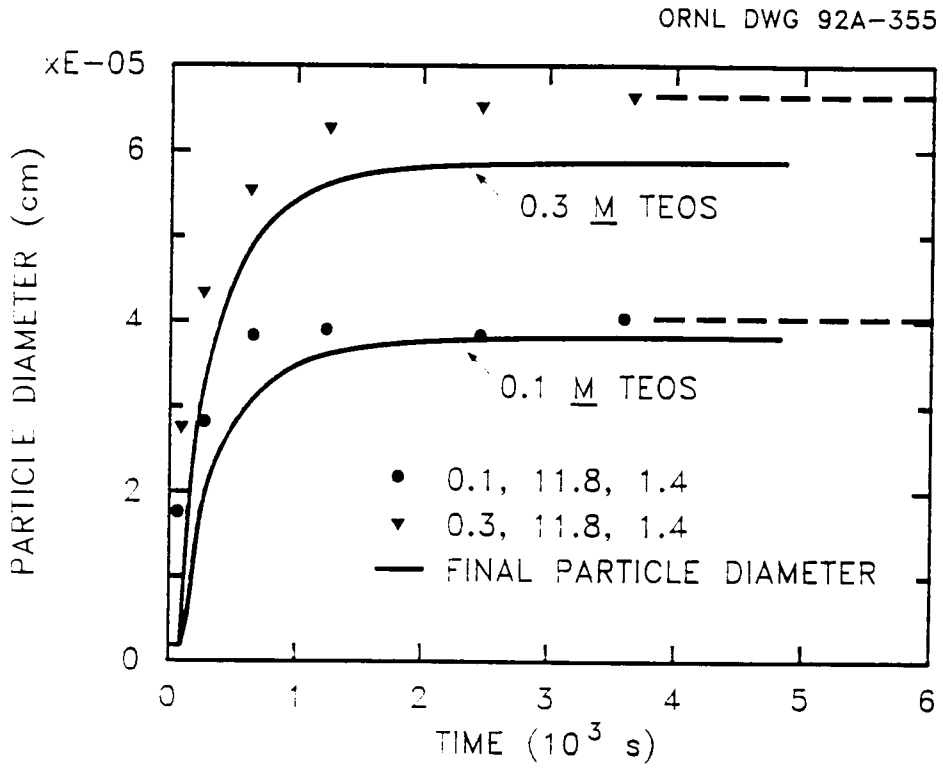



**Fig. 2.44** Predicted and experimental particle growth data: TEOS hydrolysis in ethanol (0.1 and 0.3M TEOS, 11.8M $H_2O$, 1.4M $NH_3$ 22°C).

Fig. 2.44 depicts the experimental and predicted growth kinetics of particles synthesized during the hydrolysis of 0.1M and 0.3M TEOS with 11.8M $H_2O$ and 1.4M $NH_3$ in ethanol. There is good agreement between the experimental and theoretical growth kinetics. As shown in Fig. 2.40, the final particle size increased with an increase in the initial TEOS concentration.

Figs. 2.45 and 2.46 show the change in number concentrations for the primary and aggregate particles, respectively, during the hydrolysis of 0.014, 0.05 and 0.3M TEOS with 6.0M $H_2O$ and 0.7M $NH_3$ in ethanol.

With a 10 to 20 minute time period, the number of primary particles (Fig. 2.45) rapidly increases to a maximum and quickly decreases to where the ratio of primary to aggregate particles is less than 1:100. Nucleation is still occurring during this time. Thus, the model predicts that, even during nucleation, the depletion of the smaller primary particles is very fast due to the rapid deposition of the smaller primary particles onto the surface of larger more stable aggregates. This suggests that it is quite possible not to detect primary particles during nucleation if there is a sufficient number of larger more stable colloids.

The measured and predicted aggregate number concentrations are shown in Fig. 2.46 for the hydrolysis of 0.05M TEOS, 6.0M $H_2O$ and 0.7M $NH_3$. The predicted aggregate number concentration for 0.014M TEOS, 6.0M $H_2O$ and 0.7M $NH_3$ is also shown. In all cases, the aggregate number concentration increases to a constant value. There is good agreement between the measured and predicted aggregate number concentration for 0.05M TEOS, 6.0M $H_2O$ and 0.7M $NH_3$ data. The measured particle number concentrations were determined by classical and dynamic light scattering techniques.

Figs. 2.47 and 2.48 show the predicted primary and aggregate number con-

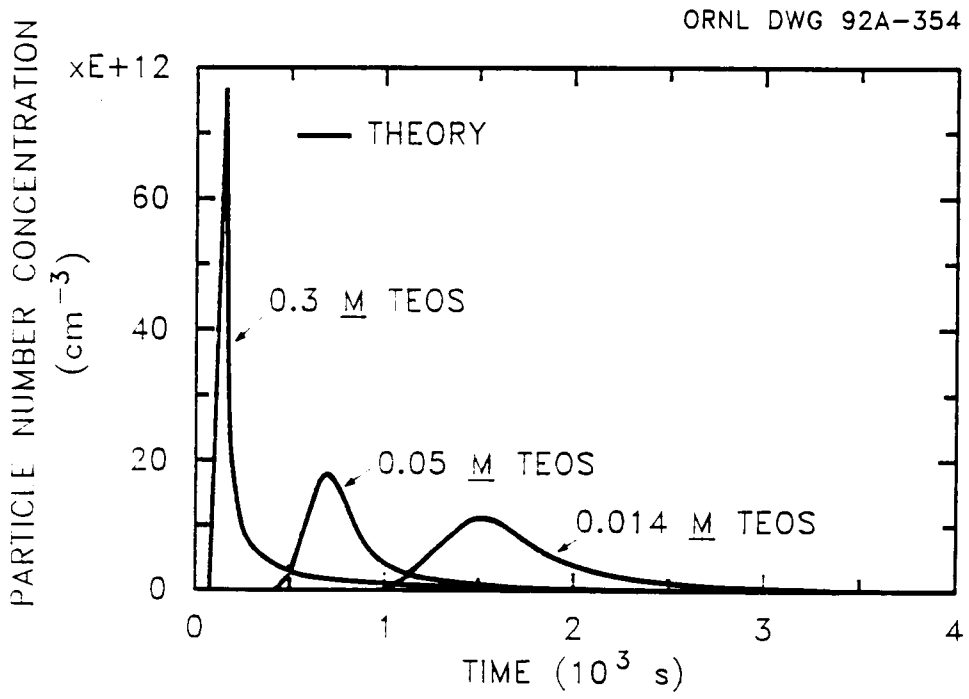



Fig. 2.45 Predicted primary particle number concentration: TEOS hydrolysis in ethanol (0.014, 0.05 and 0.3M TEOS, 6.0M $H_2O$, 0.7M $NH_3$ 22°C).

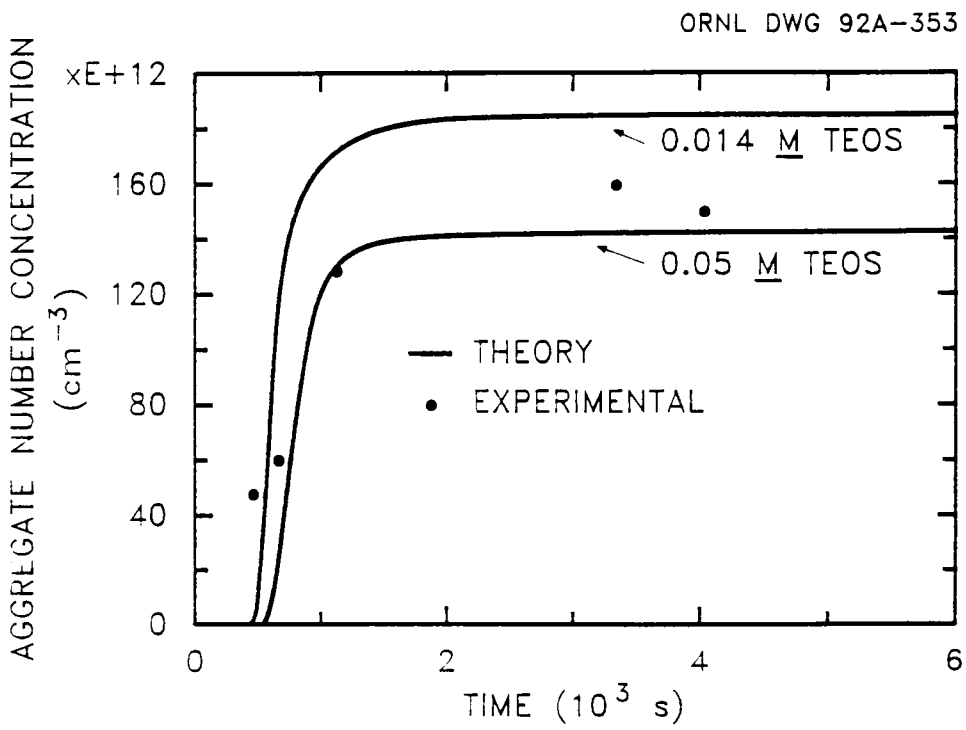



Fig. 2.46 Predicted and experimental aggregate number concentration: TEOS hydrolysis in ethanol (0.014, 0.05 and 0.3M TEOS, 6.0M $H_2O$, 0.7M $NH_3$ 22°C).

centrations, respectively, for the hydrolysis of 0.1 and 0.3M TEOS with 11.8M $H_2O$ and 1.4M $NH_3$.

Again, the primary particle number concentration (Fig. 2.47) rapidly increases to a maximum and quickly decreases to where the ratio of primary to aggregate particles is less than 1:100. The aggregate concentration (Fig. 2.48) increases to a maximum value and subsequently decreases slightly to a constant value.

To understand the kinetic behavior of the primary particle concentrations, the collision efficiency factors ($\beta_{\gamma\gamma}$, $\beta_{\lambda\lambda}$, and $\beta_{\gamma\lambda}$) are plotted as a function of time in Fig. 2.49.

The collision efficiency factor for the primary-primary interactions, $\beta_{\gamma\gamma}$, increases slightly and decreases to some steady-state value. Since the primary particles are essentially constant, the change in $\beta_{\gamma\gamma}$ is due to the change in the inverse DeBye length which is caused by changes in the silicic acid, thus, ammonium ion, concentrations. The collision efficiency factor for the aggregate-aggregate interactions decreases by several orders of magnitude as the aggregates become larger (See Fig. 2.47 for particle growth data); thus, a large aggregate will not agglomerate with another large aggregate. Conversely, the primary-aggregate collision efficiency factor, $\beta_{\gamma\lambda}$, is increased to approximately one to two orders of magnitude larger than $\beta_{\gamma\gamma}$. Thus, a primary particle will deposit on the surface of a larger aggregate faster than a primary particle will aggregate with another primary particle. In summary, Fig. 2.49 suggests that, initially, primary particles interact with other primary particles to form aggregates. However, as the concentration and size of the aggregates increases, primary particles selectively deposit on the larger more stable aggregates and consequently, the

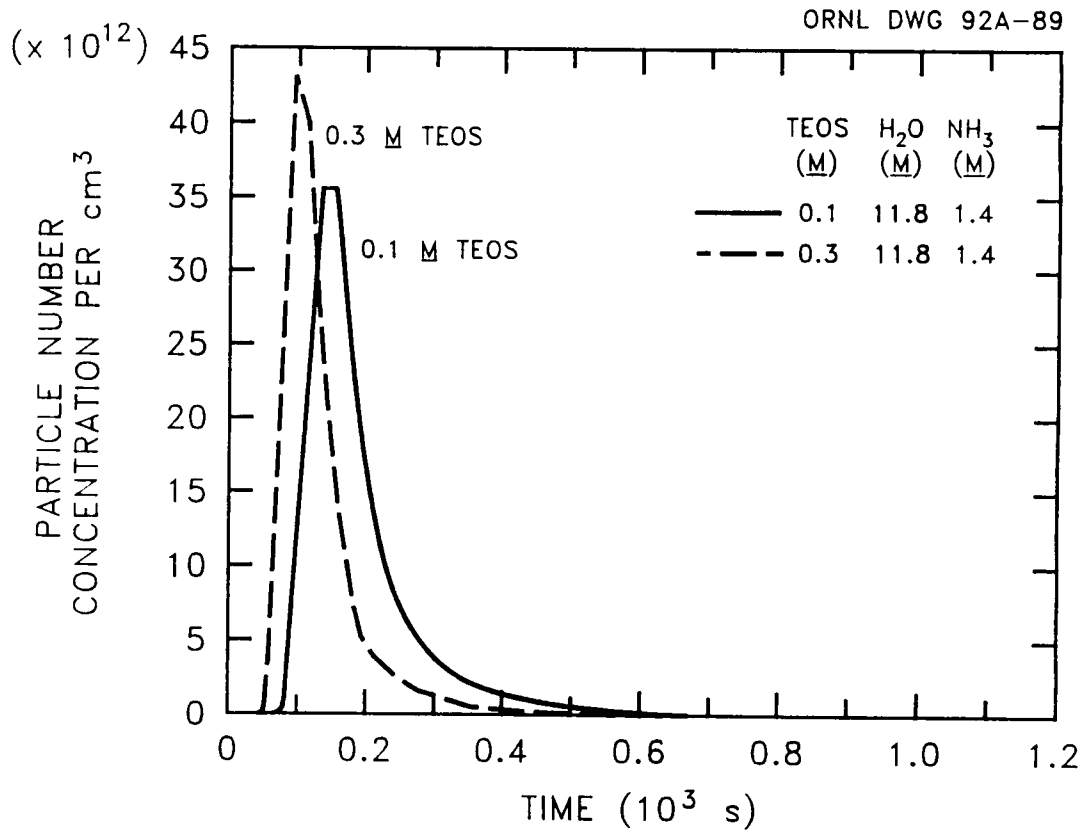



Fig. 2.47 Predicted primary particle number concentration: TEOS hydrolysis in ethanol (0.1, and 0.3M TEOS, 11.8M $H_2O$, 1.4M $NH_3$ 22°C).

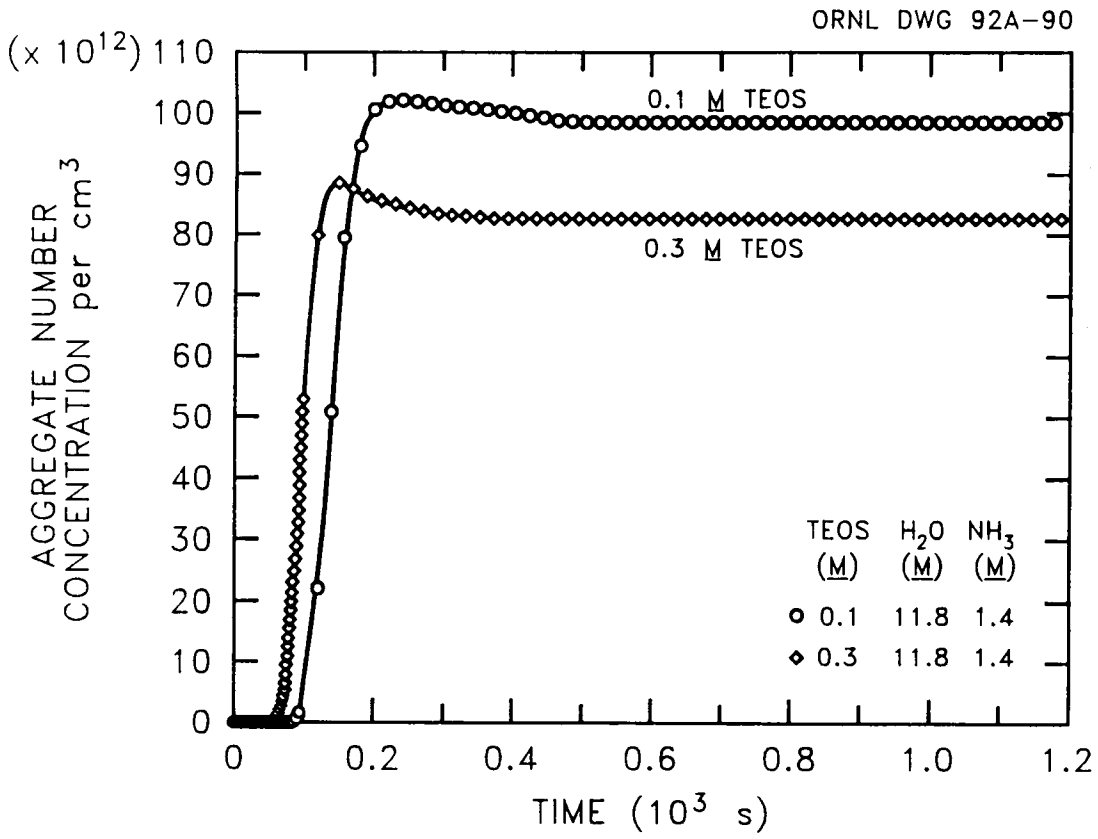



Fig. 2.48 Predicted aggregate number concentration: TEOS hydrolysis in ethanol (0.1, and 0.3M TEOS, 11.8M $H_2O$, 1.4M $NH_3$ 22°C).

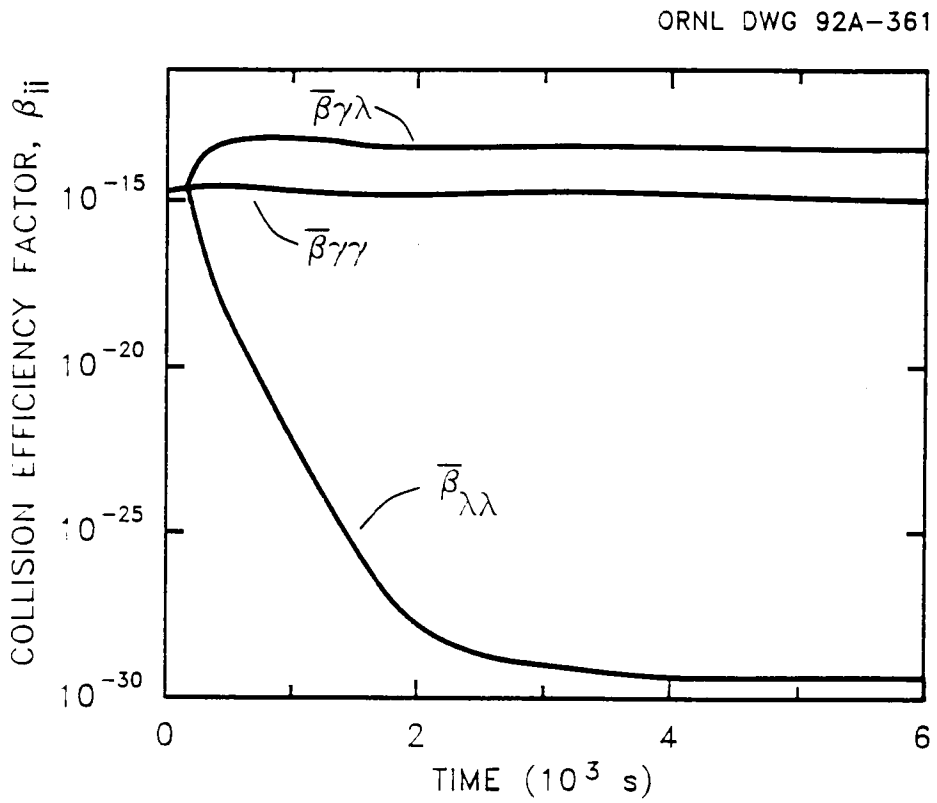



Fig. 2.49 Collision efficiency factor (0.1M TEOS, 11.8M $H_2O$, 1.4M $NH_3$ 22°C).

amount of primary particles in solution is depleted.

In addition to predicting particle growth, and size, it is also necessary to compare the theoretical and experimental particle size distribution. This determines how well the final particle size distributions are modeled by lognormal distribution and/or whether the size range is predicted by the population balance model. Figs. 2.50 and 2.51 show the predicted and experimental particle size distribution for the TEOS hydrolysis in ethanol with 6.0M $H_2O$ and 0.7M $NH_3$, and 11.8M $H_2O$ and 1.4M $NH_3$, respectively.

The model adequately predicts the experimental unimodal distributions for moderate water and ammonia concentrations (Fig. 2.50). The experimental size distributions for the high water and ammonia runs (Fig. 2.51) were bimodal. Although the algorithm that is used to solve the population balance model cannot resolve bimodal distributions, the model adequately predicts the particle size range.

Another measure of the spread in the particle size distribution is the polydispersity factor. It is defined by Pratsinis (1987) as

$$W_P = \left(\frac{\lambda_{2/3}\lambda_0}{\lambda_{1/3}^2} - 1\right)^{1/2} \tag{2.69}$$

Figs. 2.52 and 2.53 show good agreement between the predicted and final experimental polydispersity factor for the aggregate particles.

## 2.6. Conclusions

The formation of silica particles by the hydrolysis of TEOS in ethanol has been evaluated over a wide range of reactant and catalyst concentrations. Initially, the hydrolysis and condensation reactions were conducted in various low

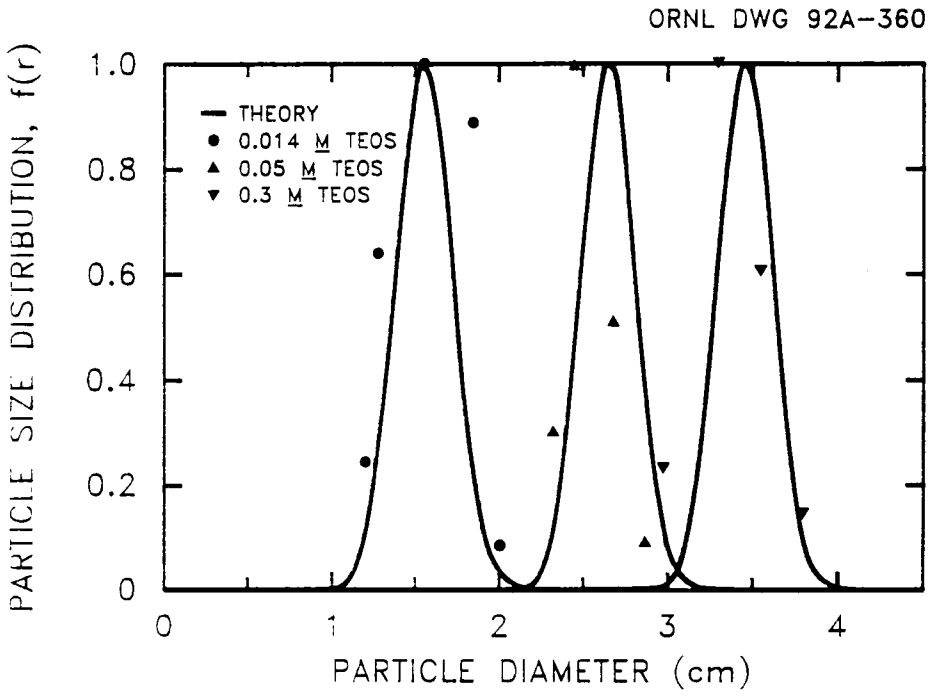



Fig. 2.50 Experimental and predicted particle size distribution (0.014, 0.05 and 0.3M TEOS; 6.0M $H_2O$; and 0.7M $NH_3$ 22°C).

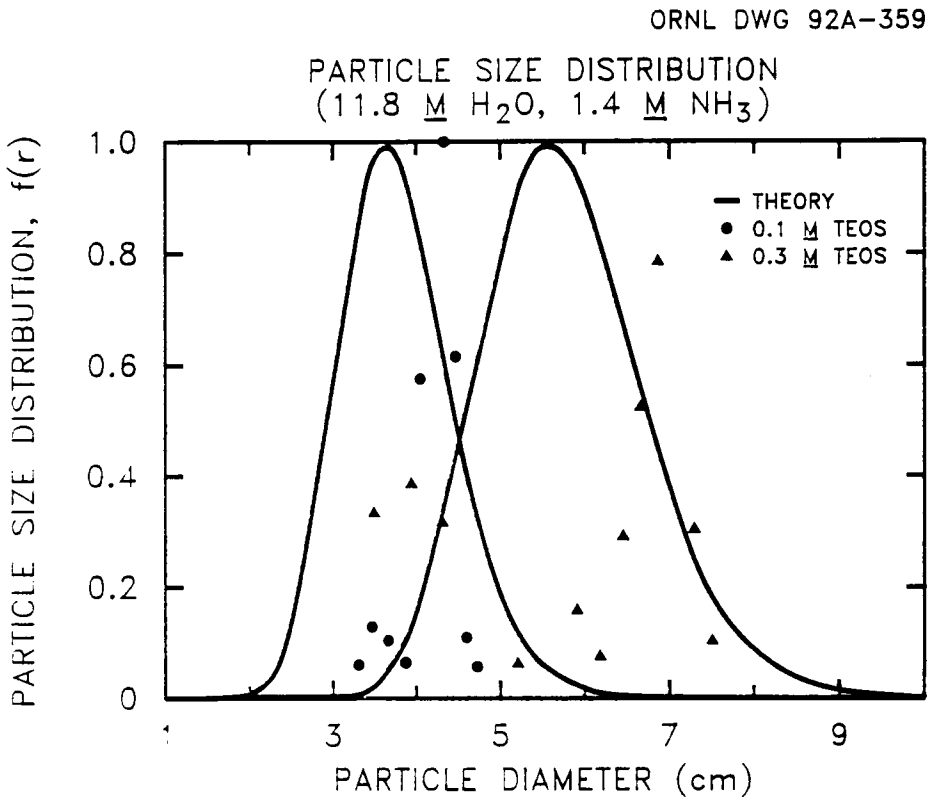



**Fig. 2.51** Experimental and predicted particle size distribution (0.1 and 0.3M TEOS; 11.8M $H_2O$; and 1.4M $NH_3$ 22°C).

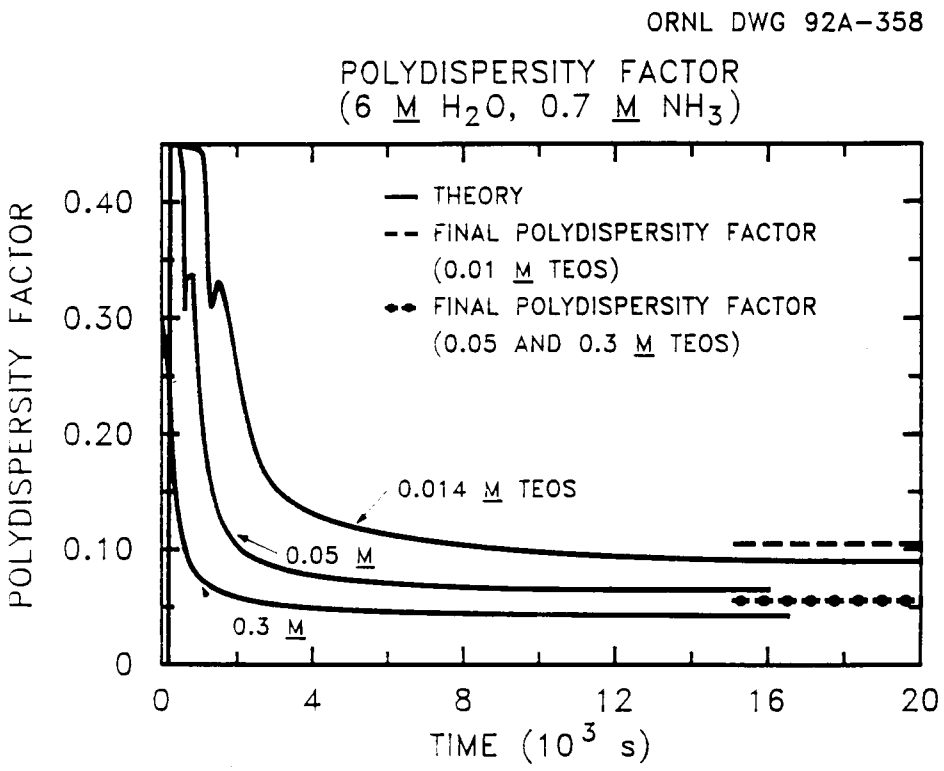



Fig. 2.52 Experimental and predicted polydispersity factor (0.014, 0.05 and 0.3M TEOS; 6.0M $H_2O$; and 0.7M $NH_3$ 22°C).

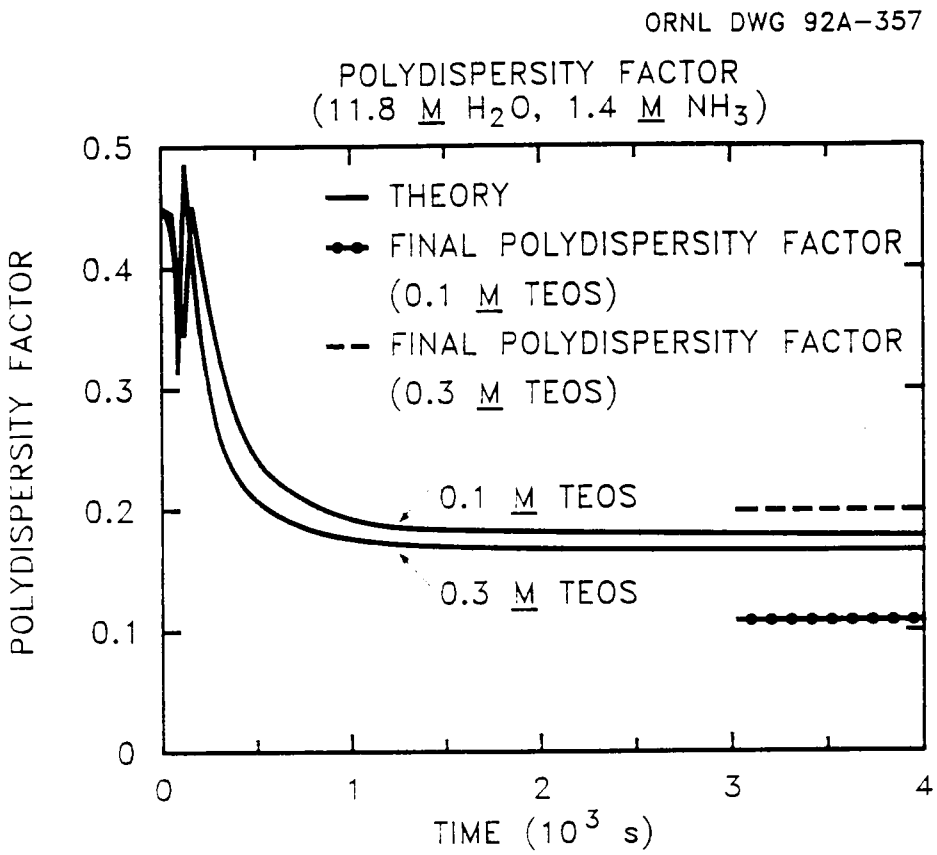



Fig. 2.53 Experimental and predicted polydispersity factor (0.1 and 0.3M TEOS; 11.8M $H_2O$; and 1.4M $NH_3$ 22°C).

molecular weight alcohols. It was observed that the hydrolysis reaction was affected by the alcohol. These effects were explained in terms of hydrogen bonding and the degree of basicity of ammonia in each alcohol. The reaction was fastest when hydrogen bonding was less and the basicity was greatest. Furthermore, the effect of temperature on the hydrolysis reaction was investigated and the hydrolysis rate constant was found to follow an Arrenhius type behavior. The activation energies ranged from 3.5 to 6.9 cal/mol.

A more extensive experimental and theoretical investigation of the hydrolysis and condensation reaction in ethanol was used to test models for silica particle formation and growth from ammonia catalyzed TEOS hydrolysis. The theoretical computations were based on solving the hydrolysis and condensation kinetic expressions and applying the method of moments to expedite the solution of the governing population balance equation. The theoretical model semi-quantitatively predicted particle growth kinetics, size and size distribution and the effect of reactant concentrations on these parameters. These data also indicated that the aggregative growth model is applicable at high water and ammonia concentrations. However, particles grow by the addition of monomer, soluble polysilicates and small ramified precipitates to the particle surface at low water and ammonia concentrations. Thus, it was implied from the current studies that the dominant mechanism varies for the growth of silica particles with reactant and catalyst concentrations.

As a result of this work, it is recommended that additional research is needed to put the rate expressions for the condensation and nucleation kinetics on a more fundamental level. It is also suggested that additional research is needed to develop computationally efficient and accurate methods to predict the

formation of multi-modal distributions of silica particles during the hydrolysis of concentrated TEOS solutions with high water and ammonia concentrations.

# 3. HYDROUS METAL OXIDE POWDER SYNTHESIS BY METAL ALKOXIDE HYDROLYSIS

## 3.1 Introduction

This chapter extends the research of Chapter 2 to oxide particle formation by "true" metal alkoxides. In contrast to TEOS, metal alkoxides exhibit a very rapid hydrolysis step followed by a fast condensation step [Bradley, Mehrotra and Gaur (1978)]. Thus, special precautionary measures must be taken to prevent these compounds from contacting moisture in the air.

Although metal alkoxides are currently expensive and difficult to handle, these materials are very attractive for synthesizing high-purity single and mixed component submicron metal oxide particles as well as thin films. Alkoxides of silicon, titanium, aluminum and zirconium are used extensively in industry and are commercially available at relatively low cost (Livage, Henry and Sanchez 1988).

The objective of this chapter is to determine the effects of pH, solvent and reactant concentration on particle morphology and to relate particle formation and growth to the chemical reactivity of the alkoxide, and the surface properties (colloidal stability) of the precipitate.

## 3.2. Literature Survey

### 3.2.1. Titania Synthesis by Titanium Alkoxide Hydrolysis

Bradley et al. (1978) have reported that the hydrolysis reaction of titanium ethoxide in boiling ethanol is instantaneous. Ishino and Minami (Bradley

et al. 1978) also concluded that the hydrolysis step of titanium 1-butoxide was fast and the condensation reaction was the controlling step for precipitation. Monodisperse particles should, therefore, be more difficult to produce from alkoxide reactions than titanium alkoxides with slower rates of hydrolysis (i.e., tetraethylothosilicate).

Barringer and Bowen (1982) reported the formation of hydrous titania particles from titanium ethoxide and titanium isopropoxide and provided a preliminary analysis of their chemical and physical properties. The reaction mixture contained 0.3 to 1.5M water and 0.1 to 0.2M titanium ethoxide. Monodisperse (0.3-0.6 $\mu$m) hydrous titania powders were formed by the hydrolysis of titanium tetraethoxide in ethanol. The major criteria for synthesizing monodisperse spherical particles included: (a) proper reagent concentrations to promote a single-nucleation regime homogeneous nucleation; (b) proper mixing of reagents to minimize localized reaction zones; and (c) the removal of very small particles ($< 0.1$ $\mu$m) by the rapid growth of the particles to approximately 0.1 $\mu$m. Equiaxed amorphous particles were formed by the hydrolysis of titanium isopropoxide in isopropyl alcohol. These particle size ranged from 0.07-0.3 $\mu$m. The particles were washed with deionized water and ultrasonically dispersed in a slightly basic aqueous solution (pH 9 to 10). Dense compacts were prepared by either gravitational settling or centrifugation. These compacts sintered at temperatures 250-600 °C lower than conventional $TiO_2$ powders.

A more thorough evaluation of the synthesis, physical properties and dispersion stability of titania synthesis by titanium ethoxide hydrolysis was given by Barringer and Bowen (1985). They showed that the removal of the fourth alkoxy group is difficult. Therefore, the following hydrolysis and condensation

reaction schemes are proposed:

$$Ti(OR)_4 + 3H_2O \rightharpoonup Ti(OR)(OH)_3 + 3ROH \ , \tag{3.1}$$

and

$$Ti(OR)(OH)_3 \rightharpoonup TiO_2 \cdot xH_2O + (1-x)H_2O + ROH \ . \tag{3.2}$$

The difficult removal of the fourth alkoxy group has also been reported by Cullinane et al. (1951) and Berglund, Tallant and Dosch (1986).

Ring (1985) used photon correlation spectroscopy and transmission electron microscopy to study the growth kinetics of $TiO_2$ particles during the hydrolysis of titanium ethoxide in ethanol. Initial titanium ethoxide and water concentrations ranged from 0.075 to 0.15M and 0.4 to 0.5M, respectively. The particle formed agglomerates during growth in the solution and, therefore, the particle sizes measured by PCS were always larger than the primary particles sizes obtained by TEM.

Since agglomeration is not desirable for advanced ceramic precursor powders, it was desirable to prevent agglomeration by electrostatic or steric stabilization. Ring (1986) stated that electrostatic forces were weak since the reaction was conducted in a low dielectric constant ($\epsilon$=24) solvent. Therefore, to minimize agglomeration, Ring (1986) used hydroxy propyl cellulose (HPC) as a sterically stabilizing surfactant. Edelson and Glaeser (1988) found that porous monosized titania particles are synthesized during the hydrolysis of titanium ethoxide in ethanol with HPC as the surfactant. Scanning electron microscopy (SEM) and BET surface area measurements showed that these spherical particles were formed by the aggregation of 6 nm primary particles.

Jean and Ring (1986) studied the nucleation and growth of titania during the hydrolysis of titanium ethoxide in ethanol. A short nucleation period (homogeneous nucleation) was assumed and diffusion of polymeric species to the surface of the particles was proposed as the rate-limiting step during growth. The decrease in the standard deviation of the particles with time and the narrow particle size distribution were explained in terms of the short nucleation period and diffusion limited growth mechanism.

Bailey and MeCartney (1990) used cyro-TEM to study the precipitation of titania particles. During the early stage, 3 nm particles were present in solution. Growth was found to occur by the aggregation of these particles.

Zukoski, Chow, Bogush and Look (1990) and Look, Bogush and Zukoski (1990) have shown that the size of titania particles can be decreased and agglomeration can be reduced by increasing the concentration of HCl. This was due to the increase in the surface charge of the titania particles which increased with HCl concentration. No precipitation occurred above a HCl concentration of $8 \times 10^{-3}$M.

### 3.2.2. Zirconia Powders by Alkoxide Reactions

Similar to titanium alkoxides, zirconium alkoxides hydrolyzed rapidly without the aid of an acid or base catalyst. Fegley, Bowen, Rigione and Todd (1983) reported the formation of zirconia powders by the hydrolysis of 0.1 M zirconium n-propoxide or zirconium isopropoxide in ethanol with excess water.

Spherical monodisperse particles (200-300 nm) were formed by zirconium n-propoxide hydrolysis. The particles that were synthesized by zirconium iso-

propoxide hydrolysis were about the same the size; however, they were not as spherical and were more agglomerated.

### 3.2.3 Alumina Powders by Alkoxide Reactions

The hydrolysis of aluminum alkoxides is very rapid; thus, the controlled precipitation of spherical-monodisperse particles has not been achieved (Blendell, Bowen and Coble 1984). However, several techniques have been developed for synthesizing spherical hydrous alumina particles.

Bruce and Matijevic (1973) presented the first method for preparing, purifying and stabilizing uniform spherical aluminum hydrous oxide sols. Dilute aluminum salt solutions ($1 \times 10^{-3}$ to $1 \times 10^{-2}$ are complexed with sulfate ions (Willard and Tang 1937) and aged at 98 °C for days. Spherical particles with a mean diameter of ≈600 nm are formed.

Uniform aluminum hydrous oxide sols were also prepared by the hydrolysis of aluminum sec-butoxide in the presence of sulfates anions (Catone and Matijevic 1974). An aliquot of a 0.4M solution of $Al(OC_4H_9)_3$ in tert-butyl alcohol was added to an aqueous solution of sulfate. A volume of 0.4 to 1.3 ml of this solution was added to 200 ml of the aqueous sulfate solution. The precipitate was ultrasonicated, slowly heated to 99 °C and aged for 2 days at that temperature. The final particles were 450 nm. Sols consisting of spherical "monodisperse" particles formed over a very limited range of concentrations of aluminum alkoxide, sulfate ions and pH. The aluminum alkoxide concentration was typically $2. \times 10^{-3}$.

Yoldas (1974) used aluminum isopropoxide and aluminum sec- butoxide to

prepare alumina sols by using acid to peptize the hydrolysis products of these alkoxides. Hydrolysis was carried out at 75 °C with 1 mole of alkoxide to 100 moles of water to produce a stable monohydroxide of alumina. Peptization was achieved by adding 0.03 to 0.1 moles of acid ($HNO_3$, HCl, or $HCLO_4$) per mol of hydroxide. The peptized solution is clear and depending on the amount of acid, the sol particles are either 5 to 35 nm round particles, or irregular and rectangular particles with dimensions 10-20 nm wide, 4-10 nm long and 5nm thick.

All of the methods discussed above result in a dilute suspension of aluminum hydrous oxide particles. Therefore, it is necessary to develop new homogeneous precipitation techniques to increase the yield of the alumina powders.

High purity alumina powders were synthesized by controlled precipitation techniques from concentrated (0.1 to 1F in Al) aluminum sulfate solutions that used urea and/or formamide as the precipitation agent (Blendell, Bowen and Coble 1984). Upon heating, urea slowly decomposes to form ammonium ions and $CO_2$.

The decomposition of formamide yields ammonium ions and $HCHOOH$. The pH of the solution increases and the solubility of aluminum sulfate hydrate in solution decreases; thus, inducing nucleation. Monodisperse spherical aluminum sulfate hydrate particles were formed in the size regime of 0.1 to 5 $\mu$m. The powders are converted to alumina by heating at 600-900 °C.

Fanelli and Burlew (1986) prepared fine alumina powder from the in situ hydrolysis of aluminum sec-butoxide in alcohol. The water for the hydrolysis reaction was produced by decomposing the solvent (sec-butyl alcohol) in an autoclave at 250 °C for 6 hours. Irregular shaped amorphous particles were

produced with an average particle size of 1350 nm and a standard deviation of 0.38.

Recently, spherical aluminum powders have been produced from initial aluminum sec-butoxide concentrations of 0.2-0.3M (Ayral, Phalippou and Droguet 1988). In this process, the alkoxide reacts with acetic acid in diethyl ether to produce sec-butyl alcohol and aluminum mono-sec-butoxy diacetate. Subsequently, sec-butyl alcohol reacts with acetic acid to produce water by esterification. These series of reactions results in the formation of $Al(OH)(OAc)_2$ which is insoluble in diethyl ether. Precipitation occurs in minutes and depending on the reaction conditions, spherical (250-400nm) amorphous aluminum basic acetate particles are formed. Heating the particles to 300 $^{o}C$ results in the formation of amorphous alumina particles.

Overall, the formation of monodisperse alumina particles by the hydrolysis of unmodified aluminum alkoxides has not been achieved. However, high purity mixed hydrous metal oxides of aluminum and titanium are important as advanced ceramics.

### 3.2.4 Alumina-titania and titania-zirconia powders by alkoxide reactions

The previous sections reviewed the formation of single component powders; however, advanced ceramics require the use of ultrafine mixed oxide powders. Ideally, each submicron particle should have the correct stoichiometry on the smallest possible level. Alkoxides can be combined to produce mixed (di-, tri-, etc.) metal alkoxides (Bradley, Mehrota and Gaur 1978). When hydrolyzed correctly, chemical homogeniety is achieved on the nanometer level.

Alumina-titania and titania-zirconia systems were studied in this research because of their relative rates of hydrolysis and importance in industry. Mixed oxide particles of alumina and titania are important in the formation of aluminum titanate-based ceramics. Ordinarily, a stoichiometric mixture of $TiO_2$ and $Al_2O_3$ powders is prepared by ball- milling and isostatic pressing (Heistand 1985). These techniques, however, do not result in homogeneity on the microscopic level and do not allow for the control of particle size and morphology. Several methods (aerosol reactor-alkoxide drops (Ingebrethsen, Matijevic and Partch 1981); coating titania, by titanium alkoxide hydrolysis, on colloidal alumina substrates Okamura, Barringer and Bowen 1986) have recently been developed to produce a more ideal powder (i.e., monodisperse, spherical, and homogeneous particles). However, little information has been reported on the synthesis of alumina-titania particles by the low-temperature hydrolysis/homogeneous precipitation of mixed metal alkoxide solutions.

This research focuses on the formation of mixed alumina-titania particles by the hydrolysis of mixed metal alkoxide solutions in low-molecular-weight alcohols. Ultimately, the goal of this research is to understand the mechanisms that govern the synthesis of monodisperse particles of aluminum titanate ($Al_2TiO_5$) by the homogeneous precipitation of mixed metal alkoxides.

The formation mixed oxide particles of zirconium and titanium have not been reported. However, such powders are of interest in the formation of $Pb(Zr_{0.53}Ti_{0.47})O_3$ (PZT) piezoelectric ceramics. Fukai, et al. (1990) have shown that PZT ceramics sinter at lower temperatures when mixed $Zr_xTi_{1-x}O_2$ powders are used. The conventional method is to mix and sinter PbO, $ZrO_2$ and $TiO_2$ powders.

In addition to their industrial importance, alumina-titania and zirconia-titania are model compounds for studying the effect of the relative rates of hydrolysis-condensation and surface properties on the mixed oxide particle synthesis by metal alkoxide hydrolysis. Titania and zirconia have similar hydrolysis-condensation kinetics and surface properties. On the other hand, the hydrolysis-condensation of alumina is much faster than that of titanium and zirconium alkoxides and the surface properties are also quite different.

### 3.2.5 Surface charge of Titania, Alumina and Zirconia Particles

Contrary to conventional theories that attempt to describe the formation of metal hydrous oxide particles by homogeneous nucleation, more recent models (Zukoski, et al. 1990, and Jee- Loon Look, Bogush and Zukoski 1990) suggest that these particles grow by the controlled aggregation of primary nanometer particles. Therefore, the surface properties of hydrous metal oxide particles are very important in controlling their size and monodispersity.

Barringer and Bowen (1985) determined the electrochemistry of titania particles that were synthesized by the hydrolysis of titania alkoxides. The point of zero charge for these powders occurred at a pH of $\approx$4.5 for freshly washed powders and $\approx$5.5 for particles aged in water for 3 months. Zeta potentials in the range of interest for this research (pH>4.5) were less between 0 to -30mV.

Baik, Bleier and Becher (1986) and Bleier and Westmoreland (1988) have examined the electrophoretic mobility of $\alpha$-alumina and $m$-zirconia particles. Points of zero charge for alumina and zirconia were pH 7.8-8.2 and pH 5.7-6.8, respectively. Lee and Hench (1987) determined the electrophoretic behavior of

alumina powders that were synthesized by the hydrolysis of aluminum alkoxides and calcined at various temperatures. The point of zero charge ranged from pH 8.3 to 10.3 for powders calcined at >500 to 25 °C.

### 3.2.6. Chemical Analyses

Infrared spectra of titanium alkoxide have been reported by Lynch et al. (1964). Barrough et al. (1963) and Bradley et al. (1978) discuss the use of infrared and NMR spectroscopy to study aluminum, zirconium and titanium alkoxides in solution. Sanchez et al. (1988) used ($^1$H, $^{13}$C) NMR and Infrared spectroscopy to study the formation of gels from titanium isopropoxide and titanium butoxide in the presence of acetic acid and acetylacetone. Time resolved UV-Raman spectroscopy has been used to study the hydrolysis kinetics of titanium isopropoxide and to determine the presence of unreacted alkoxy groups in the final powder (Berglund et al. 1986).

It is also well known that titanium in the presence of sulfate reacts with hydrogen peroxide to produce an intense orange color (Cotton and Wilkinson 1980). The main peroxo species is probably $[Ti(O_2(OH)aq]^+$. A modification of this method can be used to study the condensation of dilute solutions of titanium alkoxdies by colorimetric methods.

## 3.3. Experimental

Metal hydrous oxide particles were synthesized by the hydrolysis of either titanium ethoxide, zirconium n-butoxide or aluminum sec-butoxide (Alfa Products) in ethanol–water, 1-propanol–water, 1-butanol–water, 2-butanol–water,

and tert-butyl alcohol–water mixtures. All reagents and solvents, except for the ethoxide, were passed through a 0.22-$\mu$m filter to minimize heterogeneous nucleation. The alkoxides were purchased from ALFA products. Separate solutions of alcohol–water and alcohol–alkoxide were prepared to minimized localized reaction zones. Mixed aluminum-titanium alkoxide stock solutions are prepared that contain a total metal alkoxide concentration of 3.0 mol/L and initial $Al^{3+}$:$Ti^{4+}$ (aluminum *sec*-butoxide (ASB): titanium ethoxide (TIE)) molar ratios of 0.00:1.00, 0.39:1.00, 0.81:1.00, 1.50:1.00, and 2.00:1.00 in 1-butanol. The reaction mixtures for the homogeneous precipitation studies are prepared by diluting the pure alkoxide or stock solutions to total metal concentrations of 0.02 to 0.225 mol/L in an appropriate solvent (i.e., anhydrous ethanol, 1-propanol, 1-butanol, 2-butanol, or tert-butanol). Separate solutions of alcohol-water and alcohol-alkoxide are prepared to minimize localized reaction zones. The two solutions are rapidly mixed for approximately 5 s. Immediately after mixing, a fraction of the sample is transferred to a clean quartz-spectrophotometer cell for particle size analysis by dynamic light scattering.

Fourier transform infrared absorption spectroscopy was employed to determine if alcoholysis occurred when the metal alkoxide was mixed with alcohol solvents other than ethanol. A Michelson 100 spectrometer (Bomem Inc.) with IBM Personal computer interfacing capabilities was used to obtain these infrared absorption spectra. Liquid samples were contained in a ZnSe flowthrough cell. The characteristic peaks of the metal alkoxide and water were determined by subtracting absorption due to the solvent.

The water concentration (as an impurity) in each solvent was initially determined by the Karl-Fischer method. Water concentrations as an impurity in

the "pure" solvents ranged from 0.04 mol/l in ethanol and 1-butanol to 0.222 mol/l in tert-butyl alcohol. The water concentration during the reaction was determined by filtering the sample through 0.22 $\mu$m filter paper and reading the absorption of the 1655 $cm^{-1}$ peak of FTIR spectra. The concentration of soluble titania was determined by either filtering the sample or centrifuging a portion of the sample at 4000 to 15,000 rpm for 10 to 20 min and subsequently adding a portion of the supernatant to 4% hydrogen peroxide for the colorimetric determination of soluble titania (Sandell 1959).

TEM, SEM, and dynamic light scattering analysis were used to determine particle shape and growth kinetics. Electron dispersive X-ray (EDX) microprobe spectroscopy was employed to determine the composition of metal atoms in the particles.

## 3.4. Theory

### 3.4.1. Chemistry

The following hydrolysis and condensation reactions for the synthesis of alumina hydrous oxide particles by alkoxides have been proposed (Yoldas 1988 and Yoldas 1973):

$$Al(OR)_3 + 2H_2O \rightharpoonup Al(O)(OH) + 3ROH \ ,$$

and

$$Al(O)(OH) + H_2O \rightharpoonup Al(OH)_3, \tag{3.3}$$

$$Al(OR)_3 + H_2O \rightarrow Al(OR)_2(OH) + ROH\ , \tag{3.4}$$

and

$$2Al(OR)_2(OH) + H_2O \rightarrow (RO)(OH)AlOAl(OH)(OR) + 2ROH. \tag{3.5}$$

The hydrolysis of aluminum alkoxides is very rapid.

Mazdiyasni, Lynch and Smith II (1967) have proposed the following reactions for the hydrolysis and condensation of zirconium alkoxides

$$Zr(OR)_4 + H_2O \rightarrow Zr(O)(OR)_2 + 2ROH\ , \tag{3.6}$$

and

$$Zr(O)(OR)_2 \rightarrow ZrO_2 + Zr(OR)_4. \tag{3.7}$$

The controlling step is the first hydrolysis reaction. It is interesting that the formation of zirconium hydroxides are not proposed. Whereas, hydroxides of aluminum are easily formed.

The overall hydrolysis and condensation reactions for titanium alkoxides are given in section 3.2. . Barringer and Bowen (1985) proposed the following rate expression for the hydrolysis reaction

$$\frac{\mathrm{d}[Ti(OR)_4]}{\mathrm{d}t} = k_H[H_2O]^3[Ti(OR)_4] \tag{3.8}$$

In addition to obtaining overall hydrolysis and condensation expressions, a deeper understanding of mechanisms that govern the reactivity and polymerization of metal alkoxides is needed to explain gel-particle morphology. This is discussed in the next section.

### 3.4.2. Evaluating Chemical Reactivity by Partial Charge Analysis

The reactions of metal alkoxides can be represented by the following equation

$$M(OR)_n + mXOH \rightarrow M(OR)_{n-m}(OX)_m + mROH \qquad (3.9)$$

where for X=H, M, or R′ in Eq. 3.9 represents either a hydrolysis, condensation or alcoholysis reactions, respectively. Each of these reactions can be described by the three step process (Livage and Henry 1988):

1. Nucleophilic addition of negatively charged OH group to positively charged metal atom M.
2. Proton transfer within the transition state complex from the entering ligand (XOH) toward a negatively charged oxygen of an adjacent OR group.
3. Departure of the protonated (ROH) species.

The reaction denoted by Eq. 3.9 therefore depends on the partial charge distribution. Thus, the following conditions must be fulfilled

$$\delta(M) > 0, \delta(OR) < \delta(H), \delta(ROH) > 0$$

The limiting step for the overall reaction occurs when the above condition for that step is not met. Therefore, it is necessary to compute the partial charge of various groups in the reactant, intermediate products and transition state complexes.

A model for doing this has been developed by Livage and Henry (1988). It is based on the principle of "electronegativity equalization" (Sanderson 1951) which states: "When atoms of different electronegativity combine, they adjust to the same intermediate electronegativity in the compound". In addition to the

electronegativity equalization principle, the following are employed to develop the model by Livage and Henry:

a. Electronegativity varies linear with its charge.

$$\chi_i = \chi_i^o + \eta_i \delta_i \tag{3.10}$$

b. The hardness is determine by the equation

$$\eta_i = k\sqrt{\chi_i^o} \tag{3.11}$$

where, $k = 1.36$.

c. Charge is conserved

$$Z = \sum p_i \delta_i \tag{3.12}$$

where $p_i$ corresponds to the stoichiometry of atom i.

Eqs. 3.10 to 3.12 can be solved to show that the mean electrtonegativity of a molecule is

$$\overline{\chi} = \frac{\sum_i p_i \sqrt{\chi_i^o} + 1.36z}{\sum_i (p_i/\sqrt{\chi_i^o})} \tag{3.13}$$

The partial charge distribution on group (G) is given by

$$\delta(G) = S(G)(\overline{\chi} - \chi^o(G)) \tag{3.14}$$

where S(G), the softness of group (G), is given by

$$S(G) = \frac{\sum_i (p_i/\sqrt{\chi_i^o})}{1.36} \tag{3.15}$$

This model has been used to show that the fourth alkoxy group is difficult to remove from titanium alkoxides (Livage, Henry and Sanchez 1988). The

relative rates of hydrolysis have also been predicted by this model where it is shown that the partial charge of zirconium and titanium are greater than that of silicon in metal alkoxides. Hydrolysis is fastest in the alkoxide with the more electropositive metal atom (Ti, Zr, and Al). Various chemical modification and polymerization reactions have been predicted by analyzing the partial charge distribution (Sanchez, Livage, Henry and Babonneau 1988). Furthermore, the effect of acid and base catalyst on the hydrolysis and condensation reactions evaluated by the partial charge model. It was found that, in accordance with experiment, acid catalyst results in the formation of linear polymers; while, high cross-linked polymers are formed with base catalyst (Livage, Henry and Sanchez 1988). This method will be used in the present research to explain the chemical reactivity and polymerization of aluminum alkoxide systems.

## 3.5. Results and Discussion

### 3.5.1. Alcoholysis and Hydrolysis Reactions

#### 3.5.1.1. Titanium alkoxides

Before examining the nature of particle growth kinetics, it is necessary to understand the alcoholysis and hydrolysis reactions. Since the titanium ethoxide and water are mixed in separate portions of alcohol, it is possible that alcoholysis will occur in the "water-free" titanium ethoxide solution. Fourier transform infrared spectroscopy (FTIR) with solvent subtraction is, therefore, used to determine the chemical species in this solution. This analysis is performed in less than two minutes after adding the titanium ethoxide to the solvent. The major

characteristic peaks at 1369, 1130, 613, 600 and 574 $cm^{-1}$ are observed when titanium ethoxide is added to ethanol and 1-butanol. However, characteristic peaks at 1011, 793, and 599 $cm^{-1}$ are observed when tert-butyl alcohol is the solvent. Infrared spectra reported by other investigators show strong characteristic absorptions at 1136, 1101, 1064, 916, and 625-500 $cm^{-1}$ for titanium ethoxide in a two-solvent system of carbon disulfide and carbon tetrachloride (Barrough, et al. 1961) and 1190, 1008, 909, 797, and 597 $cm^{-1}$ for tert-butyl alcohol in carbon disulfide (Lynch et al. 1964). Spectra in the former study (Barrough et. al. 1961) were recorded over the range 500 - 1300 $cm^{-1}$. Comparison of the characteristic peaks that are observed in the present study with those given in the literature for titanium ethoxide and titanium tert-butoxide, it is seen that alcoholysis occurs very rapidly (in less than 2 minutes) between titanium ethoxide and the tert-butyl alcohol. Complete alcoholysis does not occur since it is rather difficult to replace the last ethoxy group with a tert-butoxy group (Bradley, Mehrotra, and Gaur 1978). It is also postulated that alcoholysis also occurs between titanium ethoxide and the 1-butanol solvent since alcoholysis occurs more readily with unbranched moieties than branched ones.

The hydrolysis of titanium ethoxide in 2-butanol resulted in the immediate formation of a yellow reaction complex upon the addition of water. This did not occur in the other alcohol solvents; therefore, it is postulate that the alcoholysis occurs in 2-butanol.

Several investigators (Berglund, Tallant and Dosch 1986, Barringer and Bowen 1985 and Bradley, Mehrotra and Gaur 1978) suggest that hydrolysis is fast and that the condensation reaction is slow for titanium alkoxides. Livage, Henry and Sanchez (1988) have shown from partial charge calculations that the

first two iso-propoxy groups are readily removed from titanium iso-propoxide. In this study, the rate of hydrolysis is evaluated by using the cobalt chloride method to follow the water concentration in ethanol and 1-butanol solvent systems. Water concentrations in ethanol and tert-butyl alcohol are also determined by the Karl-Fischer method and Fourier transform infrared spectroscopy. In all cases, the moles of water consumed achieved a level of approximately 2 to 3 times the initial moles of titanium ethoxide within the first minute of the reaction. During the induction period, the time between the mixing of the reagents and the first observation of particles in the mixture, the water consumption does not proceed beyond the value achieved in the first rapid period of the reaction. Table 3.1 gives the induction time, $t_i$, which is greater than the approximately 1 minute period during which hydrolysis reaction occurs. Therefore, it is concluded that the hydrolysis reaction is fast and that the condensation reaction is slow for the hydrolysis of titanium alkoxides in ethanol, 1-butanol, and tert-butyl alcohol. Furthermore, the observation that approximately 3 moles of water was consumed during this one minute hydrolysis period suggests that Eq. 3.1 is correct and that the precipitation reaction proceeds from the condensation of the titanium hydroxide alkoxide species, $Ti(OC_2H_5)(OH)_3$ or $Ti(OC_4H_9)(OH)_3$.

Barringer and Bowen (1985) used $t_i$ as a function of $[H_2O]$ and $[Ti(OC_2H_5)_4]$, to determine the reaction kinetics of the hydrolysis reaction; however, our data (Table 3.1) show that, for reactant concentrations much less than those used in Barringer and Bowen's study, most of the induction time is due to the delay period between the completion of the initial-phase hydrolysis reaction and the subsequent precipitation reaction. In this case, the variation of $t_i$ with water and $[Ti(OC_2H_5)_4]$ concentrations will not yield the correct information about

Table 3.1. Effect of initial titanium ethoxide and water concentration on the induction period.

| $[Ti(OC_2H_5)_4]$ (mol/L) | $[H_2O]$ (mol/L) | Solvent | $t_i$ min |
|---|---|---|---|
| 0.0078 | 0.36 | ethanol | 188 |
| 0.016 | 0.36 | ethanol | 15 |
| 0.023 | 0.36 | ethanol | 7.25 |
| 0.032 | 0.36 | ethanol | 5 |
| 0.016 | 0.71 | ethanol | 6.5 |
| 0.016 | 1.06 | ethanol | 3.3 |
| 0.016 | 0.38 | 1-butanol | 120 |
| 0.032 | 0.38 | 1-butanol | 51.8 |
| 0.062 | 0.38 | 1-butanol | 33.8 |
| 0.032 | 0.80 | tert-butanol | 10.3 |
| 0.047 | 0.80 | tert-butanol | 4 |
| 0.071 | 0.80 | tert-butanol | 4 |

the hydrolysis reaction kinetics. The data in Table 3.1 suggest that $t_i$ varies inversely with $[H_2O]$ and $[Ti(OC_2H_5)_4]^2$, where these concentrations represent the initial values.

3.5.1.2. Zirconium, titanium-zirconium and titanium-aluminum alkoxides

Like titanium alkoxides, the hydrolysis of zirconium butoxide is apparently faster (i.e., occurring within 1 min) than the condensation reaction in all alcohols. Based on infrared spectroscopic analysis, approximately 4 moles of water were consumed per initial mol of zirconium butoxide. This is an interesting finding since zirconium does not form hydroxides (Yoldas 1982 and Mazdiyasni, Lynch and Smith 1961; see Eq. 3.7)

This reaction scheme was developed from studies in which the water-to-alkoxide ratio was less than 2.0. In the present study, the water to zirconium butoxide ratio is greater than 6, which suggests that the zirconium alkoxide reaction is more complex than that indicated by Eqs. 3.7. Further studies are needed to elucidate the reaction mechanism of this system.

An induction period is observed after the fast hydrolysis reactions. The length of this period is affected by the solvent medium, where the period is shortest in ethanol and the branched butyl alcohols. In 1-butanol, the induction time is considerably longer than in the other alcohols, which suggests that the condensation process and/or the degree of polymerization in metal alkoxides is very dependent on "unhydrolyzed" alkoxy groups. A study of the induction period for "titania" and "zirconia" systems suggests that condensation occurs considerably faster for "zirconia".

Equations 3.1-3.6 describe the possible overall hydrolysis and condensation reactions for titanium-aluminum mixed alkoxide solutions. Considering the dialkoxides of zirconium and aluminum (Bradley, Mehrotra and Gaur 1978), the following dialkoxides are possibly formed when aluminum and titanium alkoxides are mixed

$$nAl(OR)_3 + Ti(OR)_4 \rightleftharpoons Al_2Ti(OR)_{10} \text{ and/or } AlTi(OR)_7 \qquad (3.16)$$

The formation of this dialkoxide has not been reported; however, when these aluminum and titanium alkoxides are mixed an exothermic reaction occurs and a white precipitate is formed. As the reaction proceeds, the precipitate dissolves and a clear homogeneous solution is formed. No hydrolysis or condensation reaction equations have been proposed for the aluminum-titanium dialkoxides. Therefore, the hydrolysis and condensation of mixed aluminum-titanium alkoxide solutions will be explained in terms of Eqs 3.1-3.6.

For initial ASB:TIE molar ratios of 1:1 and 2:1, 6 and 9 mol of water per initial mol of TIE are used in the hydrolysis and condensation reactions (Eqs. 3.1-3.6). This indicates that the value of $x$ in Eq. 2 is between 0 and 0.4.

### 3.5.2. Condensation and Particle Growth Kinetics

#### 3.5.2.1. Titanium hydrous oxide

The slower condensation reaction that succeeds the fast hydrolysis reaction ultimately results in the precipitation of "titania" particles. The quotation

marks are used to indicate that the precipitate is hydrated and that it also possibly contains unhydrolyzed ethoxy groups (Berglund, Tallant and Dosch 1986).

Figs. 3.1 to 3.3 show the concentration of the total soluble titania during the hydrolysis of titanium ethoxide in ethanol and 1-butanol. These data show that the total soluble titania concentration decreases to an equilibrium concentration. The reduction in the total soluble titania concentration occurs over a considerably longer time (thousands of seconds) than the very rapid hydrolysis of the first couple of alkoxy groups. During condensation, partial charge analysis suggests that the following alcoxolation and hydrolysis-alcoxolation reactions are possible:

$$Ti--OR + HO--Ti \rightarrow Ti--O--Ti + ROH \text{ and/or} \qquad (3.17)$$

$$Ti--OR + H_2O + RO--Ti \rightarrow Ti--O--Ti + 2ROH \text{ and/or} \qquad (3.18)$$

If Eq. 3.18 is the limiting reaction, the induction period, $t_i$, for our studies should varied inversely with $[Ti(OC_2H_5)_4]^2$ and $[H_2O]$. This was observed experimentally and was reported in section 3.4.1.2.

The Fig. 3.1 to 3.3 suggest that the yield of titania particles is significantly <100%. The equilibrium concentration is reduced by increasing the initial water concentration. It is also shown that the rate of condensation and yield are enhanced by increasing the reaction temperature. Fig. 3.3 also illustrates that the condensation rate is faster in ethanol than in 1-butanol; however, the yield of titania particles is improved slightly in 1-butanol.

Particle growth is followed by dynamic laser-light scattering during the very early stages of the condensation reaction such that the concentration of the disperse-phase material, $Ti(OC_2H_5)(H_2O)_3$ or $Ti(OC_4H_9)(OH)_3$, is essentially

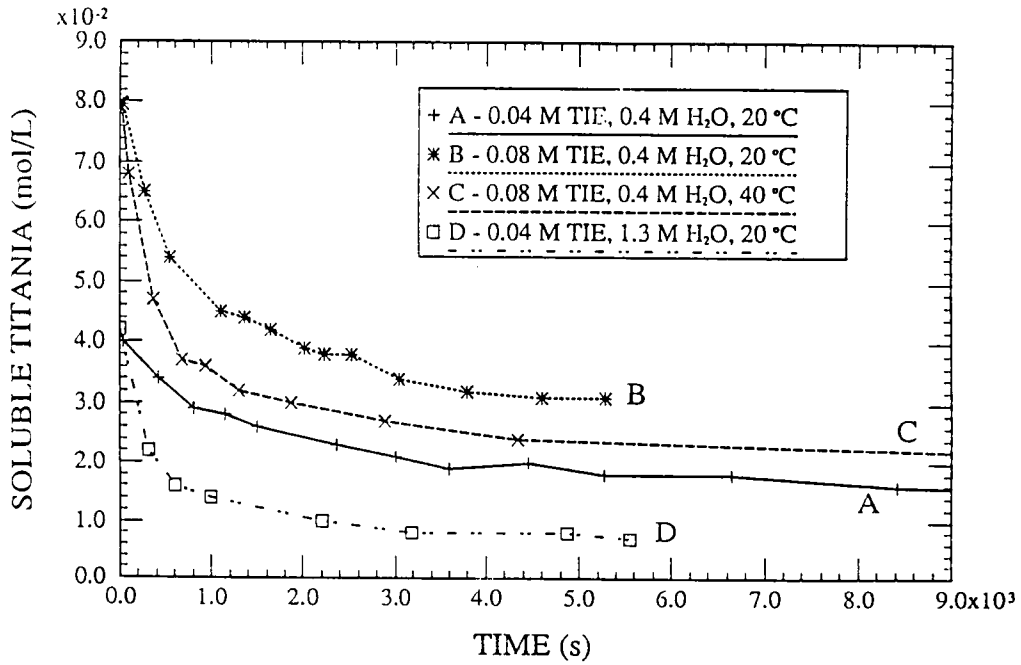



Fig. 3.1. Soluble Titania Condensation Kinetics: Hydrolysis of Titanium Ethoxide in Ethanol.

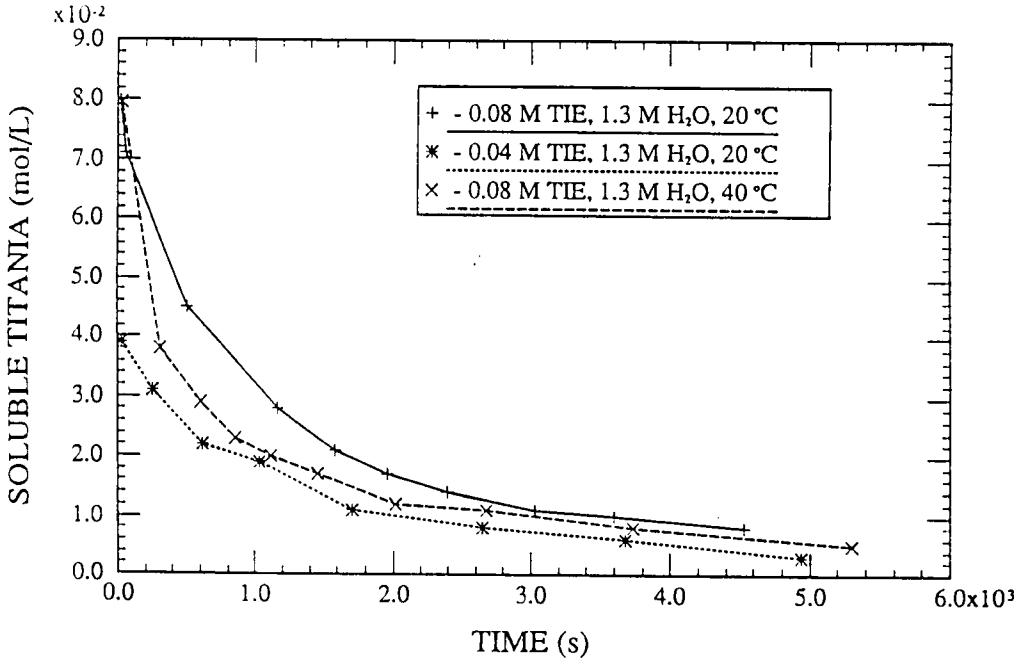



Fig. 3.2. Soluble Titania Condensation Kinetics: Hydrolysis of Titanium Ethoxide in 1-Butanol.

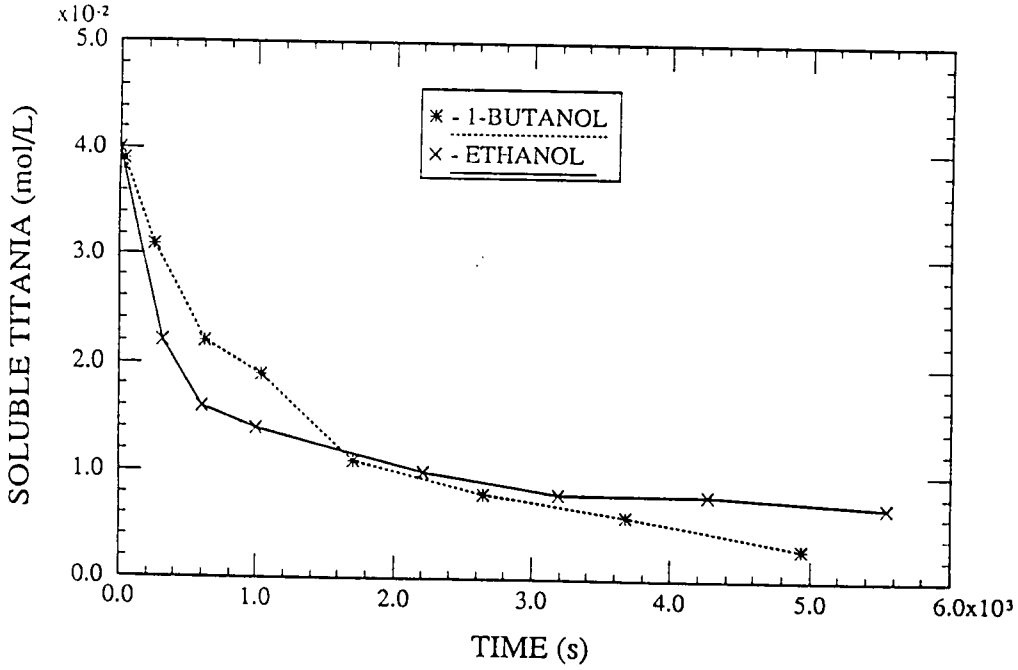



Fig. 3.3. Soluble Titania Condensation Kinetics: Comparison of Titanium Ethoxide Hydrolysis in Ethanol and 1- Butanol.

constant. Due to the fast hydrolysis reaction, the concentration of the disperse-phase material is equal to the initial concentration of $Ti(OC_2H_5)_4$. The sample is also mildly turbid during the dynamic laser-light scattering measurements. As the turbidity of the sample increases, analysis of the light scattering signal becomes complicated by multiple scattering and particle-to-particle interactions (Dahneke 1982).

Typical plots of the average hydrodynamic particle size ($d_H$) in ethanol are presented in Fig. 3.4. The data were determined by dynamic light scattering. The size increases linearly for precipitation reactions in ethanol. It is interesting to note that the first observed particle size by dynamic laser light scattering was approximately 0.2 $\mu$m. It is easily within the analytical capability of the laser-light scattering equipment to observe particles in the 0.01-$\mu$m size range; therefore, it may be concluded that no coherent mass of particles occurs until a 0.2-$\mu$m particle is "assembled".

Since particle size measurements by laser-light scattering requires approximately 1 minute for data collection and analyses, the assembling of mass to form the 0.2-$\mu$m particles must occur rapidly once the precipitation process has begun. Barringer and Bowen reports that one of the requirements for synthesizing monodisperse $TiO_2$ particles is the rapid growth of particles to a size of $>0.1$ $\mu$m [8]. This would minimize the presence of very small particles (i.e., $< 0.1$ $\mu$m) which have a tendency to flocculate, thus, resulting in uncontrolled precipitation. Under the experimental conditions of the reaction, the desired conditions are met. However, contrary to the assumption of Barringer and Bowen that titania particles are formed by homogeneous nucleation, Bailey and MeCartney (1990) observed that titania particle are formed by the controlled aggregation

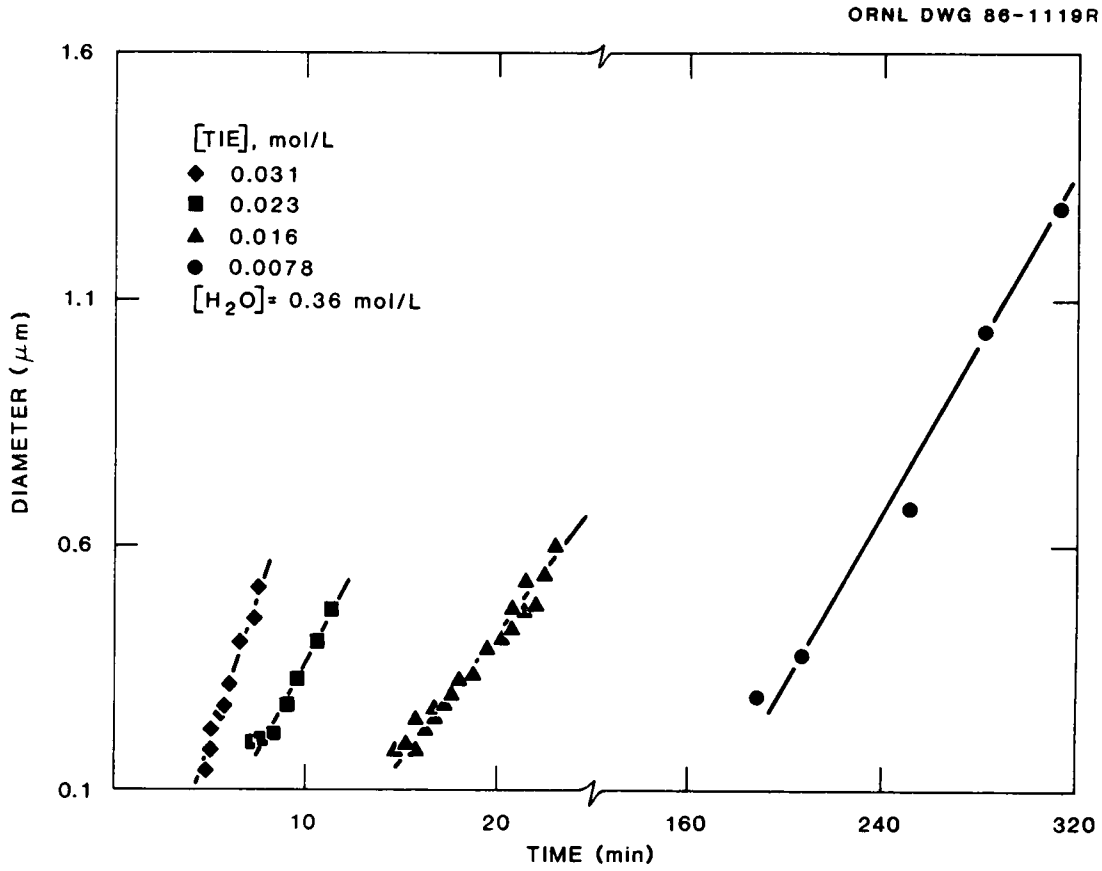



Fig. 3.4. Titania Growth Kinetics: Hydrolysis of Titanium Ethoxide in Ethanol.

of 3 nm particles. With proper kinetic data, the detailed population chemical kinetic model developed for silica in Chapter 2 can be applied to the titania system.

Fig. 3.5 shows the linear growth behavior of the "titania" particles from about 0.2- to 0.4-$\mu$m in 1-butanol. It is interesting to note that as with ethanol, the first observed particle size by dynamic laser-light scattering was approximately 0.2-$\mu$m. Similar to reactions in ethanol, dynamic laser-light-scattering measurements indicate that the particles are fairly monodisperse in solution. The effect of the initial concentration of titanium ethoxide in 1-butanol on the rate of particle growth and induction time, $t_i$, is also shown on this plot. The induction time decreases as the initial concentration of titanium ethoxide increases.

Scanning electron micrographs of dried titania particles in ethanol and 1-butanol are shown in Fig. 3.6. The powders were dried directly from the alcohol-water solutions without further preparation to minimize agglomeration upon drying; therefore, the observed particle agglomeration was probably due to precipitation of the unreacted "titania" and the drying process. Looking beyond the agglomeration, the particles are spherical and monodisperse. The particle size is $\approx$0.2-0.6 $\mu$m for reactions in ethanol and 1-butanol, and the particles are quite monodisperse. Transmission electron micrographs of titania particles synthesized in ethanol and 1-butanol are shown in Figs. 3.7 and 3.8. Once again, the particles produced in ethanol and 1-butanol appear spherical and, although agglomerated upon drying, are monodisperse.

Particle sizes measured by electron microscopy are $\approx$50% smaller than those measured by dynamic light scattering. The difference in the particle sizes can

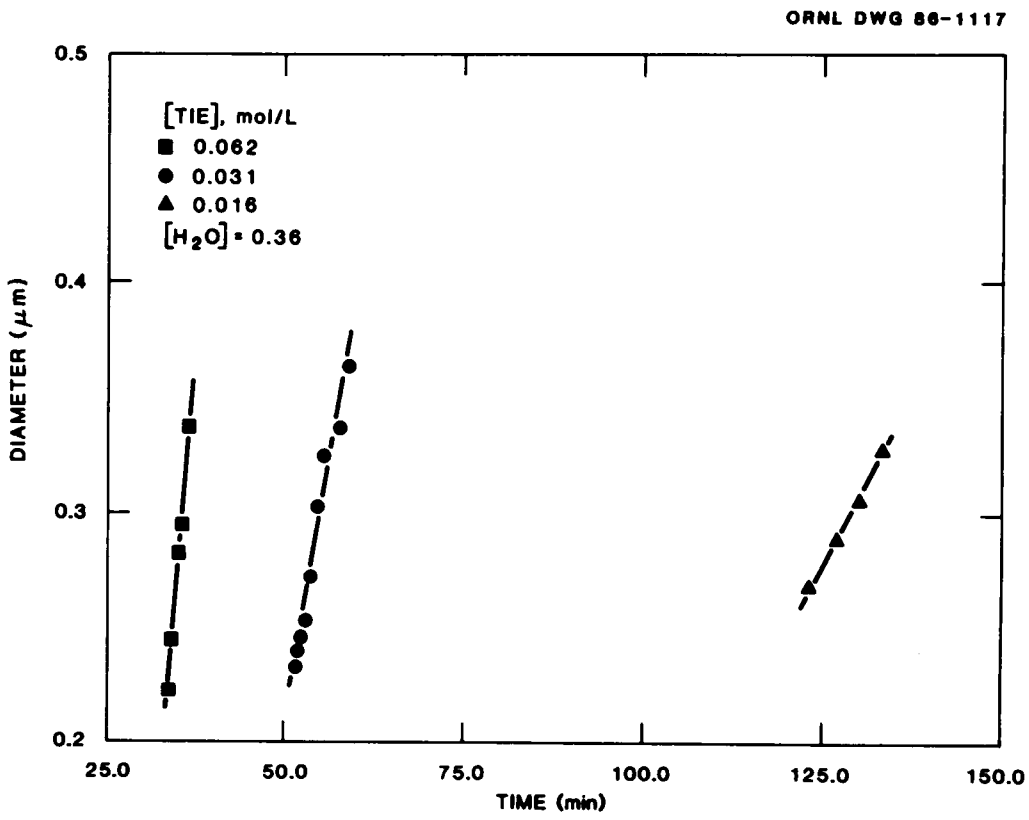



Fig. 3.5. Titania Growth Kinetics: Hydrolysis of Titanium Ethoxide in 1-Butanol.

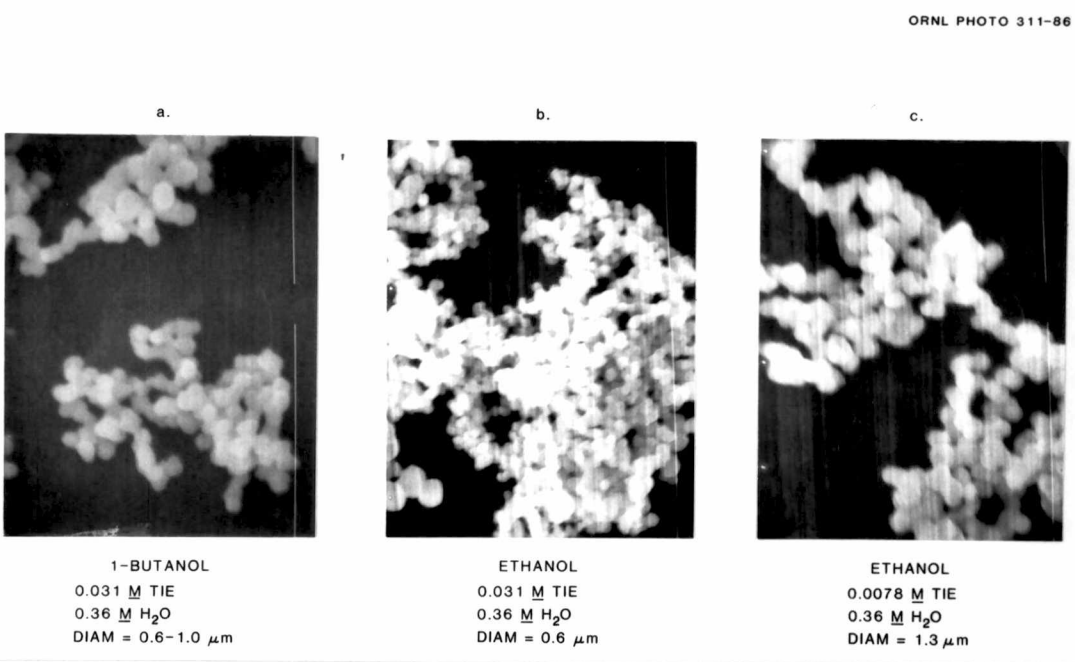



Fig. 3.6. Scanning Electron Micrographs of Titania Particles Synthesized in Ethanol and 1-Butanol.

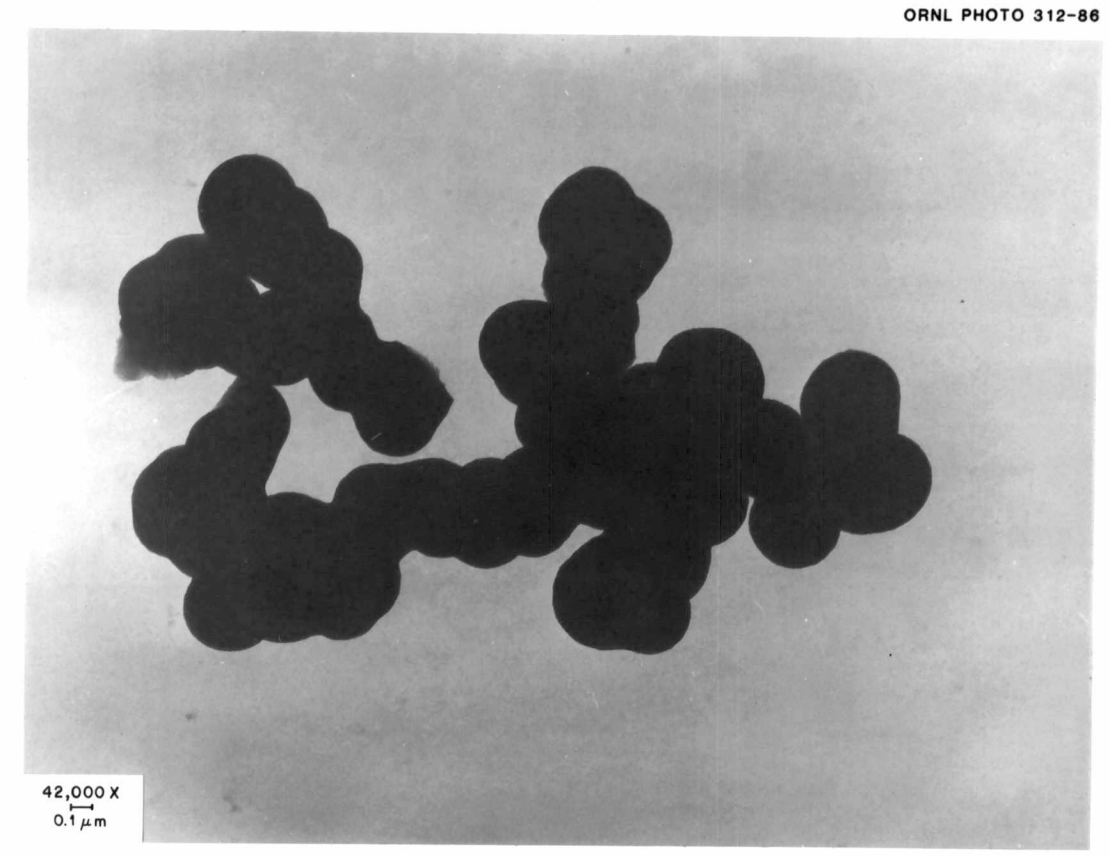



Fig. 3.7. Transmission Electron Micrograph of Titania Particles Synthesized in Ethanol.

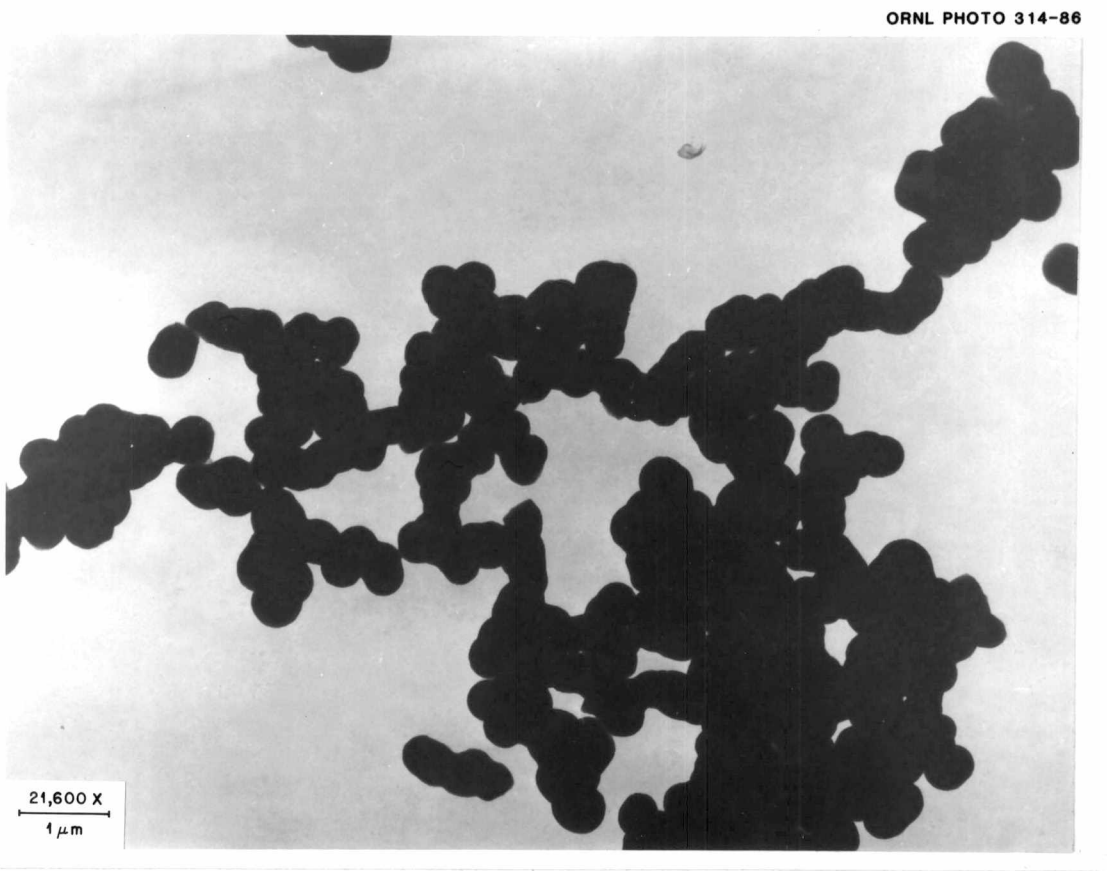



Fig. 3.8. Transmission Electron Micrograph of Titania Particles Synthesized in 1-Butanol.

not be accounted for by shrinkage during drying. Therefore, unlike the silica particles, the larger >0.1 $\mu$m titania particles are aggregating in solution which results in the larger hydrodynamic radii as measured by DLS.

The particle growth behavior in tert-butyl alcohol yield kinetic plots that are quite different from those obtained for growth in ethanol or 1-butanol. These plots show an increase in the rate of growth with time (Fig. 3.9). The condensation reactions for this system results in the growth of linear polymers, rather than, the more crosslinked polymers that are formed in ethanol and 1-butanol. It is postulated that the slow growth regime represents the situation in which most of the disperse-phase material is used to form new nuclei and the subsequent particle growth is very slow. Therefore, the initially observed particle sizes during this slow-growth regime represent the hydrodynamic diameter of the initial insoluble polymer. The particles that are produced in tert-butyl alcohol during this period are very small (i.e., diameter = 0.02 $\mu$m).

As reported for the formation of silica particles, the initial insoluble polymers must collapse to form dense primary nuclei that subsequently rapidly aggregate to formed larger particles. If these particles do not collapse, a gelatinous precipitate is formed.

In evaluating the particle growth rate behavior that is observed in tert-butyl alcohol, it is known that very small particles, < 0.1 $\mu$m, are susceptible to flocculation on collision due to Brownian motion of these particles (Barringer and Bowen 1985). Therefore, it is likely that, as the concentration of nuclei in the solution increases, the collision frequency between these nuclei increases; thus, flocculation occurs. This is depicted by the rapid increase in growth rate at later times. Futhermore, smaller nuclei will also attach to the surface of larger

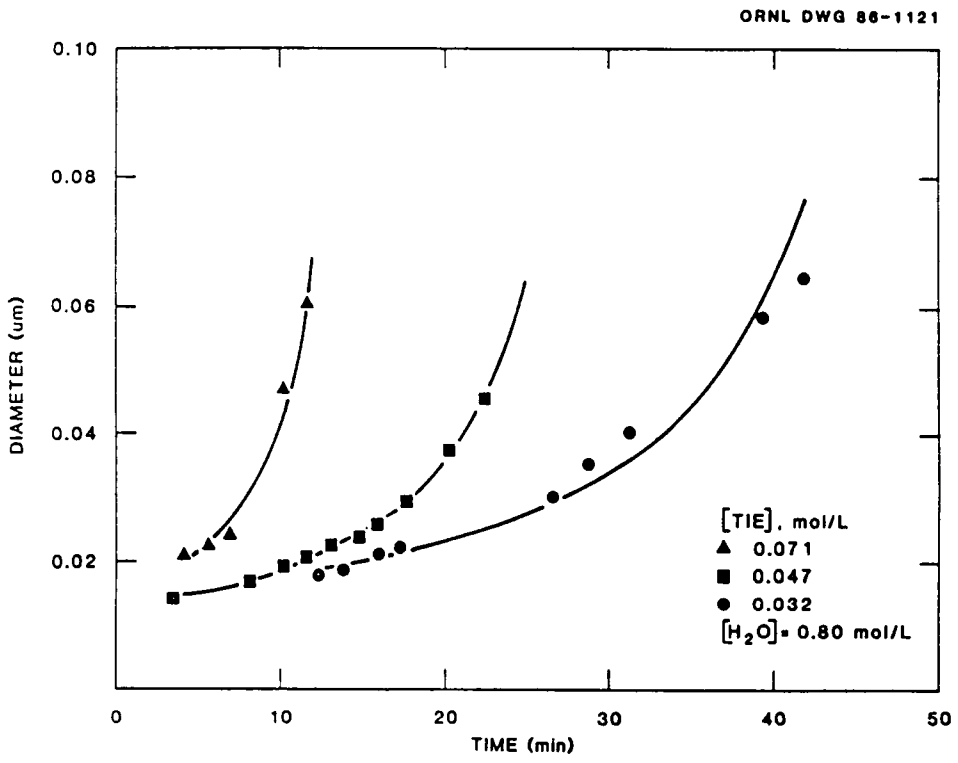



Fig. 3.9. Titania Growth Kinetics in t-Butyl Alcohol.

particles, and the consequence is a rapid growth in particle size. The result of this uncontrolled nucleation and growth is the production of an agglomerated mass with no definite shape. This is shown by Fig. 3.10, an electron micrograph of "dried titania" particles that are synthesized in tert-butyl alcohol. Although the precipitate does not have a definite shape, the stringy nature of the precipitate is possibly suitable for sol-gel processing, which is another method that is being studied for ceramic powder synthesis.

### 3.5.2.2. Zirconium, titanium-zirconium and titanium-aluminum hydrous oxides

A study of the induction period for "titania" and "zirconia" systems suggests that condensation occurs considerably faster for "zirconia" than for titania. This due to the greater ease of removing the last alkoxy group from zirconium alkoxides than from titanium alkoxides.

After the induction period, the growth of zirconia and zirconia-titania particles was monitored by dynamic light scattering. Fig. 3.11 illustrates typical kinetic plots for 1:2 "zirconia":"titania" particles during the early stages of growth in 1-butanol and ethanol and an increasing growth rate in tert-butyl alcohol. The growth patterns are similar to the patterns for "titania" that were discussed in previous section.

Figs. 3.12(a), 3.12(b), and 3.12(d) show typical transmission electron micrographs of particles that exhibit a constant growth rate. The primary particles have a definite shape.

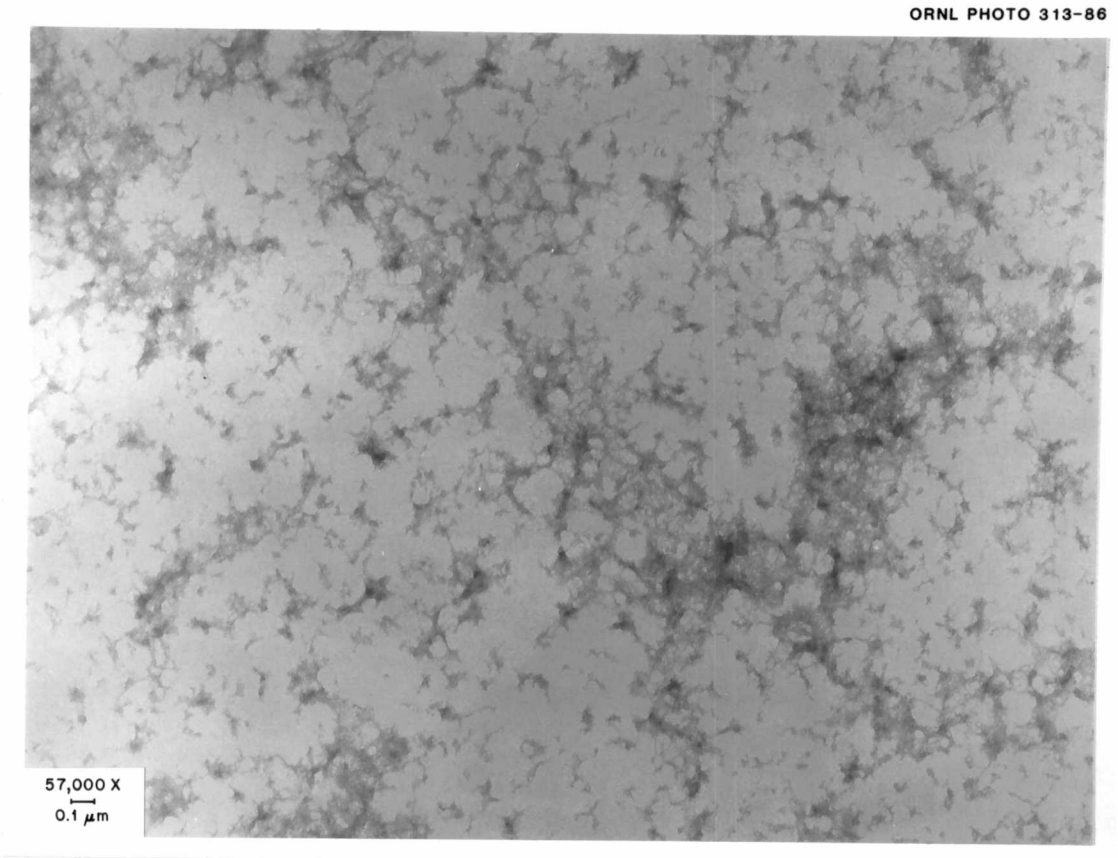



Fig. 3.10. Transmission Electron Micrograph of Titania Particles Synthesized in t-Butyl Alcohol.

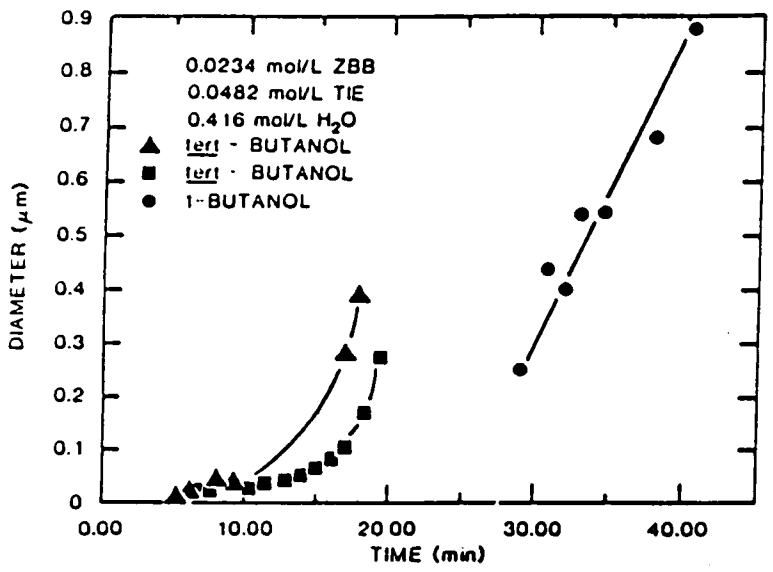



Fig. 3.11. The Growth of "Zirconia"-"Titania" Particles in 1-Butanol and t-Butyl Alcohol: Hydrolysis of Mixed Titanium-Zirconium Alkoxides.

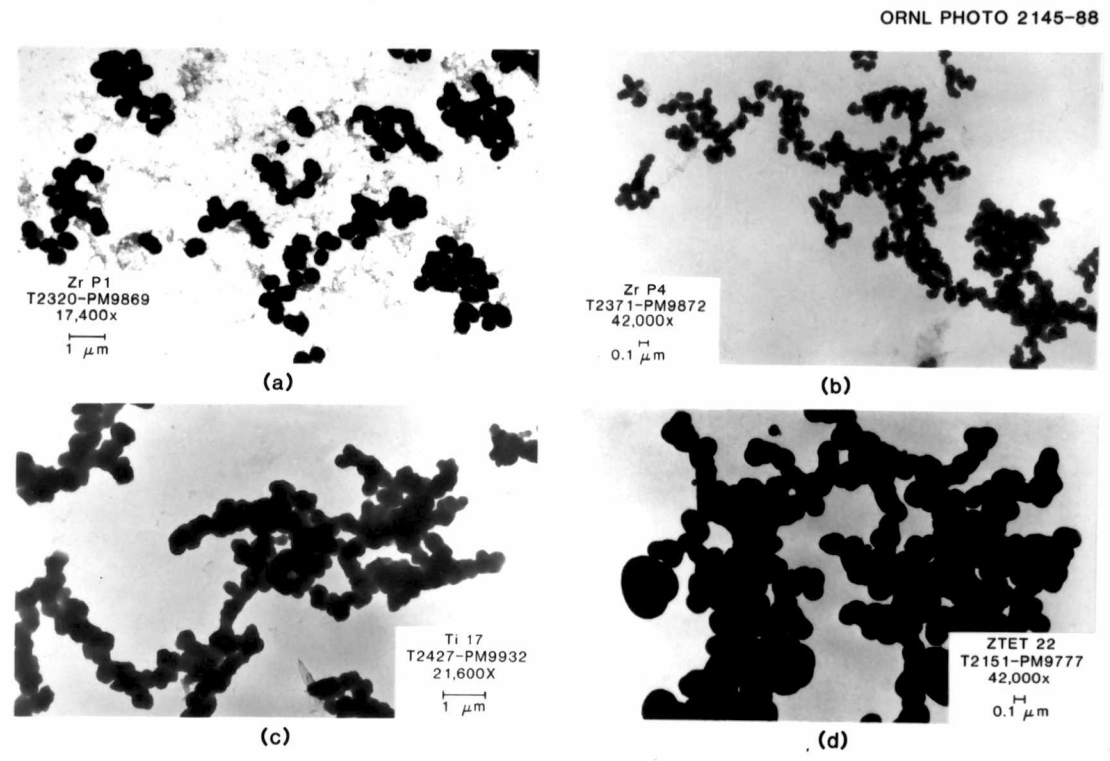



Fig. 3.12. Transmission Electron Micrograph of "Titania" and "Zirconia"-"Titania" Particles Synthesized in Ethanol and 2-Butanol.

In comparing the diameter ($\approx$0.3 $\mu$m) that was obtained by photon correlation spectroscopy with the size ($\approx$0.1 $\mu$m) of the primary particles shown in the transmission electron micrographs [Fig. 3(b)], it is observed that the particles in solution probably consist of agglomerates of approximately three primary particles. It is further noted that, in the case of a constant growth rate, the smallest observable size by photon correlation spectroscopy at the onset of nucleation is $\approx$0.1 $\mu$m. As stated in the previous section, the requirements for synthesizing monodisperse metal oxide particles is the rapid growth to a size of $\approx$0.1 $\mu$m. Particles produced in tert-butyl alcohol are irregular, as would be expected from the agglomeration of uncollapsed small particles [not shown, but similar to Fig. 3.10].

Energy Dispersive X-ray (EDX) analysis was performed on the particles shown in Fig. 12(d), and the results showed a constant composition of titanium and zirconium between the "titania-zirconia" particle with a size resolution of 0.1 $\mu$m. It was expected, however, that because of the apparently faster condensation of "zirconia" than "titania", a more heterogeneous composite material would be formed. It is, therefore, postulated that mixed alkoxides are formed, and the condensation occurs from this new species. Theoretically, these particle should have contained 32.0 wt% zirconium and 35 wt% titanium. The values from EDX analysis were 32.4 $\pm$ 0.7 and 34.1 $\pm$ 0.9.

It is seen from Eqs. 3.1-3.6 that titanium alkoxides are partially hydrolyzed, while aluminum alkoxides are completely hydrolyzed. It is assumed that the partially hydrolyzed products of titanium alkoxides should precipitate (nucleate) considerably slower than the completely hydrolyzed aluminum alkoxides. Furthermore, partial charge computations (Table 3.2 ) for aluminum alkoxides

indicate that condensation by alcoxolation will occur as readily as the removal of the last two alkoxy groups by hydrolysis.

Thus, linear aluminum hydrous oxide polymers are preferentially formed (Yoldas 1973) instead of the highly crosslinked polymers like those of silica, and titanium and zirconium hydrous oxides. Linear polymers result in the formation of gels or gelatinous precipitates.

For comparable total metal concentrations and water concentrations, the experimental data show that titanium alkoxide hydrolysis products precipitate much slower than the hydrolyzed products from the aluminum-titanium mixed alkoxide system (i.e., longer induction times before precipitation occurs; minutes to hours compared with seconds). A portion of the samples is also filtered 10 min. after precipitation has begun. In the titanium alkoxide system, the filtrate turns turbid after 5 to 10 min. This indicates that either the hydrolysis of titanium alkoxide (Eq. 3.1) is occurring after 10 min, condensation by alcoxolation is the limiting step during this regime and/or there is equilibria between the precipitate and soluble species. As stated earlier, Fourier transform infrared spectroscopy suggests that the hydrolysis reaction is fast and occurs within 1 to 2 min. Therefore, the precipitation in the filtrate is due to the shift in equilibrium condition that is caused by the removal of the precipitate and/or slow condensation by alcoxolation.

The filtrate from the aluminum-titanium mixed alkoxide system remained clear and, therefore, suggests that both the aluminum and titanium hydrolysis products are probably precipitated together within 10 min of reaction.

Fig. 3.13 shows the effect of the initial molar ratio of ASB:TIE on the shape of "alumina" [probably AlO(OH)] and "titania" [probably TiO(OH)(OR)]

Table 3.2. Particle charge distributions for aluminum ethoxide and aluminum butoxide hydrolysis products.

| $R = C_2H_5$ | $\delta$(Al) | $\delta$(OR) | $\delta$(OH) | $\delta$($OH_2$) | $\delta$(ROH) | $\delta$(H) |
|---|---|---|---|---|---|---|
| $Al(OR)_3$ | 0.4877 | -0.161 | — | — | — | — |
| $Al(OR)_3(OH_2)$ | 0.4998 | -0.073 | -0.375 | -0.277 | 0.025 | 0.098 |
| $Al(OR)_2(OH)$ | 0.5012 | -0.063 | -0.373 | — | 0.037 | 0.10 |
| $Al(OR)_2(OH)(OH_2)$ | 0.515 | 0.039 | -0.352 | -0.239 | 0.151 | 0.112 |
| $Al(OR)(OH)_2$ | 0.529 | 0.136 | -0.332 | -0.209 | 0.259 | 0.123 |
| $Al(OR)(OH)_2(OH_2)$ | 0.544 | 0.248 | -0.309 | -0.173 | 0.384 | 0.136 |
| $Al(OH)_3$ | 0.615 | — | -0.204 | -0.010 | — | — |
| $R = C_4H_9$ | $\delta$(Al) | $\delta$(OR) | $\delta$(OH) | $\delta$($OH_2$) | $\delta$(ROH) | $\delta$(H) |
| $Al(OR)_3$ | 0.483 | -0.161 | — | — | — | — |
| $Al(OR)_3(OH_2)$ | 0.491 | -0.065 | -0.40 | -0.296 | 0.027 | 0.091 |
| $Al(OR)_2(OH)$ | 0.492 | -0.053 | -0.39 | — | 0.04 | 0.092 |
| $Al(OR)_2(OH)(OH_2)$ | 0.501 | 0.068 | -0.37 | -0.269 | 0.169 | 0.101 |
| $Al(OR)(OH)_2$ | 0.514 | 0.193 | -0.35 | -0.243 | 0.304 | 0.111 |
| $Al(OR)(OH)_2(OH_2)$ | 0.528 | 0.349 | -0.33 | -0.211 | 0.472 | 0.122 |
| $[Al(OR)_2(OH)]_2(OH_2)$ | 0.498 | 0.01 | -0.378 | -0.281 | 0.108 | 0.097 |

particles that are synthesized by the hydrolysis of aluminum-titanium alkoxides in ethanol containing an excessive amount of water.

These data clearly show that as the initial ratio of ASB:TIE decreases [Figs. 13(a)-13(d)], the precipitate changes from an aggregation of nanometer-size particles that have an incoherent-open structure to an aggregation of more coherent and spherical 0.1 to 0.2-$\mu$m particles. The former structure is typical of gels while the latter, with the help of surfactants to minimize aggregation, can result in discrete submicron monodisperse particles.

The proposed mechanism that governs the growth of coherent-(spherical)-versus-incoherent particles of "alumina"-"titania" involves (a) collapse of polymeric species to form nuclei, (b)the controlled aggregation of dense nuclei to form larger more stable aggregates, (c) long term stability of aggregates and deposition of nuclei on surface of aggregates. This mechanism, which is based on the chemical reactivity of alkoxides to form linear or highly crosslinked polymer networks and electric double-layer theory, assumes that during nucleation, very small (~20-Å) primary dense nuclei, because of their colloidal instability, rapidly coagulate to form larger, more stable spherical particles. As nucleation proceeds, the primary nuclei preferentially attach to the larger particles rather than aggregate with other primary nuclei. Thus, monodisperse particles are formed. The formation of monodisperse spherical particles versus incoherent-open structures is affected by the relative rate of nucleation to the rate of aggregation (i.e., colloidal stability of the nuclei). If nucleation occurs faster than the primary nuclei are able to collapse and to form larger particles by aggregation, the precipitate will exhibit an incoherent-open structure. However, spherical particles are formed when the primary nuclei aggregate faster than the formation of primary

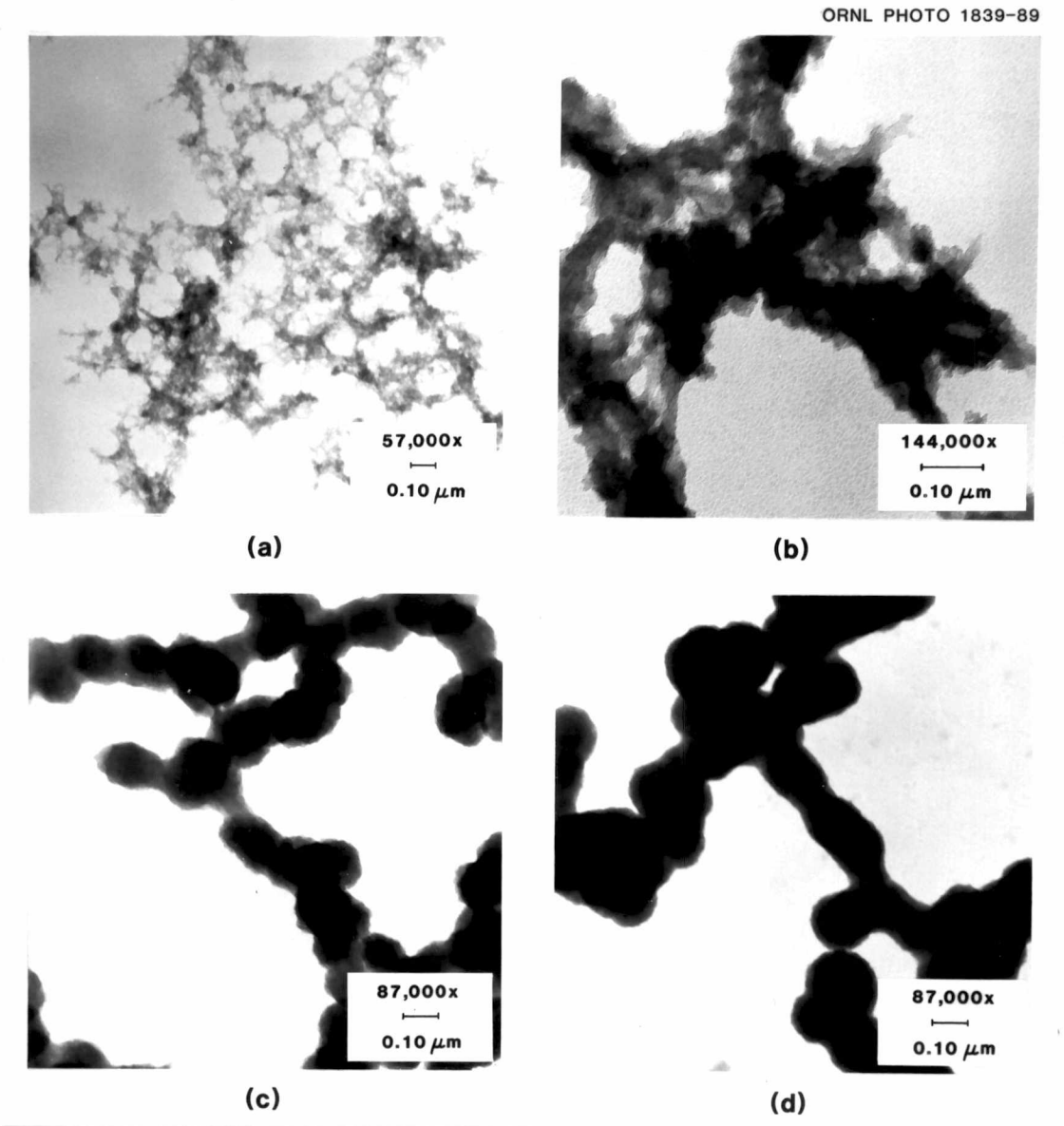



Fig. 3.13 TEM of "alumina"-"titania" particles produced in ethanol (effect of the initial molar ratio of [ASB]:[TIE]; 0.8 M $H_2O$): (a) 0.015 M TIE, 0.023 M ASB; (b) 0.023 M TIE, 0.019 M ASB; (c) 0.031 M TIE, 0.012 M ASB; (d) 0.02 M TIE.

nuclei and under the condition where larger colloids are more stable than the smaller nuclei.

Alumina precipitates that are formed by alkoxide hydrolysis form gelatinous material because of the linear polymer networks that are formed. The high zeta potential of alumina also hinders the collapse of polymeric alumina species into dense nuclei.

Zeta potentials have been determined for the precipitate from the hydrolysis of solutions with initial ASB:TIE molar ratios of 0:1, 1:0, 2:1, 1:1, and 1:2. These particles were suspended in the centrifuged reaction medium. At a pH of 6.9, the zeta potential increases from 10 mV for "titania" particles to 60 mV for "alumina" particles. This indicates that, based on the electric double-layer theory, the colloids become more stable as the "alumina" content of the particles is increased. However, this does not necessarily mean that a stable sol is formed. These particles can still aggregate; however, because of the higher rate of nucleation and the increase in colloidal stability, an increase in the "alumina" content of the particles is expected to form more incoherent-open structures [Fig. 3.13(a)-3.13(d)].

Fig. 3.14 shows growth kinetics of "alumina"-"titania" particles that are determined by dynamic-laser-light-scattering.

Since larger particles are more intense scatterers, the effective diameters are more representative of the larger particles. This figure shows that as the "alumina":"titania" molar ratios increased from 0:1 (curves E and F), 1:1 (curve A), to 2:1 (curves B, C, and D), the first observable particle size decreases from 100-200 nm to 10-20 nm. Since dynamic-laser-light-scattering techniques are capable of obtaining particle sizes in 10 to 15 s, the first observable particle

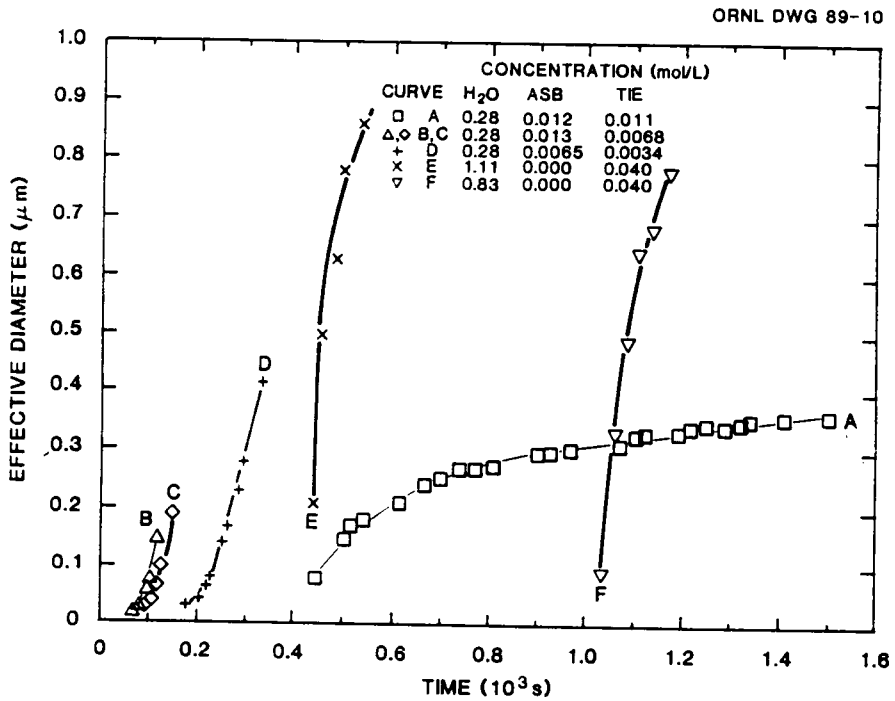



Fig. 3.14. Particle growth kinetics in 1-butanol: Effect of the initial molar ratio of ASB:TIE.

size represents 10 to 15 s of particle growth after the onset of nucleation. This growth can be due to either aggregation of smaller particles or to the addition of monomer to the surface of the nuclei. Electron microscopy (Fig. 3.13) indicates that the larger particles (>100 nm) of "alumina"-"titania" are agglomerates of smaller particles.

Since "alumina"-"titania" particles (>100 nm) are formed by aggregation of smaller particles, the previously mentioned mechanisms are used to describe the observed particle growth kinetics. In the case of 2:1 "alumina":"titania" molar ratio, it is reported above that based on zeta potential measurements, these colloids are more stable than particles with a lower "alumina":"titania" molar ratio. Therefore, it is likely that the first observable particle size after 10 to 15 s of nucleation should be smaller (because of greater colloidal stability) for particles with a higher "alumina" content than for particles with a lesser "alumina" content where, because of low colloidal stability, the very small nuclei (20-50 $\AA$) rapidly aggregate to form 100- to 200-nm particles. The subsequent increase in the measured effective diameter from the first observable particle size (Fig. 3.14) is due to aggregation.

The ultimate goal of these studies is to synthesize monodisperse spherical particles of aluminum titanate ($Al_2TiO_5$) by the homogeneous precipitation of mixed aluminum-titanium alkoxides. During a matrix of experiments in which the water concentration and solvents are varied, it is observed that more compact-spherical particles are formed when the water concentration approaches the theoretical amount needed for hydrolysis and condensation reactions (see Eqs. 3.1-3.6). Fig. 3.15 shows TEMs of particles that are synthesized by the hydrolysis of a 1:1.2 ASB:TIE solution in 1-butanol with water concentrations

of 1.6 and 0.4 mol/L.

It is clearly shown that a more incoherent-open precipitate is produced at the higher water concentration (i.e., higher rate of nucleation). At low water concentrations, aggregates of compact-near-spherical particles are obtained. The aggregation of the particles at lower water concentration can be minimized by the addition of surfactants during the reaction. To produce compact-spherical particles from the hydrolysis of a 2:1 ASB:TIE solution, it is necessary to initially add approximately 9 mol of water per mol of TIE. After this solution has reacted for 30 min, an additional 9 mol of water per mol of initial TIE are added. Fig. 3.16 shows the "alumina"-"titania" particles that are produced in ethanol, 1-propanol, and 1-butanol.

Fine powders (although aggregates of 100- to 300-nm particles) are produced in each solvent. The best powders are produced in 1- butanol.

Fig. 3.17 shows the differential thermal analysis for 2:1 "alumina"-"titania" powder that is synthesized by the above method in 1-butanol.

The plot shows an endotherm at $140^{o}C$ (removal of hydroxides) and exotherms at $360^{o}C$ (removal of alkoxide groups), $970^{o}C$(rutile and/or corundum formation), and $1400^{o}C$ (formation of $Al_2TIO_5$). The formation of the various crystalline phases is confirmed by X-ray diffraction analysis.

## 3.6 Conclusions

The solvent system used in the preparation process and alcoholysis have a profound effect on the nature of metal hydrous oxide precipitates that are synthesized by the hydrolysis of titanium ethoxide, titanium-zirconium alkoxides

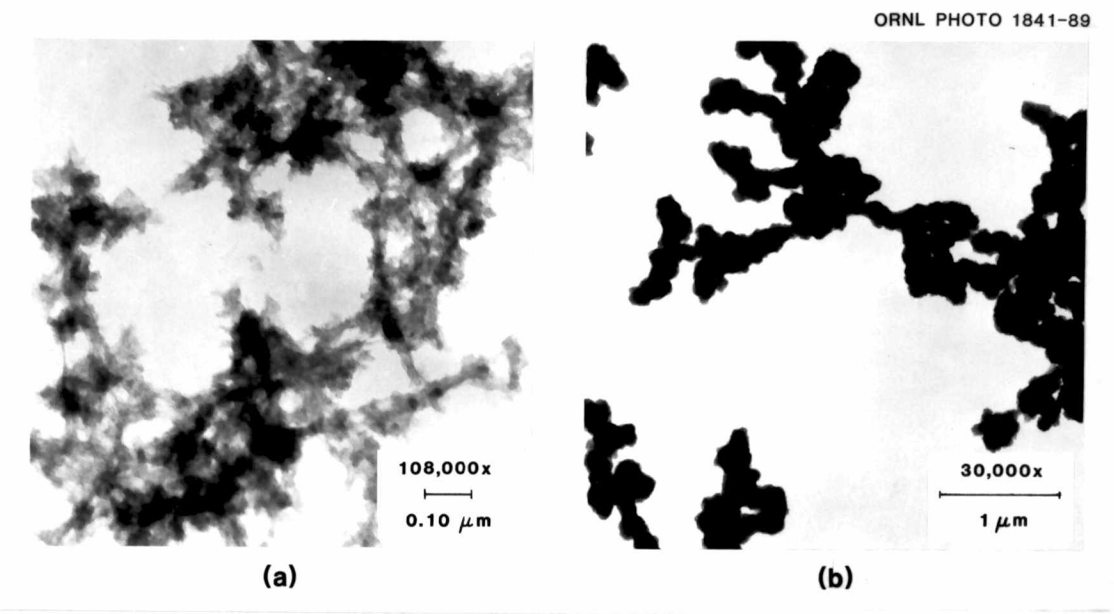



Fig. 3.15. Transmission electron micrographs of "alumina"- "titania" particles produced in ethanol (effect of initial water concentration) (0.023 M TIE, 0.019 M ASB) : (a) 1.6 M $H_2O$; (b) 0.4 M $H_2O$.

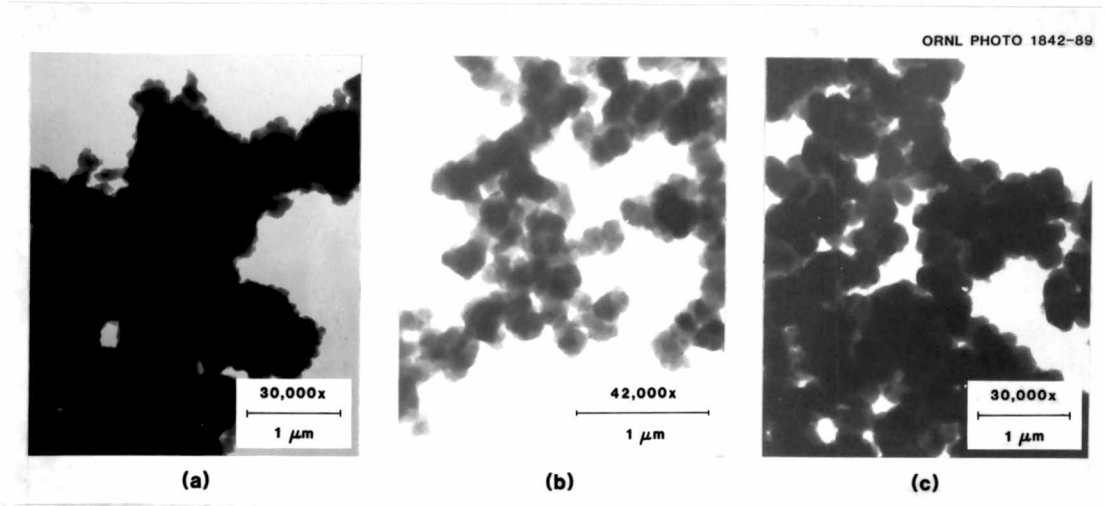



Fig. 3.16. Transmission electron micrographs of "alumina"- "titania" particles (effect of solvent: 0.56 M $H_2O$, 0.025 M TIE, 0.05 M ASB): (a) ethanol; (b) 1-propanol; (c) 1-butanol.

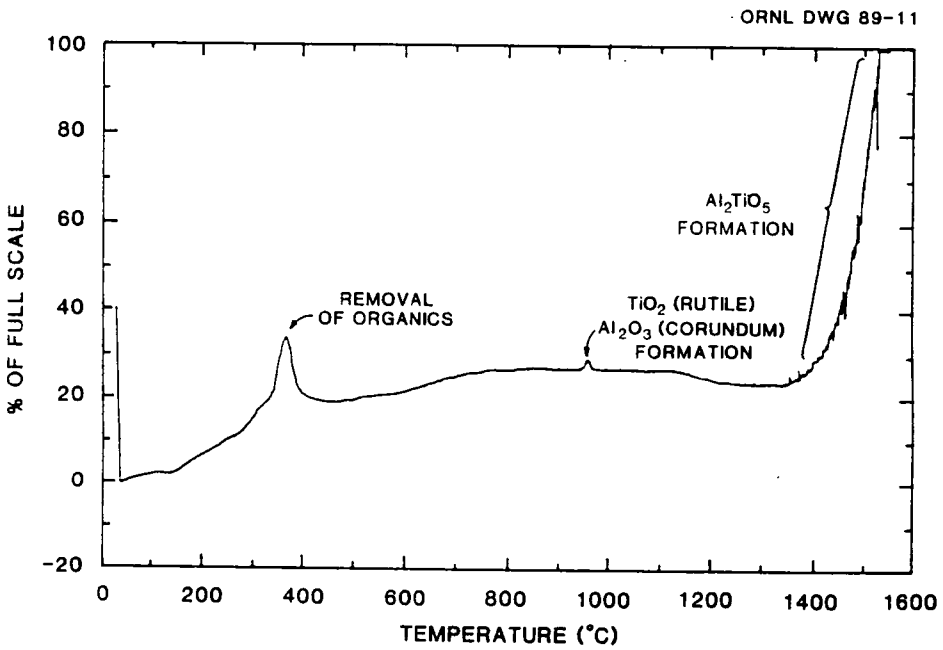



Fig. 3.17. Differential thermal analysis for "alumina"- "titania" powder.

and titanium- aluminum alkoxides in ethanol, 1-butanol, and tert-butyl alcohol. Monodisperse and spherical "titania", and "titania"-"zirconia" particles grow at constant rates when produced in ethanol and 1-butanol. However, the rate of growth in tert-butyl alcohol increases with time. The particles that are formed in tert-butyl alcohol are agglomerated and have irregular shapes. Although not monodisperse or spherical, the precipitate that is produced in tert-butyl alcohol could possibly form a sol-gel system. This system could subsequently be used to produce ceramic powders.

This investigation has shown that the "alumina" content affects of the type polymers formed, the rate of precipitation and the colloidal stability which ultimately affects particle morphology. A procedure is proposed for the synthesis of 100- to 300-nm spherical particles of 2:1 "alumina"-"titania" by the controlled hydrolysis/condensation of a homogeneous mixture of aluminum and titanium alkoxides in low-molecular-weight alcohols. However, the aggregation of these spherical particles in solution lowers the green-body density of the final powder. To produce a more ideal powder for ceramic applications, future studies should investigate the use of surfactants to minimize aggregation of these spherical particles in solution.

The experimental determination of the hydrolysis and condensation rate constants of these systems is greatly needed. Molecular dynamic and macromolecular algorithms are needed to elucidate the effects of the physical and chemical properties of the alkoxide on the initial polymeric species in solution. Such methods could evaluate steric effects of the alkoxy group on the formation of linear versus crosslinked polymers. This effect is not accounted for in partial charge models.

# 4. ELECTRIC DISPERSION REACTOR

## 4.1. Introduction

The use of high-intensity-pulsed electric fields for droplet size control in dispersed liquid systems is being investigated in the Chemical Technology Division at Oak Ridge National Laboratory (ORNL). This technology has been utilized in a device called the electric dispersion reactor (EDR) to carry out the synthesis of micron-sized particles for the production of precursor powders of advanced ceramic materials that are difficult or impossible to synthesize by homogeneous precipitation techniques. In this approach, pulsed electric fields are employed to create dispersions of microscopic conducting (aqueous-based) drops in nonconducting (organic) liquids. Each of these droplets becomes a localized microreactor where reactants in the organic phase diffuse into the aqueous droplets in which precipitation and gelation occur, while water and reaction products diffuse into the organic phase. The size of the final particle is thus controlled by the size of the initial liquid droplet. Of particular importance in this technology is the ability to alter particle morphology by varying reactant compositions in the liquid-liquid system while achieving intraparticle stoichiometric consistency. This is an extremely important characteristic for the production of composite ceramic materials. It leads to the production of high-quality precursor powders which, in turn, yields dense, consistent green-body material. Furthermore, this method requires far less energy expenditures than conventional approaches which rely on such inefficient operations as solids blending, mixing, and grinding to accomplish the formation of mixed-oxide precursor material.

4.1.1. Physicochemical Synthesis of Ceramic Precursor Powders.

The synthesis of ultrafine ceramic precursor powders by physicochemical techniques has gained increasing attention in recent years (Bowen 1984). By comparison to the strictly chemical method of homogeneous precipitation, these methods which include spray pyrolysis/aerosol synthesis, electrostatic atomization of liquid drops into air, precipitation in vesicles and precipitation in microemulsions, offer the advantage of physically controlling the particle size by creating localized reaction zones (i.e., microreactors) in which precipitation/gelation occurs. These methods are especially attractive in the synthesis of mixed hydrous metal-oxide precursor powders when intimate mixing is required on the submicron level.

Spray pyrolysis is a generic term used in describing a wide range of processes that generate ceramic particles directly from atomized precursor solutions or sols (Martin et al. 1990). Three ubiquitous transient stages are observed in most of these processes: (1) formation of a liquid vehicle droplet, (2) drying to a solid particle, and (3) chemical reaction of the solid particles to produce a ceramic. The result of these combined, serial steps is the production of high-surface-area, chemically pure ceramic powders. An intrinsic problem, however, is that most spray-pyrolyzed powders display irregular shapes with hollow morphologies (Zhang and Messing 1990). A subsequent grinding operation is necessary to crush the hollow spheres. More recently, ultrasonic nebulizers have been used in spray pyrolysis or partially hydrolyzed alkoxides to produce solid, spherical particles of $TiO_2$, $ZrO_2$ and $SiO_2$ in the size regime of 0.5 to 5 $\mu$m (Zhang and Messing 1990). However, even with the ultrasonic nebulizer, hollow irregular-

shaped particles are quite often formed as Odier et al. (1990) reported in the formation of $YBa_2Cu_3O_{7-x}$ powders by spray pyrolysis. Another problem associated with spray pyrolysis is heat transfer. The poor heat conductivity of air makes heat transfer another potential problem in the scale-up of spray pyrolysis devices.

Spray pyrolysis has several advantages when regular-shaped powders can be formed: (1) it involves simple and inexpensive chemistry; (2) a relatively high yield in a laboratory scale reactor is observed; and (3) contamination is reduced because of little contact of the powders with the container walls (Odier et al. 1990).

Powder synthesis by electrostatic atomization involves the disintegration of liquid drops (in this case, aqueous zirconium acetate) from a nozzle by a high voltage (10 to 15 kV) applied to an electrode in air (Slamovich and Lange 1988). The high potential causes the meniscus at the nozzle to form a cone. The surface of the cone, which the accumulation of electric charge makes unstable, ejects fine jets that decompose into droplets by capillary instability. The droplets are collected at a grounded substrate by which time the water has evaporated, leaving solid particles of zirconium acetate. The zirconium acetate is pyrolyzed to remove the acetate and to form $ZrO_2$.

The main disadvantage of this technique involves a high surface tension at the liquid-air interface, which leads to the use of large amounts of energy to rupture the droplet.

Unilamellar vesicles have also been used as microreactors for controlled precipitation of crystals in the nanometer size range within their internal cavity (Bhandarkar and Bose 1990). Since the vesicle wall has very specific ion-

transport properties, the internal cavity can act as a constrained domain of size in the range of hundreds of angstroms for the purpose of intravesicular reaction. The synthesis of metal-oxides in vesicles relies on the fact that the their walls are selectively permeable only to the anions.

A typical synthesis scheme involves sonicating an aqueous solution of metal salt and phosphatidylcholine until a single-compartment vesicle is formed. Since vesicle walls are impermeable to cations, only metal ions are trapped inside the vesicle. Excess cations are removed from the extravesicular region by ion exchange with sodium ions. Sodium hydroxide is added to the eluent. The hydroxide passes through the vesicle wall, and intravesicular precipitation occurs. Nanometer-sized, nearly spherically shaped crystals of aluminum oxide and mixed hydroxides of aluminum/magnesium, aluminum/calcium, aluminum/barium, and aluminum/magnesium have been synthesized by the intravesicular precipitation method. The disadvantages of this method include: 1) energy intensive sonication is required and 2) very dilute suspensions are formed.

Powder preparation using emulsions involves three general approaches (Hardy et al. 1988):

1. formation of water-oil emulsion, followed by the reaction of water with alkoxide,
2. emulsification of an aqueous sol in an organic liquid and gelation of sol droplets by ammonia, and
3. emulsification of the alkoxide with an nonreactive immiscible solvent and subsequent hydrolysis by the addition of water.

The first approach has been used to synthesize silica in the size range of ap-

proximately 1 to 10 $\mu$m. Submicron yttrium aluminum garnet (YAG) particles (approximately 1 $\mu$m) were produced by the second approach. In the third approach, alkoxides of titanium, zirconium and aluminum were emulsified in acetonitrile. Water was injected to promote hydrolysis. The resulting submicron particles were spherical and unagglomerated. Osseo-Asare and Arriagada (1990) provided a list of materials produced by microemulsions. A disadvantage with microemulsion technology is the use of large quantities of surfactants that can equal, or exceed, the amount of hydrous metal oxide produced. Furthermore, in most emulsion processes, energy-intensive mixing by mechanical agitation or ultrasonication is required.

Recently, a new concept, which is the object of this research, the electric dispersion reactor (EDR) has been developed for the synthesis of ultrafine powders by microreactor techniques (Harris, Scott, Basaran, and Byers 1990). This concept uses intense, pulsed, dc electric fields to cause jetting of a conducting liquid from a nozzle into a nonconducting organic liquid. As in the aforementioned case of electrostatic atomization in a gas, the jets are destabilized and form micron-sized droplets. An important difference is that reactants can be placed in the droplet phase and/or continuous phase. Precipitation may be induced by the diffusion of reactant into the microreactors or by temperature. In addition to the increased flexibility of use of various chemical methods, it appears that the EDR will display a decided advantage in both energy requirements and production rate because of the lower interfacial tension present in liquid-liquid systems versus liquid-gas systems.

A more-detailed description of the EDR is given in the next section. This is followed by a description of the powders that were produced by the EDR during

preliminary feasibility experiments.

In order to address the issue of powder formation in the EDR, it is necessary to touch on a number of underlying phenomena that control the system. To that end, the remainder of this technical discussion will be directed toward the dispersion of liquid drops in electric fields, chemical methods for particle formation, benefits of the EDR over other physicochemical methods, and the potential energy efficiency of the process for high-capacity operations.

### 4.1.2. Potential Benefits of The Electric Dispersion Reactor (EDR)

As mentioned above, physicochemical techniques provide an intriguing option for the manufacture of advanced composite ceramics. It is clear that more efficient production of improved precursor powders will lead to improved product quality. While there are a number of potential approaches being considered by the research community, at this time there does not appear to be a clear path toward developing a process which will be accepted by industry for use in large-scale production of these important materials. The primary pitfalls to industrial acceptance revolve around flexibility of operation (both from a sense of types of product available from a given approach and operation of the process itself) and potential for scale-up.

The EDR appears to be a good candidate for addressing both of these issues. First, the potential for taking advantage of chemistry and transport in both of the liquid phases leads to the possibility of a multitude of different products. Additionally, the process can be run in continuous mode with recycle of critical reagents to provide a realistic flowsheet which does not entail a large amount of

process waste. An important issue is the absence of dry micron-sized powders which cause potential health risks. Finally, scale-up of this system is modular by nature. That is to say that larger capacity is obtained by addition of units that are similar to the small scale system. This circumvents such issues as maintaining mechanical agitation performance, as with conventional water/organic emulsion technologies, and high temperature and heat-flux throughout large vessels such as is encountered in spray pyrolysis systems. The following two sections provide a description of the EDR and envisioned EDR process, of chemical methods used, and of the results obtained using this approach.

### 4.1.3. EDR Process Description

As in other physicochemical approaches to the production of ceramics, the EDR achieves control of the ultimate particle size by limiting particle formation processes to well-defined microscopic zones. In the case of the EDR, a high-intensity, transient electric field is utilized to disperse relatively conducting liquid droplets into a relatively nonconducting continuous liquid phase. A schematic diagram of the laboratory-scale EDR unit is given in Fig. 4.1. An aqueous solution is introduced through an electrically grounded nozzle into an organic based continuous phase. The grounded nozzle is located between two parallel-plate electrodes, which are charged to the same potential by a transient electric field. Since the electric forces applied to the dispersed fluid are proportional to the square of the electric-field-strength, the electrodes can have either polarity.

When the aqueous phase issues from the nozzle, it is immediately dispersed into a large number of micron-sized droplets and is accelerated downward by

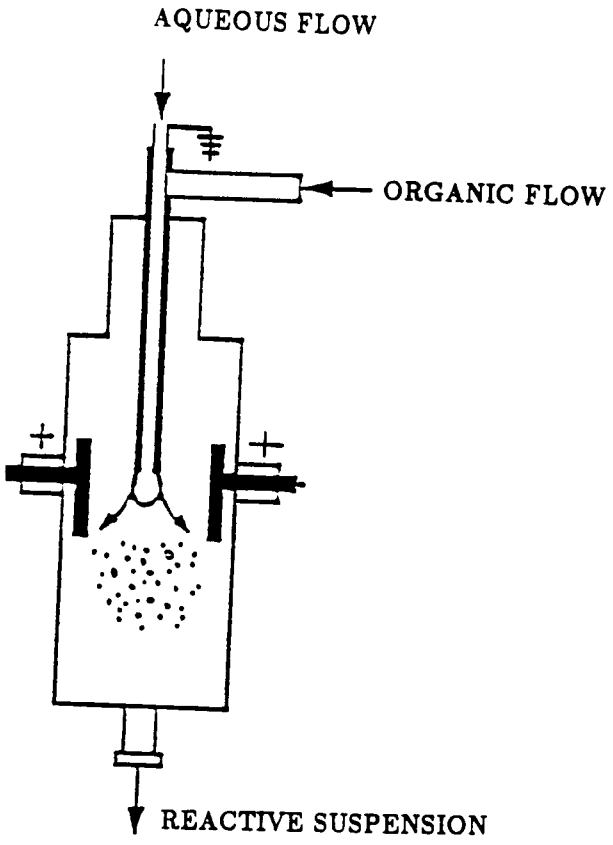



Fig. 4.1. Electric Dispersion Reactor.

the electric field. In the apparatus illustrated in Fig. 4.1, the organic phase is introduced through an annulus surrounding the grounded nozzle to provide cocurrent flow of the two liquid phases. This has the effect of ensuring quick removal of the aqueous phase from further influence of the electric field and thus avoiding droplet coalescence. Once the two liquid phases are in contact, mass transfer and chemical reaction proceed in each of the micro-drop regions. After reaction, one is left with a suspension of chemically homogeneous, micron-sized particles. Although the final reaction and precipitation occurs within the aqueous-solution droplets, initially the reactants and/or catalysts may be placed in the aqueous phase, the organic phase, or combinations thereof to achieve various effects on particle morphology.

The reactor used in laboratory initially testing the concept was a 1.5"ID cylindrical glass vessel 6" long. The single nozzle was a 0.05"ID stainless steel tube.

Flow rates of up to 5 cc/min of aqueous phase were injected while the organic phase was introduced to the column at between 20 and 50 times the volumetric rate of the aqueous phase; thus, the system typically operated with a dispersion which was between 2 to 5% by volume aqueous phase. The aqueous solution is introduced dropwise between electrodes on which is imposed an intense, pulsed, DC electric field (6 to 10kV/cm and pulsing frequencies between 100 Hz to 3 kHz). An overall schematic diagram of the continuous EDR process is illustrated in Fig. 4.2.

After the precipitation reaction has occurred between the phases, the resulting suspension is pumped into a dielectric filter (subsequently described in more detail) for continuous recovery of particles from the organic phase. The

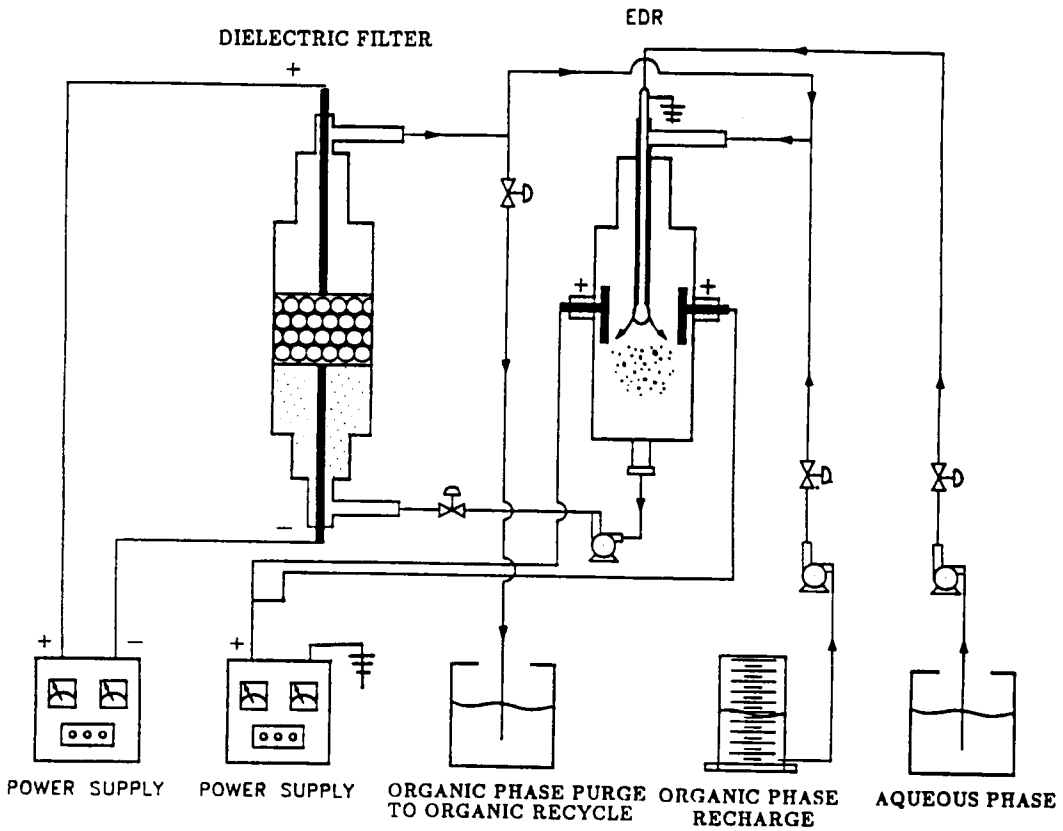



Fig. 4.2. Continuous EDR Process.

majority of the clean organic phase is then recycled to the EDR for reaction with more feed aqueous phase. In many cases the buildup of reaction byproducts is alleviated by a small purge stream of the organic phase, which is replaced by fresh organic phase which is introduced directly into the reactor along with the remainder of the recycled organic stream. Organic regeneration involves routine unit operations such as extraction or distillation and allows for reuse of the recovered reaction products in make-up of the process feed material. One of the major advantages of the EDR concept is that the environmental implications of such a process are indeed minimal.

The dielectric filter was developed in the Chemical Technology Division of ORNL for the filtration of submicron charged and/or polarizable particles from appropriate gas or liquid streams, (Barker, 1988). Also known as the "granular electro-filter" this simple and highly effective method is ideal for removing the types of particles generated by the EDR from organic media. In operation, a bed of nonconducting, dielectric solids is polarized in a DC electric field. As the suspension passes through the polarized bed, the particles are captured on the surface of the packing by electrophoretic and dielectrophoretic forces. The main requirement of the system is that the dielectric constant of the packing material be higher than that of the continuous liquid phase, collecting both the granular material and the residual aqueous solution. To regenerate the filter, one need simply turn off the field and back-flush with a small amount of the organic phase. Obviously, the continuous industrial system will require two dielectric filters, so that one can undergo regeneration by back-flushing while the other is filtering the product stream. To date, the parts of the process shown in Fig. 4.2 have been successfully tested separately.

Processing fine ceramic powders involves three fundamental steps: (1) the production of narrow size distribution fine ceramic powders, (2) the suspension of these ceramic powders in aqueous or nonaqueous liquid solutions, and (3) the fabrication of green bodies with uniform packing of particles (Ring 1990). The continuous EDR system accomplishes steps 1 and 2 without further mechanical processing and without the potential for dusting that occurs when handling ultra-fine dry powders. Slurries from the EDR should provide an expedient route for the production of high quality ceramic green bodies. As has been shown, the EDR provides a complete process for the production of ceramic precursor materials. Our preliminary work, which is described in the following sections, shows that the process can be used for an extraordinarily broad class of pure and mixed ceramic powders. Further these can be controlled in ways other technologies cannot approach, such as the control of microstoichiometry, surface agglomeration, and the continuous production of controlled materials in much the same way controls are exerted in chemical processing units. If the energy saving implications of the technology as well as its inherent safety features are also considered, the overall picture is one of an extremely attractive emerging technology, where focused new research could yield both a new technology and new insights into the nature of precipitation reactions can be achieved.

## 4.2. Chemical Methods for Particle Formation in the EDR

As mentioned above, intense-pulsed electric fields are used to produce micron-sized droplets that subsequently react to form submicron to micron size particles. However, to ensure sphericity of the final particles, it is necessary

to balance and control rates of mass transfer and reaction in the multiphase system. Two methods of chemical synthesis will be explored in the EDR: (1) external gelation, and (2) internal gelation.

### 4.2.1. External gelation

Traditionally, the external gelation method involves the precipitation of aqueous salt solutions, and dispersing the precipitate to form a stable sol. Gelation is induced by (a) removal of the water (Haas 1989) or (b) reacting the sol with ammonia (Haas 1967). The difficult step in this procedure is dispersing the precipitate to form a stable sol. To circumvent the need to disperse or peptize a precipitate into a stable sol, gel-spheres are formed in the EDR by dispersing submicron to micron size aqueous droplets containing soluble metal salts into a continuum that contains a precipitation agent such as ammonia. A schematic diagram of the technique is shown in Fig. 4.3.

In this figure, metal salts in the aqueous droplet react as the ammonia transfers from the organic continuous phase into the droplet. Precipitation and gelation occurs forming a hydrous metal oxide gel-sphere.

Another form of external gelation that is explored (Fig. 4.4) places, the metal containing species (metal alkoxide ) in the continuum and the precipitation agent water and/or ammonia (catalyst) in the disperse-phase.

This technique allows the formation of hydrous metal oxide shells that upon washing can be collapsed to create high-surface-area wafers. The external gelation technique allows the formation of oxide powders over a wider range of conditions than internal gelation because of the added flexibility of locating reactants

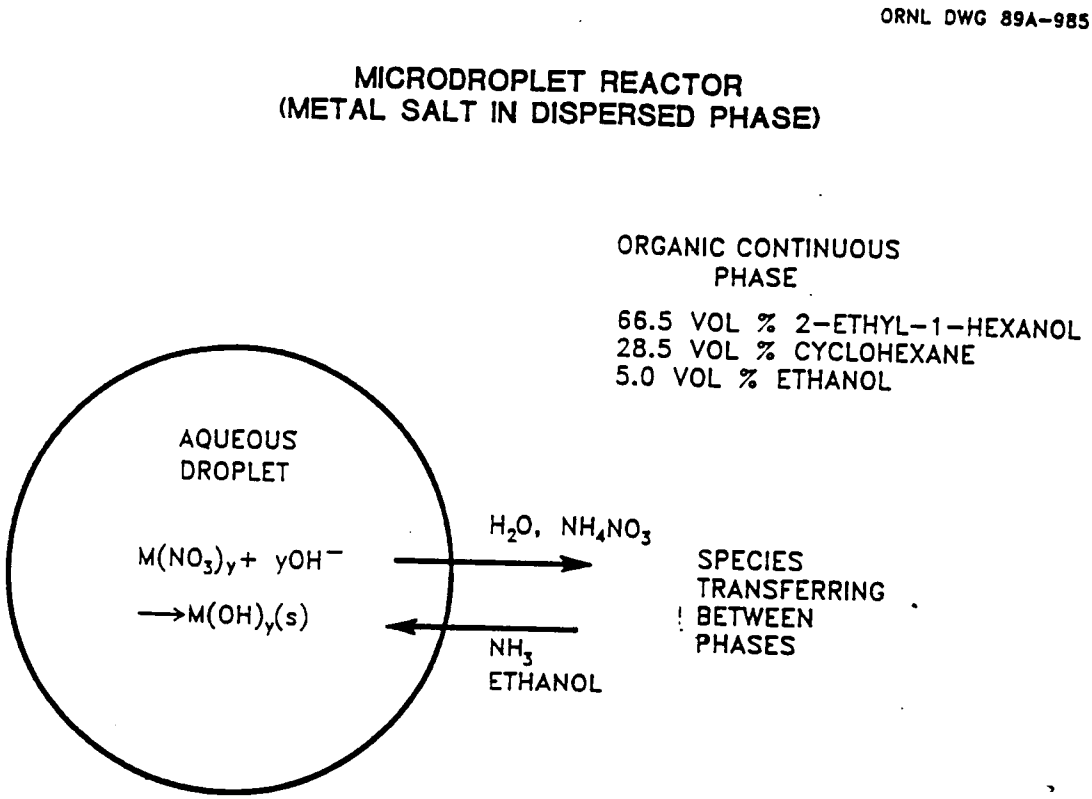



Fig. 4.3. External gelation technique for metal salt solutions.

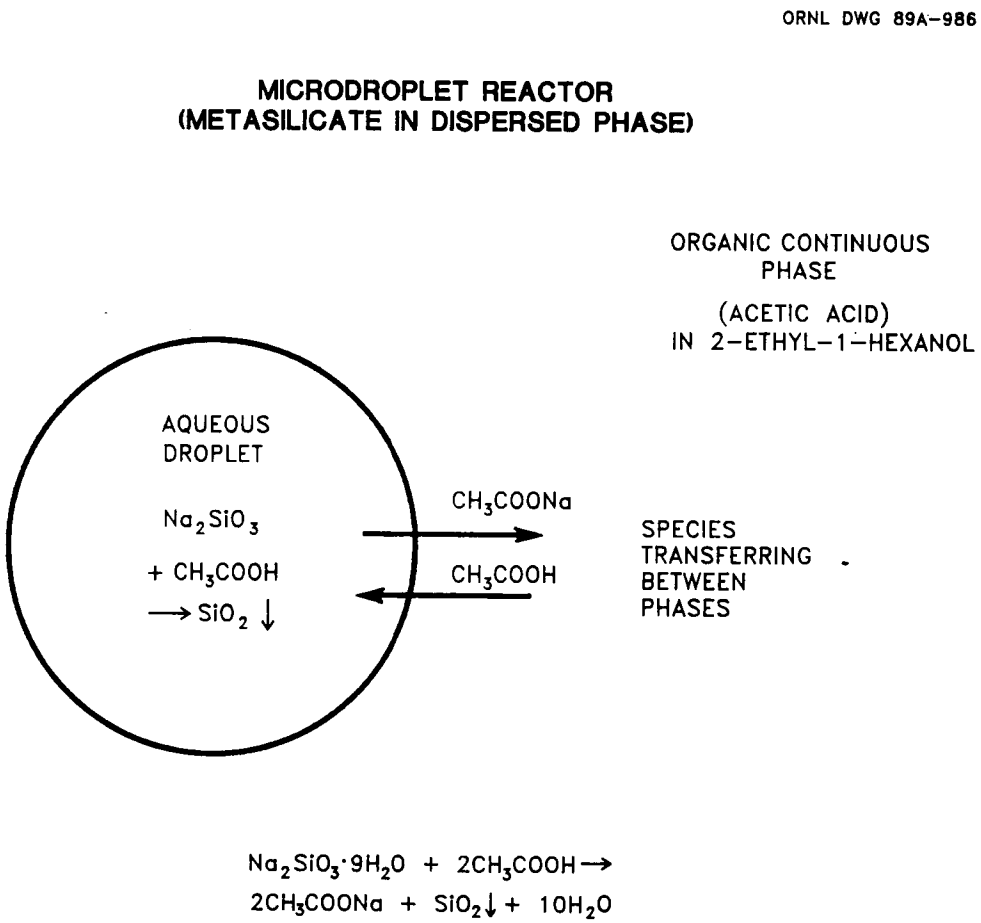



Fig. 4.4. External gelation technique for silica formation from sodium metasilicate.

in both liquid phases.

### 4.2.2. Internal Gelation

In this method, all reactants are placed in a chilled aqueous feed solution or broth. Precipitation and gelation are induced by dispensing the droplets from a nozzle into a hot continuous phase (Collins, Lloyd, and Fellows 1987). The size of the gel-spheres was controlled form several hundred microns to several millimeters by adjusting the size of the nozzle. Common chemicals in the internal gelation process include a chilled concentrated aqueous solution of metal nitrates, hexamethylenetetramine (HTMA) and urea. Upon heating, the protonation and decomposition of HTMA is enhanced (Collins, Lloyd, and Fellows 1987)

HMTA protonation

$$(CH_2)_6N_4 + H^+ \rightleftharpoons [(CH_2)_6N_4H]^+, \tag{4.13}$$

HMTA decomposition

$$(CH_2)_6N_4 \cdot H^+ + 3H^+ + 4NO_3^- + 6HOH$$

$$\rightleftharpoons 4NH_4^+ + 4NO_3^- + 6CH_2O. \tag{4.14}$$

From Eq. 4.14, it is readily observed that HMTA decomposes to form ammonia which subsequently results in hydroxide precipitation. Final particle morphology is controlled by varying the reactant concentration, gel-time, and post-processing steps (i.e. the removal of water from the gel-spheres).

This method has been used to produce gel-spheres of $UO_3$, $UO_3$-$PuO_2$, $ThO_2$-$UO_3$, $ZrO_2$, $UO_3$-C, $Al_2O_3$, and $PuO_2$-C (Haas 1989), and $TiO_2$ (Collins

1990). Internal gelation by the HMTA method is not recommended for metals that precipitate above pH 6 (Collins, Lloyd and Fellows 1987, Haas 1989).

It is envisioned that the EDR can be used to produce ultrafine (0.1 $\mu$m to 5 $\mu$m) powders by the internal gelation method. This represents a hundred-fold decrease in the size of the gel-spheres that have typically been produced by this method.

## 4.3. Results and Discussion

The EDR was developed through preliminary experiments in which several types of precursor powders were produced. In each case, reagents for reaction were placed in both liquid phases to demonstrate various effects on particle morphology. Silica particles were made by two methods, one in which the silicon source initially was in the organic phase and a second where the source of silicon was in the aqueous phase. Finally a typical example of multicomponent synthesis was demonstrated through the formation of particles of "1-2-3" (Y-Ba-Cu-oxide) precursor powders.

The first method tested for making silica particles involved an organic phase consisting entirely of the alkoxide, tetraethylorthosilicate (TEOS). In order to form the particles, distilled water containing 0.7 $\underline{M}$ $NH_4OH$ was dispersed by an electric field into the TEOS phase. Immediately upon contact, reaction occurred and particles were formed. After formation, the particles were removed by centrifugation and washed with ethanol (amounts of organic were too small to warrant use of the dielectric filter). Particles were then dried for 24 hours. The particles were imaged before and after washing and drying steps by scanning

and transmission electron microscopy. Fig. 4.5 shows particles produced in this manner indicating a collapse of porous spherical shells subsequent to their drying.

Initially, TEOS reacts with the surface of aqueous-ammonia drops to form silica. Since TEOS is virtually immiscible with water, the diffusion of TEOS into the droplet interior occurs at an extremely slow rate and one is left with a silica shell filled with the aqueous phase. When the particles are dried with or without an ethanol washing the remaining aqueous phase is removed from the interior and the silica shell collapses. These particles are similar to powder aerogels with respect to their high porosity. Particle sizes were generally around a few tenths of a micron. Several application of this type of technology to areas such as packing materials and sorbents are contemplated.

Placing the silicon source in the aqueous phase yields a significantly different result. In this case aqueous sodium metasilicate was dispersed in 2-ethyl-1-hexanol which contained acetic acid. As can be seen in Fig. 4.6, this approach rendered dense spherical particles in the size range of 1 to 3 microns.

The acetic acid was free to diffuse throughout the aqueous droplets and thus induce homogeneous precipitation. The dense particles produced in this approach to the reactions in the EDR clearly offer a route to the making of very desirable dense bodies for the production of advanced ceramics. From these two illustrations, it is evident that particle morphology can be significantly altered by strategically placing the participating reactants in one liquid phase or the other or utilizing certain combinations of liquid phases to obtain the desired effect.

Perhaps the greatest strength of the EDR approach to producing ceramic

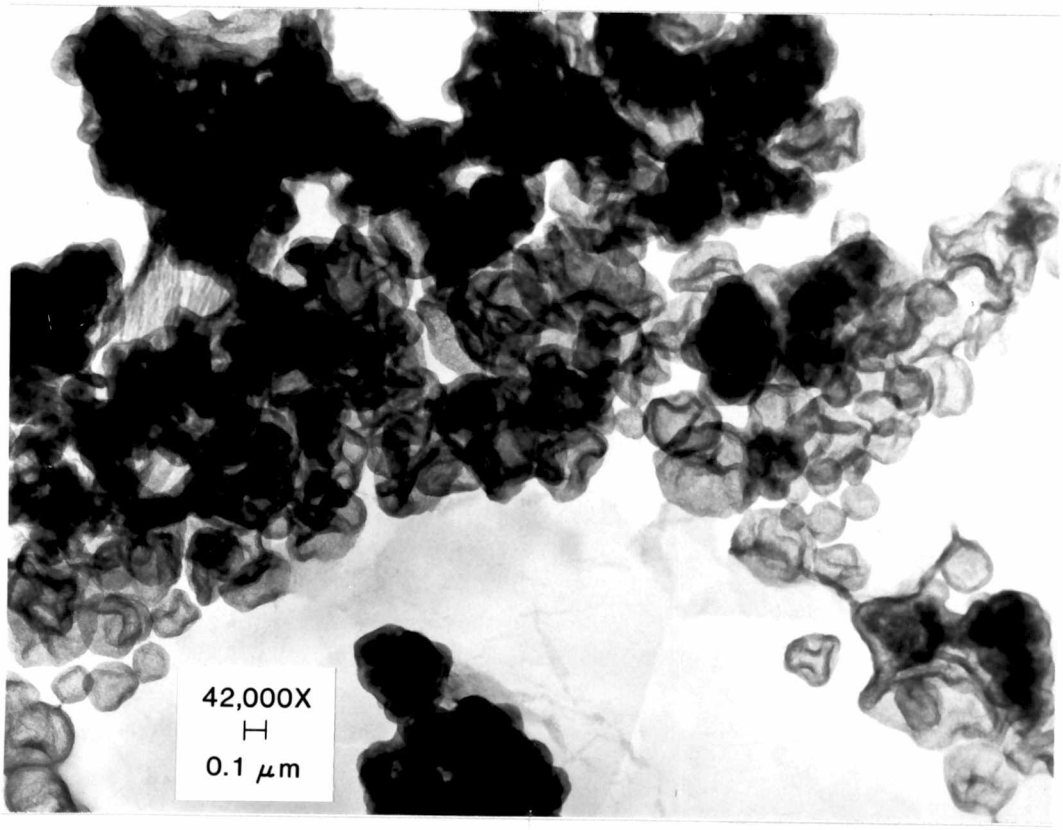



Fig. 4.5. Silica particles produced in the EDR [0.7M $NH_4OH$ (dispersed phase) and TEOS (continuous phase)].

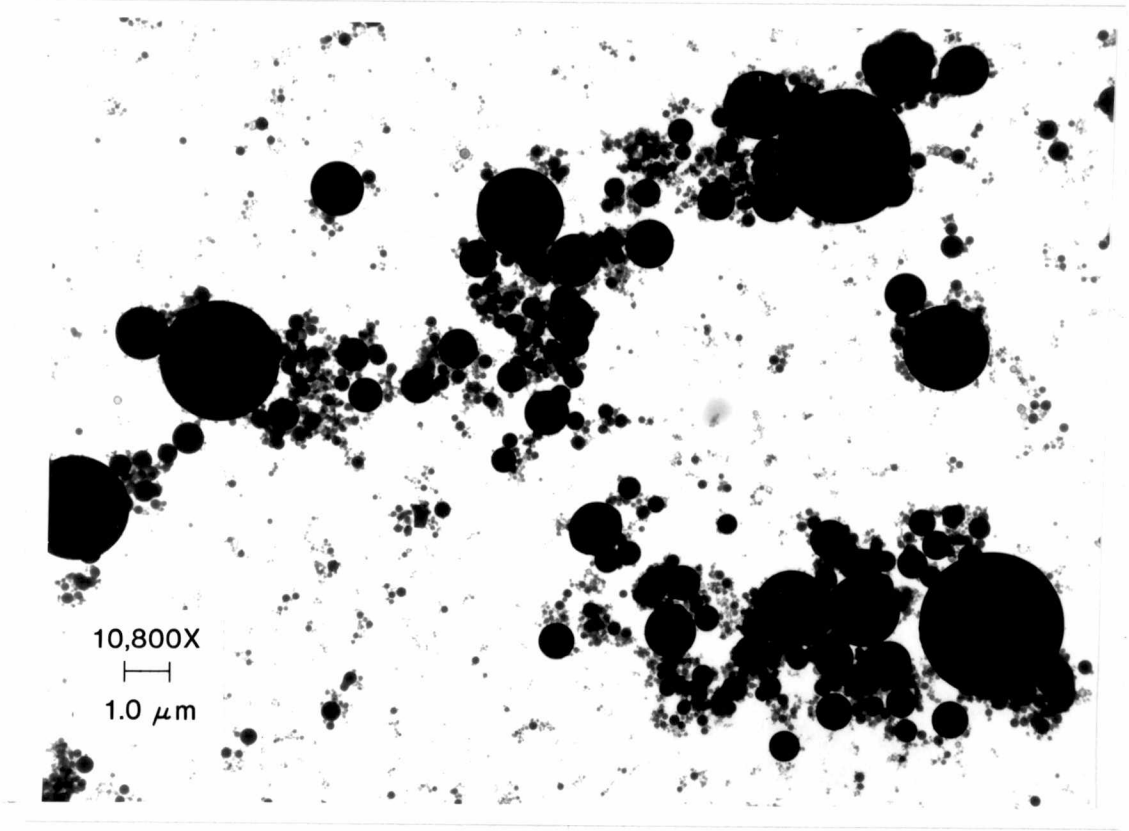



Fig. 4.6. Silica particles produced in the EDR [sodium metasilicate in water (dispersed phase) and acetic acid in 2-ethyl 1-hexanol (continuous phase)].

precursors is our ability to precisely control the composition of every particle on the precursor material, and thus guaranteeing stoichiometric control from the very start of the processing of the ceramic precursor, rather than depending on thermal processes to perform the mixing to the molecular level. An example of the effectiveness of the EDR approach in multicomponent precipitations was the selection of the "1-2-3"superconductor synthesis. An aqueous phase comprised of cupric chloride, yttrium nitrate, and barium nitrate was dispersed in an organic phase containing 2-ethyl-1-hexanol, ethanol, and ammonia. Upon contact of the two phases, ammonia diffuses into the aqueous drops and causes rapid precipitation to occur. This results in the dense, spherical particles shown in Fig. 4.7. Further analysis of these particles by energy dispersive X-ray (EDX) analysis revealed that there was chemical homogeneity both from particle to particle and within each particle. This result is extremely important to the future of producing precisely-controlled mixed ceramic precursors.

## 4.4. Conclusions

Experiments have shown that the synthesis of submicron- to micron-size metal hydrous oxide ceramic particles can be formed by imposing intense, pulsing, dc electric fields on a conducting liquid drop suspended in a nonconducting liquid. The characteristics of the particles can be changed by strategically locating the reactants in the proper phase. The ability to distribute reactants in either phase makes the EDR an attractive process for synthesizing specialty powders and for improving the synthesis of complex mixed oxide powders.Future experimental work should involve large-scale synthesis of powders in the EDR

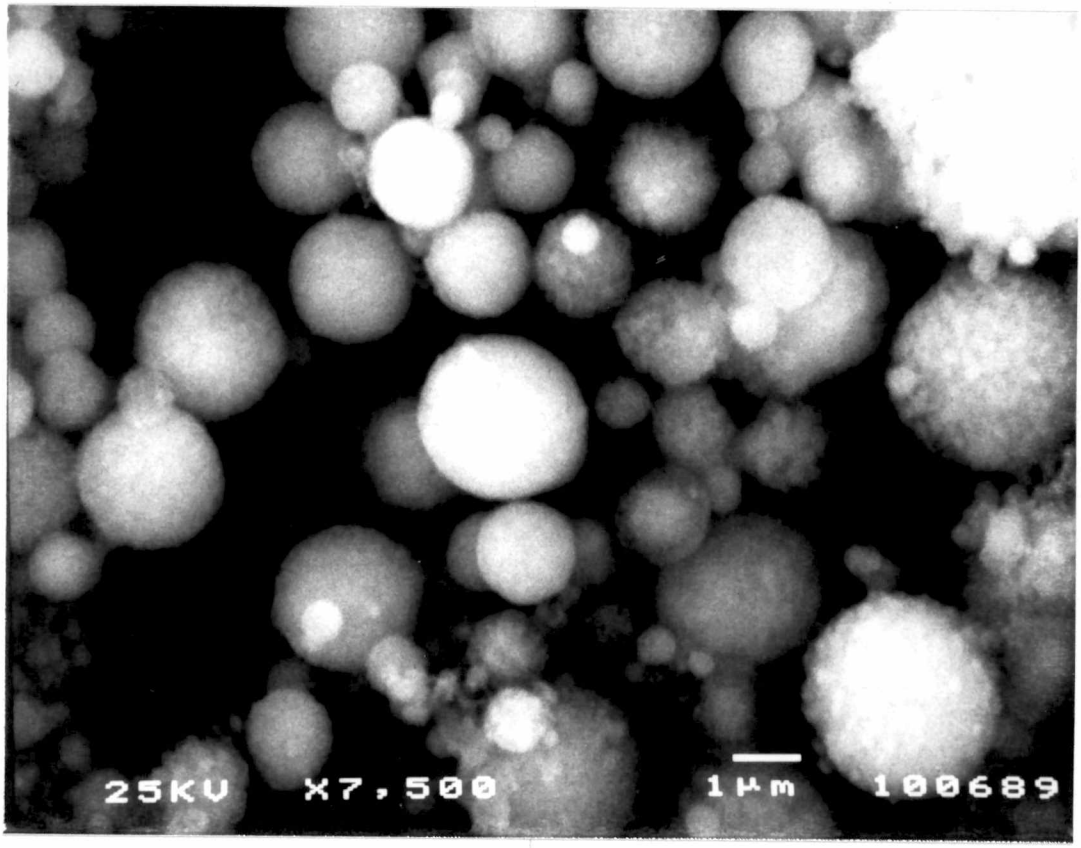



Fig. 4.7. Particles produced in the EDR containing hydrous oxides of Y-Ba-Cu (approx. 1:2:3 molar ratios).

and comparing the sinterability, composition, and the ability of these powders to produce improved ceramics to precursors produced by other methods.

# 5. ELECTROHYDROSTATICS OF AXISYMMETRIC PENDANT DROPS

## 5.1 Introduction

Placing an electric field on multiphase systems (e.g. gas-liquid, liquid-liquid, liquid-solid, etc.) will impart a force on the interfacial region if there is a significant difference in electrical permittivity of the two phases (Melcher and Taylor 1969). This operator-imposed force can then be used to control the behavior of the multiphase system. Energy usage is minimal if the continuous phase is nonconducting because the force acts only at the interface and is not dissipated throughout the bulk of the multiphase system. With this capability in hand one can envision a whole family of energy-efficient processes which could use external electric fields to manipulate and enhance multiphase operations.

In contrast to electrochemical applications, the use of electric fields to control liquid-liquid processes primarily involves physical interactions between charges, electric fields, and conducting and/or dielectric liquids. Using the fundamental and constitutive relationships for electric fields and conservation (Maxwell's equations) and transport of charge, one determines that electric field interactions are most prevalent in a region which contains a "discontinuity" of electrical properties. In liquid-liquid systems, this most often involves the interface between relatively conducting and relatively nonconducting liquids as well as interfaces between the liquids and solid and gas surfaces in the physical apparatus. Generally speaking, these interfacial effects manifest themselves as a resultant force or induced normal stress that can induce a static deformation

of the interface and even steady or transient fluid motion in one or both phase (Melcher and Taylor 1969).

## 5.2 Liquid Dispersion by an Electric Field

Placing a spherical , relatively conducting droplet that is surrounded by a relatively nonconducting continuum in a steady DC electric field will cause stresses to develop on the droplet (Taylor 1964). This force per unit area, or pressure, is imposed by the component of the electric field which is normal to the interface: the strength of the electrically induced pressure is proportional to the square of the field intensity. As the strength of the field is increased, the resultant force will cause the droplet to deform into an ellipsoid whose major axis lies parallel to the electric field lines (see Fig. 5.1). In addition, the droplet will be polarized with either the induced or net charge (for charged drops) appropriately distributed on the droplet surface. There is no electric field inside the conducting droplet. If sufficient field strength is provided, the droplet deformation will become large enough to cause disintegration of the original droplet into a number of smaller daughter droplets (Hendricks and Schneider 1962, Zeleny 1917 and Macky 1931). If a transient field is used, the droplet will elongate during times of "high" field strength and relax back toward a spherical shape when the field strength is "low", thereby forcing oscillation about the spherical form. Transient fields can also be used to cause droplet disintegration; however, the instantaneous field strength required is higher than when using a steady DC field (Vonneguet and Neubauer 1953, Scott 1987 and Scott, Basaran and Byers

1990).

Formation of droplets from a nozzle or orifice is also affected by the presence of electric fields. The resultant force which occurs at the droplet-continuum interface serves to decrease the size of the detaching droplets relative to the no-field case (Takamatsu, Hashimoto and Katayama 1981, Bailes 1981 and Perona and Byers 1987). If the electric field strength near a nozzle is increased past the point of single-drop formation, jetting occurs, which results in the formation of a dispersion of micron- sized droplets. This phenomenon has been noted in DC, AC and pulsed DC electric fields (Scott 1987, Scott and Wham 1989 and Scott 1989). The most important features of this electric dispersion technique can be understood by a more detailed look at the effects of varying the strength and transient nature of the electric field.

## 5.3. Effect of Field Strength on Dispersion

While qualitative understanding of the effects of electric fields on drop dispersion from a nozzle is relatively straight forward, the most interesting behavior (that most germane to increasing the capacity of the process) must be explored by numerical solution of coupled nonlinear partial differential equations (Basaran, 1984). For the case of a static DC field, the drop shape and electrostatic potential are governed by the dimensionless augmented Young-Laplace and Laplace equations, respectively (Basaran and Scriven, 1990):

$$-2\aleph = K - Gz + N_e H^2 E_n^2 \text{ on the droplet surface} \tag{5.1}$$

$$\nabla^2 U = 0 \text{ everywhere outside droplet.} \tag{5.2}$$

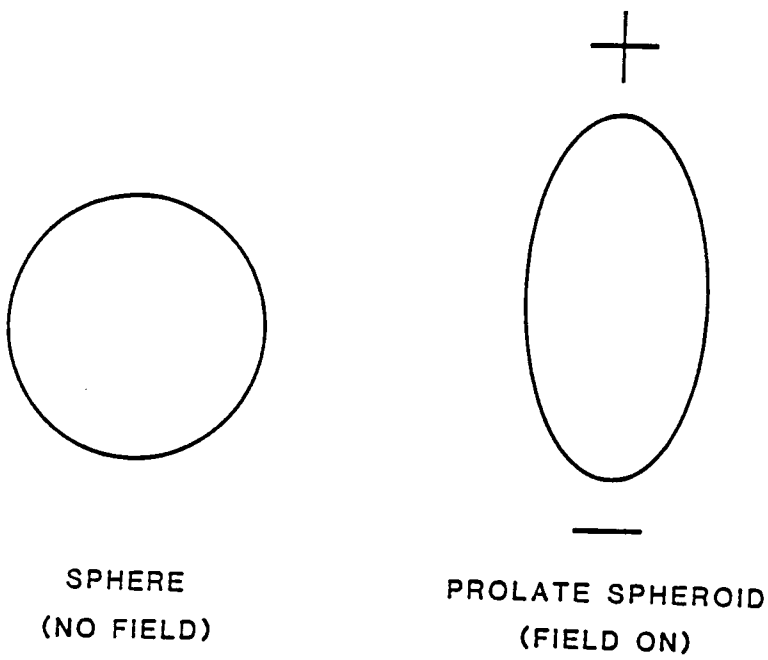



Fig. 5.1 Effect of electric field on fluid drop.

where

$2\aleph \equiv$ twice the local mean curvature of the interface $R2\overline{\aleph}$,

$K \equiv$ reference pressure $\dfrac{R\Delta p_o}{\gamma}$,

$G \equiv$ gravitational bond number $\dfrac{gR^2\Delta\rho}{\gamma}$,

$z \equiv \dfrac{\overline{z}}{R}$,

$N_e \equiv \dfrac{\epsilon R u_o^2}{2\gamma h^2}$, electric bond number,

$H \equiv \dfrac{h}{R}$,

$E_n \equiv \dfrac{R\overline{E}_n}{u_o}$, normal electric field strength,

$R \equiv$ radius of uncharged spherical drop,

$h \equiv$ distance between plates,

$\gamma \equiv$ surface tension,

$\epsilon \equiv$ dielectric constant,

$\rho \equiv$ density,

$p_o =$ reference pressure,

$z =$ distance from nozzle tip,

$u_o =$ a characteristic potential, and

$g =$ gravitational constant.

The reference pressure $K$ is determined by containing the drop volume to be a fixed amount $V_0$

$$V = V_0. \tag{5.3}$$

Inspection of Equation 5.1 reveals that the augmented Young-Laplace equation primarily differs from the base-case form by the last term on the right-hand-side: the electric field term (Basaran, 1984). Additionally, because the drop is distorted by the field, the local mean curvature ($\aleph$) becomes a highly nonlinear function. It is evident from this electric field term that the local force imposed on the droplet by the field is proportional to the square of the normal component of the local electric field in the continuous phase ($E_n^2$) and inversely proportional to the interfacial tension of the liquid-liquid system. Therefore, it requires a more intense electric field to deform a drop which has a higher interfacial tension with the surrounding fluid. This is particularly important when comparing the electric dispersion of liquid droplets in another liquid versus dispersion into a gaseous phase. In general, the liquid/vapor interfacial (surface) tension will be significantly higher than the liquid-liquid case so that liquid/vapor dispersion will require a significantly higher electric field strength. Hence, one can conclude that continuous electric field dispersion of a liquid into another liquid as utilized in the EDR will require significantly less energy than the aerosol dispersion case noted earlier.

## 5.4. Use of Transient Fields for Dispersion

Transient electric fields can also be utilized to disperse free liquid droplets or liquid streams emerging from nozzles. If a pulsed electric field is used, the drop in Fig. 5.1 will stretch when the field is "on" and recover back toward the equilibrium (spherical) shape when the field is "off". This induces a shape oscillation of the droplet about the spherical form the amplitude of which depends in

nonlinear fashion upon the frequency and amplitude of the electric field pulses. If the amplitude of oscillation is increased past a certain point, the droplet will become unstable and shatter to form a number of smaller daughter droplets (Scott 1987). The most interesting behavior occurs when the electric field pulse rate is in the vicinity of the so called "natural" frequency of the droplet.

For inviscid liquid drops in inviscid media (such as a gas), induced oscillations would continue along indefinitely because there is no mechanism for dissipation of energy. This circumstance leads to the simple expression for the natural frequency of drops given by Lamb (1945).

$$\beta^* \equiv \left[\frac{\gamma(l+1)(l-1)(l+2)}{R^3\Gamma}\right]^{1/2}, \tag{5.4}$$

$$\Gamma \equiv \rho_i l + \rho_o(l+1). \tag{5.5}$$

Here $l = 1, 2, 3, \ldots$ is the mode number, R is the droplet radius, $\gamma$ is the interfacial tension, and $\rho_o$ and $\rho_i$ are the continuous phase and droplet densities, respectively.

For the case of viscous media, induced droplet oscillations are damped out by viscous dissipation in both phases. In a comprehensive study of low amplitude oscillation, Miller and Scriven (1968, to be henceforth referred to as M & S) have given a complete description of oscillation and decay for the case of stationary viscous media. A knowledge of the damping factor allows a qualitative estimation of the amount of energy required to sustain oscillation. The results of M & S allow one to calculate the natural frequency and damping factor for liquid drops by setting the determinant of a 6×6 matrix of complex coefficients equal to zero. An analytical solution cannot be found in general; however, as-

suming the liquid viscosities to be low, yields the following asymptotic results for the frequency and damping factor:

$$\beta_I = \beta^* - \frac{(2l+1)^2(\beta^*\mu_i\mu_o\rho_i\rho_o)^{1/2}}{2\sqrt{2}R\Gamma[(\mu_i\rho_i)^{1/2}+(\mu_o\rho_o)^{1/2}]} \tag{5.6}$$

$$\begin{aligned}\beta_R = {} & \frac{(2l+1)^2(\beta^*\mu_i\mu_o\rho_i\rho_o)^{1/2}}{2\sqrt{2}R\Gamma[(\mu_i\rho_i)^{1/2}+(\mu_o\rho_o)^{1/2}]} \\ & - \frac{(2l+1)^4\mu_i\mu_o\rho_i\rho_o}{4R^2\Gamma^2[(\mu_i\rho_i)^{1/2}+(\mu_o\rho_o)^{1/2}]^2} \\ & + \frac{(2l+1)\{2l(l^2-1)\mu_i^2\rho_i + 2l(l+2)\mu_o^2\rho_o + \mu_o\mu_i\{\rho_i(l+2)-\rho_o(l-1)]\}}{2R^2\Gamma[(\mu_i\rho_i)^{1/2}+(\mu_o\rho_o)^{1/2}]^2}\end{aligned} \tag{5.7}$$

where $\mu_o$ and $\mu_i$ are the continuous phase and droplet viscosities, respectively.

In real liquid-liquid processing systems, there usually is considerable droplet motion with respect to the continuous phase. Behavior of oscillating droplets that undergo significant motion has been treated by Subramanyam (1969). In this work, it is assumed that the initial droplet deformation is taken in a direction that is parallel to the axis of droplet translation: a point that is inferred from his use of streamlines to describe the (axisymmetric ) flow. For the l=2 mode of oscillation, the frequency and decay factor are given by quite simple expressions when the Reynolds number, $Re_i \equiv \rho_i U R/\mu_i$, and Weber number, $We_i \equiv \rho_i R U^2/\gamma$, are both small:

$$\beta_I = \frac{(-4AC - B^2)^{1/2}}{2C} \tag{5.8}$$

and

$$\beta_R = \frac{B}{2C} \tag{5.9}$$

where

$$A = -\frac{40(k+1)\gamma}{\rho_i} \tag{5.10}$$

$$B = \frac{[38k^2 + 89k + 48]\mu_i}{R^2\rho_i k} \tag{5.11}$$

$$C = \frac{26k + 29}{4} - \frac{16k + 14}{\rho_i/\rho_o} \tag{5.12}$$

and $k \equiv \mu_i/\mu_o$.

The effect of fluid motion which is axisymmetric and parallel to the droplet oscillation is to further lower the frequency and decay factor relative to the values obtained by Lamb and M & S given above. After initial consideration in a paper by Prosperetti (1980), Basaran, et al. (1989) have given a comprehensive evaluation of the viscous droplet oscillation process described in M & S by converting the 6×6 matrix to a 3×3 matrix and numerically solving for the frequency of oscillation and damping factor. For the first time this allows one to calculate the natural frequency and damping factor for any mode of linear oscillation which fits the M & S criteria. Scott et al. (1990) tested the above theories by using pulsed electric fields to oscillate aqueous droplets falling through 2-ethyl-1-hexanol. Their data were bounded by predictions of Basaran et al (1989) and Subramanyam (1969). These results indicate that for isolated free drops, the natural frequency can now be calculated with reasonable accuracy. Thus, a pulsed field can be tuned-in to obtain the most efficient droplet dispersion.

The case for liquids streaming from nozzles once again appears to be much more complex. Experimental results on the electrodispersion of water in 2-ethyl-1-hexanol indicated that pulsed DC fields can accomplish the same extent of droplet dispersion utilizing a lower root-mean-square (rms) voltage than steady DC fields (Scott, 1991). In addition, the pulsed field behavior varied with pulse frequency, with 200-Hz fields being more effective for higher continuous phase

viscosities while 2000-Hz fields were more effective when the viscosity was lower. A steady DC field displayed invariant behavior with changing viscosity.

For experiments using the 2000-Hz field, the Taylor number (ratio of electric to viscous forces) remained constant for the cases studied, thus indicating that the dispersion behavior is controlled by the dynamic interactions of the forces induced by the transient field with the viscous interactions between both liquid phases. This implies that resonance is occurring and more easily forcing break-up of the liquid stream as it exits from the nozzle. This type of behavior lends a possibility to significantly increasing liquid dispersion rates from nozzles by properly adjusting the frequency of the pulsed electric field used to break-up the liquid stream.

The oscillation of drops from a nozzle must be solved by numerical methods such as three-dimensional finite element and boundary element techniques. Such problems require extensive computing capabilities that would tax even the largest supercomputer.

## 5.5. Solving the Electrohydrostatic Problem

As stated in a previous section, solving the effect of pulsed electric fields on drops hanging from a nozzle is very computer intensive. However, solving the simplier electrohydrostatic problem allows the determination of the shapes of drops at the point (instability point or turning point) where the droplet goes unstable and starts to jet. Such an analysis can be used to optimize the configuration of an electrodispersion device.

Equations 5.1 and 5.2 have been solved by finite element and boundary el-

ement methods to determine the equilibrium shapes and stability of an axisymmetric pendant or sessile conducting drop of fixed volume which is surrounded by a fluid insulator (Tsuka et. al. 1986, Basaran and Scriven, 1990, Harris and Basaran, 1991 and 1992). The drop is assumed to be attached to a variable length charged nozzle extending from a flat circular plate which is parallel to a grounded circular flat plate (Figs. 5.2 and 5.3).

The boundary conditions for this problem are

$$f_\theta = 0 \text{ at } \theta = 0 \tag{5.13}$$

$$f = 1 \text{ at } \theta = \frac{\pi}{2} \tag{5.14}$$

$$n \cdot \nabla U = 0 \text{ on the side boundaries,} \tag{5.15}$$

$$U = 1 \text{ on the top plate, nozzle and the drop, and} \tag{5.16}$$

$$U = 0 \text{ on the bottom plate.} \tag{5.17}$$

5.5.1. Finite Element Solution to the Augmented Young-Laplace Equation

The finite element method is used to convert integrodifferential equations into a system of algebraic expressions by discretizing the domain of the problem into subdomains or elements. The drop surface (Fig. 5.2) is discretized such that a fine mesh a located near the axis of symmetry (tip) and the contact line. The mesh size varies geometrically from a fine mesh to a coarse mesh where values of surface charge and drop shape functions do not vary rapidly with distance.

Each curvilinear element is mapped onto the line $\xi$, $0 \leq \xi \leq 1$, by the isoparametric transformation (Lapidus and Pinder 1982). Two linear basis functions are defined in each element . The basis functions have global numbers (1,2,

ORNL DWG 91A-846

## PROBLEM STATEMENT

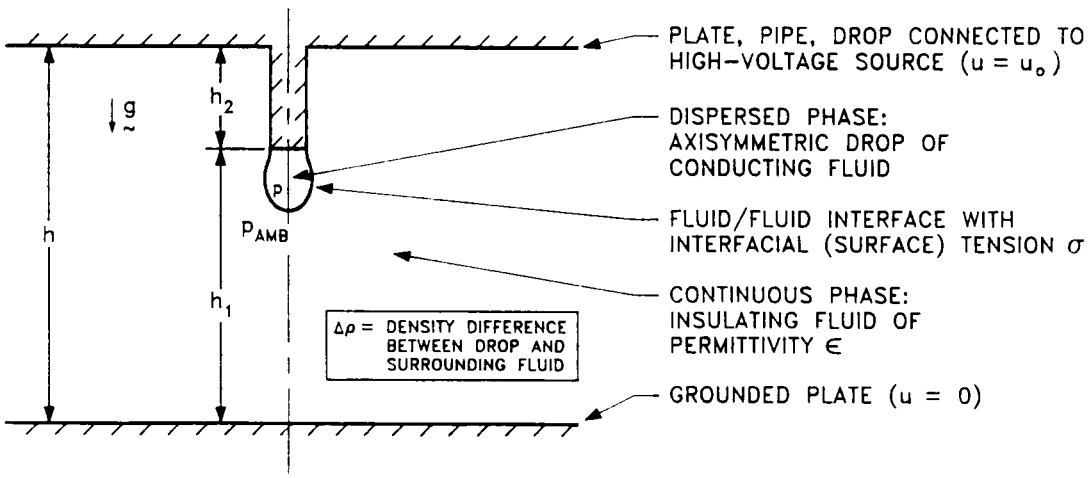
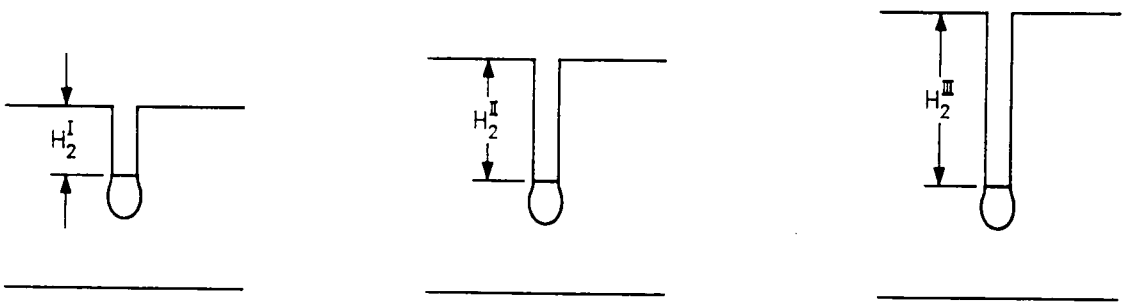



Fig. 5.2. Problem statement: a conducting drop hanging from a conducting nozzle in an insulating fluid placed between two parallel plates.




- AS $H_2$ GROWS WITHOUT BOUND, DROP NO LONGER SEES TOP PLATE
- THEREFORE, $\sqrt{N_e}$ OR $\mathcal{P}$ SHOULD APPROACH AN ASYMPTOTIC VALUE AS $H_2 \to \infty$

**Fig. 5.3. Effect of pipe length on drop shape and stability.**

$\cdots, N_\theta + 1$). The basis functions also have local numbers within each element that correspond to nodal numbering in the mapped $\xi$-domain.

The free surface of the drop and the spatial coordinate ($\theta$) are interpolated globally as

$$f(\theta) = \sum_{j=1}^{N_\theta} f_j \psi^j(\xi) \text{ and} \tag{5.18}$$

$$\theta = \sum_{j=1}^{N_\theta} \theta_j \psi^j(\xi). \tag{5.19}$$

The coefficients $\alpha_j$ and $\theta_j$ are nodal values of the free surface location and meridional angle measured from the axis of symmetry. Locally (i.e. inside each element), the free surface and $\theta$ are interpolated as

$$f(\theta) = \sum_{m=1}^{2} f_m \psi^m(\xi) \text{ and} \tag{5.20}$$

$$\theta = \sum_{m=1}^{2} \theta_m \psi^m(\xi). \tag{5.21}$$

The Galerkin weighted residual of Eq. 5.1 is formed by weighting this equation by $\psi^i(\underline{e}_r \cdot \underline{n}_{LV})$, where $\underline{e}_r$ is a radially directed unit vector, and $\psi^i$ is the global basis function

$$R_i^{YL} = \int_{S_{LV}} [-2\aleph - (K + N_e H^2 E_n^2)] \psi^i \underline{e}_r \cdot \underline{n}_{LV} dS_{LV} = 0. \tag{5.22}$$

Using the surface divergence theorem and integrating by parts, the curvature term of Eq. 5.22 is simplified and the working equation becomes

$$R_i^{YL} = \int_0^\pi \left[ \frac{f f_\theta \psi_\theta^i + \psi^i (2f^2 + f_\theta^2)}{\sqrt{f^2 + f_\theta^2}} - (K - Gz + N_e H^2 E_n^2) f^2 \psi^i \right] \sin\theta d\theta = 0 \tag{5.23}$$

Eq. 5.23is converted to the following parametric form by using equations 5.17 to 5.20

$$R_i^{YL} = \int_0^1 \left[ \frac{f f_\xi \psi_\xi^i + \psi^i (2\theta_\xi^2 f^2 + f_\xi^2)}{\sqrt{\theta_\xi f^2 + f_\xi^2}} - (K - Gz + N_e H^2 E_n^2)\theta_\xi f^2 \psi^i \right] \sin\theta \mathrm{d}\xi = 0 \tag{5.24}$$

5.5.2. Boundary Element Solution of the Laplace Equation

The fundamental equation for the BEM solution of the Laplace equation is obtained by multiplying Eq. 5.2 by the fundamental solution, i.e. Green's function, and integrating by parts twice. The initial equation, and te equations after the first and the second integration by parts are

$$\int_V \nabla^2 U G \mathrm{d}v = 0 \tag{5.25}$$

$$\int_V -\nabla G \cdot \nabla U \mathrm{d}v + \int_\Omega G n \cdot \nabla U \mathrm{d}a = 0 \tag{5.26}$$

$$\int_V U \nabla^2 G \mathrm{d}v + \int_\Omega G n \cdot \nabla U \mathrm{d}a - \int_\Omega U n \cdot \nabla G \mathrm{d}a = 0 \tag{5.27}$$

where the fundamental solution to the Laplace equation is

$$G = \frac{1}{4\pi |x - x'|}. \tag{5.28}$$

When $U$ is on the surface, eq. 5.27 reduced to

$$\varpi_{angle} U + \int_\Gamma U n \cdot \nabla G \mathrm{d}a = \int_\Gamma G n \cdot \nabla U \mathrm{d}a \tag{5.29}$$

Eq. 5.29 is the starting point for solving the Laplace equation by BEM. Either the potential or the charge density is specified over portions of the boundary $\Gamma$ bounding the domain of interest.

For axisymmetric problems, the physical variables and geometry of the domain are independent of the co-ordinate $\phi$ in a cylindrical coordinate system. The free space Green function, $G$, is , however, a function of $\phi$ (Ligget and Liu 1983). Therefore, Eq. 5.29 can be rewritten as

$$\varpi_{angle}U(r_i,z_i,t) - \oint_\Gamma \left[n\cdot U\int_0^{2\pi} g\mathrm{d}\phi\right] r\mathrm{d}\Gamma + \oint_\Gamma \left[U\int_0^{2\pi} n\cdot\nabla G\mathrm{d}\phi\right] r\mathrm{d}\Gamma = 0 \tag{5.30}$$

where the differential surface element $da = rd\theta\mathrm{d}\Gamma$ and $\Gamma$ is the generating boundary contour which is the projection of $\Omega$ in the r-z plane. An axisymmetric Green function is defined as

$$g(r,z;r_i,z_i) = \int_0^{2\pi} G\mathrm{d}\phi. \tag{5.31}$$

Substituting this into Eq. 5.30 gives the following BEM expression:

$$\varpi_{angle}U(r_i,z_i) - \oint_\Gamma gn\cdot\nabla U\ r\mathrm{d}\Gamma + \oint_\Gamma Un\cdot\nabla g\ r\mathrm{d}\Gamma = 0. \tag{5.32}$$

The axisymmetric Green's function, written in cylindrical coordinates (r,z) is

$$g(r,z,r_i,z_i) = \int_0^{2\pi} \frac{\mathrm{d}\phi}{(a-b\cos\phi)^{1/2}} = \frac{4}{(a+b)^{1/2}K(m)} \tag{5.33}$$

where

$$\begin{aligned} a &= r_i^2 + r^2 + z_d^2, \\ b &= 2rr_i, \\ z_d &= z - z_i, \end{aligned} \tag{5.34}$$

and $K(m)$ is the complete elliptic integral of the first kind,

$$K(m) = \int_0^{2\pi} \frac{\mathrm{d}\phi}{(1-m\sin^2\phi)^{1/2}},\ 0 \le m < 1 \tag{5.35}$$

The modulus, m, of the elliptic integral and its complementary modulus, $m_1 = 1 - m$, can be expressed specifically as follows:

$$m = \frac{4rr_i}{(r+r_i)^2 + z_d^2}, \tag{5.36}$$

$$m_1 = \frac{(r-r_i)^2 + z_d^2}{(r+r_i)^2 + z_d^2} \tag{5.37}$$

The elliptic integral is readily computed by the approximation

$$\begin{aligned} K(m) &= a_0 + a_1 m_1 + \cdots + a_4 m_1^4 - (b_0 + b_1 m_1 + \cdots + b_4)\log m_1 \\ &= P_K(m_1) + Q_K(m_1)\log m_1 \end{aligned} \tag{5.38}$$

where

$$\begin{cases} a_0 = 1.38629436112 & b_0 = 0.5 \\ a_1 = 0.09666344259 & b_1 = 0.121498593597 \\ a_2 = 0.03590092383 & b_2 = 0.06880248576 \\ a_3 = 0.03742563713 & b_3 = 0.03328355346 \\ a_4 = 0.01451196212 & b_4 = 0.00441787012 \end{cases}.$$

The expression $n \cdot \nabla g$ or $\frac{\partial g}{\partial n}$ along the surface of the drop can be written as

$$\begin{aligned} n \cdot \nabla g &= \frac{\partial g}{\partial n} n_r + \frac{\partial g}{\partial z} n_z \\ &= \frac{2n_r}{r(a+b)^{1/2}}[E(m) - K(m)] - 4\frac{[n_r(r-r_i) + n_z z_d]}{(a-b)(a+b)^{1/2}} E(m) \end{aligned} \tag{5.39}$$

$E(m)$ is the elliptic integral of the second kind and as with K(m), it is expressed as a polynomial approximation

$$\begin{aligned} E(m) &= 1 + c_1 m_1 + \cdots + c_4 m_1^4 - (d_1 m_1 + \cdots + d_4 m_1^4)\log m_1 \\ &= P_E(m_1) + Q_E(m_1)\log m_1 \end{aligned} \tag{5.40}$$

where

$$\begin{cases} c_1 = 0.44325141463 & d_1 = 0.24998368310 \\ c_2 = 0.06260601220 & d_2 = 0.09200180037 \\ c_3 = 0.04757483546 & d_3 = 0.04069697526 \\ c_4 = 0.01746596451 & d_4 = 0.00426449639 \end{cases}.$$

Integration of Equation 5.32 is accomplished by discretizing the boundary into $N_T$ elements as discussed in the previous section. Similar to FEM, each curvilinear element is mapped onto a line with co-ordinate $\xi$, $0 \leq \xi \leq 1$, by the isoparametric transformation. On the surface of the drop, the nodes for the boundary elements and finite elements coincide.

The unknown surface charge density is expanded in a set of linear basis functions

$$\sigma(\theta) = \sum_{i=1}^{N_T} \sigma_i \psi^i(\xi). \tag{5.41}$$

The spatial coordinates, ($r$ and $z$) are interpolated, globally and locally, respectively, as

$$\begin{aligned} z &= \sum_{i=1}^{N_T} f_i \cos\theta_i \psi^i(\xi) \\ z &= \sum_{j=1}^{2} f_j \cos\theta_j \psi^j(\xi) \\ r &= \sum_{i=1}^{N_T} f_i \sin\theta_i \psi^i(\xi) \\ r &= \sum_{j=1}^{2} f_j \cos\theta_j \psi^j(\xi) \end{aligned} \tag{5.42}$$

Converting to parametric form, the residual equation (Eq. 5.32) for the

BEM becomes

$$R_i^L = \varpi_i U_i - \sum_{j=1}^{N_T} \int_0^1 \sigma_j(\xi) - [P_K(m_1) + Q_K(m_1)\log m_1] r(\xi) J \mathrm{d}\xi$$
$$+ \sum_{j=1}^{N_T} \int_0^1 U_j(\xi) \left\{ \frac{2n_r}{r(a+b)^{1/2}} [P_E(m_1) - P_K(m_1)] \right\} r(\xi) J \mathrm{d}\xi$$
$$+ \sum_{j=1}^{N_T} \int_0^1 U_j(\xi) \left\{ \frac{2n_r}{r(a+b)^{1/2}} [(Q_E(m_1) - Q_K(m_1))\log m_1] \right\} r(\xi) J \mathrm{d}\xi$$
$$+ \sum_{j=1}^{N_T} \int_0^1 U_j(\xi) \left\{ \frac{4[n_r(r-r_i) + n_z z_d]}{(a-b)(a+b)^{1/2}} (P_E(m_1) - Q_E(m_1)\log m_1) \right\}$$
$$r(\xi) J \mathrm{d}\xi \tag{5.43}$$

where the Jacobian of the mapping is given by

$$J = \sqrt{(f_{i+1}\sin\theta_{i+1} - f_i \sin\theta_i)^2 + (f_{i+1}\cos\theta_{i+1} - f_i \cos\theta_i)^2} \tag{5.44}$$

The lengths of the $r$ and $z$ components of the unit normal vector to each surface element are computed by the following equations for linear basis functions

$$n_r = \frac{(f_{i+1}\cos\theta_{i+1} - f_i \cos\theta_i)}{Jac} \tag{5.45}$$

$$n_z = \frac{(f_i \sin\theta_i - f_{i+1}\sin\theta_{i+1})}{Jac} \tag{5.46}$$

For an interior problem, $\varpi$ can be computed from the expression

$$\varpi = -\sum_{j=1}^{N_T} \int_0^1 \frac{\partial g}{\partial n} r \mathrm{d}\xi \tag{5.47}$$

### 5.5.3 Solution of Systems of Nonlinear Equations by Newton's Method

The system of nonlinear equations (Eqs. 5.3, 5.24 and 5.43) is solved simultaneously for the drop shape, surface potentials and surface charge densities by Newton's method. This iterative method updates each successive approximation to the solution in accordance with the expressions

$$\underline{x}^{k+1} = \underline{x}^k - [\underline{\underline{J}}^{-1}(\underline{x}^k)]\underline{R}(\underline{x}^k), \tag{5.48}$$

where $\underline{\underline{J}} \equiv \frac{\partial \underline{R}}{\partial \underline{x}}$ or

$$\begin{bmatrix} \frac{\partial \underline{R}^{YL}}{\partial \underline{\alpha}} & \frac{\partial \underline{R}^{YL}}{\partial \underline{K}} & \frac{\partial \underline{R}^{YL}}{\partial \underline{N}_e} & \frac{\partial \underline{R}^{YL}}{\partial \underline{\sigma}} & \underline{0} \\ \frac{\partial \underline{R}^{VC}}{\partial \underline{\alpha}} & \underline{0} & \underline{0} & \underline{0} & \underline{0} \\ 0 & \cdots & 1 & \cdots & 0 \\ \frac{\partial \underline{R}^{L}}{\partial \underline{\alpha}} & \underline{0} & \underline{0} & \frac{\partial \underline{R}^{L}}{\partial \underline{\sigma}} & \frac{\partial \underline{R}^{L}}{\partial \underline{U}} \end{bmatrix}^{(k)} \begin{bmatrix} \Delta\underline{\alpha} \\ \Delta\underline{K} \\ \Delta\underline{N}_e \\ \Delta\underline{\sigma} \\ \Delta U \end{bmatrix}^{(k+1)} = - \begin{bmatrix} \underline{R}^{YL} \\ R^{VC} \\ \underline{0} \\ \underline{R}^{L}_{\sigma} \\ \underline{R}^{L}_{U} \end{bmatrix}^{(} \quad k) \tag{5.49}$$

The augmented Young-Laplace and Laplace residuals are given by Eqs. 5.24 and 5.43. The volume constant residual and adaptive parameterization residuals are

$$R^{VC} = R_{N_\theta+2} = V_o - V = \frac{1}{3} - \frac{\theta_\xi}{3}\int_0^1 f^3 \sin\theta \mathrm{d}\xi = 0, \text{ and} \tag{5.50}$$

$$R_{N_\theta+3} = p - p_o - \Delta p = 0, \text{ respectively.} \tag{5.51}$$

The Jacobian entries are computed from the following equations:

$$\frac{\partial R_i^{YL}}{\partial f_j} = \int_0^1 [\frac{\psi^j f_\xi \psi_\xi^i + f\psi_\xi^i \psi_\xi^j + \psi^i(4\theta_\xi^2 f\psi^j + 2f\psi_\xi^j)}{\sqrt{\theta_\xi^2 f^2 + f_\xi^2}}$$
$$- \frac{f f_\xi \psi_\xi^i + \psi^i(2\theta_\xi^2 f^2 + f_\xi^2)}{(\theta_\xi^2 f^2 + f_\xi^2)^{3/2}}(\theta_\xi^2 f\psi^j + f_\xi \psi_\xi^j)]\sin\theta \mathrm{d}\xi$$
$$- 2\int_0^1 (K + N_e H^2 E_n^2)\theta_\xi f\psi^i\psi^j)\sin\theta \mathrm{d}\xi \tag{5.52}$$

$$\frac{\partial R^{VC}}{\partial f_i} = \theta_\xi \int_0^1 f^2\psi^i \sin\theta \mathrm{d}\xi \tag{5.53}$$

$$\frac{\partial R_p}{\partial p} = 1 \tag{5.54}$$

$$\frac{\partial R_i^{YL}}{\partial K} = -\theta_\xi \int_0^1 f^2\psi^i \sin\theta \mathrm{d}\xi \tag{5.55}$$

$$\frac{\partial R_i^{YL}}{\partial N_e} = -\theta_\xi \int_0^1 H^2 E_n^2 f^2 \psi^i \sin\theta \mathrm{d}\xi \tag{5.56}$$

$$\frac{\partial R_i^{YL}}{\partial E_{nj}} = \frac{\partial R_i^{YL}}{\partial \sigma_j} = -2\theta_\xi \int_0^1 H^2 E_n f^2 \psi^i \sin\theta \mathrm{d}\xi \tag{5.57}$$

$$\frac{\partial R_i^L}{\partial f_j} = U_i \frac{\partial \varpi_i}{\partial \alpha_j} - \int_0^1 \sigma(\xi)\left[\frac{\partial g}{\partial f_j} r(\xi) J + g\frac{\partial r(\xi)}{\partial f_j} J + g r(\xi)\frac{\partial J}{\partial f_j}\right] \mathrm{d}\xi$$
$$+ \int_0^1 U(\xi)\left[\frac{\partial \frac{\partial g}{\partial n}}{\partial f_j} r(\xi) J + \frac{\partial g}{\partial n}\frac{\partial r(\xi)}{\partial f_j} J + \frac{\partial g}{\partial n} r(\xi)\frac{\partial J}{\partial f_j}\right] \mathrm{d}\xi \tag{5.58}$$

where

$$\frac{\partial g}{\partial f_j} = \frac{\partial P_K}{\partial m_1}\frac{\partial m_1}{\partial f_j} - \frac{\partial Q_k}{\partial m_1}\frac{\partial m_1}{\partial f_{-j}} - \frac{Q_k}{m_1}\frac{\partial m_1}{\partial f_j} \tag{5.59}$$

and

$$\frac{\partial \frac{\partial g}{\partial n}}{\partial f_j} = \left[\frac{2\frac{\partial n_r}{\partial f_j}}{r(a+b)^{1/2}} - \frac{2n_r}{r^2(a+b)^{1/2}}\frac{\partial r}{\partial f_j} - \frac{n_r(\frac{\partial a}{\partial f_j}+\frac{\partial b}{\partial f_j})}{r(a+b)^{3/2}}\right]$$

$$[P_E - P_K + (Q_E - Q_K)\log m_1 + \frac{2n_r}{r(a+b)^1/2}$$

$$\left[\frac{\partial P_E}{\partial m_1}\frac{\partial m_1}{\partial f_j} - \frac{\partial P_K}{\partial m_1}\frac{\partial m_1}{\partial f_j} + (\frac{\partial Q_E}{\partial m_1}\frac{\partial m_1}{\partial f_j} - \frac{\partial Q_K}{\partial m_1}\frac{\partial m_1}{\partial f_j})\log m_1\right]$$

$$+ \frac{2n_r}{r(a+b)^1/2}\left[\frac{(Q_E - Q_K)}{m_1}\frac{\partial m_1}{\partial f_j}\right]$$

$$- [\frac{4(\frac{\partial n_r}{\partial f_j}(r-r_i) + n_r\frac{\partial(r-r_i)}{\partial f_j} + \frac{\partial n_z}{\partial f_j}z_d + n_z\frac{\partial z_d}{\partial f_j})}{(a-b)(a+b)^{1/2}}$$

$$- \frac{4(n_r(r-r_i)+n_z z_d)}{(a-b)(a+b)^{1/2}} - \frac{2(n_r(r-r_i)+n_z z_d)}{(a-b)(a+b)^{3/2}}(\frac{\partial a}{\partial f_j} - \frac{\partial b}{\partial f_j})]$$

$$(P_E - Q_E\log m_1) + \frac{4(n_r(r-r_i)+n_z z_d)}{(a-b)(a+b)^{1/2}}\left(\frac{\partial P_E}{\partial f_j} - \frac{\partial Q_E}{\partial f_j}\log m_1\right) -$$

$$\frac{Q_E}{m_1}\frac{\partial m_1}{\partial f_j} \qquad (5.60.)$$

$$\frac{\partial R_i^L}{\partial U_j} = \varpi_j - \int_0^1 \sum_{j=1}^{N_T}\int_0^1 \psi^j(\xi)\left\{\frac{2n_r}{r(a+b)^{1/2}}[P_E(m_1) - P_K(m_1)]\right\} r(\xi)Jacd\xi$$

$$- \int_0^1 \sum_{j=1}^{N_T}\int_0^1 \psi^j(\xi)\left\{\frac{2n_r}{r(a+b)^{1/2}}[(Q_E(m_1) - Q_K(m_1))\log m_1]\right\}$$

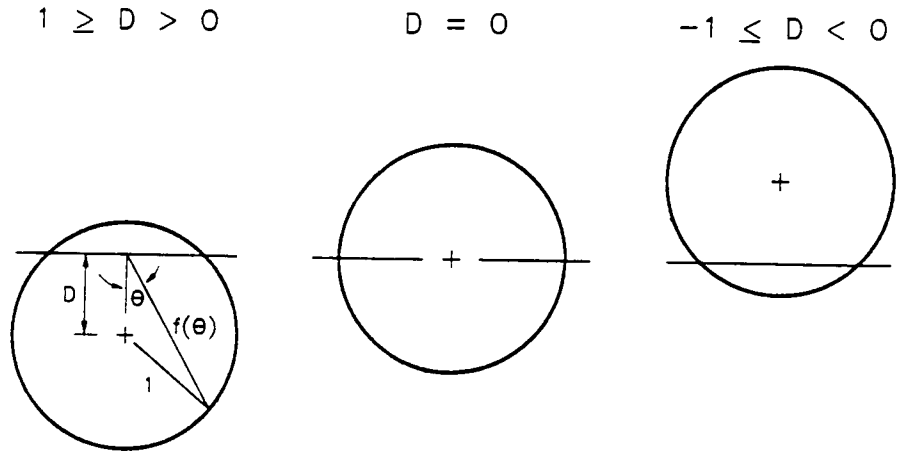
$$r(\xi)Jd\xi$$

$$+ \sum_{j=1}^{N_T}\int_0^1 \psi^j(\xi)\left\{\frac{4[n_r(r-r_i)+n_z z_d]}{(a-b)(a+b)^{1/2}}(P_E(m_1) - Q_E(m_1)\log m_1)\right\}$$

$$r(\xi)Jd\xi \qquad (5.61)$$

$$\frac{\partial R_i^L}{\partial \sigma_j} = -\sum_{j=1}^{N_T}\int_0^1 \psi^j(\xi) - [P_K(m_1) + Q_K(m_1)\log m_1]r(\xi)Jd\xi \qquad (5.62)$$

Newton's method was initiated by solving the residual equations for an initial section of a sphere of size $D$ (Fig. 5.4) for $N_e = 0$.




$$G = N_e = 0 \Rightarrow f(\theta) = D \cos\theta + \sqrt{1 - D^2 \sin^2\theta}$$

$$V_{DROP} = \frac{\pi}{3} (1 + D)^2 (2 - D)$$

- RADIUS, R, OF SPHERICAL SEGMENT CONVENIENT LENGTH SCALE (viz., D = d/R)
- DROP SIZE PARAMETER, D, IS EASILY RELATED TO PIPE RADIUS (viz., $R_{PIPE} = \sqrt{1 - D^2}$

Fig. 5.4. Initial drop shape: pendant/sessile drop in absence of external forces.

The drop shape is fixed and BEM is used to solve the uncoupled Laplace equation for the unknown values of surface charge and for potential. $N_e$, the initial marching parameter, is increased; thus, the problem becomes nonlinear and the Laplace and Young-Laplace equations are coupled and the iterative Newton's method is used. The adaptive parameterization technique is employed thereafter to optimize convergence and to continue past turning (or limit) points. A summary of the dimensionless groups are given in Table 5.1

## 5.6. Results: Theoretical Analysis of Axisymmetric Electrohydrostatics Problem

Numerical solutions to the Laplace and Young-Laplace equations were obtained to determine the optimal configuration for the axisymmetric electrode-nozzle design given in section 5.5.1. In addition to the electrode configuration, it was also of interest to determine the effect of varying the drop size on the electric field strength and drop shape at the stability limit.

Before using the numerical algorithm to perform a parametric study, several test runs were done to determine the accuracy of the method by comparing numerically and analytically computed total charges on a hemisphere, by evaluating the effect of side boundary location, and by determining the effect of the discretization on the value of the effective potential at the stability limit. The total charge on a hemisphere computed by the numerical algorithm and analytical expression were in excellent agreement, 0.94248 and 0.94422, respectively, (0.18% difference). The effect of discretization is summarized in Table 5.2, where it is shown that the combination of $N_{Drop} = 40$; $N_{Nozzle} = 20$; $N_{Top}$=$N_{Bottom}$=$N_{Side}$=10 is sufficient to obtain accurate results up to the sta-

Table 5.1. Governing Dimensionless Groups

| Dimensionless Group | |
|---|---|
| $N_E$ = Electrical bond number = $\dfrac{\text{Electrostatic}}{\text{Surface energy}}$ | $\frac{\epsilon u_o^2}{2\sigma R}$ |
| $G$ = Gravitational bond number = $\dfrac{\text{Gravitational}}{\text{Surface energy}}$ | $\frac{gR^2\Delta\rho}{\sigma}$ |
| $H$ = Distance between plates | $h/R$ |
| $H_1$ = Distance between pipe and bottom plate, or | $h_1/R$ |
| $H_2$ = Length of Pipe | $h_2/R$ |
| $D$ = Drop size parameter | $d/R$ |

$^*\mathcal{P} = \sqrt{\frac{\epsilon}{2\sigma R}}u_o$ = Dimensionless "effective" potential

$\mathcal{E} = \mathcal{P}/H$ = Dimensionless parallel-plate field strength

bility limit.

Tables 5.3 and 5.4 give the effect of the side boundary location on the accuracy of the results. It is observed that accurate solutions are obtained when the side boundary located at a distance 2-4 times the plate spacing. As the side boundary is extended very far past this distance, the solution begins to deteriorate. This situation can be rectified by employing more elements (c.f. Tables 5.2 and 5.3).

The typical deformation of an initially hemispherical drop in a static electric field is shown in Figs. 5.5 and 5.6.

Figure 5.5 illustrates how the drop shape is affected by the applied effective potential. Evidently, the droplet goes unstable and jetting occurs at an effective potential of 1.955. The solution that is represented by the dashed lines occurs beyond the turning point and, therefore, does not represent a real physical solution.

Fig. 5.6 shows how the drop aspect ratio increases with increasing in effective potential, $P$. Beyond the turning point, the aspect ratio continuous to increase whereas $P$ decreases. As the pipe length increases while keeping the distance between the tip of the pipe and bottom plate fixed (Fig. 5.6), the effective potential, $P_{TP}$, required to cause instability decreases and approaches to an asymptotic value as $H_2 \rightarrow \infty$(Fig. 5.7).

To elucidate the behavior of $P_{TP}$ with increasing pipe length, it is instructive to plot how surface charge distributes on the drop surface (Figs. 5.8 and 5.9) .

Figs. 5.8 and 5.9 make plain that the surface charge densities approach assymptotic values for $P = 0$ and $P = P_{TP}$ as the pipe length grows without bound. Fig. 5.9 also shows that the surface charge density can increase rapidly

Table 5.2. Effect of number of elements on the turning point (H=10, $H_2$=5, L=40)

| Number of Elements | | | | | | | |
|---|---|---|---|---|---|---|---|
| $N_{Drop}$ | $N_{Nozzle}$ | $N_{Top}$ | $N_{Side}$ | $N_{Bottom}$ | $N_e^*$ | a/b* | % diff |
| 10 | 10 | 10 | 10 | 10 | 0.021654 | 1.3275 | 0.494 |
| 20 | 20 | 20 | 20 | 20 | 0.021736 | 1.3488 | 0.115 |
| 30 | 30 | 30 | 30 | 30 | 0.021755 | 1.3401 | 0.028 |
| 40 | 40 | 40 | 40 | 40 | 0.021761 | 1.3372 | 0.000 |
| 10 | 40 | 40 | 40 | 40 | 0.021714 | 1.3151 | 0.216 |
| 20 | 40 | 40 | 40 | 40 | 0.021744 | 1.3413 | 0.078 |
| 30 | 40 | 40 | 40 | 40 | 0.021757 | 1.3383 | 0.018 |
| 40 | 10 | 40 | 40 | 40 | 0.021714 | 1.3327 | 0.216 |
| 40 | 20 | 40 | 40 | 40 | 0.02174 | 1.3435 | 0.097 |
| 40 | 30 | 40 | 40 | 40 | 0.021755 | 1.3390 | 0.028 |
| 40 | 40 | 10 | 40 | 40 | 0.021756 | 1.3386 | 0.023 |
| 40 | 40 | 20 | 40 | 40 | 0.021761 | 1.3374 | 0.000 |
| 40 | 40 | 30 | 40 | 40 | 0.021761 | 1.3373 | 0.000 |
| 40 | 40 | 40 | 10 | 40 | 0.021761 | 1.3372 | 0.000 |
| 40 | 40 | 40 | 20 | 40 | 0.021761 | 1.3372 | 0.000 |
| 40 | 40 | 40 | 30 | 40 | 0.021761 | 1.3372 | 0.000 |
| 40 | 40 | 40 | 40 | 10 | 0.021746 | 1.3406 | 0.069 |
| 40 | 40 | 40 | 40 | 20 | 0.021760 | 1.3375 | 0.005 |
| 40 | 40 | 40 | 40 | 30 | 0.021761 | 1.3373 | 0.000 |

Table 5.3. Effect of plate diameter on the turning point

($N_{Drop}$ = 30: $N_{Nozzle}$ = 30: $N_{Top}$ = 20: $N_{Side}$ = 10: $N_{Bottom}$ = 20)

| Plate Diameter | $N_e^*$ | a/b* | % diff |
|---|---|---|---|
| 10 | 0.021831 | 1.3327 | 0.321 |
| 20 | 0.021751 | 1.3400 | 0.046 |
| 40 | 0.021749 | 1.3405 | 0.055 |
| 80 | 0.021725 | 1.3463 | 0.166 |

Table 5.4. Effect of plate diameter on

the turning point

($N_{Drop}$ = 40: $N_{Nozzle}$ = 40: $N_{Top}$ = 40: $N_{Side}$ = 40: $N_{Bottom}$ = 40)

| Plate Diameter | $N_e^*$ | a/b* | % diff |
|---|---|---|---|
| 10 | 0.021839 | 1.3318 | 0.358 |
| 20 | 0.021761 | 1.3372 | 0.000 |
| 40 | 0.021761 | 1.3372 | 0.000 |
| 80 | 0.021759 | 1.3377 | 0.009 |

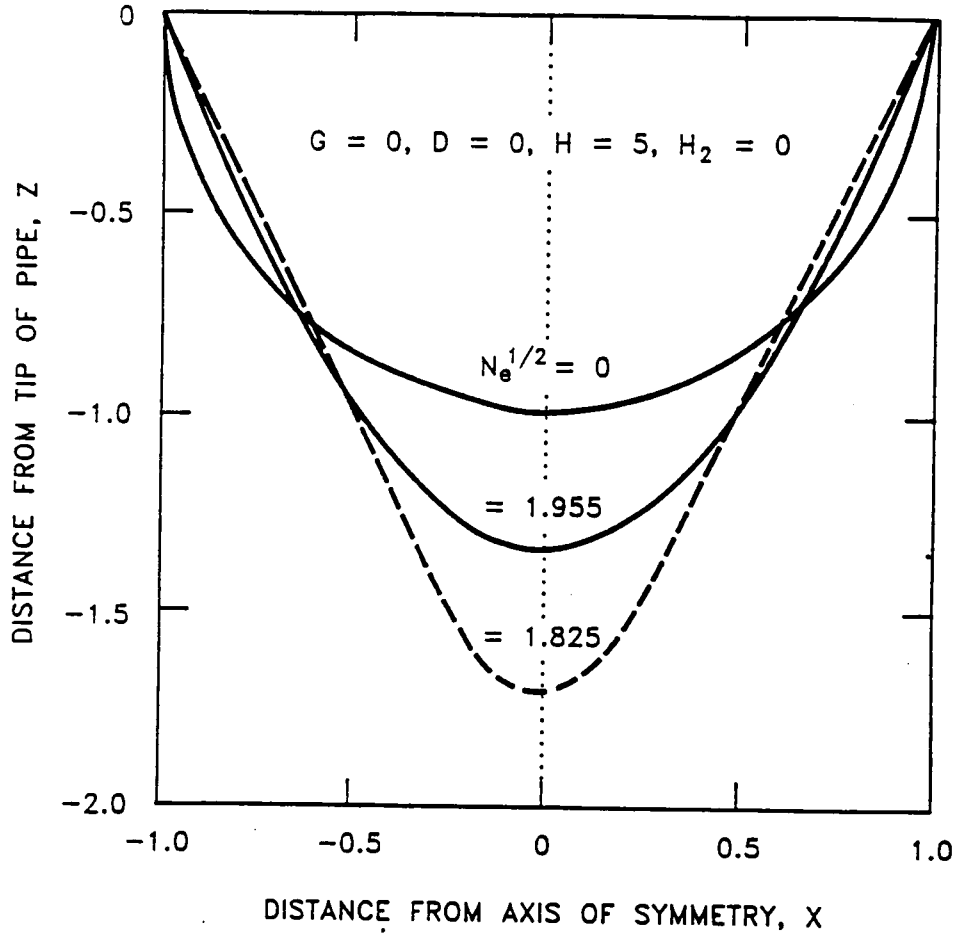



Fig. 5.5. Typical axisymmetric drop profiles in an electric field.

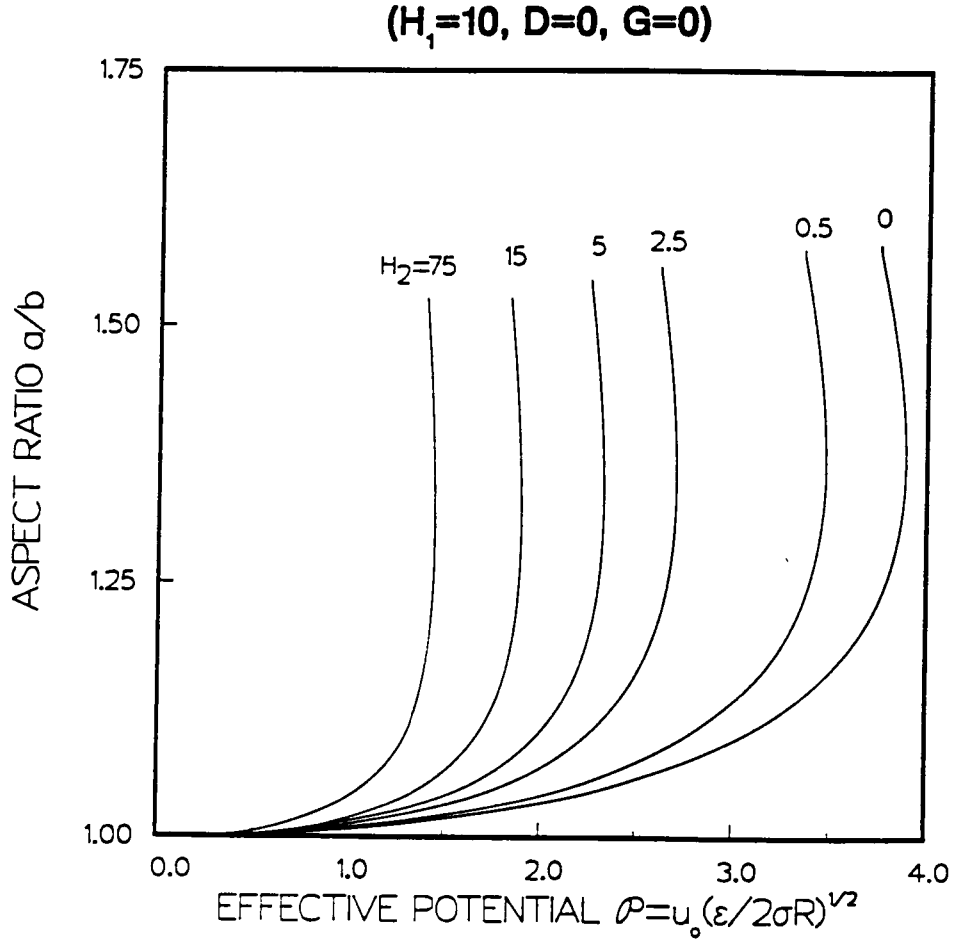



Fig. 5.6. Solution families in parameter space: effect of pipe length on aspect ratio.

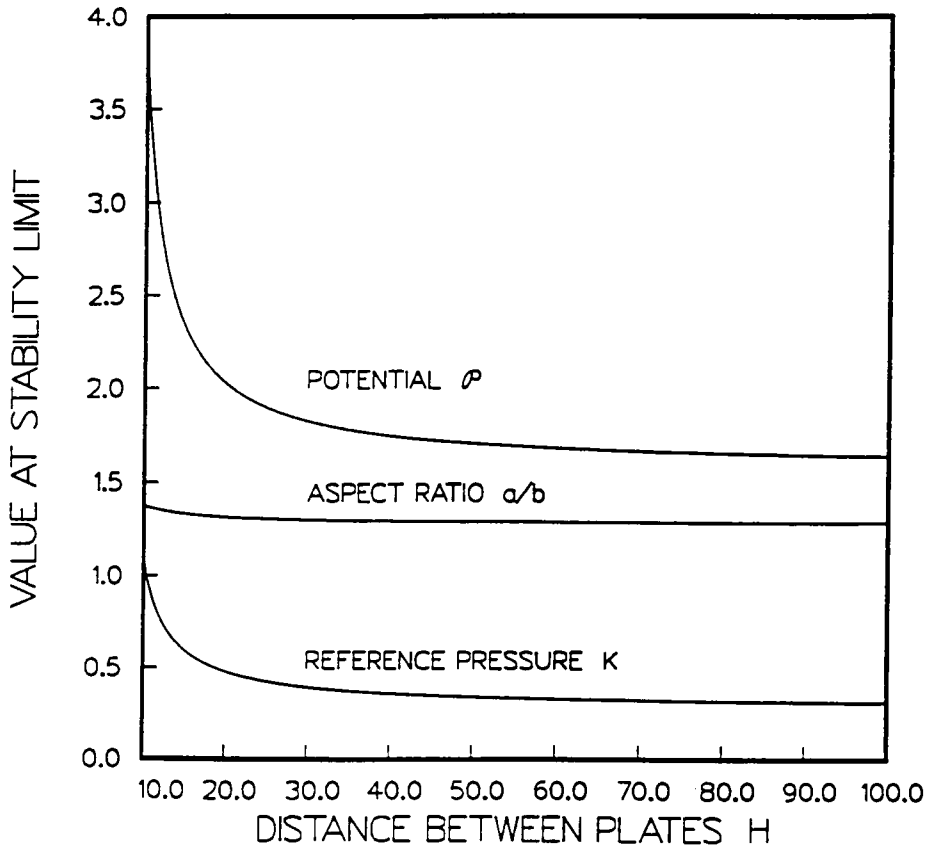



Fig. 5.7. Effect of pipe length on drop stability when distance between tip of pipe and bottom plate is held fixed ($H_1$=10, D=0, G=0).

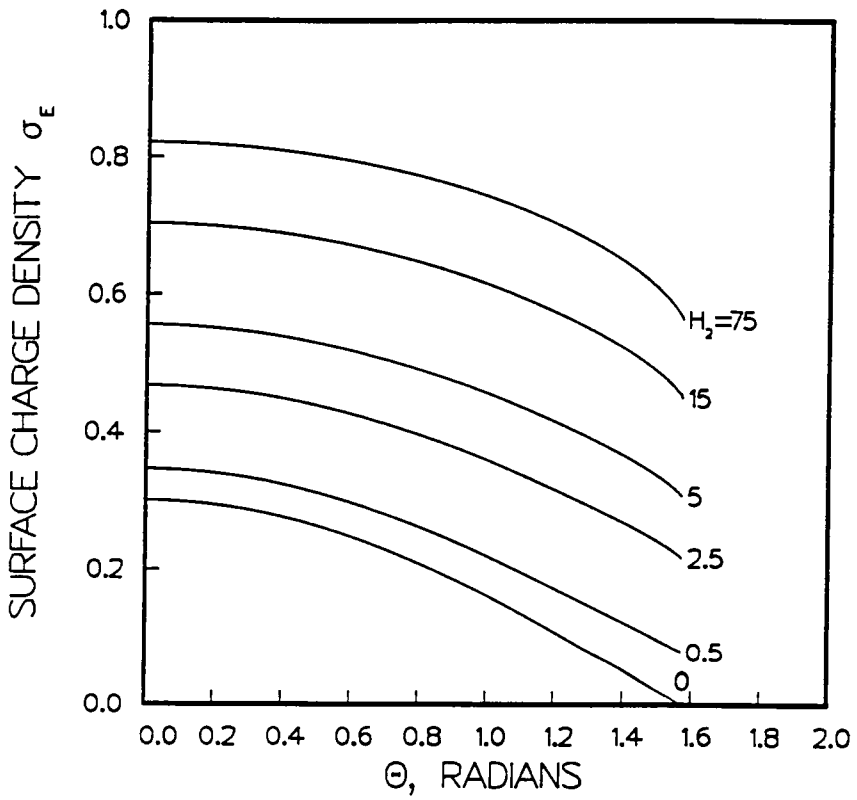



Fig. 5.8. Distribution of surface charge on supported drops when (electrical/surface forces=0) ($H_1$=10, D=0, G=0)

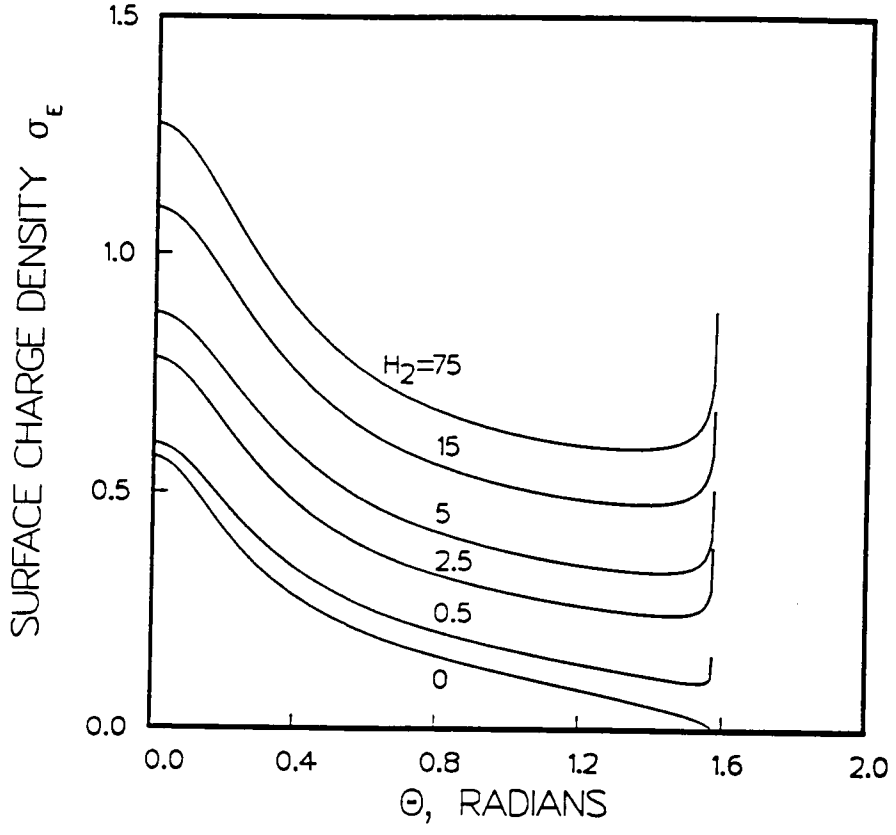



Fig. 5.9. Distribution of surface charge on supported drops at turning point (stability limit) ($H_1$=10, D=0, G=0).

near the contact line when a pipe is present. This can be explained by examining how surface charge distributes on pendant or sessile drops near a corner (see Fig. 5.10).

When $P = 0$, the drop is a hemisphere and the surface charge densities should vary as indicated by the middle figure of Case II for $\beta = \pi$. For $P = P_{TP}$, the drop deforms in such a manner that $\pi < \beta < \frac{3\pi}{2}$. In the latter case, the third figure of Case II in Fig. 5.10 shows that $\sigma_E \rightarrow \infty$ as the contact line is approached.

Since the surface charge densities increase with pipe length, the total surface charge and force on the drop should also increase and approach asymptotic values as the pipe length grows without bound (Fig. 5.11). These new results demonstrate that the presence of a pipe enhances electrodispersion by causing more charge to accumulate on the drop surface.

The effect of moving the bottom plate away from the tip of a pipe of fixed length is also evaluated. In this case, as is shown by Fig. 5.12, the electric field strength, $\mathcal{E}_{TP}$, instead of $P_{TP}$ should approach an asymptotic value as the plate spacing grows without bound. This is shown for several fixed pipe lengths (Figs. 5.13, 5.14 and 5.15).

These figures show as expected that best pipe-electrode configuration occurs when a long pipe is used and the distance between the tip of the pipe and the bottom plate is minimal. In a real experiment, the maximum deformation of the drop determines the minimum distance between the plates at which short circuiting occurs due to the drop bridging the conducting pipe and the bottom plate.

Figs. 5.16-5.20 show charge distributes along the top and bottom plates,

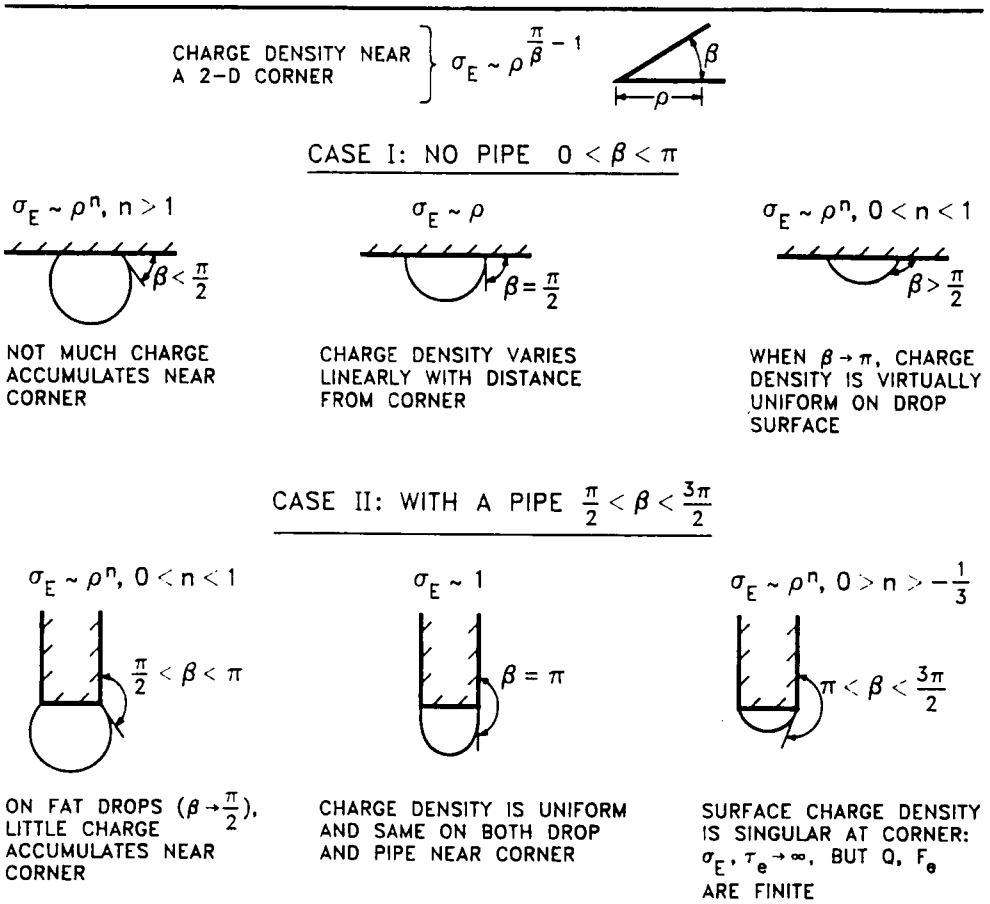



Fig. 5.10. Distribution of surface charge on pendant/sessile drops near contact line.

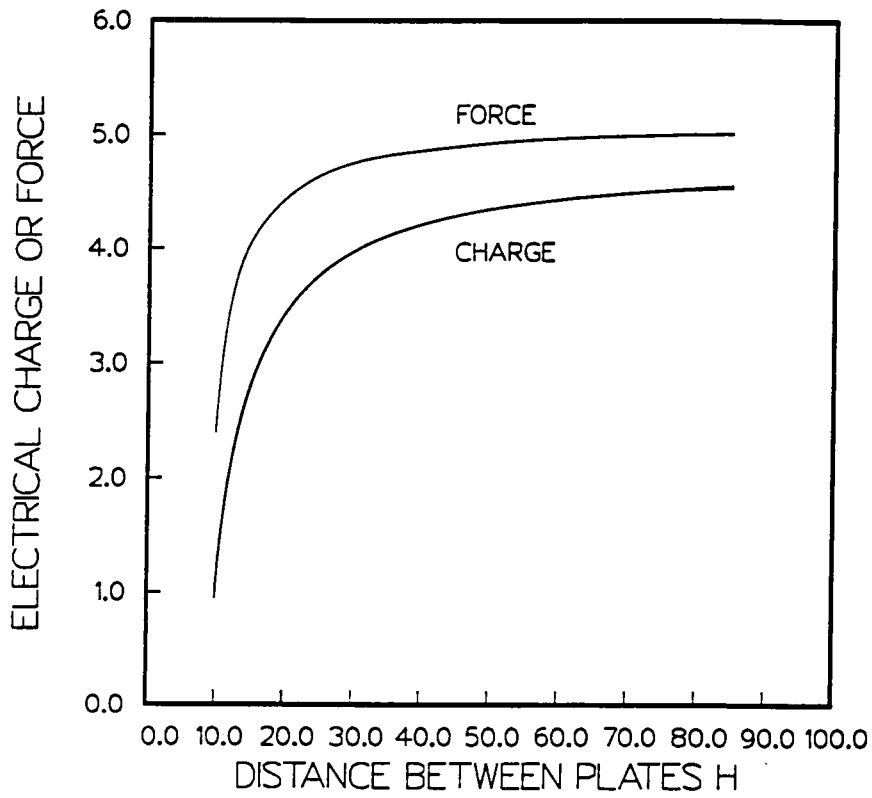
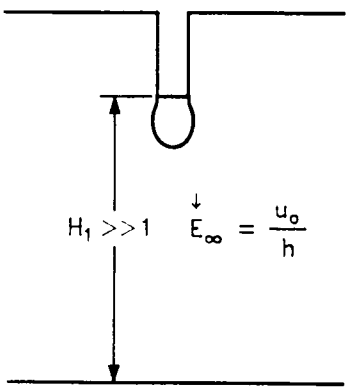



Fig. 5.11. Effect of pipe length on total surface charge and electrical force on supported drops ($H_1$=10, D=0, G=0).




- ELECTRIC STRESS = $P_e = N_e E_n^2$
- RESCALE USING $u_o/h$ AS CHARACTERISTIC FIELD INSTEAD OF $u_o/R$; THEN,

$$P_e = \frac{\epsilon R}{2\sigma} E_\infty^2 \left(\frac{\tilde{E}_n}{E_\infty}\right)^2$$

$$= \frac{N_e}{H^2} E_n^2$$

- THEREFORE, $\sqrt{N_e}/H^2$ OR $\mathcal{E}$ SHOULD APPROACH AN ASYMPTOTIC VALUE AS $H_1 \to \infty$

Fig. 5.12. Effect of moving bottom plate away from drop and tip of pipe.

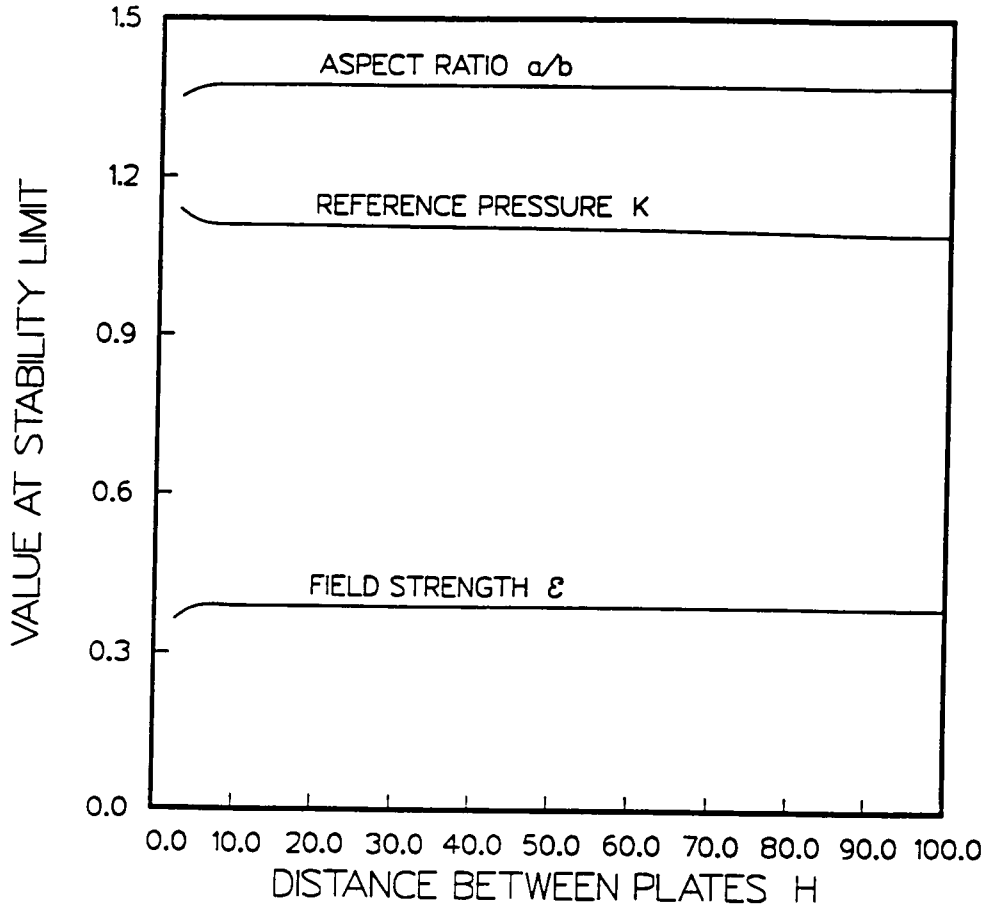



Fig. 5.13. Effect of increasing plate spacing on drop stability: case of no pipe ($H_2$=0, D=0, G=0).

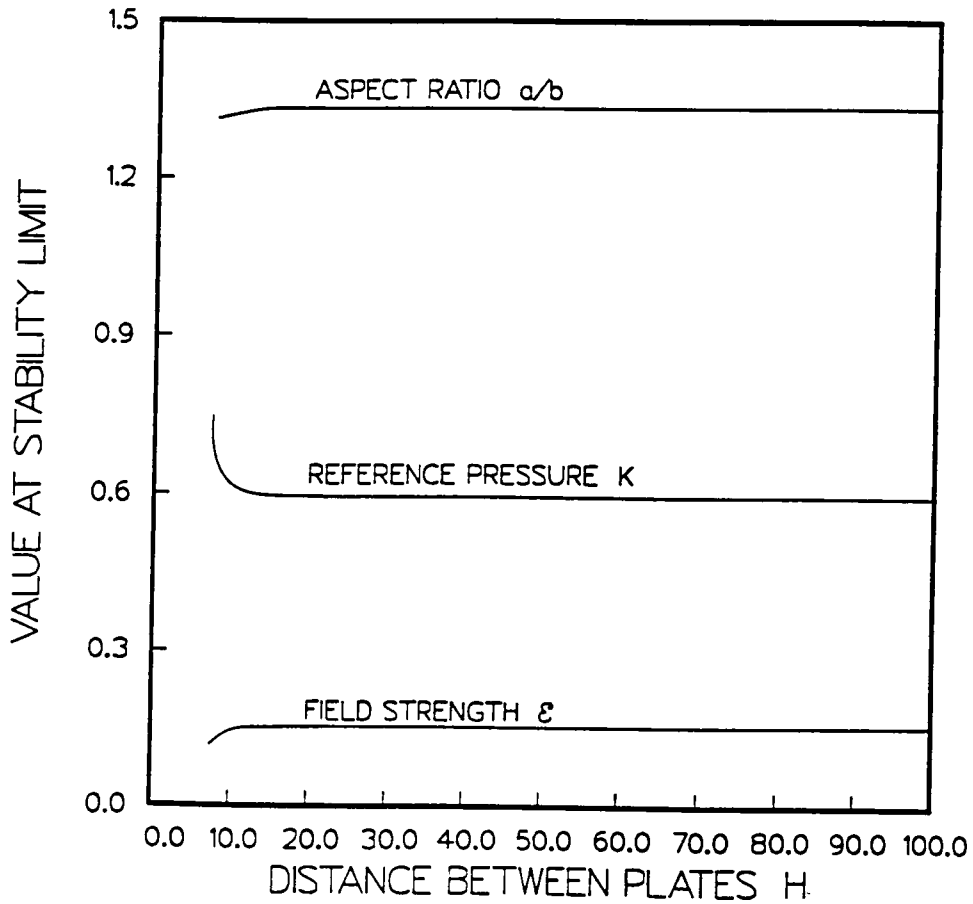



Fig. 5.14. Effect of increasing plate spacing on drop stability: case of short pipe ($H_2$=5, D=0, G=0).

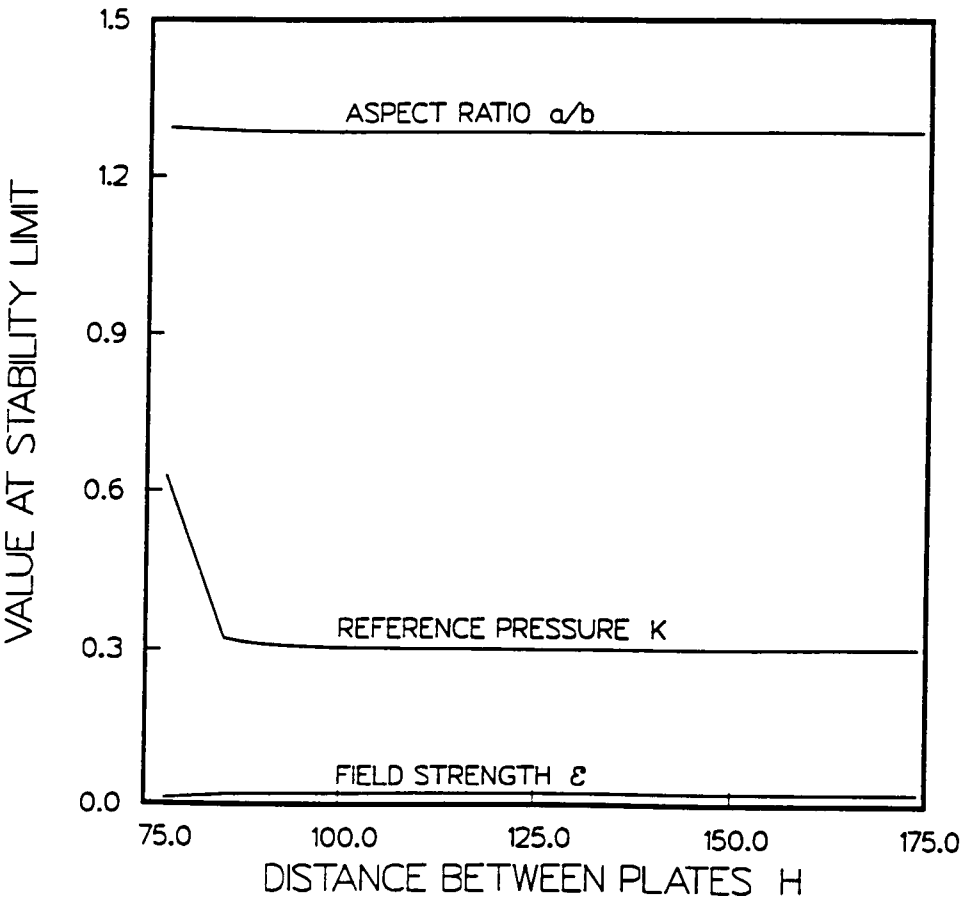



Fig. 5.15. Effect of increasing plate spacing on drop stability: case of long pipe ($H_2$=75, D=0, G=0).

and on the pipe, for situations in which there is no pipe, a short pipe and a long pipe.

The analytic asymptotic surface charge densities for the top and bottom plates in the absence of a pipe and a drop are indicated in Figs. 5.16-5.18.

As was stated earlier, a constant surface charge density is attained at a radial distance less than twice the plate separation, which shows that the assymptotic boundary conditions are met. Figs. 5.16-5.18 show that there is excellent agreement between the analytical asymptotic charge densities and those computed by the numerical method. Figs. 5.19 and 5.20 show the surface densities along the pipe for $\mathcal{P} = 0$ and $\mathcal{P} = \mathcal{P}_{TP}$. Remarkably, there is no anomalous behavior in the surface charge distribution along the pipe and plates, including the corners. These results are another testament to the accuracy of the numerical boundary element solutions to the Laplace equation given in this chapter.

The effect of the drop size on $\mathcal{E}_{TP}$ for $H_1 = 10$, $G = 0$ and $H_2 = 0$ and 5 is shown in Fig. 5.21.

$\mathcal{E}_{TP}$ decreases monotonically with increasing drop size when $H_2 = 0$ (case of no pipe). However, this is not true for $H_2 = 5$. In this situation, the monotonic decrease in $\mathcal{E}_{TP}$ occurs when D, the drop size parameter, is greater than approximately -0.646, a remarkable fact.

The difference in response between the situation in which there is no pipe and that in which there is a short pipe can be explained by examining the surface charge distribution along the drop surface (Figs. 5.22-5.27).

For the situation of no pipe (Figs. 5.22 and 5.23), the surface charge distributions display the expected behavior for $\mathcal{E} = 0$ and $\mathcal{E} = \mathcal{E}_{TP}$. The surface charge is highest new the tip of the drop and decreases to zero at the contact

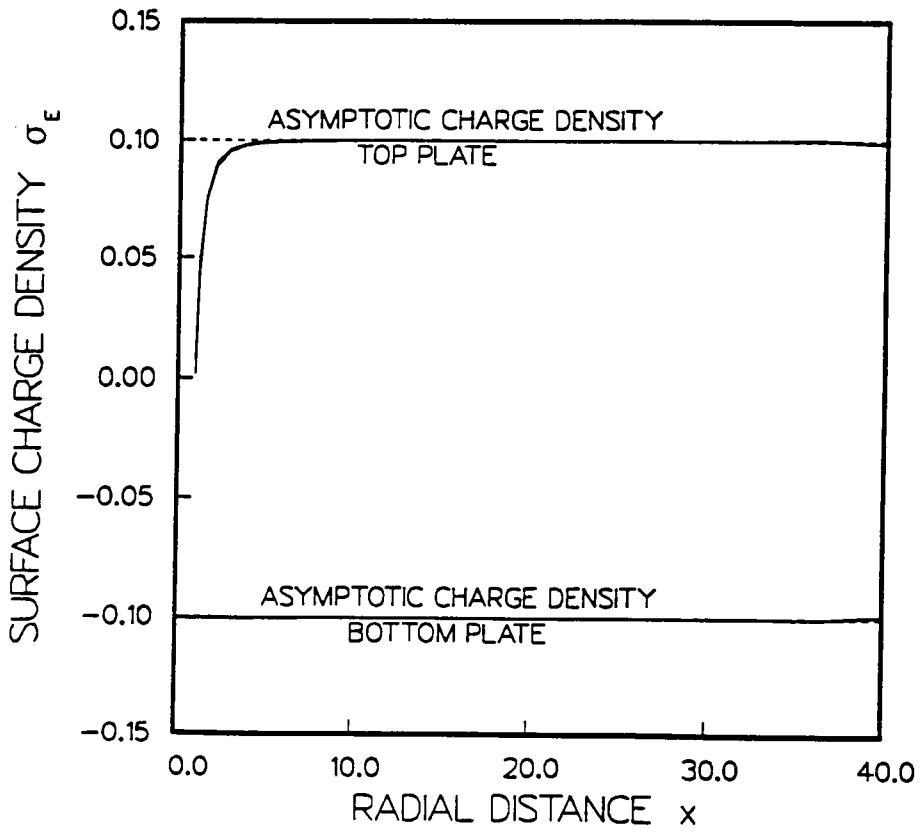



Fig. 5.16. Distribution of surface charge along the plates: no pipe and moderate plate spacing ($H_1$=10, $H_2$=0, D=0, G=0).

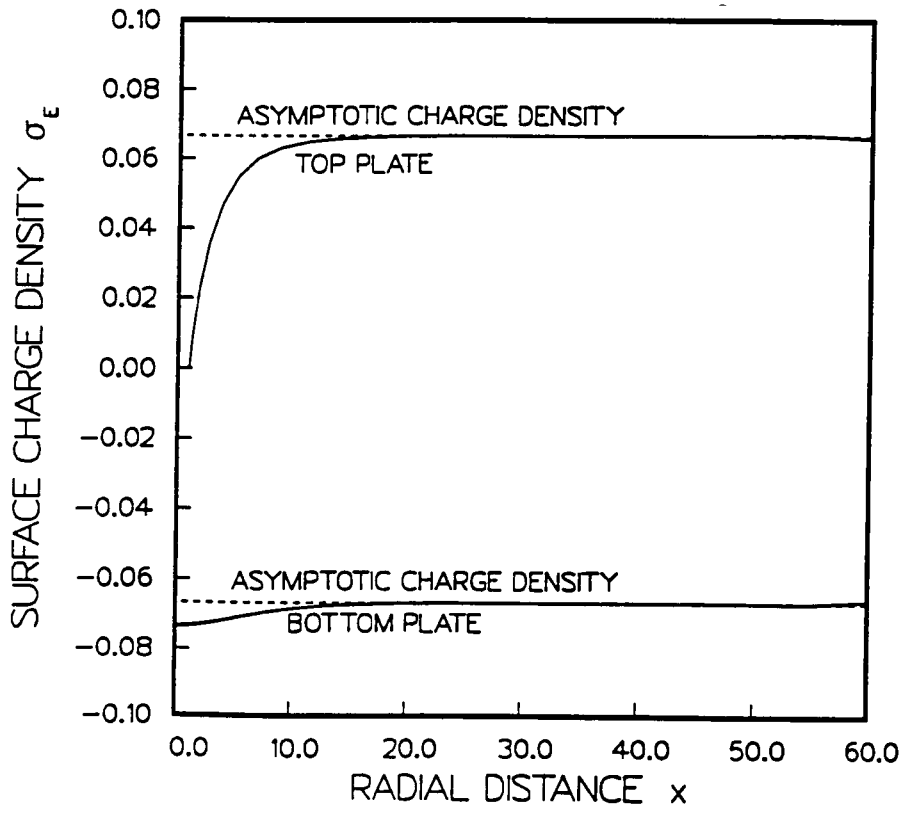



Fig. 5.17. Distribution of surface charge along the plates: case of short pipe ($H_1$=10, $H_2$=5, D=0, G=0).

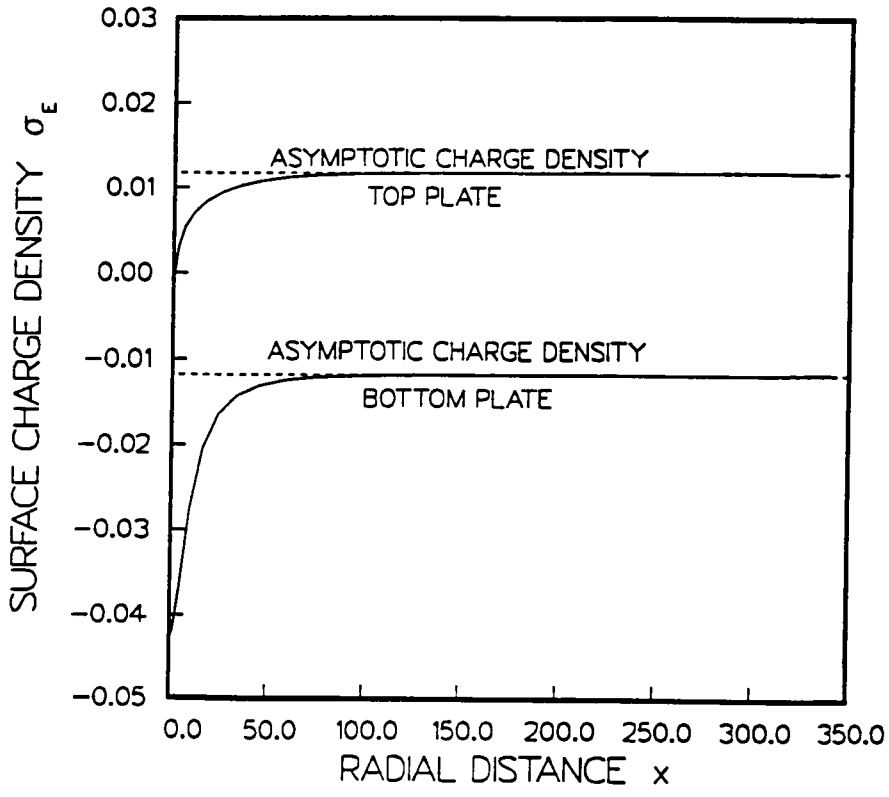



Fig. 5.18 Distribution of surface charge along the plates: case of long pipe ($H_1$=10, $H_2$=75, D=0, G=0).

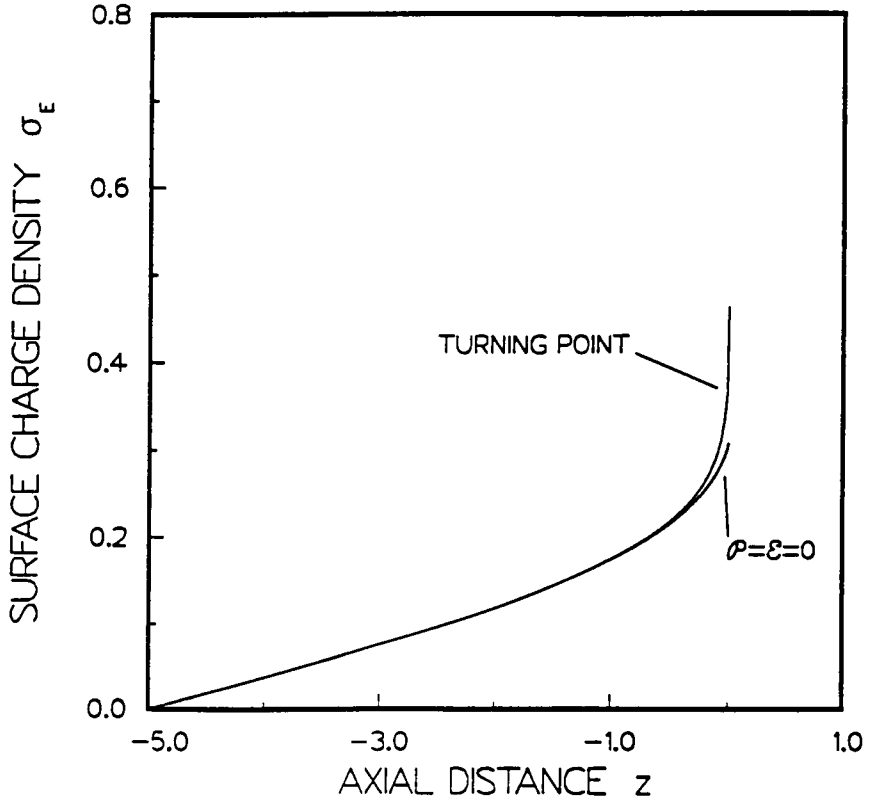



Fig. 5.19. Distribution of surface charge along the pipe: case of short pipe ($H_1$=10, $H_2$=5, D=0, G=0).

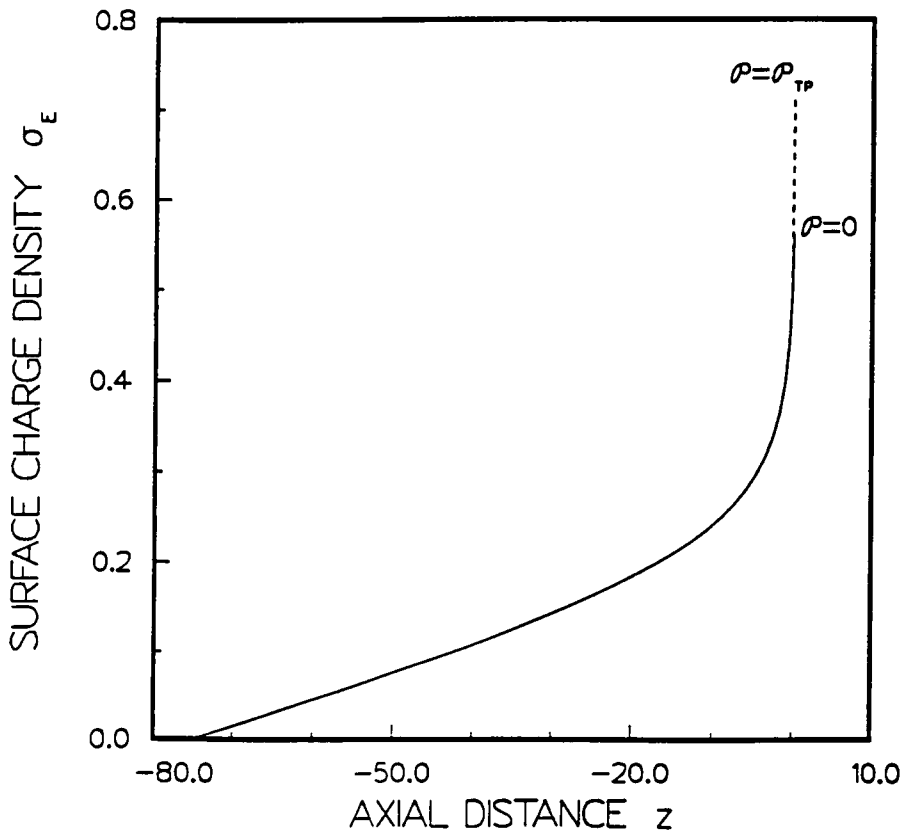



Fig. 5.20. Distribution of surface charge along pipe: case of short pipe ($H_1$=10, $H_2$=75, D=0, G=0).

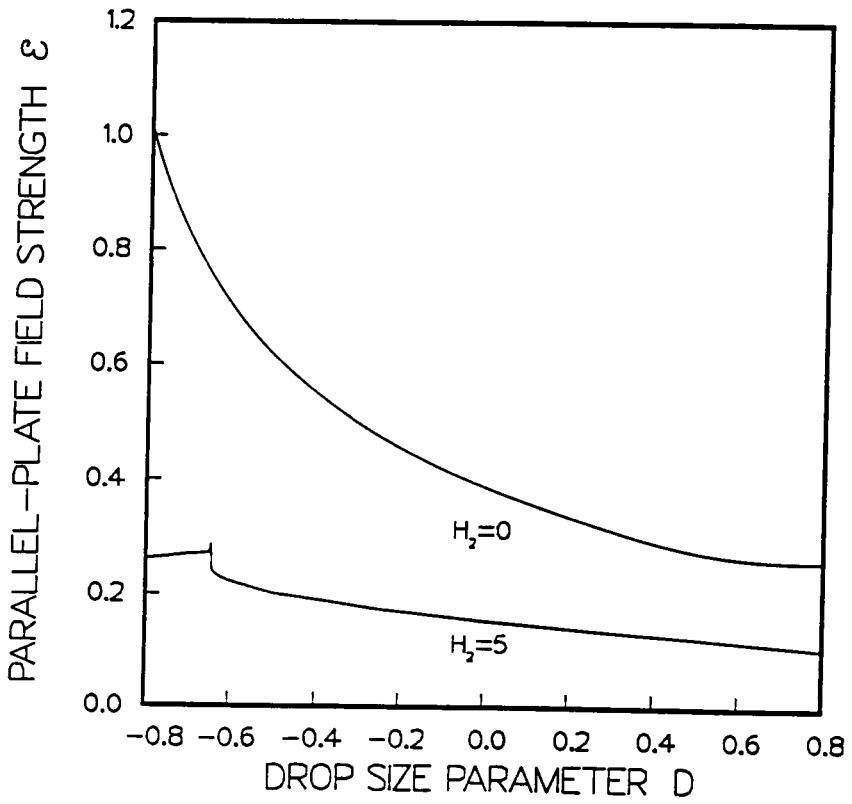



Fig. 5.21. Locus of singular points as a function of drop size ($H_1$=10, G=0).

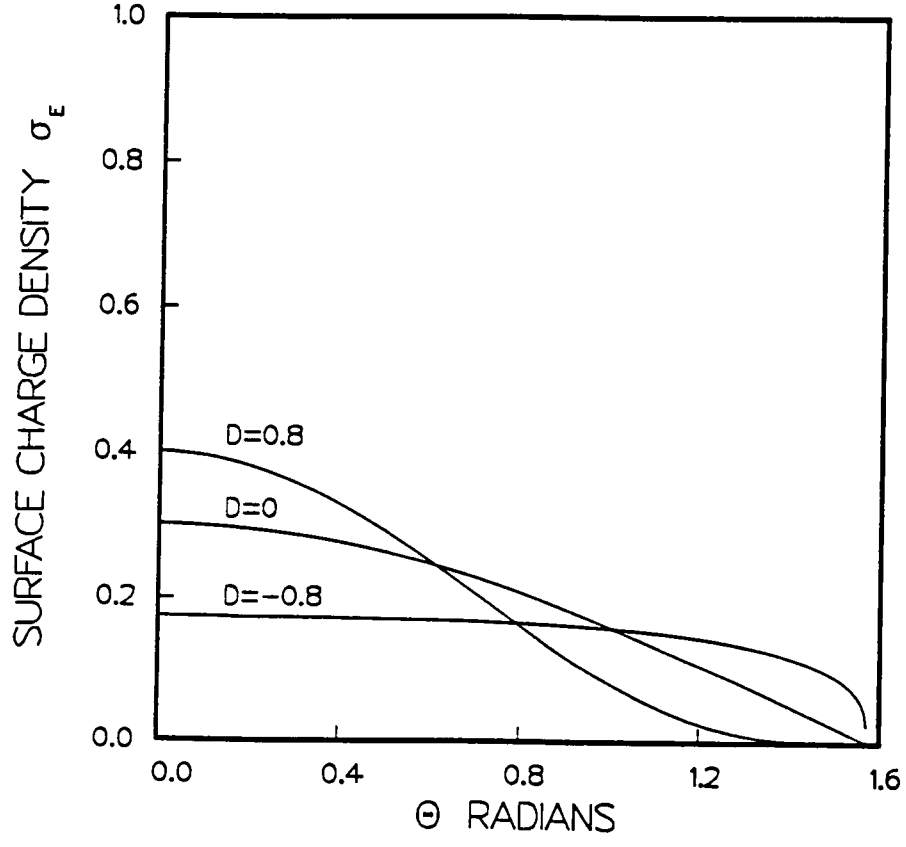



Fig. 5.22. Effect of drop size on distribution of surface charge: case of no pipe ($\mathcal{E}=\mathcal{P}=0$, $H_1=10$, $H_2=0$, $G=0$).

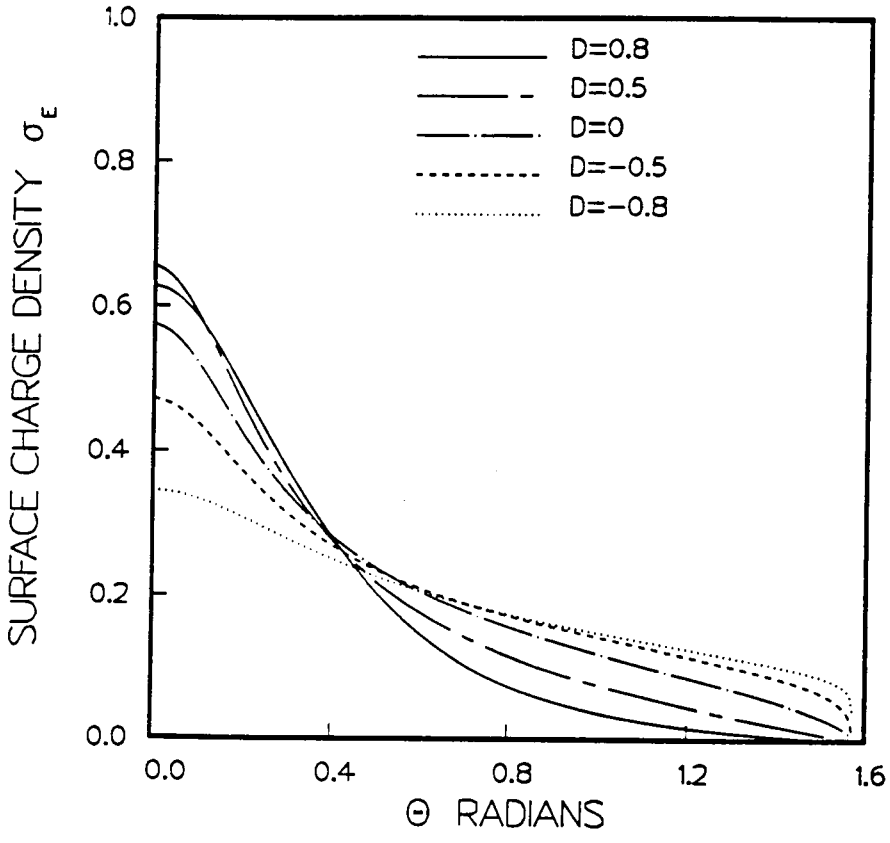



Fig. 5.23. Effect of drop size on distribution of surface charge: case of no pipe ($\mathcal{E}=\mathcal{E}_{TP}$, $H_1=10$, $H_2=0$, $G=0$).

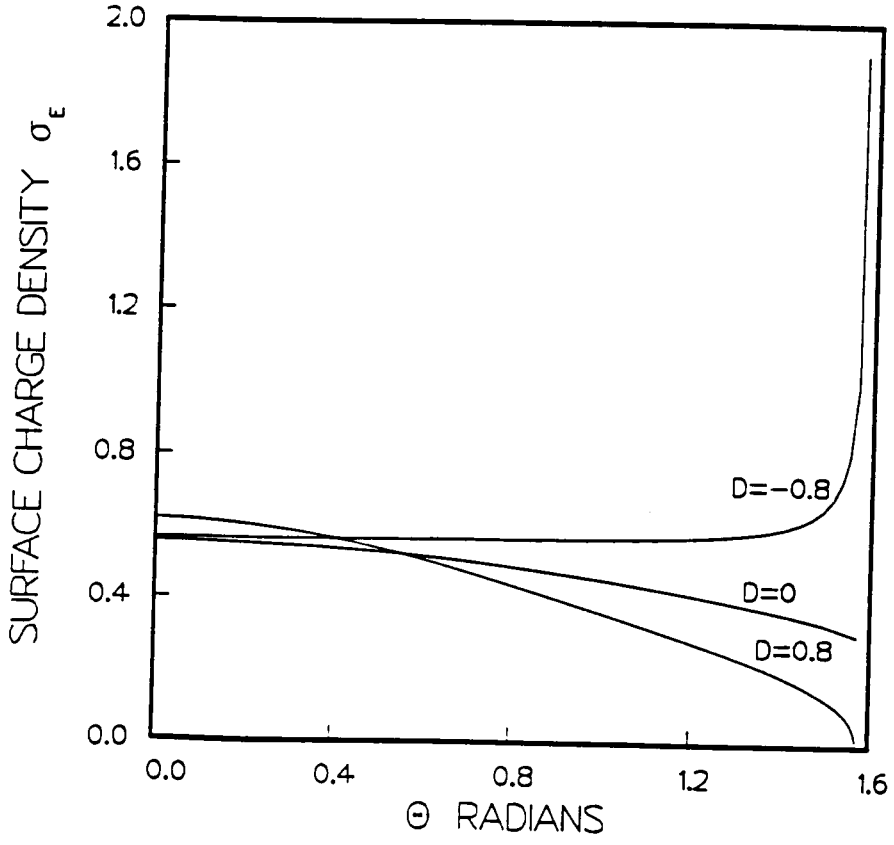



Fig. 5.24. Effect of drop size on distribution of surface charge: case with a pipe ($\mathcal{E}=P=0$, $H_1=10$, $H_2=5$, $G=0$).

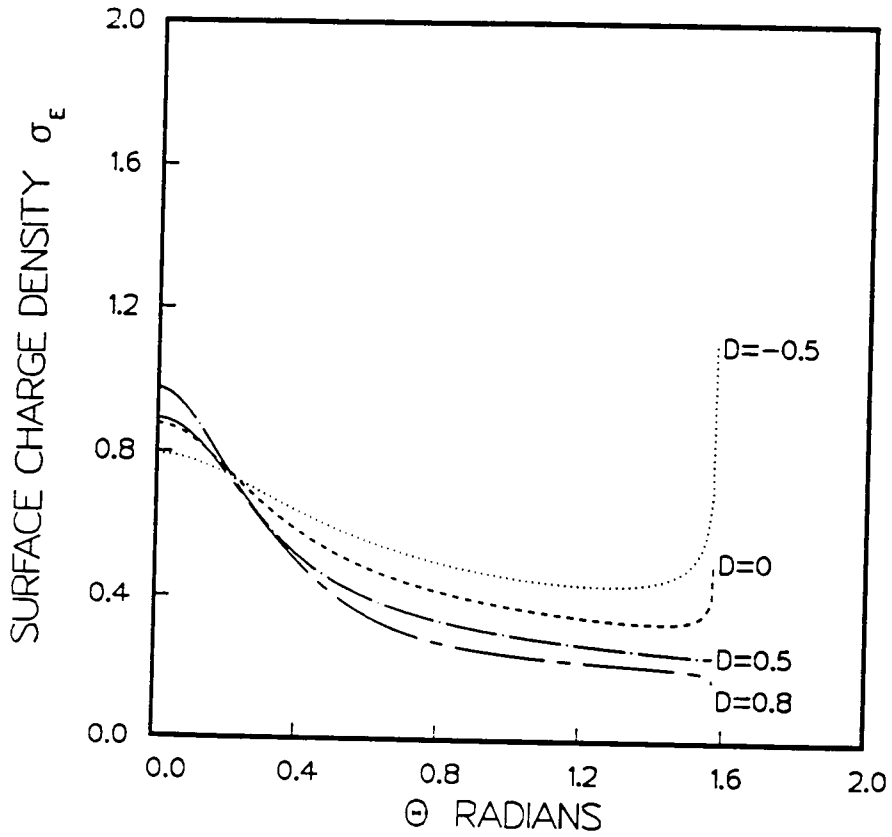



Fig. 5.25. Effect of drop size on distribution of surface charge: case with a pipe ($\mathcal{E}=\mathcal{E}_{TP}$, $H_1=15$, $H_2=5$, $G=0$).

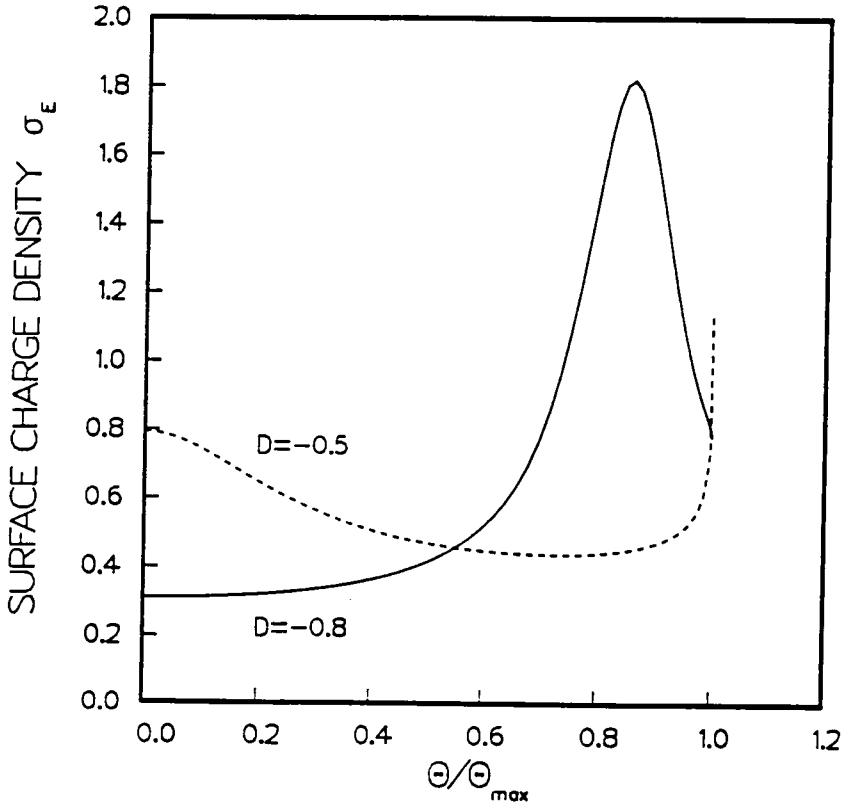



Fig. 5.26. Effect of pipe on distribution of surface charge on small drops ($\mathcal{E}=\mathcal{E}_{TP}$, $H_1=15$, $H_2=5$, $G=0$).

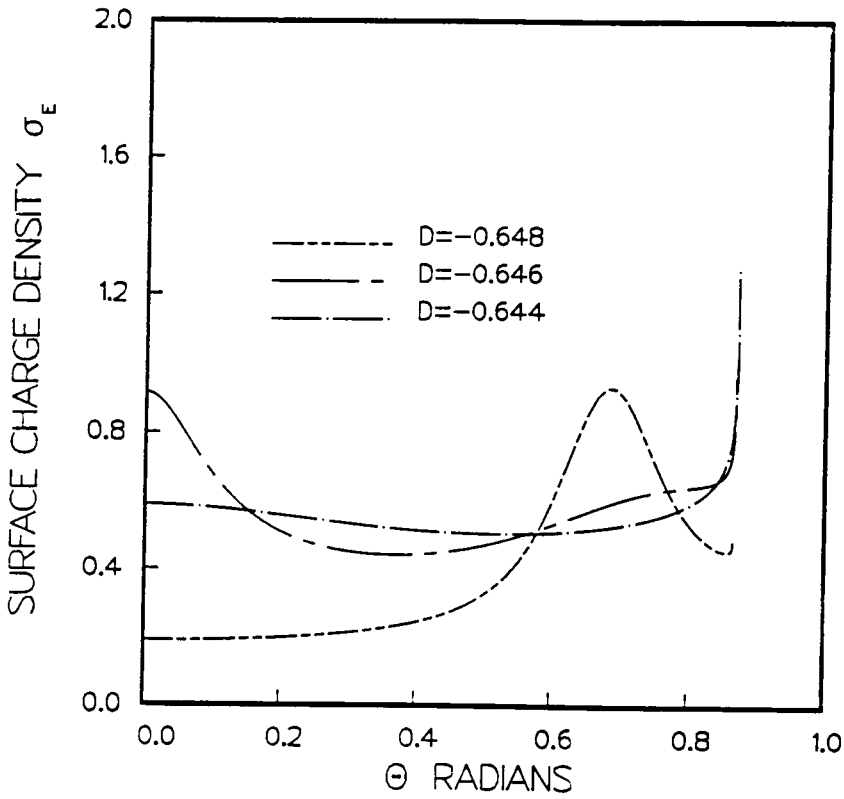



Fig. 5.27. Effect of drop size on distribution of surface charge: case with a pipe ($\mathcal{E}=\mathcal{E}_{TP}$, $H_1=15$, $H_2=5$, $G=0$).

line.

With a pipe, the surface charge densities are as expected down to a drop size parameter of ≈-0.6 (Figs. 5.24-5.27). When $-0.64 > D > -0.65$, Fig. 5.26 shows that region of high surface charge is transferred from th pole to the region near the contact line. This is further illustrated in Fig. 5.27 where the surface densities are given for $D = -0.5$ and $D = -0.8$.

Figs. 5.28-5.31 show drop shapes when $\mathcal{E} = 0$ and $\mathcal{E} = \mathcal{E}_{TP}$ for $-0.8 < D < 0.8$ in situations in which there is no pipe and also in ones in which there is a pipe.

The drop shapes at the stability limit suggest jetting occurs at the tip of the drop for all drop sizes in the absence of a pipe (Fig. 5.28). However, with a pipe, jetting from the tip occurs as long as the drop size parameter exceeds $D = -0.646$ (Figure 5.29-5.31). Below this value, a two-lobed shape appears at the turning point; thus, suggesting that jetting occurs along the periphery of the drop. This is of practical importance in electrodispersion devices where coalescence is to be minimized. Annular jetting tends to disperse microdroplets such that the distance between them is increased.

The solution families terminate past the stability limit when the radius of curvature approaches infinity or the inverse mean curvature approaches zero (Fig. 5.32). A large number of elements are required to approach the termination point (Figs. 5.32-5.36).

In each of these plots, there is no pipe and the distance between the plates is ten. Figs. 5.33 and 5.34 show the effects of mesh refinement on the variation of the aspect ratio and reference pressure, respectively, with $\mathcal{E}$. The curves show, as stated previously, that forty elements are enough to accurately determine the

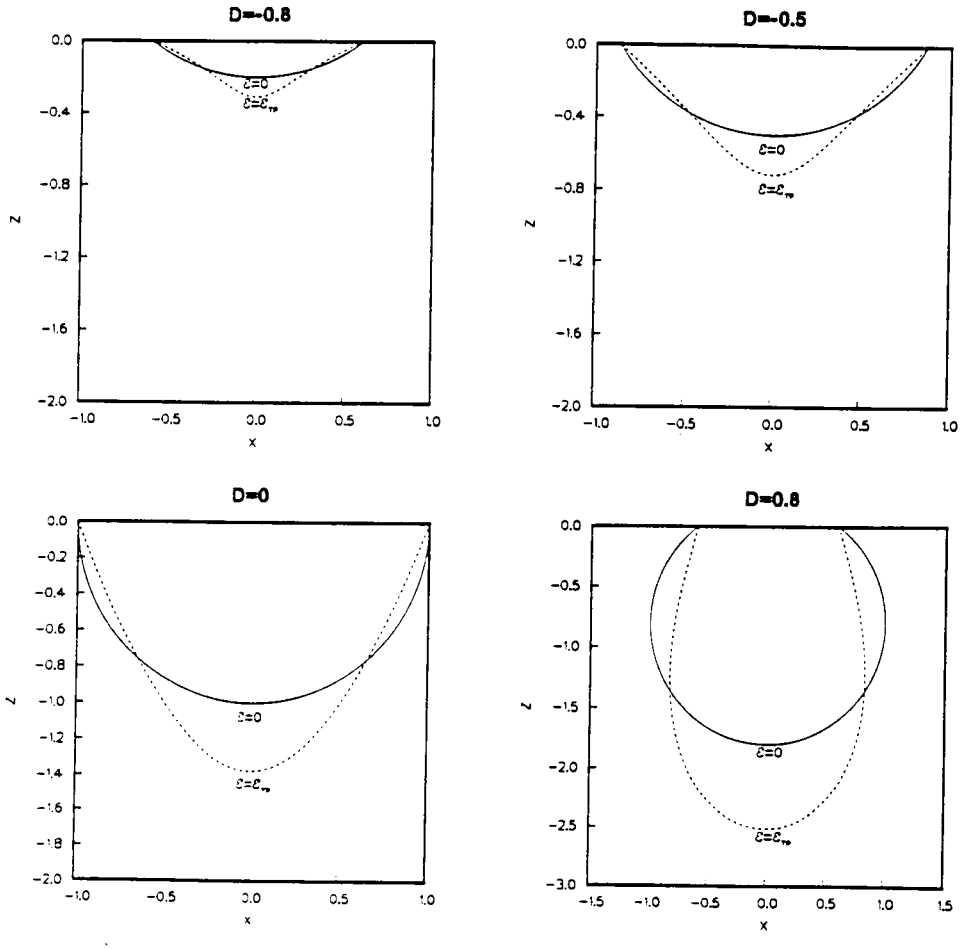



Fig. 5.28. Evolution of drop shapes with field strength: case without a pipe ($H_1$=10, $H_2$=0, G=0).

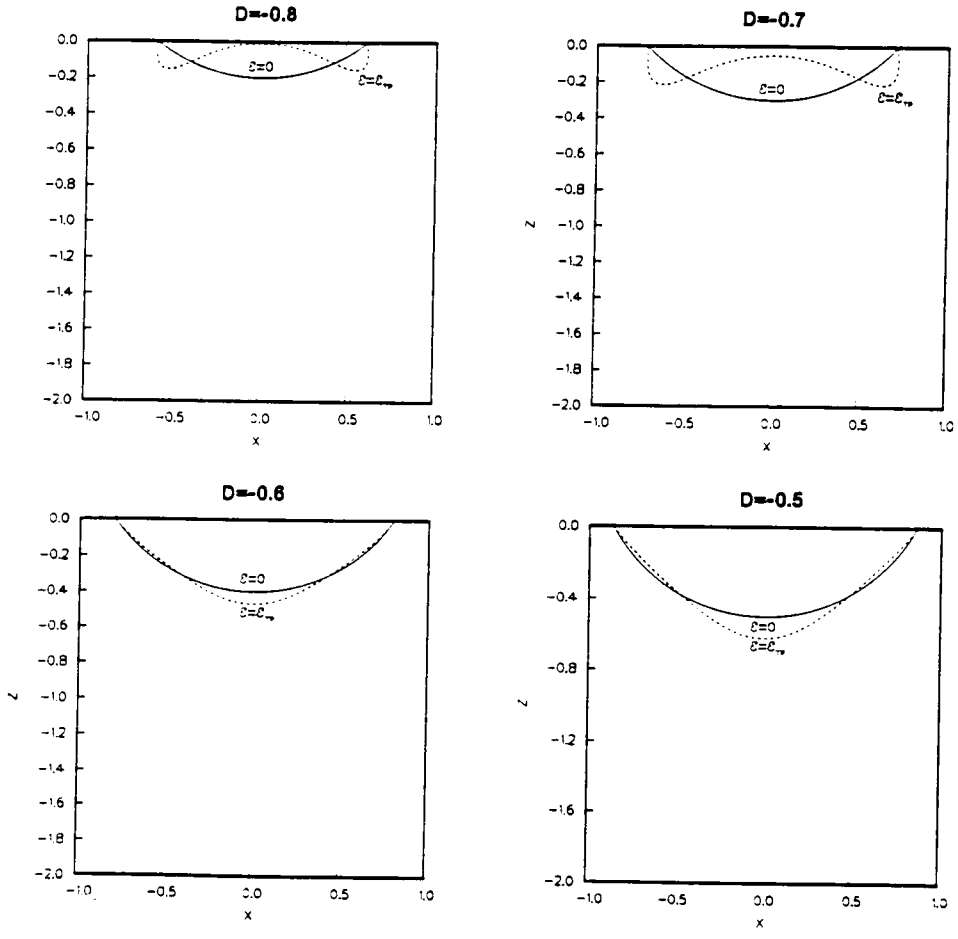



Fig. 5.29. Evolution of drop shapes with field strength: case with pipe ($H_1$=10, $H_2$=5, G=0).

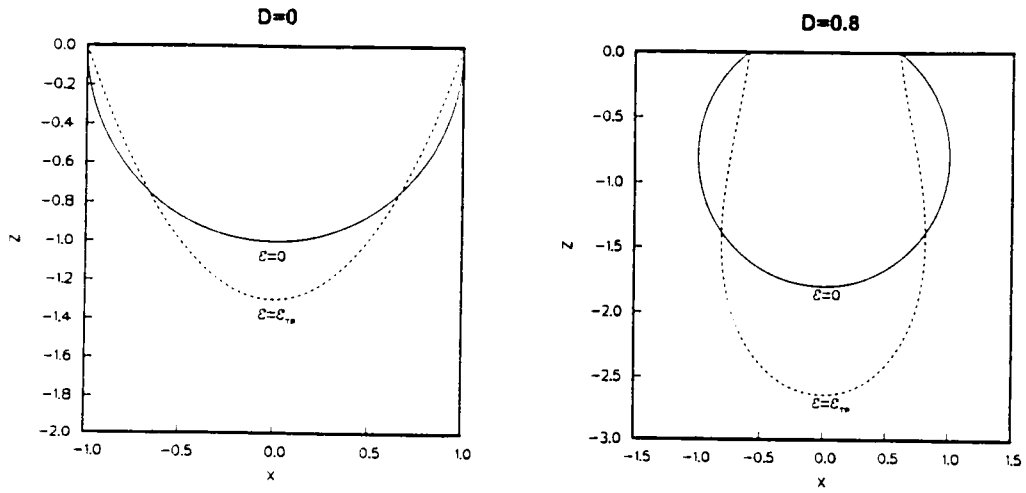



Fig. 5.30. Evolution of drop shapes with field strength: case with pipe ($H_1$=10, $H_2$=5, G=0).

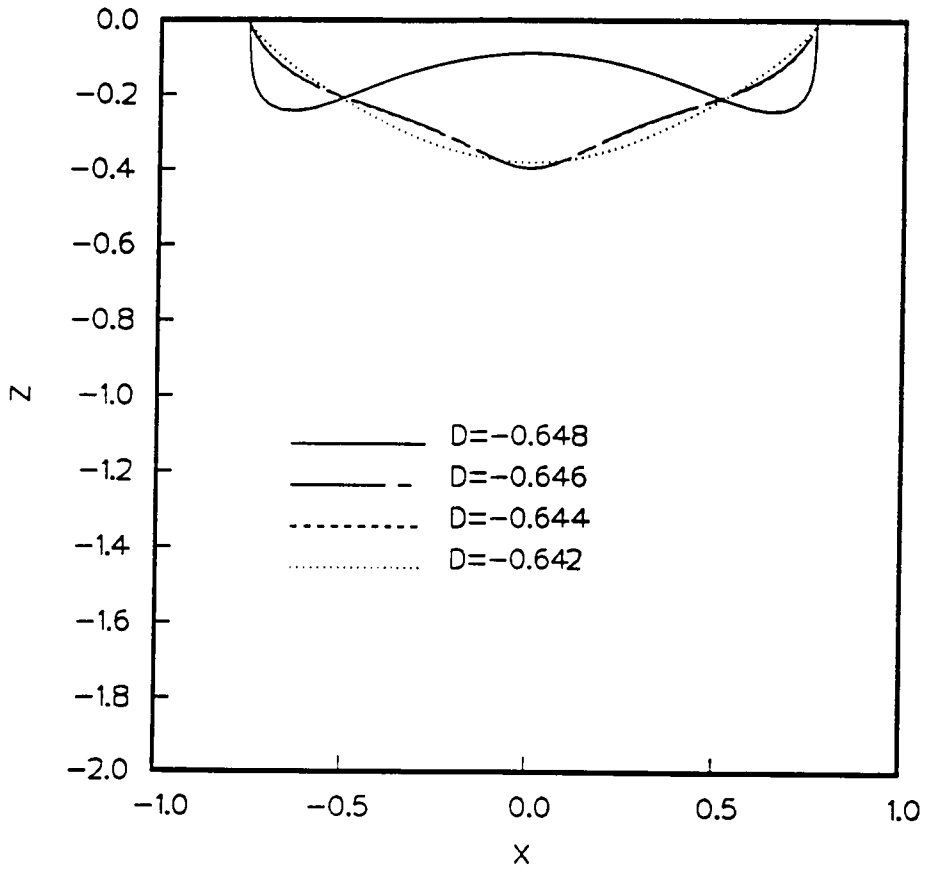



Fig. 5.31. Evolution of drop shapes with field strength: case with pipe ($\mathcal{E}=\mathcal{E}_{TP}$, $H_1=10$, $H_2=0$, $G=0$).

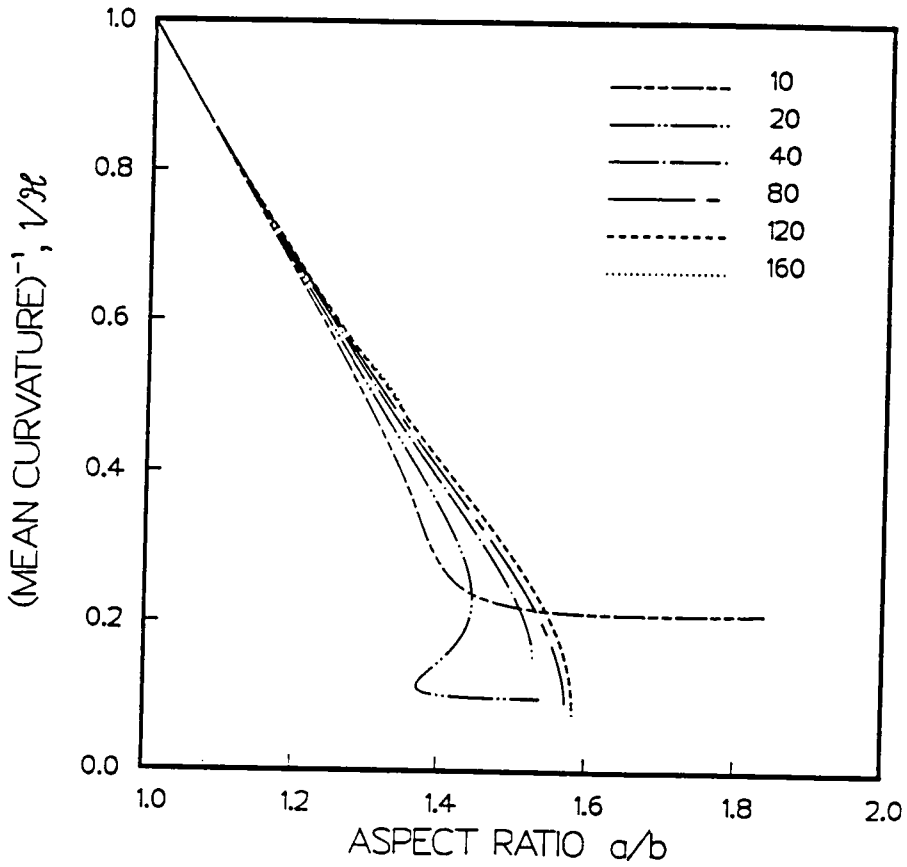



Fig. 5.32. Solution families in parameter space: effect of mesh refinement on (mean curvature)$^{-1}$ ($H_1$=10, $H_2$=0, D=0, G=0).

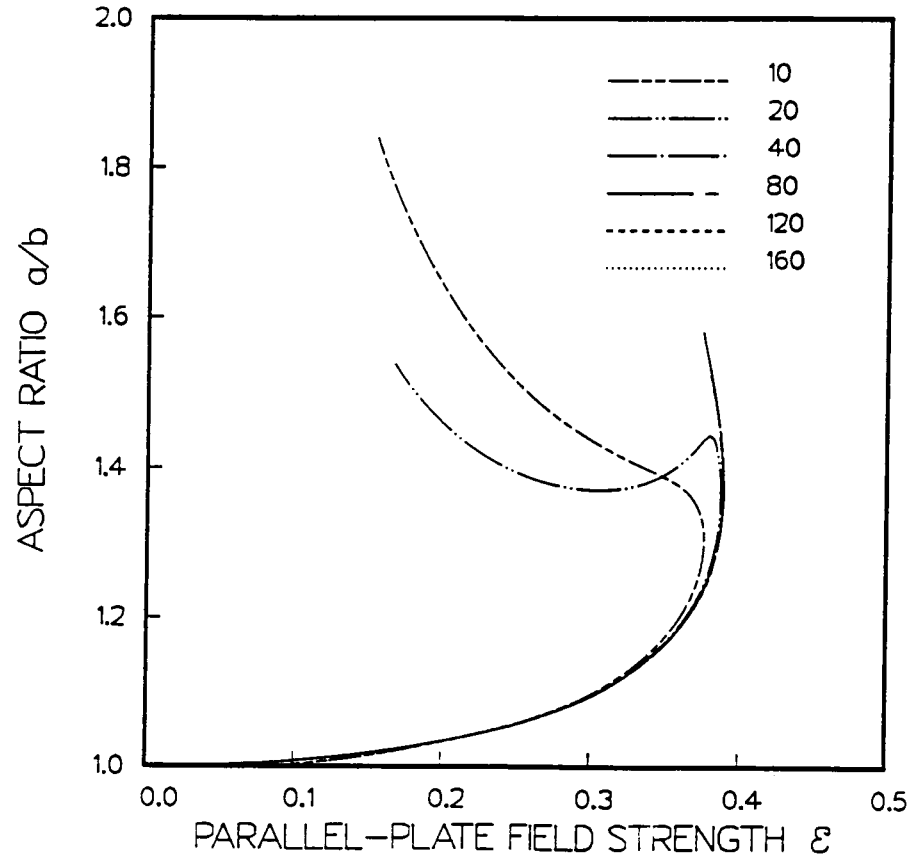



Fig. 5.33. Solution families in parameter space: effect of mesh refinement on drop aspect ratio ($H_1$=10, $H_2$=0, D=0, G=0).

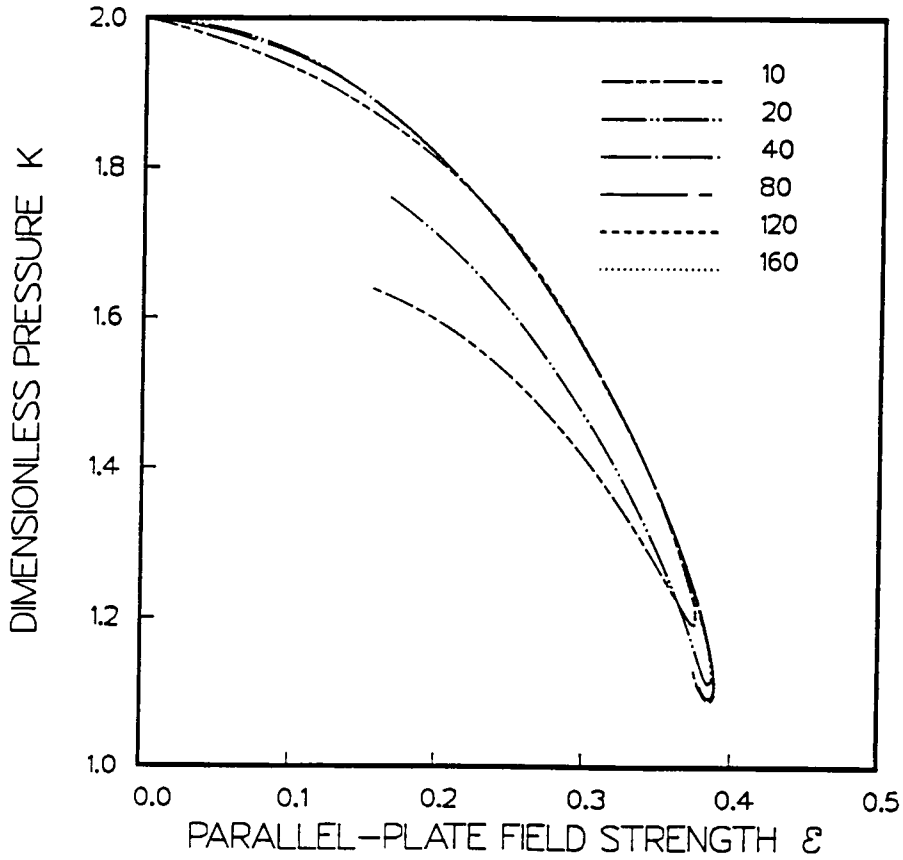



Fig. 5.34 Solution families in parameter space: effect of mesh refinement on reference pressure ($H_1$=10, $H_2$=0,D=0, G=0).

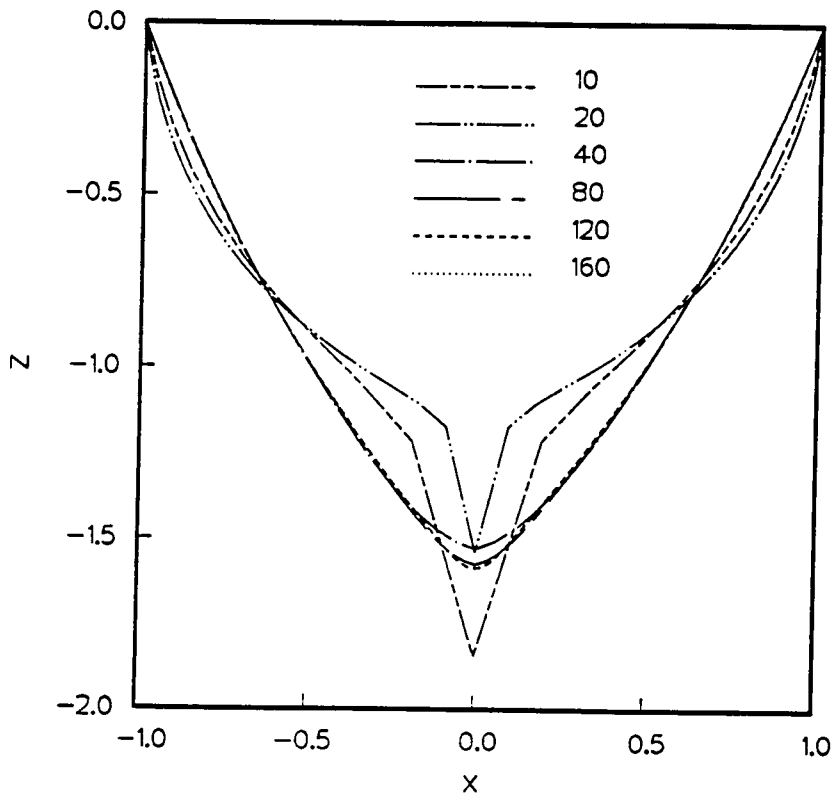



Fig. 5.35. Effect of mesh refinement on drop shape at termination of run ($H_1$=10, $H_2$=0, D=0, G=0).

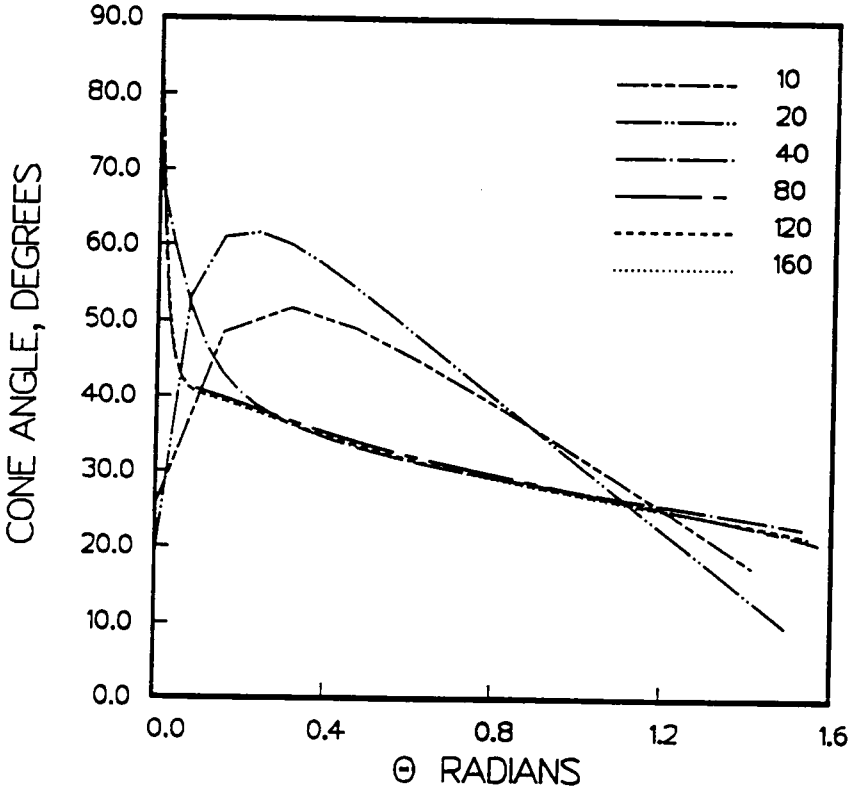



Fig. 5.36. Effect of mesh refinement on cone angle at termination of run ($H_1$=10, $H_2$=0, D=0, G=0).

stability limit. However, it is shown by Figs. 5.32, 5.35 and 5.36 that at least 120 elements must be deployed on the drop surface to get accurate information about the termination point. Fig. 5.35 shows the effect of mesh refinement on the drop shapes at termination of the run. The effect of mesh refinement on the "apparent" cone angle is illustrated in Figure 5.36. The condition of axial symmetry is violated when the number of elements is less than or equal to 80.

The effect of pipe length on the cone angles at the termination of the run is shown in Fig. 5.37.

$H_1 = 10$ for these runs. An expanded view of the cone angle near the tip of the drop is shown in Fig. 5.38.

The figure shows a rapid decrease in the angle, which is due to the fact that the drop is axisymmetric, followed by a nearly constant value. This constant value is the "apparent" cone angle and is the angle that an observer would see with the naked eye. This value increases monotonically with pipe length and ranges from between 40 degrees and the Taylor limit of 49.3 degrees.

## 5.7. Conclusions

Theoretical evaluation was completed of the electrostatics of shapes and stability of drops hanging from a pipe in an electric field. The important results obtained from this work are: (1) the presence of a pipe enhances electrodispersion by increasing the surface charge on the drop; (2) drops greater than $D = D^*$ jet from a conical tip, while annular jetting occurs for skinny drops $D < D^*$; (3) beyond the stability limit, the families of shapes terminate when the radius of curvature approaches infinity, (4) for initially hemispherical drop,

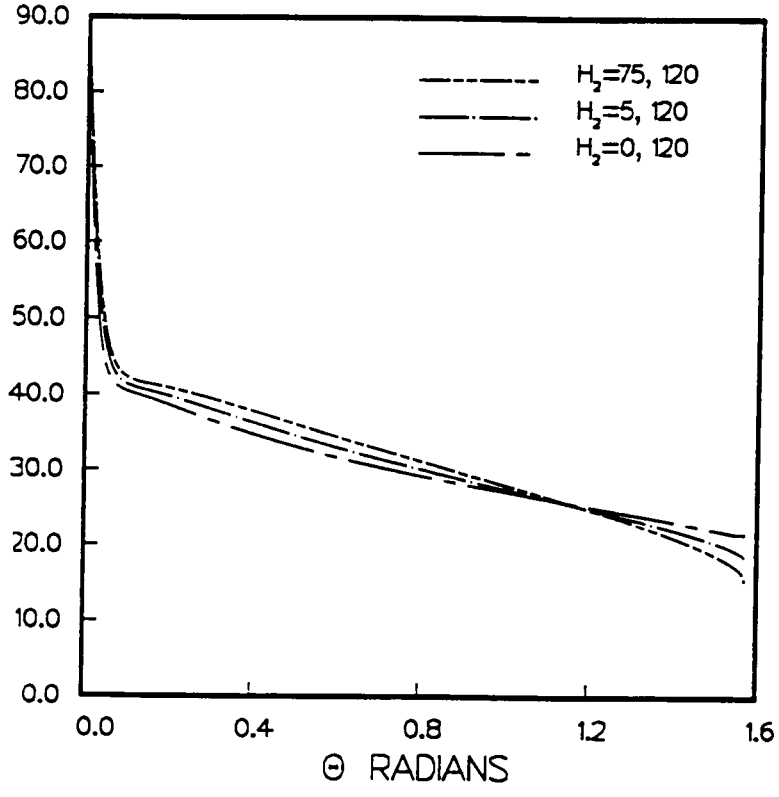



Fig. 5.37. Effect of pipe on cone angle at termination of run ($H_1$=10, D=0, G=0).

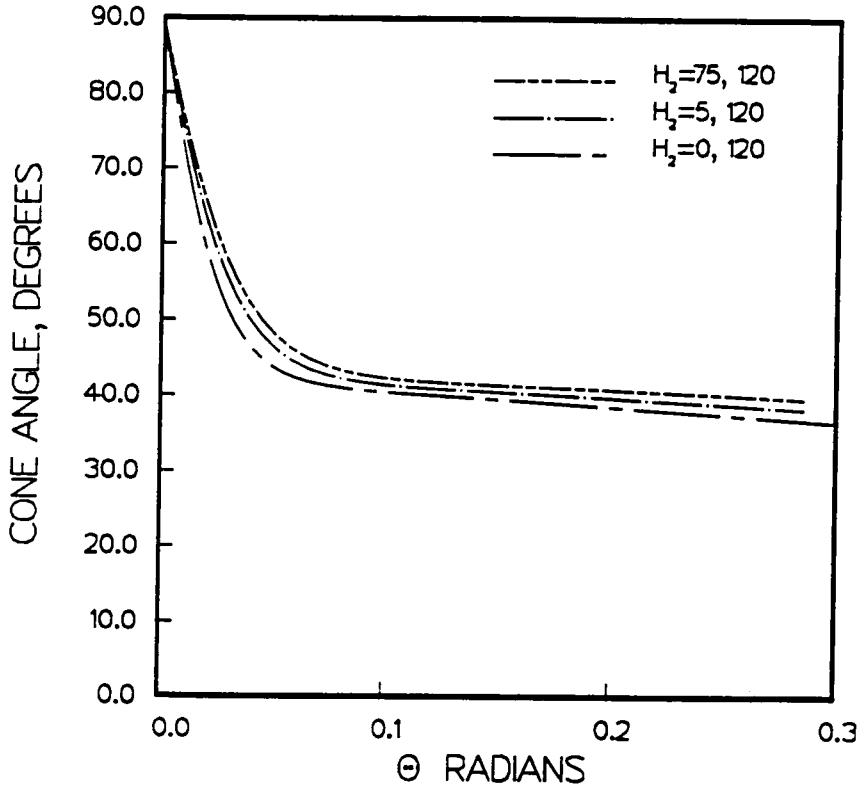



Fig. 5.38. Effect of pipe on cone angle at termination of run: Expanded region near tip of drop ($H_1$=10, D=0, G=0).

$D = 0$, the asymptotic cone angle at the tip of a drop increases monotonically with pipe length and is greater that 40 degrees and is bounded by the Taylor limit of 49.3. Future theoretical work should include (a) determining the effect of gravity on instability of electrified pendant drops, (b) the development of a three-dimensional hybrid boundary element/finite element algorithm to analyze drops hanging from a nozzle; (c) developing methods to solve the electrostatics and the hydrodynamics problems for drops flowing from or oscillating at the tip of a pipe in an electric field. Another relevant problem that is more easily solved is the effect of the "cup" electrode configuration on drop stability. In this configuration the potential on the side and bottom boundaries are set equal unity and on the top boundary $\frac{\partial V}{\partial n} = 0$. Fig. 5.39 shows that for comparable dimensions, the "cup" electrode configuration causes instability to occur at a lower value of the effective potential than the pipe/two parallel-plates configuration studied in this chapter. Future work should involve detailed modeling of the "cup" electrode configuration for both process optimization and for providing an in-depth fundamental understanding of the physics of drop deformation in this configuration.

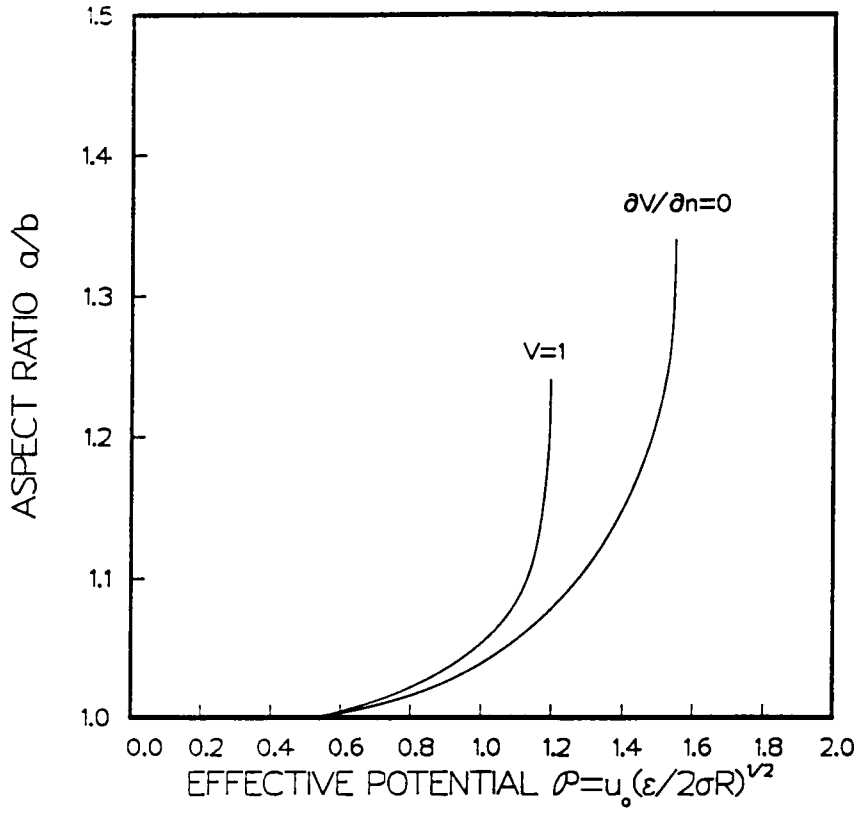



Fig. 5.39. Solution families in parameter space: effect of side boundary condition on aspect ratio ($H_2$=5, R=5, D=0, G=0).

# 6. SUMMARY AND RECOMMENDATIONS

This research has focused on the synthesis of ceramic precursor powders by two methods: (a) homogeneous precipitation of metal alkoxide solutions and (b) electrodispersion. In the first phase of this research, the synthesis of silica, titania, zirconia, zirconia-titania and zirconia-alumina powders by the hydrolysis of metal alkoxides was investigated. The formation and growth of hydrous oxide particles by the homogeneous precipitation of metal alkoxide solutions involved three major steps: (1) the growth of inorganic polymers; (2) the collapse of the polymers to form approximately 10 to 50 nm (dia.) primary dense particles; and (3) the growth of the particles by the deposition of monomer and soluble polymers on the particle surface and/or the aggregation of smaller dense particles and ramified precipitates to form large more stable colloids. The controlling step depends on the type (linear versus highly crosslinked) polymer formed, the rate of collapse of the polymer and the colloidal stability of the dense particles.

In the case of the synthesis of silica particles by the base-catalyzed hydrolysis of TEOS, it was concluded that the controlling step (mechanism) depends on the concentration of the reactants. High water and ammonia concentrations yielded larger particles because a very high conductivity or ionic strength was observed during the reaction. Thus, the primary dense particle aggregated readily to form larger particles. At even higher water concentrations, the particle size decreased because the dielectric constant of the solution increased. Below a certain TEOS concentration unimodal particle size distributions were observed. Higher TEOS concentrations resulted in the formation of bimodal particle size distributions. This occurs because, initially, the ionic strength rises very rapidly;

thus, the primary dense particles aggregate to form larger colloids. As the reaction proceeds, the primary particles are still forming; however, the ionic strength of the solution decreases. This results in increased stability of smaller aggregates and the eventual evolution of a bimodal distribution.

A detail chemical kinetic - population balance model was developed to predict the ultimate particle size and size distribution by solving the hydrolysis and condensation kinetic expressions and the population balance expression. The method of moments was used to expedite solution of the population balance equation by assuming a lognormal particle size distribution for the primary dense particles and aggregates. Separate expressions were written for the primary dense particles and aggregates. The model also assumed that the fate of the monomer, soluble polymers and ramified precipitates can all be lumped into an effective nucleation rate, which is the rate at which the primary dense particles are formed. Using experimentally determined hydrolysis, nucleation, and condensation rate parameters, and zeta potentials, this model predicted, at least semiquantitatively, the growth kinetics and the ultimate particle size and size distribution and further substantiated the growth mechanism for silica particles.

The formation of titania, zirconia and mixed titania-alumina and titania-zirconia powders by the hydrolysis of their alkoxides was also found to be governed by the three steps given above. However, solvent had a profound effect on particle morphology in these systems. This was not observed in the silica systems.

Dense titania, zirconia and titania-zirconia particles were readily formed in ethanol and 1-butanol. Ramified precipitates were formed as the alcohol solvent

became more branched. This effect was due to facile alcoholysis reactions that occur with titanium and zirconium alkoxides. After alcoholysis occurred, the hydrolysis and condensation were influenced by the bulky branched alcohols. The resulting steric hindrance caused the formation of linear polymers and, consequently, a gelatinuous precipitate produced.

In the mixed titania-zirconia system, the composition of particles had no effect on particle morphology. This was not so with the alumina-titania system. As the alumina content increased, spherical to ramified alumina-titania precipitates were formed by the hydrolysis of mixed aluminum and titanium alkoxide solutions in 1-butanol. The formation of ramified precipitates with increasing alumina content was primarily due the formation of linear polymers by the hydrolysis aluminum alkoxides. This present work has shown that a more dense precipitate can be formed by precipitating in two steps.

Although the above homogeneous precipitaiton studies have greatly enhanced our understanding of particle formation by metal alkoxide hydrolysis, the formation (size) of the primary dense particles, the deposition of monomer and soluble polymers on particle surfaces, and the collapse of the ramified precipitates are not well understood. To understand the first two phenomena, a more thorough characterization of the chemical species during the hydrolysis and condensation reactions is needed. Modeling the collapse of ramified precipitates is a formidable task which is akin to the protein folding problem. Both require the use of molecular or macromolecular computer simulations to understand, on a more fundamental and theoretical basis, the kinetics of their collapse. However, to implement these simulation techniques, more efficient algorithms are needed to solve for the hydrodynamic interactions of the particle(s). Microhydrody-

namist (Karilla and Kim 1989, Karilla, Fuentes and Kim 1989) are currently investigating this for the protein folding problem; however, this work will be easily extended to the the collapse of ramified precipitates.

As an outgrowth of the homogeneous precipitation studies, a new reactor, the electric dispersion reactor (EDR), was invented to produce ultrafine powders by electrodispersion and the subsequent reaction of aqueous drops emanating from a nozzle. By varying reactant concentrations and by strategically locating reactants in the proper phase, porous and dense silica particles have been made as well as the composite material of 1:2:3 yttrium, barium and copper.

Additional work is required to determine the effect of surfactant concentration, emulsion thickness and electric field strength on the ultimate particle size and size distribution. The prediction of such effects requires an understanding of the coalescence of drops in the presence of surfactants and an intense pulsed electric field.

Such research should provide expressions for the collision kernel, and its variance with surfactant concentration and the electric field strength. The collision kernel is used in population balance models that describe drop size kinetics during coalesence.

The commercialization of this device requires process optimization and detailed economic analysis. A recent research program at the Oak Ridge National Laboratory has been funded to address these concerns. This work is funded by the Department of Energy, Office of Basic Energy Sciences.

Before a detailed economic analysis is possible, the process should be optimized. Process optimization requires an understanding of the effect of electric field strength and reactor configuration (i.e., nozzle-electrode configuration) on

drops emanating from a nozzle.

This can be done by solving the equations that govern the electrohydrostatics and electrohydrodynamics of such systems. A comprehensive study of the electrohydrostatics of axisymmetric pendant drops hanging from a nozzle is reported in this thesis. The data clearly show that nozzle-electrode configuration has a profound effect on drop stability. However, a complete analysis of the EDR entails solving the governing macroscopic electrohydrodynamic equations, understanding the physics of and developing mathematical models for drop break-up. These are nontrivial tasks. Firstly, the macroscopic electrohydrodynamic equations must be solved on super computers using numerical techniques such as the finite element method or a hybrid finite element-boundary element methods. Secondly, the physics of drop break-up needs to be developed. This work is currently being pursued by researchers at the Oak Ridge National Laboratory.

# BIBLIOGRAPHY

R. Aeolin, A. Loebel, and F. Eirich, J. Am. Chem. Soc., 72, 5707 (1950).

M. Akinc and K. Richardson, Mat. Res. Soc. Symp. Proc., 73, 99 (1986).

I. Artaki, S. Sinha, A.D. Irwin, and J. Jonas, J. Non. Cryst. Solids, 72, 391 (1985).

I. Artaki, M. Bradley, T.W. Zerda, and J. Jonas, J. Phys. Chem., 89, 4399 (1985).

A. Ayral, J. Phalippou and J.C. Droguet, Mat. Res. Soc. Symp. Proc., 121, 239 (1988).

S. Baik, A. Bleier and P.F. Becher, Mat. Res. Soc. Symp. Proc., 73, 791 (1986).

J.P. Bailes, Ind. Eng. Chem. Process Des. Dev., 20, 564 (1981).

J.K. Bailey and M.L. McCartney, Mat. Res. Soc. Symp. Proc., 180, 153 (1990).

C.B. Bargeron, J. Chem. Phys., 61, 2134 (1974).

R.E. Barker, PhD Thesis, University of Tennessee (1988).

E. Barouch and E. Matijevic, J. Chem. Soc. Faraday Trans. 1, 81, 1797 (1985).

E. Barouch and E. Matijevic, J. Chem. Soc. Faraday Trans. 1, 81, 1819 (1985).

E.A. Barringer and H.K. Bowen, Commun. Am. Ceram. Soc., C-199 (December 1982).

E.A. Barringer and H.K. Bowen. Langmuir, 1, 414 (1985).

O.A. Basaran, PhD. Thesis, University of Minnesota (1984).

O.A. Basaran and L.E. Scriven, J. Colloid Interface Sci., 140, 10 (1990).

O.A. Basaran, T.C. Scott and C.H. Byers, AIChE J., 35, 1263 (1989).

G.W. Bell, S. Levine and L.N. McCartney, J. Colloid Interface Sci., 33, 335 (1970).

D. Bergmann and J. Hinze, J. Struct. Bonding, 66, 145 (1987).

B.J. Berne and R. Pecora, Dynamic Light Scattering, Wiley, New York (1976).

K.A. Berglund, D.R. Tallant, and R.G. Dosch, Ceramic Chemical Processing,

eds. L. L. Hench and Donald R. Ulrich, John Wiley and Sons, New York, 94 (1986).

S. Bhandarkar and A. Bose, J. Colloid Interface Sci., 135, 531 (1990).

S. Bhandardar and A. Bose, J. Colloid Interface Sci., 139, 542 (1990).

A. Bleier and G. Westmoreland, Mat. Res. Soc. Symp. Proc., 121, 145 (1988).

J.E. Blendell, H.K. Bowen and R.L. Coble, Ceram. Bull., 63, 797 (1984).

J.B. Blum and J.W. Ryan, J. Non-Cryst. Solids, 81, 221 (1986).

G.H. Bogush and C.F. Zukoski, in: Ultrastructure Processing of Advanced Ceramics, eds. J. D. MacKenzie and D. R. Ulrich, John Wiley and Sons, New York (1988).

G.H. Bogush and C.F. Zukoski, J. Colloid Interface Sci., 142, 1 (1991).

G.H. Bogush and C.F. Zukoski, J. Colloid Interface Sci., 142, 19 (1991).

D.F. Boltz and J.A. Howell, Colorimetric Determination of Nonmetals, Wiley, New York, 316 (1978).

H.K. Bowen, Mat. Sci. Eng., 44, 1 (1980).

H. K. Bowen, Mat. Res. Soc. Symp. Proc., 24, 1 (1984).

R. Brace and E. Matijevic, J. Inorg. Nucl. Chem., 35, 3691 (1975).

D.C. Bradley, R. Mehrotra, and D. P. Gaur, Metal Alkoxides, Academic Press, New York (1978).

C.J. Brinker et. al., J. Non-Cryst. Solids, 48, 47 (1982).

C.J. Brinker et. al., J. Non-Cryst. Solids, 63, 45 (1984).

J.C. Brown and P.N. Pusey, J. Chem. Phys., 62, 1136 (1975).

C.H. Byers, M.T. Harris and D.F. Williams, Ind. Eng. Research, 26, 1916 (1987).

C.H. Byers and T.C. Scott, NATO ASI Series: Physics, 193, 544 (1989).

D.L. Catone and E. Matijevic, J. Colloid Interface Sci., 48, 291 (1974).

S. Chandrasedar, Rev. Mod. Phys., 15, 1 (1943).

T.M. Che, J.J. Rafalko and P.B. Dorain, in: Ultrastructure Processing of Advanced Ceramics, eds. J.D. Mackenzie and D.R. Ulrich, Wiley, New York, 827 (1988).

H.K. Christenson and R.G. Horn, Chem. Phys. Letter, 98, 45 (1983).

H.K. Christenson, J. Chem. Soc. Faraday Trans. I, 80, 1933 (1984).

H.K. Christenson and R.G. Horn, J. Colloid Interface Sci., 103, 50 (1984).

B. Chu, Laser Light Scattering Academic Press, New York (1974).

J.L. Collins, M.H. Lloyd and R.L. Fellows, Radiochimica Acta, 42, 121 (1987).

B. Crosignoni, P. Di Porto and M. Bertolotti, Statistical Properties of Scattered Light, Academic Press, New York (1974).

F.A. Cotton and G. Wilkinson, Advanced Inorganic Chemistry, Wiley, New York (1980).

B. Dahneke, Measurements of Suspended Particles Using Quasi-Elastic Light Scattering, John Wiley and Sons, New York (1982).

P.K. Dutta and D. Shieh, Appl. Spectroscopy, 39(2), 343 (1985).

L.H. Edelson and A.M. Glaeser, J. Am. Ceram. Soc., 71, 225 (1988).

A.J. Fanelli and J.V. Burlew, J. Am. Ceram. Soc. 69, C-174 (1986).

P. Feeney, D.H. Napper, and R.G. Gilbert, Macromol., 17, 2520 (1984).

B. Fegley, H.K. Bowen, L.J. Rigione and D. Todd, Bull. Am. Ceram. Soc., 62, 374 (1983).

B. Fegley and E.A. Barringer, Mat. Res. Soc. Symp. Proc., 32, 187 (1984).

N.A. Fuchs, The Mechanics of Aerosols, Pergamon Press, New York (1964).

K. Fukai et al., Ceram. Trans., 12, 741 (1990).

H.C. Hamaker, Physica, 4, 1058 (1937).

M.T. Harris, C.H. Byers and R.R. Brunson, Mat. Res. Soc. Symp. Proc., 121, 287 (1988).

P.A. Haas, F.G. Kitts and H. Beutler, Chem. Eng. Prog. Symp. Ser., 63, 16 (1967).

P.A. Hass, Chem. Eng. Prog. April, 44 (1989).

C.D. Hendricks and J.M. Schneider, Am. J. Phys. 31, 450 (1962).

R.H. Heistand et al., Science or Ceramic Chemical Processings, eds. L.L. Hench and D.R. Ulrich, John Wiley and Sons, New York, pg 485 (1985).

R. Hogg, T.W. Healy and D.W. Fuerstenau, Trans. Faraday Soc., 62, 1638 (1966).

R.G. Horn and J.N. Israelachvili, J. Chem. Phys., 75, 1400 (1981).

R.K. Iler, The Chemistry of Silica, John Wiley and Sons, New York (1979).

B.J. Ingebrethsen, E. Matijevic, and R.E. Partch, J. Colloid Interface Sci., 95, 228 (1981).

J.N. Israelachvili and G.E. Adam, J. Chem. Soc., Faraday Trans., 74, 975 (1978).

J.H. Jean and T.A. Ring, Ceram. Bull., 65, 1574 (1986).

J.H. Jean and T.A. Ring, Langmuir, 2, 251 (1986).

D.W. Johnson, Am. Ceram. Soc. Bull., 60, 221 (1981).

K.D. Keefer, Mat. Res. Soc. Symp. Proc., 32, 15 (1984).

L.W. Kelts, N.J. Effinger, and S.M. Melpolder, J. Non–Crystalline Solids, 83, 353 (1986).

R. Klein and W. Hess, Faraday Discuss. Chem. Soc., 76, 137 (1983).

D.E. Koppel, J. Chem. Phys., 57, 4814 (1972).

H. Lamb, "Hydrodynamics," 6th Ed., Dover Publications, New York (1945).

V.K. LaMer and R.H. Dinegar, J. Amer. Chem. Soc., 72, 4847 (1950).

L. Lapidus and G.P. Pfinder, Numerical Solution of Partial Differential Equations in Science and Engineering, John Wiley and Son, New York (1982).

B.I. Lee and L.L. Hench, Colloids and Surfaces, 23, 211 (1987).

J.A. Ligget and P.L-F. Liu, The Boundary Integral Equation Method for Porous Media Flow, George Alen & Urwin, London (1983).

J.L. Lippert, S.B. Melpolder and L.M. Kelts, J. Non-Cryst. Solids, 104, 139 (1988).

J. Livage, M. Henry and C. Sanchez, Mat. Res. Soc. Symp. Proc., 18, 259 (1988).

J. Livage, M. Henry and C. Sanchez, Prog. Solid St. Chem., 18, 259 (1988).

L. Livage and M. Henry, Ultrastructure Processsing of Advanced Ceramics, eds. J.D. McKenzie and D.R. Ulrich, 183 (1988).

J.L. Look, G.H. Bogush and C.F. Zukoski, Faraday Discussion Chem. Soc., 90, 345 (1990).

C.T. Lynch et al., Anal. Chem., 36, 2333 (1964).

W.A. Macky, Proc. R. Soc. London, A 133, 565 (1931).

A.C. Makrides, M. Turner and J. Slaughter, J. Colloid Interface Sci., 61, 24 (1976).

A.R. Marsh III, G. Klein and T. Vermeulen, LBL-4415.

C.B. Martin, R.P Kurosky, G.D. Maupin, C. Han, J. Javadpour and I.A. Askay, Ceramic Trans., 12, Eds. G.L. Messing, S. Hirano and H. Hausner, 99 (1990).

E. Matijevic, Prog. Colloid Polym. Sci., 61, 24 (1976).

T. Matsoukas and E. Gulari, J. Colloid Interface Sci., 124, 252 (1988).

K.S. Mazdiyasni, C.T. Lynch and J.S. Smith, A. Amer. Ceram. Soc., 50, 532 (1967).

J.R. Melcher and G.I. Taylor, Ann. Rev. Fluid Mech., 1, 111 (1969).

C.A. Miller and L.E. Scriven, J. Fluid Mech., 32, 417 (1968).

W.T. Minehan and G.L. Messing, J. Non-Cryst. Solids, 121, 375 (1990).

A.E. Neilsen, Kinetics of Precipitation, Pergamon Press, New York (1964).

P. Odier, et. al., Ceramic Trans., 12, Eds. G.L. Messing, S. Hirano and H. Hausner, 75 (1990).

H. Okamura, E.A. Barringer and H.K. Bowen, J. Am. Ceram. Soc., 69, C-22 (1986).

K. Osseo-Asare and F.J. Arriagada, Ceramic Trans., 12, Eds. G.L. Messing, S. Hirano and H. Hausner, 3 (1990).

R.H. Ottewill and J.N. Shaw, Discuss. Faraday Soc., 42, 154 (1966).

R.M. Pashley, J. Colloid Interface Sci., 83, 531 (1981).

R.M. Pashley and J.N. Israelachvili, J. Colloid Interface Sci., 101, 511 (1984).

B.W. Peace, K.G. Mayhan, and J.F. Montle, Polymers, 14, 420 (1973).

N.A. Pelekasis, J.A. Tsamopoulos and G.D. Manolis, Phys. Fluids A, 2, 1328 (1990).

J.J. Perona and C.H. Byers, Chem. Eng. Sci., 42, 2785 (1987).

G. Peschel et al., Colloid and Polymer Sci., 260, 444 (1982).

J.C. Pouxviel, J.P. Boilot, J.C. Beloeil, and J.Y. Lallemand, J. Non–Cryst. Solids, 89, 345 (1987).

S.E. Pratsinis, Ceramic Trans., 12, Eds. G. L. Messing, S. Hirano and H. Hausner, 227 (1990).

A. Prosperetti, J. Mec., 19, 149 (1980).

S.W. Provencher, J. Hendrix, L. De Maeyer, J. Chem. Phys., 69, 4273 (1978).

S.W. Provencher, Makromol. Chem., 180, 201 (1979).

S.W. Provencher, Comput. Phys. Commun., 27, 213 (1982a).

S.W. Provencher, Comput. Phys. Commun., 27, 229, (1982b).

H. Reerink and J.G. Overbeek, Discuss. Faraday Soc., 18, 74 (1954).

R.C. Reid, J.M. Prausnitz and T.K. Sherwood, The Properties of Gases and Liquids, McGraw Hill Book Company, New York (1977).

W.H. Rhodes, J. Am. Ceram. Soc. 64, 19 (1981).

T.A. Ring, Advanced Systems for Manufacturing, 12th Conference on Production Research and Technology, 239 (1985).

T.A. Ring, MRS Bulletin, 15, 43 (1990).

S. Ross and I.D. Morrison, Colloidal Systems and Interfaces, Wiley, New York (1988).

S. Sakka, H. Kozukz and S. Kim, in: Ultrstructure Processing of Advanced Ceramics, eds. J. D. MacKenzie and D. R. Ulrich, Wiley, New York, 159 (1988).

C. Sanchez, J. Livage, M. Henry and F. Babonneau, J. NonCryst- Solids, 100, 65 (1988).

C. Sanchez et. al, in: Ultrstructure Processing of Advanced Ceramics, eds. J.D. MacKenzie and D.R. Ulrich, Wiley, New York, 77 (1988).

J. Sanchez and A. McCormick, Chem. Mater., 3, 320 (1991).

E.B. Sandell, Colorimetric Determination of Trace Metals, Interscience Publishers, Inc., New York, 868 (1959).

R.T. Sanderson, Science, 114, 670 (1951).

E. Santacesaria et. al., J. Colloid Interface Sci., 44, 111 (1986).

H. Schmidt, H. Scholze, and A. Kaiser, J. Non–Cryst. Solids, 48, 65 (1982).

H. Schmidt, H. Scholze, and A. Kaiser, J. Non–Cryst. Solids, 65, 1 (1984).

H. Schmidt, A. Laiser, M. Rudolph and A. Lentz, Science of Ceramic Chemical Processing, eds. L.L. Hench and D.R. Ulrich, John Wiley and Sons, pg. 87 (1986).

T.C. Scott, AICHE J., 33, 1557 (1987).

T.C. Scott, Sep. and Purif. Methods, 18, 65 (1989).

T.C. Scott, O.A. Basaran and C.H. Byers, I & EC Research, 29, 901 (1990).

T.C. Scott and W.G. Sisson, Sep. Sci. Techn., 23, 1563 (1988).

T.C. Scott and R.M. Wham, I & EC Research, 28, 94 (1989).

T.C. Scott, "Dimensional Analysis of Continuous High Capacity Elctrodispersion of Aqueous-Based Liquids in an Organic Continuous Phase," Sep. Sci. and Tech., 25, 1709 (1991).

D.J. Shaw, Introduction to Colloid and Surface Chemistry, Butterworths, Boston (1980).

E.B. Slamovich and F.F. Lange, Mater. Res. Soc. Proc. 121, 257 (1988).

W. Stober, A. Fink, and E. Bohn, J. Colloid Inter. Sci., 25, 62 (1968).

R.S. Stock and W.H. Ray, J. Polym. Sci. Polym. Phys. Ed., 23, 1393 (1985).

S.V. Subramanyam, J. Fluid Mech., 37, 715 (1969)

T. Takamatsu, Y. Hashimoto, M. Yamaguchi and T. Katayama, J. Chem. Eng. Japan, 14, 178 (1981).

G.I. Taylor, Proc. R. Soc. London, A 280, 383 (1964).

J. Timmermans, The Physico-Chemical Constants of Binary Systems in Concentrated Solutions, Vol. 4, Interscience Publishers, Inc., New York, (1960).

B. Tremillon, Chemistry of Nonaqueous Solvents, Dreidel Publishing Company, (1974).

T. Tsukada, et al., J. Chem. Eng (Japan), 19, 537 (1986).

C.W. Turner and K.J. Franklin, in: Ceramic Chemical Processing, eds. L.L. Hench, and D.R. Ulrich, John Wiley and Sons, New York, 81 (1986).

C.W. Turner and K.J. Franklin, J. Non-Cryst. Solids, 91, 401 (1987).

H.C. Van de Hulst, Light Scattering by Small Particles, Wiley, New York (1957).

E.J. W. Verwey and J.Th.G. Overbeek, Theory of the Stability of Lyophobic Colloids, Elsevier, New York (1948).

G.R. Weise and T.W. Healy, Trans. Faraday Soc., 66, 490 (1970).

H.H. Willard and N.K. Tang, J. Am. Chem. Soc., 59, 1190 (1937).

M. Yamane, S. Inoue and A. Yasumori, J. Non-Cryst. Solids, 63, 12 (1984).

B.E. Yoldas, J. Appl. Chem. Biotechnol., 23, 803 (1973).

B.E. Yoldas, Ceram. Bull., 54, 289 (1975).

B.E. Yoldas, J. Non-Cryst. Solids, 51, 105 (1982).

B. Yoldas, J. Non-Cryst. Solids, 83, 375 (1986).

J. Zelany, Phys. Rev., 10, 1 (1917).

T.W. Zerda, I. Artaki and J. Jonas, J. Non-Cryst. Solids, 81, 365 (1986).

S. Zhang and G.L. Messing, Ceramic Trans., 12, Eds. G.L. Messing, S. Hirano and H. Hausner, 49 (1990).

C.F. Zukoski, M.K. Chow, G.H. Bogush and J.L. Look, Mat. Res. Soc. Symp. Proc., 180, 131 (1990).

# APPENDIXES

## A.1. Computer Programs

This appendix contains the three major computer codes that were used in modeling and data evaluation. Algorithms one and two, **popcon.f** and **popsol.f**, employ the continuous method and the method of moments to solve the population balance equations, Eqs. 2.21 and 2.22 (Chapter 2), respectively. Euler's or the Runge-Kutta method is employed to integrate the time derivative and Simpson's rule is used to integrate the right hand side of the equation.

The third computer code solves the electrohydrostatic equations for an axisymmetric pendant drop hanging from a nozzle **bemfem.f**. This codes uses a hybrid finite element-boundary element to solve the augmented Young-Laplace Equation and Laplace equations, respectively.

A.1.1. popcon.f - Population Balance Model - Continuous Method

```
c       ******************************************************
c       popcon.f - Main Program
c       ******************************************************
        implicit integer (i-n)
        implicit double precision (a-h,o-z)
        character*80 ofile,ofil
        common /param/zkob,zko,beta,zrpn
        common /znlpa/zmu,zsig,znt,rlq,zfu2,xmut
        common /nj/zgn
        common /napa/zmuo,zsio,znno,tspf
        common /vbeta/zo1,zo2,zki,zpe,zlam,zhc
        common /vhn/zvhn,tcog,sten,vol,temp,csol,cinto,botz
        common/chemical/pk1,pk2,pk3,znh3,h2oo,h2o
        zo1=11.5e-3
        zo2=zo1
        zki=3.e8
        zpe=7.e-10
        zlam=0.1e-4
        zhc=1.6e-20
        open(unit=5,File='bc',status='old')
        rewind 5
        read(5,*)zki,zo1,zo2
        read(5,*)zgn,zfmax,tspf
        read(5,177) ofile
177     format(a)
        read(5,177)ofil
        read(5,*) zkob,zko,beta,vzmu,vzsig,vznt
        open (unit=2,file=ofile,status='new')
        open (unit=3,file=ofil,status='new')
        write(2,*)'IDL= ',zki,' zo1= ',zo1
        write(2,*)' zo2= ',zo2
        write(3,*)'IDL= ',zki,' zo1= ',zo1,' zo2= ',zo2
        read(5,*)dt,tstop
        read(5,*)zmuo,zsio,znno,xmut,zvhn,tcog
        read(5,*)sten,vol,temp,csol,cinto,ifip
        read(5,*)pk1,pk2,pk3,znh3,h2oo,h2o
        if(ifip.eq.1)open (unit=4,file='last.dat',status='old')
        botz=1.3805e-16
        csol=6.02e20*csol
        cinto=6.02e20*cinto
        supsat=1.00001
        rstar=5.e-7
```

```
      rp=exp(zmuo)/10.
      drp=rp
      vzmu=zmuo
      zmu=vzmu
      zsig=vzsig
      znt=vznt
      t=0.
      zmu=vzmu
      zsig=vzsig
      znt=vznt
      ni=220
      call rk4(rp,drp,t,dt,tstop,zfmax,ifip,ni)
      rp=rp+drp
      stop
      end
c     ******************************************************
c     Numerical Integration of Double Integral
c     Mechanical Cubature Method
      Subroutine MCUB(F1z,f1,F2,rp,drp,vzrpn,np1,vrp,a,h,z,vn,
     1ne1,vh,drp2)
      implicit integer (i-n)
      implicit double precision (a-h,o-z)
      Common /param/zkob,zko,beta,zrpn
      common /znlpa/zmu,zsig,znt,rlq,zfu2,xmut
      common /nj/zgn
      common /napa/zmuo,zsio,znno,tspf
      common /max/rmin,rmax
      dimension vrp(10000),a(10000),h(10000),z(10000),vn(10000)
c     ***************************
c     Calculate Formation Integral
c     ***************************
      dzmuo=zmuo
      dzsio=zsio
      dznno=znno
      irr=0
      ir=0
      irop=0
      irrd=0
      vrp(0)=0.0
      vn(0)=0.0
      rhom=(rp)*zkob/2.0**(1.0/3.0)
      f1=0.0
      rrho=vrp(1)-drp
      rhovm=rhom-rrho
      irhom=0
      if(rhom.gt.vh)rhovm=vh-rrho
      if(rhom.gt.vh)difrvh=rhom-vh
```

```
      wdrp=drp
      rfrst=vrp(1)-drp
1010  ifrp=rhovm/wdrp
      if(ifrp.le.1)ifrp=1
      vfrp=rhovm/ifrp
      zk=vfrp/zgn
      zhk=zk/2.0
      rrp=rp
690   if(rp.ge.vrp(irop).and.rp.le.vrp(irop+1))goto 790
      irop=irop+1
      if(irop.gt.np1)irop=0
      goto 690
790   continue
      in=-1
      do 100 n=1,2*ifrp*zgn+1
      in=in+1
      rrho=rfrst+(n-1)*zhk
490   if(rrho.ge.vrp(irr).and.rrho.le.vrp(irr+1))goto 590
      irr=irr+1
      if(irr.gt.np1)irr=0
      goto 490
590   continue
      rhopd=((zkob*rp)**(3.0)-rrho**(3.0))**(1.0/3.0)
      if(rp.le.rrho)goto 100
495   if(rhopd.ge.vrp(irrd).and.rhopd.le.vrp(irrd+1))goto 595
      irrd=irrd+1
      if(irrd.gt.np1)irrd=0
      goto 495
595   call FR1(irop,irr,irrd,zhk,fu1,rrho,rrp,t,np1,vrp,
     1 a,h,z,vn)
      c=2.0/3.0*zhk
      if(in.eq.1) c=4.0/3.0*zhk
      if(in.eq.1)in=-1
      if(n.eq.1.or.n.eq.2*ifrp+1) c=1.0/3.0*zhk
      f1=c*fu1+f1
100   continue
      irhom=irhom+1
      rhovm=difrvh
      wdrp=drp2
      rfrst=vh
      if(rhom.gt.vh.and.irhom.lt.2)goto 1010
46    f1=f1
c     **********************
c     Calculate Loss Integral
c     **********************
      rrp=rp
      rlq=exp(zmu)
```

```
            rrho=vrp(1)-drp
            f2=0.
            rrhop=rlq
            rmax=vrp(ne1+6)
            rvmax=rmax-rrho
            irmax=0
            ir=0
            if(rmax.gt.vh)rvmax=vh-rrho
            if(rmax.gt.vh)difrvh=rmax-vh
            wdrp=drp
            rfrst=vrp(1)-drp
1015        izk=rvmax/wdrp
            if(izk.lt.1)izk=1
            zk=(rvmax)/izk
            zk=zk/zgn
            zhk=zk/2.0
            in=-1
            do 120 n=1,izk*2*zgn+1
            in=in+1
            rrho=rfrst+(n-1)*zhk
290         if(rrho.ge.vrp(ir).and.rrho.le.vrp(ir+1))goto 390
            ir=ir+1
            goto 290
390         continue
            call FR2(irop,ir,zhk,fu2,rrho,rrp,t,np1,vrp,a,h,z,vn)
            c=2.0/3.*zhk
            if(in.eq.1) c=4.0/3.*zhk
            if(in.eq.1)in=-1
            if(n.eq.1.or.n.eq.izk*2*zgn+1) then c=1.0/3.*zhk
            f2=c*fu2+f2
            zfu2=f2
120         continue
99          continue
            irmax=irmax+1
            rvmax=difrvh
            wdrp=drp2
            rfrst=vh
            if(rmax.gt.vh.and.irmax.lt.2)goto 1015
1999        continue
            call zjmnp(dzmuo,dzsio,dznno,zpnrp,rrp)
            f2=zfu2*vzrpn
            f1z=f1+zpnrp
c           f1z=zpnrp
            return
            end
c           ******************************************************
c           Integral Representing Formation of Primary Particles
```

```
c       ****************************************************
        Subroutine FR1(irop,irr,irrd,drp,fu1,rho,rp,t,np1,vrp,
        1 a,h,z,vn)
        implicit integer (i-n)
        implicit double precision (a-h,o-z)
        Common /param/ zkob,zko,beta,zrpn
        common /znlpa/zmu,zsig,znt,rlq,zfu2,xmut
        common /max/rmin,rmax
        dimension vrp(10000),a(10000),h(10000),z(10000),vn(10000)
        rhop=((zkob*rp)**(3.0)-rho**(3.0))**(1.0/3.0)
        fu1=0.
        if (rhop.eq.0.)goto 554
        call zbeta (xbeta,rhop,rho)
        frst=zko*(rhop+rho)*(1/rhop+1/rho)*xbeta
        const=rp**(2.0)*zkob**(3.0)/((rp*zkob)**(3.0)- rho**(
        1 3.0))**(2.0/3.0)
        slope1=(vn(irrd+1)-vn(irrd))/(vrp(irrd+1)-vrp(irrd))
        slope2=(vn(irr+1)-vn(irr))/(vrp(irr+1)-vrp(irr))
        znrp=slope1*(rhop-vrp(irrd))+vn(irrd)
        znrho=slope2*(rho-vrp(irr))+vn(irr)
        zU1=const*frst*znrp*znrho
c       if(zu1.gt.1.e-20.and.zu1.lt.1.e36)fu1=zu1
        goto 558
554     zu1=0.
        fu1=0.
558     continue
        fu1=zu1
        Return
        End
c       ****************************************************
c       Integral Representing Loss of Primary Particles
c       ****************************************************
        Subroutine FR2(irop,ir,drp,fu2,rho,rp,t,np1,vrp,a,h,z,vn)

        implicit integer (i-n)
        implicit double precision (a-h,o-z)
        Common /param/ zkob,zko,beta,zrpn
        common /znlpa/zmu,zsig,znt,rlq,zfu2,xmut
        common /max/rmin,rmax
        dimension vrp(10000),a(10000),h(10000),z(10000),vn(10000)
        fu2=0.
        call zbeta (xbeta,rp,rho)
        frst=zko*(rp+rho)*(1/rp+1/rho)*xbeta
        slope1=(vn(irop+1)-vn(irop))/(vrp(irop+1)-vrp(irop))
        slope2=(vn(ir+1)-vn(ir))/(vrp(ir+1)-vrp(ir))
        znrp=slope1*(rp-vrp(irop))+vn(irop)
```

```
      znrho=slope2*(rho-vrp(ir))+vn(ir)
      zu2=frst*znrho
c     if(zu2.gt.1.e-20.and.zu2.lt.1.e38)fu2=zu2
      fu2=zu2
      Return
      End
c     ******************************************************
c     Log-normal Particle size distribution
c     ******************************************************
      subroutine zlmnp(drp,rp,rho,t,znrp,znrho)
      implicit integer (i-n)
      implicit double precision (a-h,o-z)
      common /znlpa/zmu,zsig,znt,rlq,zfu2,xmut
      f11=0.
      f12=0.
      f21=0.
      f22=0.
      if(rp.eq.0.)goto 22
      f11=znt/((2.*22./7.)**(0.5)*rp*zsig)
      f12=exp(-(log(rp)-zmu)**(2.0)/(2.0*zsig**(2.0)))
      znrp=f11*f12
22    continue
      if(rho.eq.0.)goto 23
      f21=znt/((2*22/7)**(0.5)*rho*zsig)
      f22=exp(-(log(rho)-zmu)**(2.0)/(2.0*zsig**(2.0)))
23    continue
      znrho=f21*f22
      Return
      End
c     ******************************************************


c     Runge-Kutta Routine
c     ******************************************************
      subroutine rk4(rp,drp,t,dt,tstop,zfmax,ifip,ni)
      implicit integer (i-n)
      implicit double precision (a-h,o-z)
      dimension vrp(10000),vn(10000),zrp(10000),a(10000),h(10000)
     1 ,z(10000),vn2(10000)
      common /znlpa/zmu,zsig,znt,rlq,zfu2,xmut
      common /nj/zgn
      common /napa/zmuo,zsio,znno,tspf
      common /max/rmin,rmax
      common /vhn/zvhn,tcog,sten,vol,temp,csol,cinto,botz
      common/area/sarea,pratio,r2b,r3b
      common/chemical/pk1,pk2,pk3,znh3,h2oo,h2o
      pi=3.1415926535898
```

```
      sarea=0.0
      ct=0.
      ni=100
      call vhc(vh,drp,ni)
      vh=(1.+10.0*zsio)*exp(zmuo)
      vho=(1.-10.0*zsio)*exp(zmuo)
      if(vho.lt.0.0)vho=0.0
      drp=(vh-vho)/zvhn
      vdrp=drp
      drp2=(5.e-5-vh)/2000.
      wdrp=drp
      rp=drp
      ni=2100
      n=1
      zvrp=vh
      zmax1=0.
      np1=ni
      vrp(0)=0.0
      vrp(1)=vho
      vn(1)=0.0
      vn2(1)=0.0
      do 84 k=2,np1
      if(k.gt.zvhn)wdrp=drp2
      vrp(k)=vrp(k-1)+wdrp
      crp=vrp(k)
      call zlmnp(vdrp,crp,crp,t,znrp,znrp)
      if(zmax1.le.znrp)zmax1=znrp
      rmax=vrp(k)
85    vn(k)=znrp
      vn2(k)=znrp
      vn(k)=0.0
      vn2(k)=0.0
84    continue
      vrp(0)=0.0
      rmax=1.e-5
      if(ifip.eq.1)goto 899
      rmid1=rlq
      do 444 i=1,np1
      crp=vrp(i)
      call zlmnp(vdrp,crp,crp,t,znrp,znrp)
      if(znrp.gt.zfmax*zmax1) rmin=0.0
444   continue
449   continue
      ditim=0.0
      ditim2=0.0
      dt1=1.
      znt=0.0
```

```
      call zspl3(np1,vrp,vn2,a,h,z)
      supsat=1.0001
      gfen=16.8*sten**3*vol**2/(botz**3*temp**3*
     1 (log(supsat))**2)
      diam=(6./pi*vol)**(0.33333333)
      afreq=(2.*1.e-5)/(diam)**5
      znstar=2.*gfen/log(supsat)
      znno=afreq*exp(-gfen)/znstar
      cintt=cinto
      cints=0.0
      ctie=cinto
      if(znt.ne.0.0)dt1=tcog*3.75e10/znt
      if(znno.ne.0.0)dt1=sqrt(tcog*3.75e10/znno)
      ne1=zvhn
      drp3=drp
15    continue
      vrp(0)=0.0
      vn(0)=0.0
      zfu2=0.0
      vmax=0.
      if(znt.ne.0.0)dt=tcog*3.75e10/znt
      dtj=dt
      if(znno.ne.0.0)
     1 dt=(-znt+sqrt(znt**2+tcog*1.5e11*znno))/(2.*znno)
      if(znno.ne.0.0)dtj=0.2*(cintt-csol)/znno
      if(dtj.lt.dt)dt=dtj
      if(dt.ge.10.)dt=10.
      ct=ct+dt
c     write(*,*)'dt= ',dt,znno
      ditim2=ditim2+dt
      ditim=ditim+dt
      n=0
      if(t.lt.1000.and.cints.lt.1.01*csol)goto 488
      if(znno.lt.1.0)goto 488

298   n=n+1
      f1=0.
      f2=0.
      f1z=0.
      zrpn=vn(n)
      rp=vrp(n)
      zrpn=vn(n)
      zzrpn=zrpn
      call mcub(f1z,f1,f2,rp,drp,zzrpn,np1,vrp,a,h,z,vn2,ne1,
     1 vh,drp2)
      cvole=vol*6.02e23
      ctioh=cints/6.02e20
```

```
      wdrp=drp
      if(n.gt.zvhn)wdrp=drp2
      dpndr=(vn2(n)-vn2(n-1))/(vrp(n)-vrp(n-1))
      dgrow=(1./36./pi)**0.3333333*ctioh*0.06/1.9*pk2
      dpgrw=dgrow*dpndr
      if(f2.lt.0.0)f2=0.
      fk1=(f1z-f2-dpgrw)*dt
c     fk1=f1z*dt
      goto 333
333   vn(n)=vn(n)+fk1
      if(vn(n).lt.0.0)write(*,*)n,vrp(n),vn(n)
      if(vn(n).lt.0.)vn(n)=0.
      if(vmax.le.vn(n))vmax=vn(n)
      zmax=vmax
      if(n.gt.ne1)ne1=n
      if(n.eq.np1)goto 18
      if(n.ge.nf1.and.(vn(n)*rmax).lt.1.0e-4)goto 18
      if(ditim.lt.100.)goto 14
      ditim=0.0
      write(2,195)t+dt,vrp(n),vn(n)
195   format(E12.7,' ',e12.7,' ',e12.7)
14    goto 298
18    continue
      if(n.lt.zvhn)goto 298
899   nf1=n
      if(ifip.ne.1)goto 894
      read(4,*)ne1
      n=ne1
      do 491 i=1,ne1
      read(4,*)tt,vrp(i),vn(i)
491   vn2(i)=vn(i)
      t=tt
      read(4,*)h2o,cintt,ctie
      cintt=cintt*6.02e20
      ctie=ctie*6.02e20
      ifip=0
      cints=cintt-ctie
894   vrp(0)=drp
      vn(0)=0.
      do 451 i=1,np1+1
      vn2(i)=vn(i)
      cex=0.3333333333
451   continue
      vrp(0)=drp
      call zspl3(np1,vrp,vn2,a,h,z)
      zmax1=0
      do 445 i=1,np1+1
```

```
      crp=vrp(i)
      crp1=vrp(i-1)
      crp2=vrp(i+1)
      znrp=spl3(np1,vrp,vn2,z,crp)
      zn1p=spl3(np1,vrp,vn2,z,crp1)
      zn2p=spl3(np1,vrp,vn2,z,crp2)
      if(zmax1.le.znrp)rmid=crp
      if(zmax1.le.znrp)zmax1=znrp
445   continue
      do 446 i=1,np1+1
      crp=vrp(i)
      znrp=spl3(np1,vrp,vn2,z,crp)
      if(znrp.lt.zfmax*zmax1.and.crp.lt.rmid)rmin=0.0
446   continue
      call sigm(drp,drp2,vrp,vn,n-1,r6b,zrlq,zvhn)
      if(ditim2.lt.5.)goto 137
      ditim2=0.0
      write(*,193)t+dt,r2b,r6b,znt,cintt/6.02e20,zdiff
      write(3,193) t+dt,r2b,r6b,znt,cintt/6.02e20,zdiff
193   format(e10.5,' ',e10.5,' ',e10.5,' ',e10.5,' '
     1 ,e10.5,' ',e14.5)
137   continue
488   continue
      t=t+dt
      if(ct.ge.xmut*dt)ct=0.
      if(ifip.eq.1)goto 893
      if(dt1.gt.1.5*dt.or.dt1.lt.0.5*dt)dt1=dt
      cintt=cintt-(znno*znstar+pk2*sarea*(cints)-
     1 pk3*h2o**2*sarea*(cinto-cintt))*dt
      ctie=ctie-pk1*h2o**1.5*znh3**0.9*ctie*dt
      h2o=h2oo-(4.*(cinto-ctie)-2.0*(cinto-cintt))/6.02e20
      cints=cintt-ctie
      cscalc=pk3*h2o**2/pk2*(cinto-cintt)
      if(csol.le.cscalc)csol=cscalc
893   znno=0.0
      if((cints/csol).lt.1.01)goto 915
      supsat=cints/csol
      gfen=16.8*sten**3*vol**2/(botz**3*temp**3*
     1 (log(supsat))**2)
      diam=(6./pi*vol)**(0.333333333)
      afreq=(2.*1.e-5)/(diam)**5
      znstar=2.*gfen/(log(supsat))
c     rstar=2.*sten*vol/(botz*temp*log(supsat))
c     if(rstar.lt.5.e-7) rstar=5.e-7
      rstar=exp(zmuo)
      znstar=(4.*pi/3.*rstar**3)/vol
```

```
      znno=afreq*exp(-gfen)/znstar
      zmuo=log(rstar)
      zcint=(cinto-cintt)/6.02e20
      zpart=4.18879/vol*r3b**3*znt/6.02e20
      zdiff=(zcint-zpart)/zcint
c     write(*,*)t,zdiff

915   continue
      if(t.lt.tstop) goto 15
      return
      end
c     ***************************************************
c     Adjustment of Lognormal Distribution Parameters
c     ***************************************************
      Subroutine sigm(drp,drp2,vrp,vn,ni,r6b,zrlq,zvhn)
      implicit integer (i-n)
      implicit double precision (a-h,o-z)
      dimension vrp(10000),vn(10000)
      common /znlpa/zmu,zsig,znt,rlq,zfu2,xmut
      common/area/sarea,pratio,r2b,r3b
      pi=3.1415926535898
      vmu=0.
      vsi=0.
      vnt=0.
      vaa=0.
      r6b=0.
      r2b=0.0
      r3b=0.0
      vvnt=0.
      sarea=0.0
      pratio=0.0
      do 46 i=1,ni-2
      wdrp=drp
      if(i.gt.zvhn)wdrp=drp2
      vmu=0.5*(vn(i+1)+vn(i))*wdrp*log(vrp(i))+vmu
      vnt=vn(i)*wdrp+vnt+0.5*wdrp*(vn(i+1)-vn(i))
      rhos=2.*22./7.*vrp(i)/0.6328e-4*1.5
      zqs=2.-4./rhos*sin(rhos)+4./rhos**2.*(1.-cos(rhos))
      sarea=sarea+4*pi*vrp(i)**2*wdrp*0.5*(vn(i+1)+vn(i))
      vrpav=(vrp(i+1)+vrp(i))/2.
      r6b=wdrp*(vrpav**6)*(0.5*vn(i+1)+0.5*vn(i))+r6b
      r2b=wdrp*(vrpav**2)*(0.5*vn(i+1)+0.5*vn(i))+r2b
      r3b=wdrp*(vrpav**3)*(0.5*vn(i+1)+0.5*vn(i))+r3b
      pratio=5.4e22*vrp(i)**6*0.5*(vn(i+1)+vn(i))*wdrp+pratio
      vvnt=0.5*(vn(i+1)+vn(i))*wdrp+vvnt
46    continue
      r6b=(r6b/vvnt)**(1./6.)
```

```
      r2b=(r2b/vvnt)**(0.5)
      r3b=(r3b/vvnt)**(1./3.)
      vmu=vmu/vnt
      zrlq=exp(vmu)
      rlq=exp(vmu)
      do 48 i=1,ni-2
      vsi=vn(i)*wdrp*(log(vrp(i))-log(rlq))**2.+vsi
c     vaa=vn(i)*wdrp*((vrp(i)-rlq)**2.)**(0.5) +vaa
48    continue
      zmu=vmu
      zsig=(vsi/vnt)**(0.5)
      znt=vnt
      return
      end
c     ************************************************************
c     Calculate where distribution density is less than 0.1
c     ************************************************************
      subroutine vhc(vrh,drp,ni)
      implicit integer (i-n)
      implicit double precision (a-h,o-z)
      common /znlpa/zmu,zsig,znt,rlq,zfu2,xmut
      dzmu=zmu
      dzsi=zsig
      dznt=znt
      rlq=exp(zmu)
      rrho=rlq
      rrhop=rlq
      nt=0
      zk=rrhop/ni
      zmax=0.
110   continue
      nt=nt+1
      call zjmnp(dzmu,dzsi,dznt,znrp,rrho)
      if(rrho.gt. rlq.and.znrp.le.0.1) goto 115
      rrho=rrho+nt*zk
      goto 110
115   continue
      vrh=rrho
      rrho=rlq
      rrhop=rlq
      nt=0
      zk=rrhop/ni
114   continue
      nt=nt+1
      call zjmnp(dzmu,dzsi,dznt,znrp,rrho)
      if(rrho.lt. rlq.and.znrp.le.0.1) goto 117
      rrho=rrho-nt*zk
```

```
      goto 114
117   continue
      drp=rlq/5.
      return
      end
c     ****************************************************
c     Log-normal Particle size distribution of Nuclei
c     ****************************************************
      subroutine zjmnp(zzmu,zzsi,zznt,znrp,rp)
      implicit integer (i-n)
      implicit double precision (a-h,o-z)
      common /znlpa/zmu,zsig,znt,rlq,zfu2,xmut
      f11=0.
      f12=0.
      f21=0.
      f22=0.
      if(rp.eq.0.)goto 22
      f11=zznt/((2.*22./7.)**(0.5)*rp*zzsi)
      f12=exp(-(log(rp)-zzmu)**(2.0)/(2.0*zzsi**(2.0)))
      znrp=f11*f12
22    continue
      return
      end

      subroutine zbeta(xbeta,aa1,aa2)
      implicit integer (i-n)
      implicit double precision (a-h,o-z)
      common /vbeta/zo1,zo2,zki,zpe,zlam,zhc
      zlim=10./zki
      a1=aa1/100.
      a2=aa2/100.
      smin=2.
      smax=zlim/(a1+a2)*2.+2.0
      if(a1.lt.a2)smax=zlim/(a1+a2)*2.+2.
      if(a1.gt.a2)smax=zlim/(a2+a1)*2.+2.
      dls=(smax-smin)/8.
      smin=smin+dls/40.
      in=-1
      zce=0.
      zce2=0.
      s=smin
      vmax=4.45e-9*a1*a2/(a1+a2)*zo1**2
      xbeta=1./exp(vmax/4.142e-21)
      goto 130
      do 55 i=1,8
      in=in+1
```

```
      call wr(s,a1,a2,ce,ce2)

      c=4.0/3.0*dls
      if(in.eq.2) c=2./3.*dls
      if(in.eq.2) in=0
      if(i.eq.1.or.i.eq.8) c=1.0/3.0*dls
      zce=c*ce+zce
      zce2=c*ce2+zce2
      s=s+dls
55    continue
      r1=a1
      r2=a2
      if(a1.lt.a2)goto 113
      r2=a1
      r1=a2
113   continue
      if(zce2.eq.0.0.and.zce.eq.0.0)goto 129
      if(zce.eq.0.0)goto 129
111   xbetah=zce2/(1.*zce)
112   xbeta=xbetah
      goto 130
129   xbeta=1.0
130   continue
97    continue
      return
      end

      subroutine wr(s,aa1,aa2,ce,ce2)
      implicit integer (i-n)
      implicit double precision (a-h,o-z)
      common /vbeta/zo1,zo2,zki,zpe,zlam,zhc
110   continue
      a1=aa1
      a2=aa2
      zho=s*(a1+a2)/2.-(a1+a2)
      if(a1.lt.a2)zho=s*(a1+a2)/2.-(a1+a2)
      if(a2.lt.a1)zho=s*(a2+a1)/2.-(a1+a2)
      zpo=2.*(22./7.)*zho/zlam
      x=zho/(a1+a2)
      y=a1/a2
      if(a2.gt.a1)y=a2/a1
      vr=0.
      if(zo1.eq.0.0.and.zo2.eq.0.) goto 215
      vr=zpe*a1*a2*(zo1**2.+zo2**2.)/(4.*(a1+a2))*(
     1 2.*zo1*zo2/(zo1**2.+zo2**2.)*
     1 log((1.+exp(-zki*zho))/(1.-exp(-zki*zho)))+log(1.-exp
     1 (-2.*zki*zho)))
```

```
215     continue
        zla1=(exp(20.1*zo1)-1.)/(exp(20.1*zo1)+1)
        zla2=(exp(20.1*zo2)-1.)/(exp(20.1*zo2)+1)
        vr=0.125*a1*a2/(a1+a2)*zla1*zla2*zpe*(exp(-zki*zho))
        va=-zhc*a1*a2/(6.*zho*(a1+a2))*(1./(1.+1.77*zpo))
        if(zpo.le.2.0)goto 410
        va=2.*zhc*a1*a2/(zho*(a1+a2))*(-2.48/(60.*zpo)+
       1 2.17/(180.*zpo**2.)-0.59/(420.*zpo**3.))
        va=-zha/12.*(y/(x**2.+x*y+x)+y/(x**2.+x*y+x+y)+2.
       1 *log((x**2.+x*y+x)/(x**2.+x*y+x+y)))
410     continue
        va=-zhc/12.*(y/(x**2.+x*y+x)+y/(x**2.+x*y+x+y)+2.
       1 *log((x**2.+x*y+x)/(x**2.+x*y+x+y)))
        zkt=4.e-21
        ce=exp((vr+va)/(4.e-21))/(s**2.)
        ce2=exp(va/4.e-21)/(s**2.)
        return
        end

        subroutine zspl3(n,t,y,d,c,z)
        implicit integer (i-n)
        implicit double precision (a-h,o-z)
        dimension t(n),y(n),d(n),c(n),z(n)
        d(1)=1.0
        c(1)=0.
        z(1)=0.
        do 2 i=2,n-1
        d(i)=2.*(t(i+1)-t(i-1))
        c(i)=t(i+1)-t(i)
        temp=(y(i+1)-y(i))/(t(i+1)-t(i))
2       z(i)=6.*(temp-(y(i)-y(i-1))/(t(i)-t(i-1)))
        d(n)=1.0
        c(n-1)=0.
        z(n)=0.
        call tri(n,c,d,c,z)
        return
        end

        subroutine tri(n,a,d,c,b)
        implicit integer (i-n)
        implicit double precision (a-h,o-z)
        dimension a(n),d(n),c(n),b(n)
        do 2 i=2,n
        xmult=a(i-1)/d(i-1)
        d(i)=d(i)-xmult*c(i-1)
2       b(i)=b(i)-xmult*b(i-1)
```

```
      b(n)=b(n)/d(n)
      do 3 i=1,n-1
3     b(n-i)=(b(n-i)-c(n-i)*b(n-i+1))/d(n-i)
      return
      end

      function spl3(n,t,y,z,x)
      implicit integer (i-n)
      implicit double precision (a-h,o-z)
      dimension t(n),y(n),z(n)
      do 2 j=1,n-2
      i=n-j
      temp=x-t(i)
      if(temp.ge.0.0) goto 3
2     continue
      i=1
      temp=x-t(1)
3     h=t(i+1)-t(i)
      a=temp*(z(i+1)-z(i))/(6.0*h)+0.5*z(i)
      b=temp*a+(y(i+1)-y(i))/h-h*(2.0*z(i)+z(i+1))/6.0
      spl3=temp*b+y(i)
      return
      end
```

A.1.2. popsol.f - Population Balance Model - Method of Moments

```
c       popsol.f - DEVELOPED BY - M. T. HARRIS
c       DATE - SEPTEMBER 12, 1990

        IMPLICIT REAL*8(A-H,O-Z)
        CHARACTER*80 IFILE,OFILE,OFILE2,OFILE3,OFILE4,
        INFILE
        COMMON/PARAM/ZKH,ZKC,ZKD,SIGMA,CSTAR,VSTAR,
        BCSTAR,ALPHA
        1,FVSTAR,CFRAC,FVINIT
        COMMON/CHEMICAL/TEOS,H2O,ZNH3,ZETA,EPSI
        COMMON/SOLVA/SOSHEL

C       *** OPEN FILES AND INPUT DATA ***
        OPEN(UNIT=11,FILE='INFILE',STATUS='OLD')
        READ(11,*)IFILE,OFILE,OFILE2,OFILE3,OFILE4
        c IFILE='INMOM2A'
        c OFILE='OUTMO2A'
        c OFILE2='OUTDI2A'
        c OFILE3='OUTCHE2A'
        OPEN(UNIT=5,FILE=IFILE,STATUS='OLD')
        OPEN(UNIT=10,FILE=OFILE,STATUS='NEW')
        OPEN(UNIT=3,FILE=OFILE2,STATUS='NEW')
        OPEN(UNIT=4,FILE=OFILE3,STATUS='NEW')
        OPEN(UNIT=12,FILE=OFILE4,STATUS='NEW')
        REWIND 5
        READ(5,*)ZKH,ZKC,ZKD,SIGMA,CSTAR,VSTAR,
        BCSTAR,ALPHA
        READ(5,*)TMAX,TEOS,H2O,ZNH3,DT,FRAC,POW,
        FVSTAR,FVINIT,CFRAC
        READ(5,*)COSI,CONH,ZETA,EPSI,HAMCON,
        SOLCON,SOSHEL
c       SIGMA=-2.94520+119.61*H2O
c       SIGMA=349.1+0.061249*H2O**4
        WRITE(10,*)'KH=',ZKH,' KC=',ZKC,' KD=',ZKD
        WRITE(10,*)'SIGMA=',SIGMA,' CSTAR=',CSTAR
        WRITE(10,*)'VSTAR=',VSTAR,' BCSTAR=',BCSTAR,
        1 ' ALPHA=',ALPHA
        WRITE(10,*)'TMAX=',TIME
        WRITE(10,*)'TEOS=',TEOS,' H2O=',H2O,' NH3=',ZNH3

        CALL INTEGR(DT,TMAX,FRAC,POW,COSI,CONH,
        HAMCON,SOLCON)
        STOP
```

```
      END


c     **** USE EULER'S METHOD TO SOLVE MOMENT AND
c     CHEMICAL KINETIC EQS. ****

      SUBROUTINE INTEGR(DT,TMAX,FRAC,POW,COSI,
     CONH,HAMCON,SOLCON)
      IMPLICIT REAL*8(A-H,O-Z)
      CHARACTER*80 IFIL1,IFIL2,IFIL3,IFIL4
      CHARACTER*80 IFILE,OFIL
      COMMON/PARAM/ZKH,ZKC,ZKD,SIGMA,CSTAR,
     VSTAR,BCSTAR,ALPHA
     1,FVSTAR,CFRAC,FVINIT
      COMMON/CHEMICAL/TEOS,H2O,ZNH3,ZETA,EPSI

c     *** SET INITIAL VALUES ***
      ZH4ION=0.0
      PI=3.1415926535898
      TNUC2=0.0
      TNUC=0.0
      ZMU0=0.0
      ZMU1=0.0
      ZMU2=0.0
      ZMU23=0.0
      ZMU123=0.0
      G13MA=0.0
      GM13=0.0
      GMA=0.0
      G0A=0.0
      GM13A=0.0
      G113MA=0.0
      G1M13A=0.0
      G213MA=0.0
      G2M13A=0.0
      G2M13=0.0
      GMA=0.0
      G1MA=0.0
      G2MA=0.0
      G0=0.0
      G1=0.0
      G23=0.0
      G123=0.0
      G2=0.0
      G2A=0.0
      G13=0.0
      GM13=0.0
```

```
G113=0.0
G1M13=0.0
G213=0.0
G2M13=0.0
ZL0=0.0
ZL1=0.0
ZL2=0.0
ZL23=0.0
ZL123=0.0
ZLMA=0.0
ZL1MA=0.0
ZL2MA=0.0
ZL13=0.0
ZLM13=0.0
ZLM13A=0.0
ZL13MA=0.0
ZL113=0.0
ZL113MA=0.0
ZL1M13A=0.0
ZL1M13=0.0
ZL113=0.0
ZL1M13=0.0
ZL213=0.0
ZL2M13=0.0
G0A=0.0
G1A=0.0
G2A=0.0
ZL0A=0.0
ZL1A=0.0
ZL2A=0.0
SIOH=0.0
T=0.0
ZL23=0.0
tnut=0.0
BGG=0.0
BGL=0.0
BLL=0.0
TEOS0=TEOS
TOTSOL=TEOS0
H2O0=H2O
VSTAR0=FVINIT*4.188e-21*0.001
VSTAR3=FVSTAR*4.188e-21*0.001
VSTAR8=8.*4.188e-21*0.001
SCALFA=1./(FVINIT*4.188E-21*0.001)
SCALFA=1.
VSTAR0=VSTAR0*SCALFA
VSTARB=VSTAR3*SCALFA
BCSTA2=BCSTAR
POW=0.0
```

```
c       *** SOLVE EQUATIONS BY EULER'S METHOD ***

        BOTZ=1.3805E-16
100     CONTINUE
        SUPSAT=SIOH/CSTAR
        IF(ZL0.EQ.0.0.AND.SUPSAT.LT.1.01)GOTO 500
        VSTAR2=VSTAR*1000.
        DIAM=(6./PI*VSTAR2)**0.333333
        AFREQ=0.0
        IF(SUPSAT.GT.1.001)THEN
        AFREQ=(2.*1.E-5)*LOG(SUPSAT)/DIAM**5
        ENDIF
        GFEN=SIGMA*(LOG(SUPSAT))**(-2)
        RN=0.0
        IF(GFEN.LT.120.)RN=AFREQ*EXP(-GFEN)*1000.
        RN0=RN
        RN=RN*VSTAR/4.188e-21*1000./FVSTAR
450     CONTINUE
        DTS=DT
        v=1.
c       IF((R6*12.4).GE.1.E-5)v=0.0
c       IF(G0.LE.0.05*ZL0)v=0.0
        RATE=(RN-BGG*(2.*G13MA*GM13+4.*GMA*G0A+
        12.*GM13A*G13)
        1 -BGL*(G13MA*ZLM13+2.*GMA*ZL0A+GM13A*ZL13+
        1G13*ZLM13A+
        1 2.*G0A*ZLMA+GM13*ZL13MA))
        RATE2=(BGG*(G13MA*GM13+2.*GMA*G0A+G13*GM13A)-
        1 BLL*(ZL13MA*ZLM13+2.*ZLMA*ZL0A+ZL13*ZLM13A))
        DTS2=1.0
        DTS=1.0
        IF(ABS(RATE2).GT.0.0)DTS2=FRAC*ABS(ZL0)/ABS(RATE2)
        IF(ABS(RATE).GT.0.0)DTS=FRAC*ABS(G0)/ABS(RATE)
        IF(ZL0.GT.0.0.AND.DTS2.LT.DTS)DTS=DTS2
c       IF(G0.GT.100.0.AND.DTS2.LT.DTS)DTS=DTS2
        IF(G0.GT.0.0.OR.ZL0.GT.0.0)DT=DTS
c       IF(ZL0.GT.1.00.AND.G0.GT.1.0)DT=DTS
        IF(G0.LT.100.0.AND.ZL0.GT.1.E7)DT=1.0
        IF(DTS.GT.1.)DT=1.0
c       IF(DT.LT.0.0001)DT=0.0001

c       write(*,*)'dt-g0-zl0',dt,g0,zl0,rate,rate2
c       ****************************************
c       **********************_ ****
c       MOMENT EQUATION FOR FREE PARTICLES
c       ****************************************
```

```
c          ********************_ ****

c          *** ZEROTH MOMENT ***

           G0=(RN-BGG*(2.*G13MA*GM13+4.*GMA*G0A+
           12.*GM13A*G13)
           1 -BGL*(G13MA*ZLM13+2.*GMA*ZL0A+GM13A*ZL13
           1+G13*ZLM13A+
           2 2.*G0A*ZLMA+GM13*ZL13MA))*DT+G0

c          IF(G0.LT.1.0)GOTO 949
c          *** FIRST MOMENT ***

           G1=(GROWTH*G23+RN*VSTARB-BGG*(G113MA*GM13+
           1 2.*G1MA*G0A+G1M13A*G13+G113*GM13A+2.*G1A*GMA+
           2 G1M13*G13MA)-BGL*(G113MA*ZLM13+2.*G1MA*ZL0A
           1+G1M13A*ZL13
           3 +G113*ZLM13A+2.*G1A*ZLMA+G1M13*ZL13MA))*DT+G1

c          *** SECOND MOMENT ***

           G2=(2.*GROWTH*G123+RN*VSTARB**2-BGG*(G213MA*GM13
           1 2.*G2MA*G0A+
           1 G2M13A*G13+G213*GM13A+2.*G2A*GMA+G2M13*G13MA)-
           2 BGL*(G213MA*ZLM13+2.*G2MA*ZL0A+G2M13A*ZL13
           1+G213*ZLM13A
           3 +2.*G2A*ZLMA+G2M13*ZL13MA))*DT+G2


c          ************************************
c          MOMENT EQUATIONS FOR AGGREGATES
c          ************************************


c          *** ZERO MOMENT ***
c
c

           ZL0=(BGG*(G13MA*GM13+2.*GMA*G0A+
           1 G13*GM13A)-BLL*(ZL13MA*ZLM13+2.*ZLMA*ZL0A
           1+ZL13*ZLM13A))*DT+ZL0

c
c          *** FIRST MOMENT ***

           ZL1=(GROWTH*ZL23+BGG/2.*(G113MA*GM13+
           12.*G1MA*G0A
           1 +G1M13A*G13+G113*GM13A+2.*G1A*GMA+G113*G13MA
```

```
     3 )+BGL*(ZL13MA*G1M13
     4 +2.*ZLMA*G1A+ZLM13A*G113+ZL13*G1M13A+
     12.*ZL0A*G1MA
     5 +ZLM13*G113MA))*DT+ZL1

c    *** SECOND MOMENT ***

     ZL2=(2.*GROWTH*(ZL123)+BLL*(2.*ZL113MA*ZL1M13
     1 +4.*ZL1MA*ZL1A+2.*ZL1M13A*ZL113)+BGG*
     1(G213MA*GM13+2.*G2MA*G0A
     2 +G2M13A*G13+G213*GM13A+2.*G2A*GMA+G2M13*G13MA
     3 2.*G113MA*G1M13+4.*G1MA*G1A+2.*G1M13A*G113)+
     4 BGL*(ZL13MA*G2M13+2.*ZLMA*G2A+ZLM13A*G213
     1+ZL13*G2M13A+
     5 2.*ZL0A*G2MA+ZLM13*G213MA+2.*ZL113MA*G1M13+
     6 4.*ZL1MA*G1A+2.*ZL1M13A*G113+2.*ZL113*G1M13A
     7 +4.*ZL1A*G1MA+2.*ZL1M13*G113MA))*DT+ZL2
949  continue
     TNUC=ZMU0
     TNUC2=G0
     TNUC3=ZL0
     IF(ZMU0.LE.0.0)ZMU0=0.00
     IF(ZMU1.LE.0.0)ZMU1=0.0
     IF(ZMU2.LE.0.0)ZMU2=0.0
     IF(G0.LE.0.0)G0=0.0
     IF(G0.LE.0.0)G1=0.0
     IF(G0.LE.0.0)G2=0.0
     IF(G1.LE.0.0)G1=0.0
     IF(G2.LE.0.0)G2=0.0
     IF(ZL0.LE.0.0)ZL0=0.0
     IF(ZL1.LE.0.0)ZL1=0.0
     IF(ZL2.LE.0.0)ZL2=0.0
     IF(ZL0.LE.0.0)ZL1=0.0
     IF(ZL0.LE.0.0)ZL2=0.0
     G0A=G0
     G1A=G1
     G2A=G2
     ZL0A=ZL0
     ZL1A=ZL1
     ZL2A=ZL2
     G13MA=0.0
     GM13=0.0
     GMA=0.0
     GM13A=0.0
     G113MA=0.0
     G1M13A=0.0
     G213MA=0.0
```

```
      G2M13A=0.0
      G2M13=0.0
      GMA=0.0
      G1MA=0.0
      G2MA=0.0
      G23=0.0
      G123=0.0
      G13=0.0
      GM13=0.0
      G113=0.0
      G1M13=0.0
      G213=0.0
      G2M13=0.0
      ZL23=0.0
      ZL123=0.0
      ZLMA=0.0
      ZL1MA=0.0
      ZL2MA=0.0
      ZL13=0.0
      ZLM13=0.0
      ZLM13A=0.0
      ZL13MA=0.0
      ZL113=0.0
      ZL113MA=0.0
      ZL1M13A=0.0
      ZL1M13=0.0
      ZL113=0.0
      ZL1M13=0.0
      ZL213=0.0
      ZL2M13=0.0
      IF(ZMU0.LE.0.0)GOTO 503
      IF(ZMU2.LE.0.0.OR.ZMU1.LE.0.0)GOTO 503
      SIGMU=LOG(ZMU2)-2.*LOG(ZMU1)+LOG(ZMU0)
      ZLOGL=LOG(ZMU1)-0.5*(SIGMU)-LOG(ZMU0)
      ZN=2./3.
      ZMU23=(EXP(ZLOGL))**(ZN)*EXP(0.5*(ZN**2)*SIGMU)
     1*ZMU0
      ZN=1.+2./3.
      ZMU123=(EXP(ZLOGL))**(ZN)*EXP(0.5*(ZN**2)*SIGMU)
     1*ZMU0
503   CONTINUE
      IF(G0.LE.0.0)GOTO 501
      IF(G2.LE.0.0.OR.G1.LE.0.0)GOTO 501
      SIGG=LOG(G2)-2.*LOG(G1)+LOG(G0)
      IF(SIGG.LT.0.0)SIGG=0.0
c     SIGG=0.0
c     G1=VSTARB*G0
c     G2=VSTARB**2*G0
```

```
      ZLOGL=LOG(G1)-0.5*(SIGG)-LOG(G0)
      ZN=2./3.
      G23=(EXP(ZLOGL))**(ZN)*EXP(0.5*(ZN**2)*SIGG)*G0
      ZN=2./3.+1.
      G123=(EXP(ZLOGL))**(ZN)*EXP(0.5*(ZN**2)*SIGG)*G0
      ZN=-POW
      GMA=(EXP(ZLOGL))**(ZN)*EXP(0.5*(ZN**2)*SIGG)*G0
      ZN=1.-POW
      G1MA=(EXP(ZLOGL))**(ZN)*EXP(0.5*(ZN**2)*SIGG)*G0
      ZN=2.-POW
      G2MA=(EXP(ZLOGL))**(ZN)*EXP(0.5*(ZN**2)*SIGG)*G0
      ZN=1./3.
      G13=(EXP(ZLOGL))**(ZN)*EXP(0.5*(ZN**2)*SIGG)*G0
      ZN=-1./3.
      GM13=(EXP(ZLOGL))**(ZN)*EXP(0.5*(ZN**2)*SIGG)*G0
      ZN=1.+1./3.
      G113=(EXP(ZLOGL))**(ZN)*EXP(0.5*(ZN**2)*SIGG)*G0
      ZN=1.-1./3.
      G1M13=(EXP(ZLOGL))**(ZN)*EXP(0.5*(ZN**2)*SIGG)*G0
      ZN=2.+1./3.
      G213=(EXP(ZLOGL))**(ZN)*EXP(0.5*(ZN**2)*SIGG)*G0
      ZN=2.-1./3.
      G2M13=(EXP(ZLOGL))**(ZN)*EXP(0.5*(ZN**2)*SIGG)*G0
      ZN=-POW+1./3.
      G13MA=(EXP(ZLOGL))**(ZN)*EXP(0.5*(ZN**2)*SIGG)*G0
      ZN=-(1./3.+POW)
      GM13A=(EXP(ZLOGL))**(ZN)*EXP(0.5*(ZN**2)*SIGG)*G0
      ZN=1+1./3.-POW
      G113MA=(EXP(ZLOGL))**(ZN)*EXP(0.5*(ZN**2)*SIGG)*G0
      ZN=1.-(1./3.+POW)
      G1M13A=(EXP(ZLOGL))**(ZN)*EXP(0.5*(ZN**2)*SIGG)*G0
      ZN=2.-(1./3.+POW)
      G2M13A=(EXP(ZLOGL))**(ZN)*EXP(0.5*(ZN**2)*SIGG)*G0
      ZN=2.+1./3.-POW
      G213MA=(EXP(ZLOGL))**(ZN)*EXP(0.5*(ZN**2)*SIGG)*G0

501   CONTINUE
      IF(ZL0.LE.0.0)GOTO 500
      IF(ZL2.LE.0.0.OR.ZL1.LE.0.0)GOTO 500
      SIGG=LOG(ZL2)-2.*LOG(ZL1)+LOG(ZL0)
      IF(SIGG.LT.0.0)SIGG=0.0
1023  CONTINUE
      ZLOGL=LOG(ZL1)-0.5*SIGG-LOG(ZL0)
      ZN=-POW
      ZLMA=(EXP(ZOGL))**(ZN)*EXP(0.5*(ZN**2)*SIGG)*ZL0
      ZN=1.-POW
```

```
      ZL1MA=(EXP(ZLOGL))**(ZN)*EXP(0.5*(ZN**2)*SIGG)*ZL0
      ZN=2.-POW
      ZL2MA=(EXP(ZLOGL))**(ZN)*EXP(0.5*(ZN**2)*SIGG)*ZL0

      ZN=2./3.
      ZL23=(EXP(ZLOGL))**(ZN)*EXP(0.5*(ZN**2)*SIGG)*ZL0
      ZN=1.+2./3.
      ZL123=(EXP(ZLOGL))**ZN*EXP(0.5*ZN**2*SIGG)*ZL0
      ZN=1./3.
      ZL13=(EXP(ZLOGL))**(ZN)*EXP(0.5*(ZN**2)*SIGG)*ZL0
      ZN=-1./3.
      ZLM13=(EXP(ZLOGL))**(ZN)*EXP(0.5*(ZN**2)*SIGG)*ZL0
      ZN=1.+1./3.
      ZL113=(EXP(ZLOGL))**(ZN)*EXP(0.5*(ZN**2)*SIGG)*ZL0
      ZN=1.-1./3.
      ZL1M13=(EXP(ZLOGL))**(ZN)*EXP(0.5*(ZN**2)*SIGG)*ZL0
      ZN=1./3.-POW
      ZL13MA=(EXP(ZLOGL))**(ZN)*EXP(0.5*(ZN**2)*SIGG)*ZL0
      ZN=-1./3.-POW
      ZLM13A=(EXP(ZLOGL))**(ZN)*EXP(0.5*(ZN**2)*SIGG)*ZL0
      ZN=1.-1./3.-POW
      ZL1M13A=(EXP(ZLOGL))**(ZN)*EXP(0.5*(ZN**2)*SIGG)*ZL0
      ZN=1.+1./3.-POW
      ZL113MA=(EXP(ZLOGL))**(ZN)*EXP(0.5*(ZN**2)*SIGG)*ZL0
      ZN=2.+1./3.
      ZL213=(EXP(ZLOGL))**(ZN)*EXP(0.5*(ZN**2)*SIGG)*ZL0
      ZN=2.-1./3.
      ZL2M13=(EXP(ZLOGL))**(ZN)*EXP(0.5*(ZN**2)*SIGG)*ZL0
      ZN=2.
      ZL6=(EXP(ZLOGL))**(ZN)*EXP(0.5*(ZN**2)*SIGG)*ZL0


c     *** CHEMICAL KINETIC EQUATIONS ***

500   DTEOSD=-(ZKH*H2O**1.5*ZNH3**0.9*TEOS)
      TEOS=DTEOSD*DT+TEOS
      CORECTI=4.*PI*(3./(4.*PI))**0.66666667
      SAREA=0.1*(G23+ZL23)*CORECTI*SCALFA**(-0.6666667)
c     DIFSIOH=ZNH3*(SIOH-CSTAR)
      DIFSIOH=(SIOH-CSTAR)
      IF(DIFSIOH.LT.0.0)DIFSIOH=0.0
      TOTSOL=(-ZKC*SAREA*DIFSIOH
     1 -RN0/6.02E23)*DT+TOTSOL
      H2O=H2O0-(4.*(TEOS0-TEOS)-2.*(TEOS0-TOTSOL))
      RSURF=ZKC*SAREA*DIFSIOH
      IF(RSURF.GT.0.0)THEN
```

```
      RATIO2=RN0/(ZKC*SAREA*DIFSIOH)/6.02e23
      ENDIF
      SIOH=TOTSOL-TEOS
      CALL NEWTON(ZH4ION,COSI,SIOH)
      ZKAPPA=2.98E10*SQRT(EPSI**(-1)*(CONH+ZH4ION))
      CTIME=CTIME+DT
      C2TIM=C2TIM+DT
      CONST=60./2000.*0.1*CORECTI
      GROWTH=CONST*(ZKC*DIFSIOH)*SCALFA**(0.3333333)
      DCTIME=1.0
      IF(T.LT.100.)DCTIME=1.0
      IF(C2TIM.LT.DCTIME)GOTO 652
      C2TIM=0.0
      IF(G0.NE.0.0.AND.G1.NE.0.0)THEN
      RA1=(G1/G0/SCALFA)**(1./3.)*6.2
      CALL BETA(RA1,RA1,ZKAPPA,RESU,HAMCON,SOLCON)
      BGG=RESU*BCSTA2
      ENDIF
      IF(ZL0.NE.0.0.AND.ZL1.NE.0.0)THEN
      RA2=(ZL1/ZL0/SCALFA)**(1./3.)*6.2
      CALL BETA(RA2,RA2,ZKAPPA,RESU,HAMCON,SOLCON)
      BLL=RESU*BCSTA2
      ENDIF
      IF(ZL0.NE.0.0.AND.G0.NE.0.0)THEN
      CALL BETA(RA1,RA2,ZKAPPA,RESU,HAMCON,SOLCON)
      BGL=RESU*BCSTA2
      ENDIF
652   CONTINUE
      DCTIME=20.
      IF(T.LT.100.)DCTIME=1.
      IF(CTIME.LT.DCTIME)GOTO 600
      CTIME=0.0
      IF(ZL0+G0.GT.0.)R6=((G1+ZL1)/SCALFA/(ZL0+G0))**(1./3.)
      IF(ZL13.GT.0.0)ROOT2=(ZL23*ZL0/ZL13**2-1.)
      IF(ROOT2.GT.0.0)POLY=SQRT(ROOT2)
      WRITE(10,1100)T+DT,G0,ZL0,R6*12.4,POLY
      WRITE(4,1100)T+DT,TOTSOL,TEOS,SIOH,H2O,RATIO2
      SCHEM=0.03*(TEOS0-TOTSOL)
      SPOP=(ZL1+G1)*SCALFA
      IF(SCHEM.GT.0.0)DIFF=(SCHEM-SPOP)/SCHEM
      WRITE(*,1100)T+DT,G0,ZL0,BLL,ZH4ION,R6*12.4
      WRITE(12,1100)T+DT,BGG,BLL,BGL,ZH4IOH
      IF(G0.LE.0.0.OR.G1.LE.0.0)GOTO 611
      IF(G2.LE.0.0)GOTO 611
      SIGG1=LOG(G2)-2.*LOG(G1)+LOG(G0)
      IF(SIGG1.LT.0.0)SIGG1=0.0
```

```
      ZLOGL1=LOG(G1)-0.5*SIGG1-LOG(G0)-LOG(SCALFA)
611   CONTINUE
      IF(ZL0.LE.0.0.OR.ZL1.LE.0.0)GOTO 600
      IF(ZL2.LE.0.0)GOTO 600
      SIGG2=LOG(ZL2)-2.*LOG(ZL1)+LOG(ZL0)
      IF(SIGG2.LT.0.0)SIGG2=0.0
      ZLOGL2=LOG(ZL1)-0.5*SIGG2-LOG(ZL0)-LOG(SCALFA)
      WRITE(3,1101)T+DT,SIGG1,ZLOGL1,SIGG2,ZLOGL2
1000  FORMAT(7E8.4)
1100  FORMAT(10(e10.5,1X))
1101  FORMAT(10(e12.6,1x))
600   T=T+DT
      tnut=rn*dt+tnut
      IF(T.LT.TMAX+DT)GOTO 100
      RETURN
      END


      SUBROUTINE NEWTON(X,COSI,SIOH)
      IMPLICIT REAL*8(A-H,O-Z)
      COMMON/CHEMICAL/TEOS,H2O,ZNH3,ZETA,EPSI
      X=0.3
      DO 10 I=1,100
      TERM1=X**3
      DTERM1=3.*X**2
      TERM2=(COSI*ZNH3)*X**2
      DTERM2=2.*(COSI*ZNH3)*X
      TERM3=-(COSI*ZNH3*SIOH+3.16e-8*ZNH3)*X
      DTERM3=-(COSI*ZNH3*SIOH+3.16e-8*ZNH3)
      TERM4=-3.16E-8*COSI*ZNH3**2
      F=TERM1+TERM2+TERM3+TERM4
      FP=DTERM1+DTERM2+DTERM3
      X0=X
      FDFP=0.0
      IF(COSI.NE.0.0.OR.X.NE.0.0)FDFP=F/FP
      X=X-FDFP
      X1=X
      IF(ABS(X0-X1).LT.1.E-8)THEN
      X=2.*X
      RETURN
      ENDIF
10    CONTINUE
      WRITE(*,*)'****SOLUTION DID NOT CONVERGE****'
      WRITE(*,*)X,ABS(X1-X0)
      RETURN
      END
```

```
SUBROUTINE BETA(RA1,RA2,ZKAPPA,RESU,HAMCON,
1SOLCON)
IMPLICIT REAL*8(A-H,O-Z)
CHARACTER*80, OFILE,OFILE2
COMMON/CHEMICAL/TEOS,H2O,ZNH3,ZETA,EPSI
COMMON/SOLVA/SOSHEL
DIMENSION W(30),ZG(10),ZH(10)
ZK=ZKAPPA
INC=2000
INC2=2000
DECAY=1.E-9
A=ZETA
A=A/1000.
B=A
P=3.1415926536
E=8.854E-12
ZJ=78.4*EPSI**(-1)*HAMCON
ZM=1.38047E-23
F=EPSI
T=298.0
CORREC=1.0
LF=1
G=RA1/100.
H=RA2/100.
COUNT=0.0
ZN=0
Q=10.E-9/(2.*INC)
START=10.E-9
ZO=1e-20
DO 200 I=1,2*INC+1,1
R=(I-1)*Q+G+H+ZO
S=R-G-H
U=P*E*F*G*H*2*A*B*LOG((1.0+EXP(-ZK*S))/
1(1-EXP(-ZK*S)))
U=U/(G+H)
V=P*E*F*G*H*(A**2+B**2)*LOG(1.0-EXP(-ZK*S*2))/(G+H)
X=(S+2.*SOSHEL)/(G+H)
Y=H/G
Z=-ZJ*(Y/(X**2+X*Y+X)+Y/(X**2+X*Y+X+Y)+
1 2*LOG((X**2+X*Y+X)/(X**2+X*Y+X+Y)))/12.
VS=P*SOLCON*DECAY*2.*G*H/(G+H)*EXP(-S/DECAY)
D=U+V+Z+VS
ZL= (G+H)*Q*EXP(D/(ZM*T))/R**2
```

```
      IF(COUNT/2-INT(COUNT/2).EQ.0) ZN=ZN+2*ZL
      IF(COUNT/2-INT(COUNT/2).GT.0)ZN=ZN+4*ZL
      IF (COUNT.EQ.0.OR.COUNT.EQ.2*INC) ZN=ZN+ZL
      COUNT=COUNT+1.0
200   CONTINUE
      W(LF)=ZN/3.
      ZN=0.0
      COUNT=0.0
      Q=(10./ZK-10.E-9)/(2.*INC)
      DO 400 I=1,2*INC2+1,1
      R=(I-1)*Q+G+H+START
      S=R-G-H
      U=P*E*F*G*H*2*A*B*LOG((1.0+EXP(-ZK*S))/
     1(1-EXP(-ZK*S)))
      U=U/(G+H)
      V=P*E*F*G*H*(A**2+B**2)*LOG(1.0-EXP(-ZK*S*2))/(G+H)
      X=(S+2.*SOSHEL)/(G+H)
      Y=H/G
      Z=-ZJ*(Y/(X**2+X*Y+X)+Y/(X**2+X*Y+X+Y)+
     1 2*LOG((X**2+X*Y+X)/(X**2+X*Y+X+Y)))/12.
      VS=P*SOLCON*DECAY*2.*G*H/(G+H)*EXP(-S/DECAY)
      D=U+V+Z+VS
      ZL= (G+H)*Q*EXP(D/(ZM*T))/R**2
      IF(COUNT/2-INT(COUNT/2).EQ.0) ZN=ZN+2*ZL
      IF(COUNT/2-INT(COUNT/2).GT.0)ZN=ZN+4*ZL
      IF (COUNT.EQ.0.OR.COUNT.EQ.2*INC2) ZN=ZN+ZL
      COUNT=COUNT+1.0
400   CONTINUE
      W(LF)=ZN/3.0+W(LF)
      RESU=1./W(LF)
      RETURN
      END
```

A.1.3. bemfem.f - Algorithm for Solving Electrohydrostatic Problem

noindent by Hibrid Finite Element-Boundary Element Method

```
c       PROGRAM bemfem.f: PROGRAM TO CALCULATE
c       AXISYMMETRIC SHAPES
c       AND STABILITY OF PENDANT AND SESSILE
c       DROPS.
c       THIS IS NAMED pdsim.f.
c       PROGRAMMER: OSMAN A. BASARAN (FINITE ELEMENT
c       ANALYSIS), AND
c       MICHAEL T. HARRIS (BOUNDARY ELEMENT ANALYSIS)
c       ORNL.
c
        IMPLICIT REAL*8(A-H,O-Z)
        DIMENSION ALPA(300),BETTA(300),ASEC(50),FSEC(50),
       1ASECP(50)
        COMMON / PRIP / RHOS(500,1),ZS(500,1),
       1HQS(500)
        COMMON/BOEL/SIGM(500)
        COMMON/WIR/ A, B
        COMMON / MON /NIPT,RFAC,NBLA,NPTP
        COMMON/BC/IBEG(500),IEND(500),BEG(500),EXIT(500)
        COMMON/FRON/NP,NE,NELL,NH,NPL,HNOZ,NNOZ
        COMMON/FE/QQ(600),QK(600),AMAT(600,600),RHS(600,2),
       1X(500),R(500),DETV(500),IDETV(500),DXOLD(500)
        COMMON/OTHER/EPSI,ITMAX,H,IDROP,NPARA,VOL,PI
        COMMON/GEL/G,HBP
        COMMON/INO/IN1
        COMMON/BOEL2/NT,NB,NBT,NRS,IEP,DBP,RDBP,ZKLL,
       1ZKLP,ZSUM
        COMMON/TET/THETA(500,1)
        CHARACTER*80 IFIL1,IFIL2,IFIL3,IFIL4,IFIL5,IFIL6,IFIL7,IFIL8
c
c       *** IMOVE = 0: FINITE ELEMENT METHOD ON A FIXED
c       MESH
c       *** = 1 : MOVING FINITE ELEMENT METHOD (MFEM)
c       *** IBOUND = 0 : DO NOT BOUND ERROR
c       *** = 1 : BOUND ERROR
c
c       *** INITIALIZE CLOCK TO MEASURE CPU TIME.

c
```

```
c       *** IDENTIFY INPUT AND OUTPUT FILES.
        OPEN(UNIT=9,FILE='FILE2T.DAT',STATUS='OLD')
        READ(9,*)IFIMAZ
        DO 829 IFIL=1,IFIMAZ
        READ(9,*)IFIL1,IFIL2,IFIL3,IFIL4,IFIL5,IFIL6,IFIL7,
        IFIL8
c       OPEN (UNIT=1,FILE='IN.DAT',STATUS='OLD')
        OPEN(UNIT=2,FILE='OUT3.DAT',STATUS='OLD')
        OPEN(UNIT=5,FILE=IFIL1,STATUS='OLD')
        OPEN(UNIT=10,FILE=IFIL2,STATUS='NEW')
        OPEN(UNIT=8,FILE=IFIL3,STATUS='NEW')
        OPEN(UNIT=11,FILE=IFIL4,STATUS='NEW')
        OPEN(UNIT=12,FILE=IFIL5,STATUS='NEW')
        OPEN(UNIT=13,FILE=IFIL6,STATUS='NEW')
        OPEN(UNIT=14,FILE=IFIL7,STATUS='NEW')
        OPEN(UNIT=15,FILE=IFIL8,STATUS='NEW')

c
        NPTP=0
        NQQC=1
        CURV3=200.
c       ************************************************************
c       ************************************************************

c       * LIST OF SYMBOLS *
c       ************************************************************
c       * NE - NUMBER OF ELEMENTS ON DROP *
c       * IN1 - *
c       * ITMAX - MAXIMUM NUMBER OF INTERATIONS *
c       * NPTMAX - MAXIMUM NUMBER OF STEPS TO MARCH *
c       * IMOVE - FLAG WHETHER TO HAVE MOVABLE MESH *
c       * IBOUND - *
c       * ITP - *
c       * IDROP - PENDANT OR SESSILE DROP *
c       * VOL - VOLUME OF DROP *
c       * DELP - AMOUNT TO CHANGE MARCH PARAMETER *
c       * H - PARAMETER TO DEFINE INITIAL HEMISPHERE *
c       * EPSI - LEVEL TO TERMINATE NEWTON ITERATION *
c       * ERR - ERROR *
c       * TP - *
c       * ECF - ECCENTRICITY *
c       * NE - NUMBER OF ELEMENTS ON DROP *
c       * NT - NUMBER OF ELEMENTS ON TOP PLATE NOT
c       CLOSE TO *
c       * CLOSE TO DROP *
c       * NB - NUMBER OF ELEMENTS ON BOTTOM PLATE
c       NOT CLOSE *
c       * TO DROP *
```

```
c       * NBLA - NUMBER OF ELEMENTS ON TOP OR BOTTOM
c       PLATE *
c       * CLOSE TO DROP *
c       * NRS - NUMBER OF ELEMENTS ON RIGHT BOUNDARY *
c       * NLS - NUMBER OF ELEMENTS ON LEFT BOUNDARY *
c       * NIPT - NUMBER OF INTERIOR POINTS—BOUNDARY
c       ELEMENT*
c       * IEP - N/A *
c       * DBP - DISTANCE BETWEEN PLATES *
c       * RDBP - HOW MANY MUTIPLES OF DBP TO END OF
c       PLATE *
c       * ZKLL - HOW CLOSE TO SINGULAR POINT– (0.99¡k¡1.0) *
c       * ZKLP - SAME AS ZKLL *
c       * RFAC - DEFINE STEP SIZE FOR DETERMINING WHERE *
c       * ZKLL OR ZKLP OCCUR IN EACH ELEMENT *
c       * DFRACC - FRACTIONAL CHANGE OF NEWTION *
c       * ITERATION PARAMETER *
c       * ZSUM - N/A *
c       * HBP - DISTANCE BETWEEN PLATES (SAME AS DBP) *
c       * G - GRAVITATIONAL BOND NUMBER *
c       * HNOZ - HEIGHT OF NOZZLE *
c       * NNOZ - NUMBER OF ELEMENTS ON NOZZLE *
c       * NH - NUMBER OF NODES ON DROP (NE+1) *
c       * NP - STORAGE NUMBER FOR ELECTRIC BOND NO.
c       (NH+2) *
c       * NPL - TOTAL NO. OF NODES ON PLATES AND NOZZLE *
c       * NTOT - TOTAL NUMBER OF PARAMETER STORED IN
c       VECTOR QQ*
c       * NPARA - STORAGE LOCATION OF MARCH PARAMETER *
c       * QQ(I)[1¡=I¡=NE+1) - STORAGE LOCATION OF DROP
c       SHAPE *
c       * COORDINATE ALPHA(I) *
c       * QQ(NP) - ELECTRIC BOND NO. *
c       * QQ(NP-1) - REFERENCE PRESSURE *
c       * QQ(NP+I)[1¡=I¡=NE+NPL] - STORAGE LOCATION OR SUR-
c       * FACE CHARGE DENSITIES IN ELEMENT I *
c       * QQ(NP+NE+NPL) - STORAGE LOCATION OF NODAL *
c       * POSITION ON PLATES AND NOZZLES *
c       * X(I)[1¡=I¡=NE+1] - THETA VALUES OF NODE I *
c       ******************************************************
c       ******************************************************

        PI=3.1415926535898
c
c       *** INPUT DATA AND INITIALIZAION
        READ(5,*)NE,IN1,ITMAX,NPTMAX,IMOVE,IBOUND,ITP
c       *** IDROP=+1, PENDANT DROP; -1, SESSILE DROP.
```

```
      READ(5,*)IDROP,VOL
c     *** NOTE: H WHICH IS INPUT ONLY AN INITIAL GUESS
      READ(5,*)DELP,H,EPSI,ERR,TP
      READ(5,*)ECF,NT,NB,NBLA,NRS
      READ(5,*)NIPT
      READ(5,*)IEP,DBP
      READ(5,*)RDBP,ZKLL,RFAC,ZSUM,G,DFRACC,HNOZ,NNOZ
      READ(5,*)IDBP,IHNOZ,DBHNMX,SUSQMX
c     ********************************************************
c     ********************************************************
      DELKP=DELP

      ZKLP=ZKLL
      NNNOZ=NNOZ
      IF(HNOZ.EQ.0.0)NNOZ=0
      NH=NE+1
      NP=NH+2
      NPARA=NP
      NPL=NT+NB+2*NBLA+NNOZ+NRS
      NTOT=2*NE+NT+NB+2*NBLA+NNOZ+NRS+4
      DO 831 I=1,NTOT
831   QK(I)=0.0
c     WRITE(6,950)
c     ********************************************************
c     CALCULATE BASIS FUNCTIONS
c     ********************************************************
      CALL TFUNGP
c     ********************************************************
c     WRITE IMPORTANT INPUT DATA TO DATA FILE
c     ********************************************************
c     WRITE(6,951)NE,NT,NB,NBLA,NRS,NLS,NIPT
c     WRITE(6,952)DELP,H,EPSI,ERR,TP

c     ********************************************************
c     ********************************************************

c     *** IF IN1=0, CONSTRUCT FINITE ELEMENT MESH AND
c     *** ASSIGN DROP SHAPE; OTHERWISE, JUST CALCULATE
c     H.
c     ********************************************************
      ICONT=1
      WRITE(10,*)'H= ',H,' EPSILON= ',ECF
715   CONTINUE
      IF(ICONT.EQ.1)GOTO 1799
      WRITE(10,1013)DBP,HNOZ,QQ(NP),QQ(NP-1),
     1QQ(1)/QQ(NE+1)
1013  FORMAT(5F12.6)
```

```
      IF(IDBP.EQ.1)DBP=DBP+5.0
      IF(IHNOZ.EQ.1)THEN
      DBP=DBP+1.0
      HNOZ=HNOZ+1.
      NNNOZ=NNNOZ+1
      ENDIF
      IF(HNOZ.NE.0.)NNOZ=NNNOZ
      NPL=NT+NB+2*NBLA+NNOZ+NRS
      NTOT=2*NE+NT+NB+2*NBLA+NNOZ+NRS+4
1799  CONTINUE
      ICONT=2
      CALL MESH
      HBP=DBP
      IF(IDBP.EQ.1.AND.DBP.GT.DBHNMX)GOTO 713
      IF(IHNOZ.EQ.1.AND.DBP.GT.DBHNMX)GOTO 713
      IF(IN1.EQ.0)GO TO 40

c     ********************************************************
c     *** DATA FROM PREVIOUS POINT
c     ********************************************************

c     READ(1,930)(X(I),I=1,NH)
c     READ(1,930)(QQ(I),I=1,NTOT)
c     READ(1,*)NPARA
c     WRITE(6,954)(X(I),I=1,NH)
c     WRITE(6,954)(QQ(I),I=1,NTOT)

c     ********************************************************
c     DISCRETIZE FOR BOUNDARY ELEMENT COMPUTATIONS
c     ********************************************************

c     CALL BODEPH

c     ********************************************************
c     SURFACE CHARGE DENSITIES IN VECTOR SIGM(I)
c     ********************************************************

      40 CONTINUE

c     ********************************************************
c     STORE POSITIONS IN TEMPORARY VECTOR QK(I)
c     ********************************************************

      DO 10 I=1,NTOT
10    QK(I)=QQ(I)

c     ********************************************************
```

```
c       *** ASSIGN VALUES TO BOUNDARY CONDITION ARRAYS
c       ********************************************************

        IBEG(1)=1
        IEND(1)=0
        BEG(1)=0.0
        EXIT(1)=1.0

c       ********************************************************
c       *** START MARCHING IN SOLUTION SPACE
c       ********************************************************
        IN1=1

        NPTCO=0
        DO 170 NPT=1,NPTMAX
        write(*,*)'NPTMAX= ',NPTMAX
        IF(NPT.EQ.1)QPKMIN=QQ(NP-1)

c       ********************************************************
c       *** UPDATE PARAMETER
c       ********************************************************

        IF(NPT.NE.1)QQ(NPARA)=QQ(NPARA)+DELP
c
        NPTCO=NPTCO+1
        IF(IMOVE.EQ.0)GO TO 73
        IF(NPT.EQ.1)GO TO 73
        CALL MOVE(1,IBOUND,TP,ITP,NTOT,ISIN)
73      CONTINUE
        GOTO 711
        K1P=0
        K2P=0
        IF(NPARA.EQ.NP)K1P=1
        IF(NPARA.EQ.1)K2P=1
        FSEC(NPT+K1P)=QQ(NP)
        ASECP(NPT+1)=QQ(NPARA)
        ASEC(NPT+KP)=QQ(1)/QQ(NE+1)

        IF(NPT.EQ.5)DELP=0.0
        IF(NPT.LT.5)GOTO 711
        DSEC1=(FSEC(NPT-1)-FSEC(NPT-2))/(ASEC(NPT-1)
        1-ASEC(NPT-2))
        DSEC2=(FSEC(NPT)-FSEC(NPT-1))/(ASEC(NPT)
        -ASEC(NPT-1))

        ASEC2=(ASECP(NPT)+ASECP(NPT-1))/2.
        ASEC1=(ASECP(NPT-1)+ASECP(NPT-2))/2.
```

```
      QQ(NPARA)=ASEC2-1.0*DSEC2*(ASEC2-ASEC1)/
      1(DSEC2-DSEC1)
      IF(ABS(QQ(NP)-QK(NP)).LE.3.E-4)THEN
      QQ(NPARA)=ASEC2
      GOTO 91
      ENDIF
      IF(ABS(QQ(NPARA)-ASEC2).GT.0.1)
      1QQ(NPARA)=ASEC2+0.01*(QQ(NPARA)-ASEC2)/
      1ABS(QQ(NPARA)-ASEC2)
      ASECP(NPT+1)=QQ(NPARA)
      FSEC(NPT+K1P)=QQ(NP)
      ASEC(NPT+K2P)=QQ(1)/QQ(NE+1)
711   CONTINUE

      DO 50 I=1,NE
50    DXOLD(I)=X(I+1)-X(I)
      NCON=0
919   CONTINUE
      DO 90 ITER=1,ITMAX


      RHOS(1,1)=QQ(1)*SIN(X(1))
      ZS(1,1)=QQ(1)*COS(X(1))

      CALL DRIVER(ITER,NPTCO,ERR,NTOT,NBLA)

      QPK=QQ(NP-1)
      QPNE=QQ(NP)
      NS1=0
      CALL RESIDU(ITER,INDEX,NTOT,NBLA,DELP,NPT,NS1
      1,SUSQMX,NPPT,
      1NCON,NQQC,NPTMAX,CURV3)
      IF(NCON.EQ.20)GOTO 91
      IF(NS1.EQ.1)GOTO 919
      NPTP=2
      IF(INDEX.EQ.2)GO TO 91
      IF(INDEX.EQ.1)GO TO 100
90    CONTINUE

100   CONTINUE
      IF(NPT.GT.1.AND.ITER.GT.15)DFRACC=15./FLOAT(ITER)
      IF(NPT.GT.1.AND.ITER.LT.4)DFRACC=(4./FLOAT(ITER))

c     ********************************************************
c     *** FIND UNKNOWN THAT'S CHANGING THE MOST
c     RAPIDLY
c     ********************************************************
```

```
      DEL=0.0
      DO 110 I=1,NP
      TEMP=ABS(QQ(I)-QK(I))
      IF(TEMP.LT.DEL)GO TO 110
      IPARA=I
      DEL=TEMP
110   CONTINUE
      DFRACC=1.
      IF(IPARA.GT.1.AND.IPARA.LT.NP-1)IPARA=1
      IF(NPT.NE.1)THEN
      DELP=DFRACC*(QQ(IPARA)-QK(IPARA))
      NPARA=IPARA
      ENDIF
      IF(NPT.NE.1)DELP=DFRACC*(QQ(NPARA)-QK(NPARA))

      ZMDIFF=QQ(NPARA)-QK(NPARA)

c     ********************************************************
c     *** STORE SOLUTION
c     IF(NPT.GT.1.AND.QQ(NP).LT.QK(NP))GO TO 91
c     IF(NPT.GT.1.AND.QQ(1).LT.QK(1))GOTO 91
c     ********************************************************

      DO 120 I=1,NTOT
120   QK(I)=QQ(I)

c     ********************************************************
170   CONTINUE

c     ********************************************************
c     *** STORE LAST COMPUTED SOLUTION
c     ********************************************************

91    CONTINUE

      DO 116 I=1,NE+NPL+1
116   WRITE(8,933)RHOS(I,1),ZS(I,1),QQ(NE+3+I)
      DELP=0.001
      GOTO 713
      GOTO 715
713   CONTINUE

c     ********************************************************
c     *** CALCULATE TOTAL CPU TIME.
c     ********************************************************

      CLOSE(2)
```

```
      CLOSE(5)
      CLOSE(15)
      CLOSE(8)
829   CONTINUE
      CLOSE(9)
      STOP
993   FORMAT(/,1X,'DETERMINANT=',10(1X,E10.3))
971   FORMAT(/,1X,'NPARA=',I2)
974   FORMAT(1X,'IDET=',3X,10(1X,I10))
900   FORMAT(7I10,E13.6)
901   FORMAT(5E13.6)
902   FORMAT(I10,E13.6)
950   FORMAT(//,1X,'AXISYMMETRIC PENDANT AND
      1SESSILE DROPS',//)
951   FORMAT(1X,'NE=',I2,2X,'IN1=',I2,2X,'ITMAX=',
      *I2,2X,'NPTMAX=',
      * I2,2X,'IMOVE=',I1,2X,'IBOUND=',I1,2X,'ITP=',I1)
952   FORMAT(1X,'DELP=',E11.4,1X,'H=',E11.4,1X,'EPSI=',E11.4,
      * 1X,'ERR=',E11.4,1X,'TP=',E11.4)
953   FORMAT(//,1X,'FINITE ELEMENT MESH=')
954   FORMAT(10(1X,E12.5))
930   FORMAT(5(1X,E13.6))
961   FORMAT(///,1X,'*************************************
      *********'
      *,/,1X,'NPT=',I2,2X,'VOLUME=',E12.5,2X,'TP=',E12.5)
999   FORMAT(/,1X,'CPU TIME IN SECONDS=',E11.4)
977   FORMAT(/,1X,'ELEMENT SIZES=')
933   FORMAT(3F10.4)
      END

      SUBROUTINE MESH
      IMPLICIT REAL*8(A-H,O-Z)
      COMMON/BC/IBEG(500),IEND(500),BEG(500),EXIT(500)
      COMMON/FRON/NP,NE,NELL,NH,NPL,HNOZ,NNOZ
      COMMON/FE/QQ(600),QK(600),AMAT(600,600),RHS(600,2),
      1X(500),R(500),DETV(500),IDETV(500),DXOLD(500)
      COMMON/BOEL/SIGM(500)
      COMMON/INO/IN1
      COMMON/OTHER/EPSI,ITMAX,H,IDROP,NPARA,VOL,PI
      DIMENSION HVEC(500),RVEC(500)

      ILAST=0
      TERM=(1.0+H**2)**0.5
      IF(H.NE.0.0)GOTO 492
      DO 100 I=1,20
      ILAST=ILAST+1
```

```
      TERM=(1.0+H**2)**0.5
      RESID=VOL-PI/3.0*(TERM+H)**2*(2.0*TERM-H)
      RJAC=-PI/3*(TERM+H)*(2.0*(2.0*TERM-H)*(H/TERM+1.0)
     1 +(2.0*H/TERM-1.0)*(TERM+H))
      DH=-RESID/RJAC
      H=H+DH
      HVEC(I)=DH
      RVEC(I)=RESID
      INDEXX=1
      IF(ABS(RESID).LT.EPSI.AND.ABS(DH).LT.EPSI)GO TO 120
      INDEXX=2
100   CONTINUE
c
      GO TO 120
492   VOL=PI/3.0*(1.+H)**2*(2.0-H)
120   CONTINUE
      IF(IN1.EQ.1)CALL BODEPH
      IF(IN1.EQ.1)RETURN
      COMAX=0.0
      DO 898 I=1,NE
      SIUM=FLOAT(I)
      IF(I.GT.NE/2)SIUM=FLOAT(NE-I+1)
898   COMAX=SIUM+COMAX
      C2MAX=0.0
      DO 150 I=1,NH
      SIUM=FLOAT(I-1)
      IF(I-1.GT.NE/2)SIUM=FLOAT(NH-I+1)
      C2MAX=SIUM+C2MAX
      X(I)=C2MAX*PI/2.0/COMAX
c     X(I)=FLOAT(I-1)*PI/2.0/FLOAT(NE)
      RSTART=(1.-H**2)
150   QQ(I)=H*COS(X(I))+(RSTART+(H*COS(X(I)))**2)**0.5
      QQ(NP-1)=2.0
      QQ(NP)=0.0
      ********************************************
C     CALCULATE SURFACE CHARGE DENSITIES BY
C     BOUNDARY ELEMENT METHOD
C
      ********************************************

      CALL BODEPH
901   FORMAT(/,1X,'VOLUME=',E12.5)
950   FORMAT(/,1X,'DH=',6(1X,E12.5))
951   FORMAT(/,1X,'R=',6(1X,E12.5))
960   FORMAT(/,1X,'CONVERGENCE. ',I2,1X,'ITERATIONS.',
     1 ' H=',E12.5)
961   FORMAT(/,1X,'FAILURE. ',I2,1X,'ITERATIONS.')
```

```
      RETURN
      END

      SUBROUTINE ABFIND(NTOT)
      IMPLICIT REAL*8(A-H,O-Z)
      COMMON/BC/IBEG(500),IEND(500),BEG(500),EXIT(500)
      COMMON/FRON/NP,NE,NELL,NH,NPL,HNOZ,NNOZ
      COMMON/FE/QQ(600),QK(600),AMAT(600,600),RHS(600,2),
     1X(500),R(500),DETV(500),IDETV(500),DXOLD(500)
      COMMON/OTHER/EPSI,ITMAX,H,IDROP,NPARA,VOL,PI
      COMMON/PHI/PHI(2),PHIX(2),PHICE(4,3),W(3),GP(3)
      COMMON/GEL/G,HBP
      COMMON/BOEL/SIGM(500)
      COMMON/MOOR/VOLT(500),FCODE(500)
      DIMENSION XLOC(2),ALPHA(2),RLOC(2),ESTIFM(2,2),
     *PSI(2),DPSI(2),SLOC(2)

      DO 10 I=1,2
      RLOC(I)=0.0
      DO 10 J=1,2
10    ESTIFM(I,J)=0.0
      DO 20 I=1,2
      LI=NELL-1+I
      SLOC(I)=SIGM(LI)
      XLOC(I)=X(LI)
20    ALPHA(I)=QQ(LI)
      DX=XLOC(2)-XLOC(1)
      ZNE=QQ(NP)
      IF(FCODE(NELL).EQ.2.)THEN
      SLOC(1)=0.0
      SLOC(2)=0.0
      ENDIF
      C
      DO 150 NGP=1,3
      TH=0.0
      F=0.0
      FC=0.0
      SIGMA=0.0
      DO 30 II=1,2
      SIGMA=SIGMA+PHICE(II,NGP)*SLOC(II)
      TH=TH+PHICE(II,NGP)*XLOC(II)
      F=F+PHICE(II,NGP)*ALPHA(II)
30    FC=FC+PHICE(II+2,NGP)*ALPHA(II)
      FT=FC/DX
      DO 35 II=1,2
      PSI(II)=PHICE(II,NGP)
```

```
35          DPSI(II)=PHICE(II+2,NGP)/DX
c
            WSIN=W(NGP)*SIN(TH)*DX
            SAREA=(F**2+FT**2)**0.5
c
            RHS(NP-1,1)=RHS(NP-1,1)+2.0*PI/3.0*F**3*WSIN
            DO 100 I=1,2
            DRVC=-F**2*PSI(I)*WSIN
            AMAT(NELL+I-1,NP-1)=AMAT(NELL+I-1,NP-1)+DRVC
            AMAT(NP-1,NELL+I-1)=AMAT(NP-1,NELL+I-1)+2.0*PI*
            1DRVC
            AMAT(NELL+I-1,NP)=AMAT(NELL+I-1,NP)
            1 -(HBP*F*SIGMA)**2*PSI(I)
            1*WSIN

            RLOC(I)=RLOC(I)+
            1 ((F*FT*DPSI(I)+PSI(I)*(2.0*F**2+FT**2))/SAREA-
            2 (QQ(NP-1)+FLOAT(IDROP)*G*F*COS(TH)+ZNE*
            3 (HBP*SIGMA)**2
            4 )*F**2*PSI(I))*WSIN
            DO 100 J=1,2
100         ESTIFM(I,J)=ESTIFM(I,J)+
            1 ((F**3*(2.0*PSI(I)*PSI(J)+DPSI(I)*DPSI(J))+
            2 FT**3*(DPSI(I)*PSI(J)+PSI(I)*DPSI(J))+
            3 3.0*F*FT**2*PSI(I)*PSI(J))/SAREA**3-
            4 (2.0*F*QQ(NP-1)+3.0*F**2*FLOAT(IDROP)*
            5 G*COS(TH))*PSI(I)*PSI(J)-2.*F*ZNE*SIGMA**
            6 2*HBP**2*PSI(I)*PSI(J))
            7 *WSIN
150         CONTINUE
c
c           *** INSERT ELEMENT RESIDUAL VECTOR AND ELEMENT
c           JACOBIAN
c           *** MATRIX INTO GLOBAL RESIDUAL VECTOR AND
c           GLOBAL JACOBIAN
c           *** MATRIX
            II=NELL-1
            JJ=NELL-1
            DO 200 I=1,2
            RHS(II+I,1)=RHS(II+I,1)-RLOC(I)
            DO 200 J=1,2
200         AMAT(II+I,JJ+J)=AMAT(II+I,JJ+J)+ESTIFM(I,J)
c

            RETURN
            END
```

```
      SUBROUTINE TFUNGP
      IMPLICIT REAL*8(A-H,O-Z)
      COMMON/PHI/PHI(2),PHIX(2),PHICE(4,3),W(3),GP(3)
c     *** ASSIGN GAUSS POINTS AND WEIGHTS

      W(1)=0.27777777777778
      W(2)=0.44444444444444
      W(3)=W(1)
      GP(1)=0.11270166537926
      GP(2)=0.5
      GP(3)=1.0-GP(1)
c     *** CALCULATE 1-D BASIS FUNCTIONS AND THEIR
c     *** DERIVATIVES AT GAUSS POINTS
      DO 10 I=1,3
      Veta=GP(I)
      CALL TFUN(VETA)
      DO 10 J=1,2
      PHICE(J,I)=PHI(J)
10    PHICE(J+2,I)=PHIX(J)

      RETURN
      END

      SUBROUTINE TFUN(ETA)
      IMPLICIT REAL*8(A-H,O-Z)
      COMMON/PHI/PHI(2),PHIX(2),PHICE(4,3),W(3),GP(3)

      PHI(1)=1.0-ETA
      PHI(2)=ETA
      PHIX(1)=-1.0
      PHIX(2)=1.0

      RETURN
      END

      SUBROUTINE RESIDU(ITER,INDEX,NTOT,NBLA,DELP,NPT,
     1NS1,SUSQMX,NPPT
     1,NCON,NQQC,NPTMAX,CURV3)
      IMPLICIT REAL*8(A-H,O-Z)
      COMMON/BC/IBEG(500),IEND(500),BEG(500),EXIT(500)
      COMMON/FRON/NP,NE,NELL,NH,NPL,HNOZ,NNOZ
      COMMON / PRIP / RHOS(500,1),ZS(500,1),
     1HQS(500)
      COMMON/FE/QQ(600),QK(600),AMAT(600,600),RHS(600,2),
     1X(500),R(500),DETV(500),IDETV(500),DXOLD(500)
      COMMON/OTHER/EPSI,ITMAX,H,IDROP,NPARA,VOL,PI
```

```
      COMMON/BOEL2/NT,NB,NBT,NRS,IEP,DBP,RDBP,ZKLL,
     1ZKLP,ZSUM
      COMMON/BOEL/SIGM(500)
      COMMON/CONVERG/ S1(50),S2(50)
      COMMON/MOOR/VOLT(500),FCODE(500)
c     *** CALCULATE NORMS OF SOLUTION CHANGE AND
c     *** RESIDUALS UPDATE FINITE ELEMENT COEFFICIENTS
      NS1=0
      S1(ITER)=0.0
      S2(ITER)=0.0
      WRITE(*,*)'ITER=',ITER
      DO 30 I=1,NTOT
c     QQ(I)=QQ(I)+RHS(I,1)

      S1(ITER)=S1(ITER)+RHS(I,1)*RHS(I,1)
      S2(ITER)=S2(ITER)+R(I)*R(I)

30    CONTINUE
      WRITE(*,*)'NPT= ',NPT
      WRITE(*,*)'ASPECT RATIO= ',QQ(1)/QQ(NE+1)
      WRITE(*,*)'ELECTRIC BOND NO., Ne= ',QQ(NP)
      WRITE(*,*)'K = ',QQ(NP-1)
      WRITE(*,*)'ITER= ',ITER,' S1= ',S1(iter)
     1,' S2= ',S2(iter)
      IF(NPT.NE.1.AND.S1(ITER).GT.1.0)THEN
      NCON=NCON+1
      DELP=0.5*DELP
      NS1=1
      GOTO 37
      ENDIF
      IF(ITER.GT.6)THEN
      NCON=NCON+1
      DELP=0.5*DELP
      NS1=1
      GOTO 37
      ENDIF
      DO 35 I=1,NTOT
35    QQ(I)=QQ(I)+RHS(I,1)


      GOTO 47
37    CONTINUE
      DO 299 I=1,NTOT
299   QQ(I)=QK(I)
      QQ(NPARA)=QK(NPARA)+DELP
47    CONTINUE
      IF(NCON.EQ.20)GOTO 802
```

```
      DO 496 I=1,NE
      RHOS(I,1)=QQ(I)*SIN(X(I))
      ZS(I,1)=QQ(I)*COS(X(I))
      RHO2=QQ(I+1)*SIN(X(I+1))
      Z2=QQ(I+1)*COS(X(I+1))
496   HQS(I)=SQRT((RHO2-RHOS(I,1))**2+(Z2-ZS(I,1))**2)
      Z123=ZKLL
      DO 599 I=1,NE+NNOZ+NBLA+NT+1
      SIGM(I)=QQ(I+NE+3)
599   CONTINUE
      DO 549 I=NE+NNOZ+NBLA+NT+2,NE+NNOZ+NBLA
     1+NT+NRS
      IF(FCODE(I).EQ.2.)THEN
      VOLT(I)=QQ(I+NE+3)
      ENDIF
      IF(FCODE(I).EQ.1.)THEN
      SIGM(I)=QQ(I+NE+3)
      ENDIF
549   CONTINUE

      DO 539 I=NE+NNOZ+NBLA+NT+NRS+1,NE+NPL+1
539   SIGM(I)=QQ(I+NE+3)
      IF(NS1.EQ.1)RETURN
      S1(ITER)=DSQRT(S1(ITER))
      S2(ITER)=DSQRT(S2(ITER))
c     *** PRINT OUT RESIDUALS AND SOLUTION CHANGE
c     AT EACH
c     *** ITERATION DURING DEBUGGING STAGE
      INDEX=1
c     *** CHECK FOR CONVERGENCE
      IF(S1(ITER).LE.EPSI.AND.S2(ITER).LE.EPSI)GO TO 60
      INDEX=2
c     *** CHECK FOR DIVERGENCE
c     *** HAS MAXIMUM NUMBER OF ITERATIONS BEEN
c     EXCEEDED
      IF(ITER.GE.ITMAX)GO TO 60
c     *** HAS FREE SURFACE LOCATION BECOME LESS THAN 0?
c     *** OTHERWISE, CONTINUE NEWTON ITERATION
      INDEX=0
      RETURN
      60 CONTINUE
      IF(NPT.EQ.NPTMAX)GOTO 802
c     *** PRINT INFORMATION FOR ALL ITERATIONS
      NPPT=NPPT+1
      IF(NPPT.GT.1)NPPT=0
      CALL CONE(ACURV,CHARGE,FORCE)
      ACURV=-1./ACURV
```

```
      WRITE(10,943)QQ(NP),QQ(NP-1),QQ(1)/QQ(NE+1),ACURV
c     WRITE(*,943)QQ(NP),QQ(NP-1),QQ(1)/QQ(NE+1),ACURV
      CURV3=ACURV
      IF(QQ(NP).LT.QK(NP))THEN
      GOTO 802
      ENDIF
      IF(NPT.EQ.1.OR.NPT.EQ.3)GOTO 802

      GOTO 801


802   CONTINUE
      IF(NQQC.EQ.2.AND.NCON.EQ.20)GOTO 807
      IF(NQQC.EQ.2.AND.NPT.NE.NPTMAX)GOTO 801
807   CONTINUE
      WRITE(2,*)'ASPECT RATIO= ',QQ(1)/QQ(NE+1)
      WRITE(2,*)'ELECTRIC BOND NO., Ne= ',QQ(NP),
     1SQRT(QQ(NP))
      WRITE(2,*)'K = ',QQ(NP-1)
      WRITE(2,912)(S1(I),I=1,ITER)
      WRITE(2,913)(S2(I),I=1,ITER)
      WRITE(15,*)NE+1
      CONANG=0.0
      DO 349 I=1,NE+1
      DTET=X(I+1)-X(I)
      DFDP=QQ(I+1)-QQ(I)
      TOP=QQ(I)*DTET*SIN(X(I))-DFDP*COS(X(I))
      BOTT=SQRT(DTET**2*QQ(I)**2+DFDP**2)
      IF(I.NE.NE+1)CONANG=TOP/BOTT
      CONANG=180./3.1415926536*ACOS(CONANG)
349   WRITE(15,944)X(I),QQ(I)*SIN(X(I)),QQ(I)*COS(X(I))
     1,QQ(NE+3+I),CONANG
      WRITE(15,*)'TOTAL CHARGE= ',CHARGE
      WRITE(15,*)'FORCE= ',FORCE
      WRITE(11,*)NNOZ+1
      DO 342 I=NE+1,NE+NNOZ+1
342   WRITE(11,943)RHOS(I,1),ZS(I,1),QQ(NE+3+I)
      WRITE(12,*)NBLA+NT+1
      DO 344 I=NE+NNOZ+1,NE+NNOZ+NBLA+NT+1
344   WRITE(12,943)RHOS(I,1),ZS(I,1),QQ(NE+3+I)
      WRITE(13,*)NRS+1
      DO 346 I=NE+NNOZ+NBLA+NT+1,NE+NNOZ+NBLA
     1+NT+NRS+1
346   WRITE(13,943)RHOS(I,1),ZS(I,1),QQ(NE+3+I)
      WRITE(14,*)NBLA+NB+1
      DO 347 I=NE+NNOZ+NBLA+NT+NRS+1,NE+NPL+1
```

```
347       WRITE(14,943)RHOS(I,1),ZS(I,1),QQ(NE+3+I)
          IF(QQ(NP).LT.QK(NP))NQQC=2

801       CONTINUE
944       FORMAT(1X,5(2X,E12.5))
943       FORMAT(1X,2X,E12.5,2X,E12.5,2X,E22.15,2X,E12.5,2X,E12.5)

          IF(INDEX.EQ.1)RETURN
c         *** PRINT OUT RESIDUALS AND SOLUTION CHANGE
c         *** BECAUSE NEWTON ITERATION HAS FAILED

          RETURN
882       FORMAT(/,1X,'SURFACE CHARGE DENSITIES')
906       FORMAT(10(1X,E12.5))
912       FORMAT(1X,'QNORM=',10(2X,E9.3))
913       FORMAT(1X,'RNORM=',10(2X,E9.3))
921       FORMAT(/,1X,'CONVERGENCE:',I4,2X,'ITERATIONS')
922       FORMAT(/,1X,'FAILURE:',I4,2X,'ITERATIONS')
950       FORMAT(/,1X,'FREE SURFACE LOCATION AT NODES,
          *FINITE ELEMENT',1X,
          * 'SOLUTION=')
952       FORMAT(/,1X,'RESIDUALS=')
954       FORMAT(/,1X,'CHANGES IN NODAL VALUES=')
959       FORMAT(6F8.4)
          END


          SUBROUTINE DRIVER(ITER,NPTCO,ERR,NTOT,NBLA)
          IMPLICIT REAL*8(A-H,O-Z)
          COMMON/BC/IBEG(500),IEND(500),BEG(500),EXIT(500)
          COMMON/FRON/NP,NE,NELL,NH,NPL,HNOZ,NNOZ
          COMMON/FE/QQ(600),QK(600),AMAT(600,600),RHS(600,2),
          1X(500),R(500),DETV(500),IDETV(500),DXOLD(500)
          COMMON/OTHER/EPSI,ITMAX,H,IDROP,NPARA,VOL,PI
          COMMON/BOEL/SIGM(500)
          COMMON/MOOR/VOLT(500),FCODE(500)
          COMMON/BOEL2/NT,NB,NBT,NRS,IEP,DBP,RDBP,ZKLL,
          1ZKLP,ZSUM

c         *** SUBROUTINE THAT CALLS SUBROUTINE ABFIND FOR
c         *** ELEMENT BY ELEMENT ASSEMBLY OF LINEAR SYSTEM
c         *** OF EQUATIONS AND THEN SUBROUTINE MULSOL FOR
c         *** SOLUTION OF LINEAR SYSTEM
          NELL=0
c         *** INITIALIZE GLOBAL ARRAYS
          DO 50 I=1,NTOT
```

```
      RHS(I,1)=0.0D000
      DO 50 J=1,NTOT
50    AMAT(I,J)=0.0D000

c     ********************************************************
c     IMPOSE VOLUME CONSTRAINT
c     ********************************************************

      RHS(NP-1,1)=-VOL-PI*(1.-H**2)*ABS(H)/3.
      CALL TFUNGP
c
c     *** ASSEMBLE EQUATIONS ELEMENT BY ELEMENT

c     ********************************************************
c     COMPUTE dRj(YL)/dALPHAi
c     ********************************************************
      DO 100 I=1,NE

      NELL=NELL+1
      CALL ABFIND(NTOT)
100   CONTINUE


c     ********************************************************
c     COMPUTE dRj(YL)/dSIGMAi
c     ********************************************************

      DO 300 I=1,NE
300   CALL ABFIN2(I,NTOT)



c     ********************************************************
c     COMPUTE dRj(L)/dALPHAi
c     ********************************************************

      DO 400 I=1,NE+NPL+1
      SIP=0.0D000
      DO 410 J=1,NE+NPL
      IF(J.EQ.I)THEN
      CALL SING1(I,J,SID,NTOT)
      GOTO 410
      ENDIF
      IF(I.EQ.J+1)THEN
      CALL SING2(I,J,SID,NTOT)
      GOTO 410
      ENDIF
```

```
            CALL ABFIN3(I,J,SID,NTOT)

410         SIP=SIGM(J)*SID+SIP
400         RHS(I+NE+3,1)=-1.D000+SIP

c           ********************************************************
c           COMPUTE dRj(L)/dSIGMAi
c           ********************************************************

            DO 500 I=1,NE+NPL+1
            SIP=0.0D000
            SIPW=0.0
            SIDPP=0.0
            DO 510 J=1,NE+NPL
            IF(I.EQ.J)THEN
            CALL SING3(I,J,SID,NTOT)
            GOTO 510
            ENDIF
            IF(I.EQ.J+1)THEN
            CALL SING4(I,J,SID,NTOT)
            GOTO 510
            ENDIF
            CALL ABFIN4(I,J,SID,NTOT,SIDP,SIDW)
            SIPW=SIDW+SIPW
            SIDPP=SIDP+SIDPP
510         SIP=SID+SIP

c           ********************************************************
c           IMPOSE DIRICHLET B.C.
c           ********************************************************

            IF(FCODE(I).EQ.2.0.AND.FCODE(I-1).NE.1.)
           1AMAT(I+NE+3,I+NE+3)=-SIPW

            RHS(I+NE+3,1)=SIPW*VOLT(I)+SIP-SIDPP


500         CONTINUE


c           ********************************************************
c           *** IMPOSE DIRICHLET (ESSENTIAL) B.C.; TAKE CARE OF
c           *** ADAPTIVE PARAMETRIZATION.
c           ********************************************************

            DO 150 J=1,2*NE+NPL+4
            AMAT(NH,J)=0.0D000
150         AMAT(NP,J)=0.0D000
```

```
      AMAT(NH,NH)=1.0D000
      AMAT(NP,NPARA)=1.0D000
      RHS(NH,1)=0.0D000
      RHS(NP,1)=0.0D000

c     ********************************************************
c     STORE DIRICHLET B.C. IN TEMPORARY VECTOR
c     ********************************************************

      DO 200 I=1,NTOT
200   R(I)=RHS(I,1)
      NRHS=1



      CALL MULSOL(ERR,DET,IDET,NRHS,NTOT)
      DETV(ITER)=DET
      IDETV(ITER)=IDET

      RETURN
      END
      SUBROUTINE ABFIN2(MNEL,NTOT)
c     ****************************************************
c     CALCULATES dR(YL)/dSIGMA MATRIX
c     ****************************************************

      IMPLICIT REAL*8(A-H,O-Z)
      COMMON/BC/IBEG(500),IEND(500),BEG(500),EXIT(500)
      COMMON/FRON/NP,NE,NELL,NH,NPL,HNOZ,NNOZ
      COMMON/FE/QQ(600),QK(600),AMAT(600,600),RHS(600,2),
     1X(500),R(500),DETV(500),IDETV(500),DXOLD(500)
      COMMON/OTHER/EPSI,ITMAX,H,IDROP,NPARA,VOL,PI
      COMMON/PHI/PHI(2),PHIX(2),PHICE(4,3),W(3),GP(3)
      COMMON/BOEL/SIGM(500)
      COMMON/GEL/G,HBP
      COMMON/MOOR/VOLT(500),FCODE(500)
      DIMENSION XLOC(2),ALPHA(2),RLOC(2),ESTIFM(2,2),
     *PSI(2),DPSI(2),SLOC(2)
c
      MNEJ=NE+3+MNEL
      NELL=MNEL
      DO 10 I=1,2
      RLOC(I)=0.0
      DO 10 J=1,2
      10 ESTIFM(I,J)=0.0
c
      DO 20 I=1,2
```

```
      LI=NELL-1+I
      SLOC(I)=SIGM(LI)
      XLOC(I)=X(LI)
20    ALPHA(I)=QQ(LI)
      DX=XLOC(2)-XLOC(1)
      ZNE=QQ(NP)
      IF(FCODE(MNEL).EQ.2)THEN
      SLOC(1)=0.0
      SLOC(2)=0.0
      ENDIF
C
      DO 150 NGP=1,3
      TH=0.0
      F=0.0
      FC=0.0
      SIGMA=0.0
      DO 30 II=1,2
      SIGMA=SIGMA+PHICE(II,NGP)*SLOC(II)
      TH=TH+PHICE(II,NGP)*XLOC(II)
      F=F+PHICE(II,NGP)*ALPHA(II)
30    FC=FC+PHICE(II+2,NGP)*ALPHA(II)
      FT=FC/DX
      DO 35 II=1,2
      PSI(II)=PHICE(II,NGP)
35    DPSI(II)=PHICE(II+2,NGP)/DX
C
      WSIN=W(NGP)*SIN(TH)*DX
      SAREA=(F**2+FT**2)**0.5
C
      AMAT(MNEL,MNEJ)=-2.*SIGMA*ZNE*HBP**2*F**2*
     1PSI(1)*WSIN*PHICE(1,NGP)+
     1AMAT(MNEL,MNEJ)
      AMAT(MNEL,MNEJ+1)=-2.*SIGMA*ZNE*HBP**2*F**2*
     1PSI(1)*WSIN*PHICE(2,NGP)+
     1AMAT(MNEL,MNEJ+1)
      AMAT(MNEL+1,MNEJ)=-2.*SIGMA*ZNE*HBP**2*F**
     12*PSI(2)*WSIN*PHICE(1,NGP)+AMAT(MNEL+1,MNEJ)
440   AMAT(MNEL+1,MNEJ+1)=-2.*SIGMA*ZNE*HBP**2*F**
      12*PSI(2)*WSIN*PHICE(2,NGP)+AMAT(MNEL+1,MNEJ+1)
150   CONTINUE
      RETURN
      END

      SUBROUTINE ABFIN3(MNEL,MNEJ,SID,NTOT)
```

```
c     ********************************************************
c     CALCULATES dR(L)/Da MATRIX
c     ********************************************************
      IMPLICIT REAL*8(A-H,O-Z)
      COMMON/BC/IBEG(500),IEND(500),BEG(500),EXIT(500)
      COMMON/FRON/NP,NE,NELL,NH,NPL,HNOZ,NNOZ
      COMMON/FE/QQ(600),QK(600),AMAT(600,600),RHS(600,2),
     1X(500),R(500),DETV(500),IDETV(500),DXOLD(500)
      COMMON/OTHER/EPSI,ITMAX,H,IDROP,NPARA,VOL,PI
      COMMON/PHI2/PHI2(2),PHIX2(2),PHICE2(4,13)
      COMMON / PRIP / RHOS(500,1),ZS(500,1),
     1HQS(500)
      COMMON/BOEL/SIGM(500)
      COMMON/TET/THETA(500,1)
      COMMON/MOOR/VOLT(500),FCODE(500)
      DIMENSION XLOC(2),ALPHA(2),RLOC(2),ESTIFM(2,2),
     *PSI(2),DPSI(2),GAUS(4),WE(4)
      GAUS(4)=0.930565
      GAUS(3)=0.669994
      GAUS(2)=0.33003
      GAUS(1)=0.069435
      WE(1)=0.34785/2.
      WE(2)=0.65214/2.
      WE(3)=WE(2)
      WE(4)=WE(1)
      PI=3.1415926535898
      PIF=1./(4.*PI)
      STIP=0.
      NELL=MNEJ
      DO 10 I=1,2
      RLOC(I)=0.0
      DO 10 J=1,2
10    ESTIFM(I,J)=0.0
c
      DO 20 I=1,2
      LI=NELL-1+I
      XLOC(I)=X(LI)
20    ALPHA(I)=QQ(LI)
      DX=XLOC(2)-XLOC(1)
      ZNE=QQ(NP)
      ZNR=(ZS(MNEJ+1,1)-ZS(MNEJ,1))/HQS(MNEJ)
      ZNZ=(RHOS(MNEJ,1)-RHOS(MNEJ+1,1))/HQS(MNEJ)
      SIPD1=0.0
      SIPD2=0.0
      SIPD3=0.0
      SIPD4=0.0
```

```
SIP32=0.
SIP31=0.0
SIP41=0.
SIP42=0.0
SIP11=0.
SIP12=0.0
SIP21=0.
SIP22=0.0
SID=0.
HICC=0.0
SIGM1=SIGM(MNEJ)
SIGM2=SIGM(MNEJ+1)
IF(FCODE(MNEJ).EQ.2.)THEN
SIGM1=0.0
SIGM2=0.0
ENDIF
DO 150 NGP=1,4
FU1=1.-GAUS(NGP)
FU2=1.-FU1
TH=0.0
F=0.0
FCR=0.0
FCZ=0.0
THPSI=0.0
THMM=X(MNEL)
RHOP=RHOS(MNEL,1)
IF(RHOP.LT.0.0)RHOP=0.0
Z=ZS(MNEL,1)
ZSP=ZS(MNEJ,1)*FU1+ZS(MNEJ+1,1)*FU2
RSP=RHOS(MNEJ,1)*FU1+RHOS(MNEJ+1,1)*FU2
VOLTA=VOLT(MNEJ)*FU1+VOLT(MNEJ+1)*FU2
IF(RSP.LT.0.0)RSP=0.0
THETRO= XLOC(1)*(1.-GAUS(NGP))+XLOC(2)*GAUS(NGP)
THETRP= XLOC(2)-XLOC(1)
DROF1=(1.-GAUS(NGP))*SIN(X(MNEJ))
DROF2=GAUS(NGP)*SIN(X(MNEJ+1))
DROFP1=-SIN(X(MNEJ))
DROFP2=SIN(X(MNEJ+1))
DZDFP1=-COS(X(MNEJ))
DZDFP2=COS(X(MNEJ+1))
DZDF1=(1.-GAUS(NGP))*COS(X(MNEJ))
DZDF2=GAUS(NGP)*COS(X(MNEJ+1))
DRMF1=SIN(THMM)
DRMF2=0.0
DZMF1=COS(THMM)
DZMF2=0.0
DFFDZ=ALPHA(2)-ALPHA(1)
```

```
      DFDO=ALPHA(1)*(1.-GAUS(NGP))
     1+ALPHA(2)*GAUS(NGP)
      FCR=RHOS(MNEJ+1,1)-RHOS(MNEJ,1)
      FCZ=ZS(MNEJ+1,1)-ZS(MNEJ,1)
      IF(MNEJ.GT.NE)GOTO 912
      DEDRZ1=(FCR**2+FCZ**2)**(-0.5)*(FCR*DROFP1
     1+FCZ*DZDFP1)
      DEDRZ2=(FCR**2+FCZ**2)**(-0.5)*(FCR*DROFP2
     1ddddddddsqab1+FCZ*DZDFP2)
  912 ZBOT=(Z-ZSP)**2+(RHOP+RSP)**2
      NTTE=NE
      SIGMA=FU1*SIGM1+FU2*SIGM2
      IF(MNEL.LE.NTTE+1.AND.MNEJ.GT.NTTE)GOTO 560
      IF(MNEL.GT.NTTE+1.AND.MNEJ.GT.NTTE)GOTO 555
      DXDA=-4.*RHOP*DROF1/ZBOT+8.*RHOP*RSP*
     1((Z-ZSP)*(-DZDF1)+(RHOP+RSP)*DROF1)/
     1ZBOT**2
      DXDA2=-4.*RHOP*DROF2/ZBOT+8.*RHOP*RSP*
     1((Z-ZSP)*(-DZDF2)+(RHOP+RSP)*(DROF2))/
     1ZBOT**2
      DZBOT=2.*((Z-ZSP)*(-DZDF1)+(RHOP+RSP)*DROF1)
      DZBOT2=2.*((Z-ZSP)*(-DZDF2)+(RHOP+RSP)*DROF2)
      ZK=4.*RHOP*RSP/ZBOT
      ZKV=SQRT(4./ZBOT)
      ZKE=-ZBOT**(-1.5)*DZBOT
      ZKE2=-ZBOT**(-1.5)*DZBOT2
      CALL VK(ZK,FKE,DXDA,GKE)
      SIP11=FU1*(1./(4.*PI)*2.*
     1WE(NGP)*(ZKE*RSP*FKE+
     1DROF1
     1*ZKV*FKE+ZKV*RSP*GKE)*SQRT(FCR**2+FCZ**2)+
     11./(4.*PI)*2.0*
     1WE(NGP)*ZKV*
     1RSP*FKE*DEDRZ1)+SIP11
      SIP12=FU2*(1./(4.*PI)*2.*
     1WE(NGP)*(ZKE*RSP*FKE+
     1DROF1
     1*ZKV*FKE+ZKV*RSP*GKE)*SQRT(FCR**2+FCZ**2)+
     11./(4.*PI)*2.0*
     1WE(NGP)*ZKV*
     1RSP*FKE*DEDRZ1)+SIP12
      CALL VK(ZK,FKE,DXDA2,GKE)
      SIP21=FU1*(1./(4.*PI)*2.*
     1WE(NGP)*(ZKE2*RSP*FKE+
     1DROF2
```

```
1*ZKV*FKE+ZKV*RSP*GKE)*SQRT(FCR**2+FCZ**2)+
1 1./(4.*PI)*2.0*
1WE(NGP)*ZKV*
1RSP*FKE*DEDRZ2)+SIP21
SIP22=FU2*(1./(4.*PI)*2.*
1WE(NGP)*(ZKE2*RSP*FKE+
1DROF2
1*ZKV*FKE+ZKV*RSP*GKE)*SQRT(FCR**2+FCZ**2)+
1 1./(4.*PI)*2.0*
1WE(NGP)*ZKV*
1RSP*FKE*DEDRZ2)+SIP22
ZD=-(Z-ZSP)
A=RHOP**2+RSP**2+ZD**2
B=2.*RSP*RHOP

DSQAB1=-1.*(DROF1*(RHOP+RSP)-DZDF1*(Z-ZSP))/
1((A+B)**1.5)
DSQAB2=-1.*(DROF2*(RHOP+RSP)-DZDF2*(Z-ZSP))/
1((A+B)**1.5)
R1=QQ(MNEJ)*SIN(XLOC(1))
R2=QQ(MNEJ+1)*SIN(XLOC(2))
Z1=QQ(MNEJ)*COS(XLOC(1))
Z2=QQ(MNEJ+1)*COS(XLOC(2))
RDEN=SQRT((R2-R1)**2+(Z2-Z1)**2)
S1=SIN(XLOC(1))
S2=SIN(XLOC(2))
CO1=COS(XLOC(1))
CO2=COS(XLOC(2))
ABH=SQRT(A+B)
DZNRF1=((Z2-Z1)/RDEN**3.0*((R2-R1)*S1+(Z2-Z1)*CO1)
1-CO1/RDEN)
DZNRF2=(-(Z2-Z1)/RDEN**3.0*((R2-R1)*S2+(Z2-Z1)*CO2)
1+CO2/RDEN)
DZNZF1=-((R2-R1)/RDEN**3.0*((R2-R1)*S1+(Z2-Z1)*CO1)
1-S1/RDEN)
DZNZF2=-(-(R2-R1)/RDEN**3.0*((R2-R1)*S2+(Z2-Z1)*CO2)
1+S2/RDEN)
DC1D1=2.*ZNR/RSP*DSQAB1+2.*DZNRF1/RSP/ABH-2.*ZNR
1 /RSP**2*DROF1/ABH
DC1D2=2.*ZNR/RSP*DSQAB2+2.*DZNRF2/RSP/ABH-2.*ZNR
1 /RSP**2*DROF2/ABH
C1=2.*ZNR/RSP/ABH
AMB=A-B
C2=4.*ZNR*(RSP-RHOP)/ABH/AMB
C3=4.*ZNZ*ZD/ABH/AMB
```

```
      DABD1=-2.*(-(RHOP-RSP)*DROF1-(Z-ZSP)*DZDF1)/AMB**2
      DABD2=-2.*(-(RHOP-RSP)*DROF2-(Z-ZSP)*DZDF2)/AMB**2
      DC2D1=4.*(ZNR*(DROF1/(ABH*AMB)+(RSP-RHOP)
     1*(DSQAB1/AMB
     1 +DABD1/ABH))+(RSP-RHOP)/AMB/ABH*DZNRF1)
      DC2D2=4.*(ZNR*(DROF2/(ABH*AMB)+(RSP-RHOP)
     1*(DSQAB2/AMB
     1 +DABD2/ABH))+(RSP-RHOP)/AMB/ABH*DZNRF2)
      DC3D1=4.*(ZNZ*(DZDF1/AMB/ABH+(DSQAB1/AMB
     1 +DABD1/ABH)*ZD)+ZD/AMB/ABH*DZNZF1)
      DC3D2=4.*(ZNZ*(DZDF2/AMB/ABH+(DSQAB2/AMB
     1 +DABD2/ABH)*ZD)+ZD/AMB/ABH*DZNZF2)
      CALL VK(ZK,FKE,DXDA,GKE)
      CALL VK2(ZK,FKE2,DXDA,GKE2)
      DJOC=SQRT(FCZ**2+FCR**2)
      SIPD1=((DC1D1*(FKE2-FKE)+C1*(GKE2-GKE)-
     1 (DC2D1*FKE2+C2*GKE2)
     1 -DC3D1*FKE2-C3*GKE2)*WE(NGP)*PIF*DJOC*RSP+
     1 PIF*(C1*(FKE2-FKE)-C2*FKE2-C3*FKE2)*WE(NGP)
     1 *DEDRZ1*RSP+DROF1*PIF*WE(NGP)*
     1 (C1*(FKE2-FKE)-C2*FKE2-C3*FKE2)*DJOC)*VOLTA
     1+SIPD1
     1 -((DC1D1*(FKE2-FKE)+C1*(GKE2-GKE)-(DC2D1*FKE2
     1+C2*GKE2)
     1 -DC3D1*FKE2-C3*GKE2)*WE(NGP)*PIF*DJOC*RSP+
     1 PIF*(C1*(FKE2-FKE)-C2*FKE2-C3*FKE2)*WE(NGP)
     1 *DEDRZ1*RSP+DROF1*PIF*WE(NGP)*
     1 (C1*(FKE2-FKE)-C2*FKE2-C3*FKE2)*DJOC)*VOLT(MNEL)
      CALL VK(ZK,FKE,DXDA2,GKE)
      CALL VK2(ZK,FKE2,DXDA2,GKE2)
      SIPD2=((DC1D2*(FKE2-FKE)+C1*(GKE2-GKE)-
     1 (DC2D2*FKE2+C2*GKE2)
     1 -DC3D2*FKE2-C3*GKE2)*WE(NGP)*PIF*DJOC*RSP+
     1 PIF*(C1*(FKE2-FKE)-C2*FKE2-C3*FKE2)*WE(NGP)
     1 *DEDRZ2*RSP+DROF2*PIF*WE(NGP)*
     1 (C1*(FKE2-FKE)-C2*FKE2-C3*FKE2)*DJOC)*VOLTA+SIPD2
     1 -((DC1D2*(FKE2-FKE)+C1*(GKE2-GKE)-(DC2D2*FKE2
     1 +C2*GKE2)
     1 -DC3D2*FKE2-C3*GKE2)*WE(NGP)*PIF*DJOC*RSP+
     1 PIF*(C1*(FKE2-FKE)-C2*FKE2-C3*FKE2)*WE(NGP)
     1 *DEDRZ2*RSP+DROF2*PIF*WE(NGP)*
     1 (C1*(FKE2-FKE)-C2*FKE2-C3*FKE2)*DJOC)*VOLT(MNEL)
550   CONTINUE
      IF(MNEL.GT.NE+1)GOTO 555
      DXDA=8.*RHOP*RSP*
```

```
1((Z-ZSP)*(DZMF1)+(RHOP+RSP)*(DRMF1))/
1ZBOT**2-4.*RSP*DRMF1/ZBOT
DXDA2=8.*RHOP*RSP*
1((Z-ZSP)*(DZMF2)+(RHOP+RSP)*(DRMF2))/
1ZBOT**2-4.*RSP*DRMF2/ZBOT
DZBOT=2.*((Z-ZSP)*DZMF1+(RHOP+RSP)*DRMF1)
DZBOT2=2.*((Z-ZSP)*DZMF2+(RHOP+RSP)*DRMF2)
ZKV=SQRT(4./ZBOT)
ZK=4.*RHOP*RSP/ZBOT
ZKE=-ZBOT**(-1.5)*DZBOT
ZKE2=-ZBOT**(-1.5)*DZBOT2
CALL VK(ZK,FKE,DXDA,GKE)
SIP31=FU1*(1./(4.*PI)*2.*
1WE(NGP)*(ZKE*RSP*FKE+
1ZKV*RSP*GKE)*SQRT(FCR**2+FCZ**2))
1+SIP31
SIP32=FU2*(1./(4.*PI)*2.*
1WE(NGP)*(ZKE*RSP*FKE+
1ZKV*RSP*GKE)*SQRT(FCR**2+FCZ**2))
1+SIP32
CALL VK(ZK,FKE,DXDA2,GKE)
SIP41=FU1*(1./(4.*PI)*2.*
1WE(NGP)*(ZKE2*RSP*FKE+
1ZKV*RSP*GKE)*SQRT(FCR**2+FCZ**2))
1+SIP41
SIP42=FU2*(1./(4.*PI)*2.*
1WE(NGP)*(ZKE2*RSP*FKE+
1ZKV*RSP*GKE)*SQRT(FCR**2+FCZ**2))
1+SIP42
ZD=-(Z-ZSP)
A=RHOP**2+RSP**2+ZD**2
B=2.*RSP*RHOP
DSQAB1=-1.*(DRMF1*(RHOP+RSP)+DZMF1*(Z-ZSP))
1 /((A+B)**1.5)
DSQAB2=-1.*(DRMF2*(RHOP+RSP)+DZMF2*(Z-ZSP))/
1((A+B)**1.5)
DC1D1=2.*ZNR/RSP*DSQAB1
DC1D2=2.*ZNR/RSP*DSQAB2
ABH=SQRT(A+B)
C1=2.*ZNR/RSP/ABH
AMB=A-B
C2=4.*ZNR*(RSP-RHOP)/ABH/AMB
C3=4.*ZNZ*ZD/ABH/AMB
DABD1=-2.*((RHOP-RSP)*DRMF1+(Z-ZSP)*DZMF1)/AMB**2
DABD2=-2.*((RHOP-RSP)*DRMF2+(Z-ZSP)*DZMF2)/AMB**2
DC2D1=4.*ZNR*(-DRMF1/(ABH*AMB)+(RSP-RHOP)*
```

```
     1(DSQAB1/AMB
     1 +DABD1/ABH))
     DC2D2=4.*ZNR*(-DRMF2/(ABH*AMB)+(RSP-RHOP)
     1*(DSQAB2/AMB
     1 +DABD2/ABH))
     DC3D1=4.*ZNZ*(-DZMF1/AMB/ABH+(DSQAB1/AMB
     1 +DABD1/ABH)*ZD)
     DC3D2=4.*ZNZ*(-DZMF2/AMB/ABH+(DSQAB2/AMB
     1 +DABD2/ABH)*ZD)
     CALL VK(ZK,FKE,DXDA,GKE)
     CALL VK2(ZK,FKE2,DXDA,GKE2)
     SIPD3=(DC1D1*(FKE2-FKE)+C1*(GKE2-GKE)-(DC2D1*
     1 FKE2+C2*GKE2)
     1 -DC3D1*FKE2-C3*GKE2)*WE(NGP)*HQS(MNEJ)*PIF
     *RSP*VOLTA+SIPD3
     1 -(DC1D1*(FKE2-FKE)+C1*(GKE2-GKE)-(DC2D1*FKE2
     1+C2*GKE2)
     1 -DC3D1*FKE2-C3*GKE2)*WE(NGP)*HQS(MNEJ)
     1*PIF*RSP*VOLT(MNEL)
     CALL VK(ZK,FKE,DXDA2,GKE)
     CALL VK2(ZK,FKE2,DXDA2,GKE2)
     SIPD4=(DC1D2*(FKE2-FKE)+C1*(GKE2-GKE)-(DC2D2
     1*FKE2+C2*GKE2)
     1 -DC3D2*FKE2-C3*GKE2)*WE(NGP)*HQS(MNEJ)
     1*PIF*RSP*VOLTA+SIPD4
     1 -(DC1D2*(FKE2-FKE)+C1*(GKE2-GKE)-(DC2D2*FKE2
     1+C2*GKE2)
     1 -DC3D2*FKE2-C3*GKE2)*WE(NGP)*HQS(MNEJ)*PIF
     1*RSP*VOLT(MNEL)
     GOTO 555
560  DXDA=8.*RHOP*RSP*((Z-ZSP)*DZMF1+(RHOP+RSP)
     1*DRMF1)/ZBOT**2-4.*RSP*DRMF1/ZBOT
     DXDA2=8.*RHOP*RSP*((Z-ZSP)*DZMF2+(RHOP+RSP)
     1*DRMF2)/ZBOT**2-4.*RSP*DRMF2/ZBOT
     ZK=4.*RHOP*RSP/ZBOT
     DZBOT=2.*((Z-ZSP)*DZMF1+(RHOP+RSP)*DRMF1)
     DZBOT2=2.*((Z-ZSP)*DZMF2+(RHOP+RSP)*DRMF2)
     ZKV=SQRT(4./ZBOT)
     ZK=4.*RHOP*RSP/ZBOT
     ZKE=-ZBOT**(-1.5)*DZBOT
     ZKE2=-ZBOT**(-1.5)*DZBOT2
     CALL VK(ZK,FKE,DXDA,GKE)
     SIP31=FU1*(1./(4.*PI)*2.*HQS(MNEJ)*
     2 WE(NGP)*(ZKE*RSP*FKE+ZKV*RSP*GKE))
     3 +SIP31
```

```
SIP32=FU2*(1./(4.*PI)*2.*HQS(MNEJ)*
2 WE(NGP)*(ZKE*RSP*FKE+ZKV*RSP*GKE)
2 )
3 +SIP32
CALL VK(ZK,FKE,DXDA2,GKE)
SIP41=FU1*(1./(4.*PI)*2.*HQS(MNEJ)*
2 WE(NGP)*(ZKE2*RSP*FKE+ZKV*RSP*GKE)
2 )
3 +SIP41
SIP42=FU2*(1./(4.*PI)*2.*HQS(MNEJ)*
2 WE(NGP)*(ZKE2*RSP*FKE+ZKV*RSP*GKE)
2 )
3 +SIP42
ZD=-(Z-ZSP)
A=RHOP**2+RSP**2+ZD**2
B=2.*RSP*RHOP
DSQAB1=-1.*(DRMF1*(RHOP+RSP)+DZMF1*(Z-ZSP))/
1((A+B)**1.5)
DSQAB2=-1.*(DRMF2*(RHOP+RSP)+DZMF2*(Z-ZSP))/
1((A+B)**1.5)
DC1D1=2.*ZNR/RSP*DSQAB1
DC1D2=2.*ZNR/RSP*DSQAB2
ABH=SQRT(A+B)
C1=2.*ZNR/RSP/ABH
AMB=A-B
C2=4.*ZNR*(RSP-RHOP)/ABH/AMB
C3=4.*ZNZ*ZD/ABH/AMB
DABD1=-2.*((RHOP-RSP)*DRMF1+(Z-ZSP)*DZMF1)
1/AMB**2
DABD2=-2.*((RHOP-RSP)*DRMF2+(Z-ZSP)*DZMF2)
1/AMB**2
DC2D1=4.*ZNR*(-DRMF1/(ABH*AMB)+(RSP-RHOP)*
1(DSQAB1/AMB
1 +DABD1/ABH))
DC2D2=4.*ZNR*(-DRMF2/(ABH*AMB)+(RSP-RHOP)*
1(DSQAB2/AMB
1 +DABD2/ABH))
DC3D1=4.*ZNZ*(-DZMF1/AMB/ABH+(DSQAB1/AMB
1 +DABD1/ABH)*ZD)
DC3D2=4.*ZNZ*(-DZMF2/AMB/ABH+(DSQAB2/AMB
1 +DABD2/ABH)*ZD)

CALL VK(ZK,FKE,DXDA,GKE)
CALL VK2(ZK,FKE2,DXDA,GKE2)
SIPD3=(DC1D1*(FKE2-FKE)+C1*(GKE2-GKE)-(DC2D1
```

```
     1*FKE2+C2*GKE2)
     1 -DC3D1*FKE2-C3*GKE2)*WE(NGP)*HQS(MNEJ)*PIF
     1*RSP*VOLTA+SIPD3
     1 -(DC1D1*(FKE2-FKE)+C1*(GKE2-GKE)-(DC2D1*FKE2
     1+C2*GKE2)
     1 -DC3D1*FKE2-C3*GKE2)*WE(NGP)*HQS(MNEJ)
     1*PIF*RSP*VOLT(MNEL)
     CALL VK(ZK,FKE,DXDA2,GKE)
     CALL VK2(ZK,FKE2,DXDA2,GKE2)
     SIPD4=(DC1D2*(FKE2-FKE)+C1*(GKE2-GKE)-(DC2D2*
     1FKE2+C2*GKE2)
     1 -DC3D2*FKE2-C3*GKE2)*WE(NGP)*HQS(MNEJ)
     1*PIF*RSP*VOLTA+SIPD4
     1 -(DC1D2*(FKE2-FKE)+C1*(GKE2-GKE)-(DC2D2*FKE2
     1+C2*GKE2)
     1 -DC3D2*FKE2-C3*GKE2)*WE(NGP)*HQS(MNEJ)
     1*PIF*RSP*VOLT(MNEL)
555  CONTINUE

150  CONTINUE



140  AMAT(MNEL+NE+3,MNEJ+1)=-SIGM1*SIP21+
     1AMAT(MNEL+NE+3,MNEJ+1)
     1-SIGM2*SIP22+SIPD2
     AMAT(MNEL+NE+3,MNEJ)=-SIGM1*SIP11+
     1AMAT(MNEL+NE+3,MNEJ)
     1-SIGM2*SIP12+SIPD1
     AMAT(MNEL+NE+3,MNEL)=-SIGM1*SIP31+
     1AMAT(MNEL+NE+3,MNEL)
     1-SIGM2*SIP32+SIPD3
     AMAT(MNEL+NE+3,MNEL+1)=-SIGM1*SIP41+
     1AMAT(MNEL+NE+3,MNEL+1)-SIGM2*SIP42+SIPD4
945  CONTINUE
     RETURN
     END

     SUBROUTINE SING1(MNEL,MNEJ,SID,NTOT)
c    ****************************************************
c    CALCULATES dR(L)/Da MATRIX, SINGULARITY (I=J)
c    ****************************************************
     IMPLICIT REAL*8(A-H,O-Z)
     COMMON / PRIP / RHOS(500,1),ZS(500,1),
     1HQS(500)
     COMMON/BOEL/SIGM(500)
```

```
      COMMON/WIR/ A, B
      COMMON / MON /NIPT,RFAC,NBLA,NPTP
      COMMON/BC/IBEG(500),IEND(500),BEG(500),EXIT(500)
      COMMON/FRON/NP,NE,NELL,NH,NPL,HNOZ,NNOZ
      COMMON/FE/QQ(600),QK(600),AMAT(600,600),RHS(600,2),
     1X(500),R(500),DETV(500),IDETV(500),DXOLD(500)
      COMMON/OTHER/EPSI,ITMAX,H,IDROP,NPARA,VOL,PI
      COMMON/GEL/G,HBP
      COMMON/INO/IN1
      COMMON/BOEL2/NT,NB,NBT,NRS,IEP,DBP,RDBP,ZKLL,
     1ZKLP,ZSUM
      COMMON/TET/THETA(500,1)
      COMMON/PHI2/PHI2(2),PHIX2(2),PHICE2(4,13)
      COMMON/MOOR/VOLT(500),FCODE(500)
      DIMENSION XLOC(2),ALPHA(2),RLOC(2),ESTIFM(2,2),
     *PSI(2),DPSI(2),GAUS(4),WE(4),GSPEC(4),WSPEC(4)
C
      SIGM1=SIGM(MNEJ)
      SIGM2=SIGM(MNEJ+1)
      IF(FCODE(MNEJ).EQ.2.)THEN
      SIGM1=0.0
      SIGM2=0.0
      ENDIF
      ZNR=(ZS(MNEJ+1,1)-ZS(MNEJ,1))/HQS(MNEJ)
      ZNZ=(RHOS(MNEJ,1)-RHOS(MNEJ+1,1))/HQS(MNEJ)

      GSPEC(1)=0.04144848
      GSPEC(2)=0.24527491
      GSPEC(3)=0.55616545
      GSPEC(4)=0.84898239
      WSPEC(1)=-0.3834641
      WSPEC(2)=-0.3868753
      WSPEC(3)=-0.1904351
      WSPEC(4)=-0.0392255
      GAUS(4)=0.930565
      GAUS(3)=0.669994
      GAUS(2)=0.33003
      GAUS(1)=0.069435
      WE(1)=0.34785/2.
      WE(2)=0.65214/2.
      WE(3)=WE(2)
      WE(4)=WE(1)
      PI=3.1415926535898
      PIF=1./(4.*PI)
      STIP=0.
      NELL=MNEJ
```

```
      DO 10 I=1,2
      RLOC(I)=0.0
      DO 10 J=1,2
10    ESTIFM(I,J)=0.0
c
      DO 20 I=1,2
      LI=NELL-1+I
      XLOC(I)=X(LI)
20    ALPHA(I)=QQ(LI)
      DX=XLOC(2)-XLOC(1)
      ZNE=QQ(NP)
      SIPD1=0.0
      SIPD2=0.0
      SIPD3=0.0
      SIPD4=0.0
      SIP32=0.
      SIP31=0.0
      SIP41=0.
      SIP42=0.0
      SIP11=0.
      SIP12=0.0
      SIP21=0.
      SIP22=0.0
      SID=0.
      HICC=0.0
      DO 150 NGP=1,4
      FU1=1.-GAUS(NGP)
      FU2=1.-FU1
      VOLTA=VOLT(MNEJ)*FU1+VOLT(MNEJ+1)*FU2
      TH=0.0
      F=0.0
      FCR=0.0
      FCZ=0.0
      THPSI=0.0
      THMM=X(MNEL)
      RHOP=RHOS(MNEL,1)
      IF(RHOP.LT.0.0)RHOP=0.0
      Z=ZS(MNEL,1)
      ZSP=ZS(MNEJ,1)*FU1+ZS(MNEJ+1,1)*FU2
      RSP=RHOS(MNEJ,1)*FU1+RHOS(MNEJ+1,1)*FU2
      IF(RSP.LT.0.0)RSP=0.0
      THETRO= XLOC(1)*(1.-GAUS(NGP))+XLOC(2)*GAUS(NGP)
      THETRP= XLOC(2)-XLOC(1)
      DROF1=(1.-GAUS(NGP))*SIN(X(MNEJ))
      DROF2=GAUS(NGP)*SIN(X(MNEJ+1))
      DROFP1=-SIN(X(MNEJ))
      DROFP2=SIN(X(MNEJ+1))
```

```
      DZDFP1=-COS(X(MNEJ))
      DZDFP2=COS(X(MNEJ+1))
      DZDF1=(1.-GAUS(NGP))*COS(X(MNEJ))
      DZDF2=GAUS(NGP)*COS(X(MNEJ+1))
      DRMF1=SIN(THMM)
      DRMF2=0.0
      DZMF1=COS(THMM)
      DZMF2=0.0
      DFFDZ=ALPHA(2)-ALPHA(1)
      DFDO=ALPHA(1)*(1.-GAUS(NGP))
     1+ALPHA(2)*GAUS(NGP)
      FCR=RHOS(MNEJ+1,1)-RHOS(MNEJ,1)
      FCZ=ZS(MNEJ+1,1)-ZS(MNEJ,1)
      IF(MNEJ.GT.NE)GOTO 912
      DEDRZ1=(FCR**2+FCZ**2)**(-0.5)*(FCR*DROFP1
     1+FCZ*DZDFP1)
      DEDRZ2=(FCR**2+FCZ**2)**(-0.5)*(FCR*DROFP2
     1+FCZ*DZDFP2)
  912 ZBOT=(Z-ZSP)**2+(RHOP+RSP)**2
      NTTE=NE
      SIGMA=FU1*SIGM1+FU2*SIGM2
      IF(MNEJ.GT.NTTE)GOTO 945
      S1=SIN(XLOC(1))
      S2=SIN(XLOC(2))
      CO1=COS(XLOC(1))
      CO2=COS(XLOC(2))
      DXDA=-4.*(RHOP*DROF1+DRMF1*RSP)/ZBOT
     1+8.*RHOP*RSP*
     1((Z-ZSP)*(DZMF1-DZDF1)+(RHOP+RSP)
     1*(DRMF1+DROF1))/
     1ZBOT**2
      DXDA2=-4.*(RHOP*DROF2+DRMF2*RSP)/ZBOT
     1+8.*RHOP*RSP*
     1((Z-ZSP)*(DZMF2-DZDF2)+(RHOP+RSP)*
     1 (DRMF2+DROF2))/
     1ZBOT**2
      DZBOT=2.*((Z-ZSP)*(DZMF1-DZDF1)+(RHOP+RSP)
     1*(DRMF1+DROF1))
      DZBOT2=2.*((Z-ZSP)*(DZMF2-DZDF2)+(RHOP+RSP)
     1*(DRMF2+DROF2))
      ZK=4.*RHOP*RSP/ZBOT
      ZKV=SQRT(4./ZBOT)
      ZKE=-ZBOT**(-1.5)*DZBOT
      ZKE2=-ZBOT**(-1.5)*DZBOT2
      Z2=ZS(MNEJ+1,1)
```

```
Z1=ZS(MNEJ,1)
R2=RHOS(MNEJ+1,1)
R1=RHOS(MNEJ,1)
DXDSF1=-2*((R2-R1)*S1+(Z2-Z1)*CO1)/ZBOT-HQS(MNEJ)*
1DZBOT/ZBOT**2
DXDSF2=2*((R2-R1)*S2+(Z2-Z1)*CO2)/ZBOT-HQS(MNEJ)*
1DZBOT2/ZBOT**2
ZTOP=ZBOT/HQS(MNEJ)
ZD=(Z-ZSP)
AQ=RHOP**2+ZD**2+RSP**2
BQ=2.*RHOP*RSP
REST=(LOG((R2-R1)**2+(Z2-Z1)**2)-LOG(AQ+BQ))
IF(MNEL.EQ.1)THEN
REST=0.0
DXDA=0.0
DXDA2=0.0
ENDIF
CALL VKR(ZK,FKE,DXDA,GKE,REST)
SIP11=FU1*(1./(4.*PI)*2.*
1WE(NGP)*(ZKE*RSP*FKE+
1DROF1
1*ZKV*FKE+ZKV*RSP*GKE)*SQRT(FCR**2+FCZ**2)+
11./(4.*PI)*2.0*
1WE(NGP)*ZKV*
1RSP*FKE*DEDRZ1)+SIP11
SIP12=FU2*(1./(4.*PI)*2.*
1WE(NGP)*(ZKE*RSP*FKE+
1DROF1
1*ZKV*FKE+ZKV*RSP*GKE)*SQRT(FCR**2+FCZ**2)+
11./(4.*PI)*2.0*
1WE(NGP)*ZKV*
1RSP*FKE*DEDRZ1)+SIP12
CALL VKR(ZK,FKE,DXDA2,GKE,REST)
SIP21=FU1*(1./(4.*PI)*2.*
1WE(NGP)*(ZKE2*RSP*FKE+
1DROF2
1*ZKV*FKE+ZKV*RSP*GKE)*SQRT(FCR**2+FCZ**2)+
1 1./(4.*PI)*2.0*
1WE(NGP)*ZKV*
1RSP*FKE*DEDRZ2)+SIP21
SIP22=FU2*(1./(4.*PI)*2.*
1WE(NGP)*(ZKE2*RSP*FKE+
1DROF2
1*ZKV*FKE+ZKV*RSP*GKE)*SQRT(FCR**2+FCZ**2)+
1 1./(4.*PI)*2.0*
1WE(NGP)*ZKV*
```

```
     1RSP*FKE*DEDRZ2)+SIP22
     ZD=-(Z-ZSP)
     A=RHOP**2+RSP**2+ZD**2
     B=2.*RSP*RHOP
     DSQAB1=-1.*((DRMF1+DROF1)*(RHOP+RSP)
     1+(DZMF1-DZDF1)*(Z-ZSP))/
     1((A+B)**1.5)
     DSQAB2=-1.*((DRMF2+DROF2)*(RHOP+RSP)
     1+(DZMF2-DZDF2)*(Z-ZSP))/
     1((A+B)**1.5)
     R1=QQ(MNEJ)*SIN(XLOC(1))
     R2=QQ(MNEJ+1)*SIN(XLOC(2))
     Z1=QQ(MNEJ)*COS(XLOC(1))
     Z2=QQ(MNEJ+1)*COS(XLOC(2))
     RDEN=SQRT((R2-R1)**2+(Z2-Z1)**2)
     S1=SIN(XLOC(1))
     S2=SIN(XLOC(2))
     CO1=COS(XLOC(1))
     CO2=COS(XLOC(2))
     ABH=SQRT(A+B)
     DZNRF1=((Z2-Z1)/RDEN**3.0*((R2-R1)*S1+(Z2-Z1)
* 1*CO1)-CO1/RDEN)
     DZNRF2=(-(Z2-Z1)/RDEN**3.0*((R2-R1)*S2+(Z2-Z1)
     1*CO2)+CO2/RDEN)
     DZNZF1=-((R2-R1)/RDEN**3.0*((R2-R1)*S1+(Z2-Z1)
     1*CO1)-S1/RDEN)
     DZNZF2=-(-(R2-R1)/RDEN**3.0*((R2-R1)*S2+(Z2-Z1)
     1*CO2)+S2/RDEN)

     DC1D1=2.*ZNR/RSP*DSQAB1+2.*DZNRF1/RSP/ABH-2.*ZNR
     1 /RSP**2*DROF1/ABH
     DC1D2=2.*ZNR/RSP*DSQAB2+2.*DZNRF2/RSP/ABH-2.*ZNR
     1 /RSP**2*DROF2/ABH
     C1=2.*ZNR/RSP/ABH
     AMB=A-B
     C2=4.*ZNR*(RSP-RHOP)/ABH/AMB
     C3=4.*ZNZ*ZD/ABH/AMB
     DABD1=-2.*((RHOP-RSP)*(DRMF1-DROF1)+(Z-ZSP)
     1*(DZMF1-DZDF1))/
     1AMB**2
     DABD2=-2.*((RHOP-RSP)*(DRMF2-DROF2)+(Z-ZSP)
     1*(DZMF2-DZDF2))/
     1AMB**2
     DC2D1=4.*(ZNR*((DROF1-DRMF1)/(ABH*AMB)
     1+(RSP-RHOP)*(DSQAB1/
```

```
1AMB
1 +DABD1/ABH))+(RSP-RHOP)/AMB/ABH*DZNRF1)
DC2D2=4.*(ZNR*((DROF2-DRMF2)/(ABH*AMB)
1+(RSP-RHOP)*(DSQAB2/
1AMB
1 +DABD2/ABH))+(RSP-RHOP)/AMB/ABH*DZNRF2)
DC3D1=4.*(ZNZ*((DZDF1-DZMF1)/AMB/ABH
1+(DSQAB1/AMB
1 +DABD1/ABH)*ZD)+ZD/AMB/ABH*DZNZF1)
DC3D2=4.*(ZNZ*((DZDF2-DZMF2)/AMB/ABH
1+(DSQAB2/AMB
1 +DABD2/ABH)*ZD)+ZD/AMB/ABH*DZNZF2)
CALL VK2R(ZK,FKE2,DXDA,GKE2,REST)
DJOC=SQRT(FCZ**2+FCR**2)
SIPD1=((DC1D1*(FKE2-FKE)+C1*(GKE2-GKE)-
1(DC2D1*FKE2+C2*GKE2)
1 -DC3D1*FKE2-C3*GKE2)*WE(NGP)*PIF*DJOC*RSP+
1 PIF*(2.*ZNR/(RSP*SQRT(A+B))*(FKE2-FKE)-
1 4.*(RSP-RHOP)*ZNR/(SQRT(A+B)*(A-B))*FKE2-
1 4.*ZNZ*ZD/((A-B)*SQRT(A+B))*FKE2)*WE(NGP)
1 *DEDRZ1*RSP+DROF1*PIF*WE(NGP)*
1 (C1*(FKE2-FKE)-C2*FKE2-C3*FKE2)*DJOC)*VOLTA+SIPD1
1 -((DC1D1*(FKE2-FKE)+C1*(GKE2-GKE)-(DC2D1*FKE2+
1C2*GKE2)
1 -DC3D1*FKE2-C3*GKE2)*WE(NGP)*PIF*DJOC*RSP+
1 PIF*(2.*ZNR/(RSP*SQRT(A+B))*(FKE2-FKE)-
1 4.*(RSP-RHOP)*ZNR/(SQRT(A+B)*(A-B))*FKE2-
1 4.*ZNZ*ZD/((A-B)*SQRT(A+B))*FKE2)*WE(NGP)
1 *DEDRZ1*RSP+DROF1*PIF*WE(NGP)*
1 (C1*(FKE2-FKE)-C2*FKE2-C3*FKE2)*DJOC)*VOLT(MNEL)
CALL VK2R(ZK,FKE2,DXDA2,GKE2,REST)
SIPD2=((DC1D2*(FKE2-FKE)+C1*(GKE2-GKE)-(DC2D2*
1FKE2+C2*GKE2)
1 -DC3D2*FKE2-C3*GKE2)*WE(NGP)*PIF*DJOC*RSP+
1 PIF*(2.*ZNR/(RSP*SQRT(A+B))*(FKE2-FKE)-
1 4.*(RSP-RHOP)*ZNR/(SQRT(A+B)*(A-B))*FKE2-
1 4.*ZNZ*ZD/((A-B)*SQRT(A+B))*FKE2)*WE(NGP)
1 *DEDRZ2*RSP+DROF2*PIF*WE(NGP)*
1 (C1*(FKE2-FKE)-C2*FKE2-C3*FKE2)*DJOC)*VOLTA+SIPD2
1 -((DC1D2*(FKE2-FKE)+C1*(GKE2-GKE)-(DC2D2*FKE2
1+C2*GKE2)
1 -DC3D2*FKE2-C3*GKE2)*WE(NGP)*PIF*DJOC*RSP+
1 PIF*(2.*ZNR/(RSP*SQRT(A+B))*(FKE2-FKE)-
1 4.*(RSP-RHOP)*ZNR/(SQRT(A+B)*(A-B))*FKE2-
1 4.*ZNZ*ZD/((A-B)*SQRT(A+B))*FKE2)*WE(NGP)
```

```
     1 *DEDRZ2*RSP+DROF2*PIF*WE(NGP)*
     1 (C1*(FKE2-FKE)-C2*FKE2-C3*FKE2)*DJOC)*VOLT(MNEL)

      GIP1=GSPEC(NGP)
      FU1=1.-GIP1
      FU2=1.-FU1
      VOLTA=VOLT(MNEJ)*FU1+VOLT(MNEJ+1)*FU2
      TH=0.0
      F=0.0
      FCR=0.0
      FCZ=0.0
      THPSI=0.0
      THMM=X(MNEL)
      RHOP=RHOS(MNEL,1)
      IF(RHOP.LT.0.0)RHOP=0.0
      Z=ZS(MNEL,1)
      ZSP=ZS(MNEJ,1)*FU1+ZS(MNEJ+1,1)*FU2
      RSP=RHOS(MNEJ,1)*FU1+RHOS(MNEJ+1,1)*FU2
      IF(RSP.LT.0.0)RSP=0.0
      THETRO= XLOC(1)*(1.-GIP1)+XLOC(2)*GIP1
      THETRP= XLOC(2)-XLOC(1)
      DROF1=(1.-GIP1)*SIN(X(MNEJ))
      DROF2=GIP1*SIN(X(MNEJ+1))
      DROFP1=-SIN(X(MNEJ))
      DROFP2=SIN(X(MNEJ+1))
      DZDFP1=-COS(X(MNEJ))
      DZDFP2=COS(X(MNEJ+1))
      DZDF1=(1.-GIP1)*COS(X(MNEJ))
      DZDF2=GIP1*COS(X(MNEJ+1))
      DRMF1=SIN(THMM)
      DRMF2=0.0
      DZMF1=COS(THMM)
      DZMF2=0.0
      DFFDZ=ALPHA(2)-ALPHA(1)
      DFDO=ALPHA(1)*(1.-GIP1)
     1+ALPHA(2)*GIP1
      FCR=RHOS(MNEJ+1,1)-RHOS(MNEJ,1)
      FCZ=ZS(MNEJ+1,1)-ZS(MNEJ,1)
      IF(MNEJ.GT.NE)GOTO 1912
      DEDRZ1=(FCR**2+FCZ**2)**(-0.5)*(FCR*DROFP1
     1+FCZ*DZDFP1)
      DEDRZ2=(FCR**2+FCZ**2)**(-0.5)*(FCR*DROFP2
     1+FCZ*DZDFP2)
1912  ZBOT=(Z-ZSP)**2+(RHOP+RSP)**2
      NTTE=NE
      SIGMA=FU1*SIGM1+FU2*SIGM2
```

```
IF(MNEJ.GT.NTTE)GOTO 945
S1=SIN(XLOC(1))
S2=SIN(XLOC(2))
CO1=COS(XLOC(1))
CO2=COS(XLOC(2))
DXDA=-4.*(RHOP*DROF1+RSP*DRMF1)/ZBOT
1+8.*RHOP*RSP*
1((Z-ZSP)*(DZMF1-DZDF1)+(RHOP+RSP)*(DRMF1
1+DROF1))/
1ZBOT**2
DXDA2=-4.*(RHOP*DROF2+RSP*DRMF2)/ZBOT
1+8.*RHOP*RSP*
1((Z-ZSP)*(DZMF2-DZDF2)+(RHOP+RSP)*(DRMF2+DROF2))/
1ZBOT**2
DZBOT=2.*((Z-ZSP)*(DZMF1-DZDF1)+(RHOP+RSP)*
1(DRMF1+DROF1))
DZBOT2=2.*((Z-ZSP)*(DZMF2-DZDF2)+(RHOP+RSP)*
1(DRMF2+DROF2))
ZK=4.*RHOP*RSP/ZBOT
ZKV=SQRT(4./ZBOT)
ZKE=-ZBOT**(-1.5)*DZBOT
ZKE2=-ZBOT**(-1.5)*DZBOT2
Z2=ZS(MNEJ+1,1)
Z1=ZS(MNEJ,1)
R2=RHOS(MNEJ+1,1)
R1=RHOS(MNEJ,1)
DXDSF1=-2*((R2-R1)*S1+(Z2-Z1)*CO1)/ZBOT-HQS(MNEJ)*
1DZBOT/ZBOT**2
DXDSF2=2*((R2-R1)*S2+(Z2-Z1)*CO2)/ZBOT-HQS(MNEJ)*
1DZBOT2/ZBOT**2
ZTOP=ZBOT/HQS(MNEJ)
CALL VKS(ZK,FKE,DXDA,GKE)
IF(MNEL.EQ.1)THEN
FKE=0.0
GKE=0.0
ENDIF
SIP11=FU1*(1./(4.*PI)*2.*
1WSPEC(NGP)*(ZKE*RSP*FKE+
1DROF1
1*ZKV*FKE+ZKV*RSP*GKE)*SQRT(FCR**2+FCZ**2)+
11./(4.*PI)*2.0*
1WSPEC(NGP)*ZKV*
1RSP*FKE*DEDRZ1)+SIP11
SIP12=FU2*(1./(4.*PI)*2.*
1WSPEC(NGP)*(ZKE*RSP*FKE+
```

```
1DROF1
1*ZKV*FKE+ZKV*RSP*GKE)*SQRT(FCR**2+FCZ**2)+
11./(4.*PI)*2.0*
1WSPEC(NGP)*ZKV*
1RSP*FKE*DEDRZ1)+SIP12
CALL VKS(ZK,FKE,DXDA2,GKE)
IF(MNEL.EQ.1)THEN
FKE=0.0
GKE=0.0
ENDIF
SIP21=FU1*(1./(4.*PI)*2.*
1WSPEC(NGP)*(ZKE2*RSP*FKE+
1DROF2
1*ZKV*FKE+ZKV*RSP*GKE)*SQRT(FCR**2+FCZ**2)+
1 1./(4.*PI)*2.0*
1WSPEC(NGP)*ZKV*
1RSP*FKE*DEDRZ2)+SIP21
SIP22=FU2*(1./(4.*PI)*2.*
1WSPEC(NGP)*(ZKE2*RSP*FKE+
1DROF2
1*ZKV*FKE+ZKV*RSP*GKE)*SQRT(FCR**2+FCZ**2)+
1 1./(4.*PI)*2.0*
1WSPEC(NGP)*ZKV*
1RSP*FKE*DEDRZ2)+SIP22
ZD=-(Z-ZSP)
A=RHOP**2+RSP**2+ZD**2
B=2.*RSP*RHOP
DSQAB1=-1.*((DRMF1+DROF1)*(RHOP+RSP)+
1(DZMF1-DZDF1)*(Z-ZSP))/
1((A+B)**1.5)
DSQAB2=-1.*((DRMF2+DROF2)*(RHOP+RSP)+
1(DZMF2-DZDF2)*(Z-ZSP))/
1((A+B)**1.5)
R1=QQ(MNEJ)*SIN(XLOC(1))
R2=QQ(MNEJ+1)*SIN(XLOC(2))
Z1=QQ(MNEJ)*COS(XLOC(1))
Z2=QQ(MNEJ+1)*COS(XLOC(2))
RDEN=SQRT((R2-R1)**2+(Z2-Z1)**2)
S1=SIN(XLOC(1))
S2=SIN(XLOC(2))
CO1=COS(XLOC(1))
CO2=COS(XLOC(2))
ABH=SQRT(A+B)
DZNRF1=((Z2-Z1)/RDEN**3.0*((R2-R1)*S1+
1(Z2-Z1)*CO1)-CO1/RDEN)
```

```
DZNRF2=(-(Z2-Z1)/RDEN**3.0*((R2-R1)*S2+
1(Z2-Z1)*CO2)+CO2/RDEN)
DZNZF1=-((R2-R1)/RDEN**3.0*((R2-R1)*S1+
1(Z2-Z1)*CO1)-S1/RDEN)
DZNZF2=-(-(R2-R1)/RDEN**3.0*((R2-R1)*S2+
1(Z2-Z1)*CO2)+S2/RDEN)

DC1D1=2.*ZNR/RSP*DSQAB1+2.*DZNRF1/RSP/ABH-2.*ZNR
1 /RSP**2*DROF1/ABH
DC1D2=2.*ZNR/RSP*DSQAB2+2.*DZNRF2/RSP/ABH-2.*ZNR
1 /RSP**2*DROF2/ABH
C1=2.*ZNR/RSP/ABH
AMB=A-B
C2=4.*ZNR*(RSP-RHOP)/ABH/AMB
C3=4.*ZNZ*ZD/ABH/AMB
DABD1=-2.*((RHOP-RSP)*(DRMF1-DROF1)+(Z-ZSP)
1*(DZMF1-DZDF1))/
1AMB**2
DABD2=-2.*((RHOP-RSP)*(DRMF2-DROF2)+(Z-ZSP)*
1(DZMF2-DZDF2))/
1AMB**2
DC2D1=4.*(ZNR*((DROF1-DRMF1)/(ABH*AMB)+
1(RSP-RHOP)*(DSQAB1/
1AMB
1 +DABD1/ABH))+(RSP-RHOP)/AMB/ABH*DZNRF1)
DC2D2=4.*(ZNR*((DROF2-DRMF2)/(ABH*AMB)+
1(RSP-RHOP)*(DSQAB2/
1AMB
1 +DABD2/ABH))+(RSP-RHOP)/AMB/ABH*DZNRF2)
DC3D1=4.*(ZNZ*((DZDF1-DZMF1)/AMB/ABH+(DSQAB1/AMB
1 +DABD1/ABH)*ZD)+ZD/AMB/ABH*DZNZF1)
DC3D2=4.*(ZNZ*((DZDF2-DZMF2)/AMB/ABH+(DSQAB2/AMB
1 +DABD2/ABH)*ZD)+ZD/AMB/ABH*DZNZF2)
CALL VK2S(ZK,FKE2,DXDA,GKE2)
IF(MNEL.EQ.1)THEN
FKE2=0.0
GKE2=0.0
ENDIF
DJOC=SQRT(FCZ**2+FCR**2)
SIPD1=((DC1D1*(FKE2-FKE)+C1*(GKE2-GKE)-
1(DC2D1*FKE2+C2*GKE2)
1 -DC3D1*FKE2-C3*GKE2)*WSPEC(NGP)*PIF*DJOC*RSP+
1 PIF*(2.*ZNR/(RSP*SQRT(A+B))*(FKE2-FKE)-
1 4.*(RSP-RHOP)*ZNR/(SQRT(A+B)*(A-B))*FKE2-
1 4.*ZNZ*ZD/((A-B)*SQRT(A+B))*FKE2)*WSPEC(NGP)
1 *DEDRZ1*RSP+DROF1*PIF*WSPEC(NGP)*
```

```
     1 (C1*(FKE2-FKE)-C2*FKE2-C3*FKE2)*DJOC)*VOLTA+SIPD1
     1 -((DC1D1*(FKE2-FKE)+C1*(GKE2-GKE)-(DC2D1*FKE2
     1+C2*GKE2)
     1 -DC3D1*FKE2-C3*GKE2)*WSPEC(NGP)*PIF*DJOC*RSP+
     1 PIF*(2.*ZNR/(RSP*SQRT(A+B))*(FKE2-FKE)-
     1 4.*(RSP-RHOP)*ZNR/(SQRT(A+B)*(A-B))*FKE2-
     1 4.*ZNZ*ZD/((A-B)*SQRT(A+B))*FKE2)*WSPEC(NGP)
     1 *DEDRZ1*RSP+DROF1*PIF*WSPEC(NGP)*
     1 (C1*(FKE2-FKE)-C2*FKE2-C3*FKE2)*DJOC)*VOLT(MNEL)
     CALL VK2S(ZK,FKE2,DXDA2,GKE2)
     IF(MNEL.EQ.1)THEN
     FKE2=0.0
     GKE2=0.0
     ENDIF
     SIPD2=((DC1D2*(FKE2-FKE)+C1*(GKE2-GKE)-
     1(DC2D2*FKE2+C2*GKE2)
     1 -DC3D2*FKE2-C3*GKE2)*WSPEC(NGP)*PIF*DJOC*RSP+
     1 PIF*(2.*ZNR/(RSP*SQRT(A+B))*(FKE2-FKE)-
     1 4.*(RSP-RHOP)*ZNR/(SQRT(A+B)*(A-B))*FKE2-
     1 4.*ZNZ*ZD/((A-B)*SQRT(A+B))*FKE2)*WSPEC(NGP)
     1 *DEDRZ2*RSP+DROF2*PIF*WSPEC(NGP)*
     1 (C1*(FKE2-FKE)-C2*FKE2-C3*FKE2)*DJOC)*VOLTA+SIPD2
     1 -((DC1D2*(FKE2-FKE)+C1*(GKE2-GKE)-(DC2D2*FKE2
     1+C2*GKE2)
     1 -DC3D2*FKE2-C3*GKE2)*WSPEC(NGP)*PIF*DJOC*RSP+
     1 PIF*(2.*ZNR/(RSP*SQRT(A+B))*(FKE2-FKE)-
     1 4.*(RSP-RHOP)*ZNR/(SQRT(A+B)*(A-B))*FKE2-
     1 4.*ZNZ*ZD/((A-B)*SQRT(A+B))*FKE2)*WSPEC(NGP)
     1 *DEDRZ2*RSP+DROF2*PIF*WSPEC(NGP)*
     1 (C1*(FKE2-FKE)-C2*FKE2-C3*FKE2)*DJOC)*VOLT(MNEL)
1550 CONTINUE
1555 CONTINUE

150  CONTINUE

140  AMAT(MNEL+NE+3,MNEJ+1)=-SIGM1*SIP21+
     1AMAT(MNEL+NE+3,MNEJ+1)
     1-SIGM2*SIP22+SIPD2
     AMAT(MNEL+NE+3,MNEJ)=-SIGM1*SIP11+
     1AMAT(MNEL+NE+3,MNEJ)
     1-SIGM2*SIP12+SIPD1
     AMAT(MNEL+NE+3,MNEL)=-SIGM1*SIP31+
     1AMAT(MNEL+NE+3,MNEL)
     1-SIGM2*SIP32+SIPD3
     AMAT(MNEL+NE+3,MNEL+1)=-SIGM1*SIP41+
     1AMAT(MNEL+NE+3,MNEL+1)-SIGM2*SIP42+SIPD4
```

```
945     CONTINUE
        RETURN
        END


        SUBROUTINE SING2(MNEL,MNEJ,SID,NTOT)
c       ****************************************************
c       CALCULATES dR(L)/Da MATRIX, SINGULARITY (I=J)
c       ****************************************************
        IMPLICIT REAL*8(A-H,O-Z)
        COMMON / PRIP / RHOS(500,1),ZS(500,1),
        1HQS(500)
        COMMON/BOEL/SIGM(500)
        COMMON/WIR/ A, B
        COMMON / MON /NIPT,RFAC,NBLA,NPTP
        COMMON/BC/IBEG(500),IEND(500),BEG(500),EXIT(500)
        COMMON/FRON/NP,NE,NELL,NH,NPL,HNOZ,NNOZ
        COMMON/FE/QQ(600),QK(600),AMAT(600,600),RHS(600,2),
        1X(500),R(500),DETV(500),IDETV(500),DXOLD(500)
        COMMON/OTHER/EPSI,ITMAX,H,IDROP,NPARA,VOL,PI
        COMMON/GEL/G,HBP
        COMMON/INO/IN1
        COMMON/BOEL2/NT,NB,NBT,NRS,IEP,DBP,RDBP,ZKLL,
        1ZKLP,ZSUM
        COMMON/TET/THETA(500,1)
        COMMON/PHI2/PHI2(2),PHIX2(2),PHICE2(4,13)
        COMMON/MOOR/VOLT(500),FCODE(500)
        DIMENSION XLOC(2),ALPHA(2),RLOC(2),ESTIFM(2,2),
        *PSI(2),DPSI(2),GAUS(4),WE(4),GSPEC(4),WSPEC(4)
c
        ZNR=(ZS(MNEJ+1,1)-ZS(MNEJ,1))/HQS(MNEJ)
        ZNZ=(RHOS(MNEJ,1)-RHOS(MNEJ+1,1))/HQS(MNEJ)

        SIGM1=SIGM(MNEJ)
        SIGM2=SIGM(MNEJ+1)
        IF(FCODE(MNEJ).EQ.2.)THEN
        SIGM1=0.0
        SIGM2=0.0
        ENDIF
        GSPEC(1)=0.04144848
        GSPEC(2)=0.24527491
        GSPEC(3)=0.55616545
        GSPEC(4)=0.84898239
        WSPEC(1)=-0.3834641
        WSPEC(2)=-0.3868753
        WSPEC(3)=-0.1904351
```

```
      WSPEC(4)=-0.0392255
      GAUS(4)=0.930565
      GAUS(3)=0.669994
      GAUS(2)=0.33003
      GAUS(1)=0.069435
      WE(1)=0.34785/2.
      WE(2)=0.65214/2.
      WE(3)=WE(2)
      WE(4)=WE(1)
      PI=3.1415926535898
      PIF=1./(4.*PI)
      STIP=0.
      NELL=MNEJ
      DO 10 I=1,2
      RLOC(I)=0.0
      DO 10 J=1,2
10    ESTIFM(I,J)=0.0
      C
      DO 20 I=1,2
      LI=NELL-1+I
      XLOC(I)=X(LI)
20    ALPHA(I)=QQ(LI)
      DX=XLOC(2)-XLOC(1)
      ZNE=QQ(NP)
      SIPD1=0.0
      SIPD2=0.0
      SIPD3=0.0
      SIPD4=0.0
      SIP32=0.
      SIP31=0.0
      SIP41=0.
      SIP42=0.0
      SIP11=0.
      SIP12=0.0
      SIP21=0.
      SIP22=0.0
      SID=0.
      HICC=0.0
      DO 150 NGP=1,4
      GIP1=GAUS(NGP)
      FU1=1.-GIP1
      FU2=1.-FU1
      TH=0.0
      F=0.0
      FCR=0.0
      FCZ=0.0
      THPSI=0.0
```

```
      THMM=X(MNEL)
      RHOP=RHOS(MNEL,1)
      IF(RHOP.LT.0.0)RHOP=0.0
      Z=ZS(MNEL,1)
      ZSP=ZS(MNEJ,1)*FU1+ZS(MNEJ+1,1)*FU2
      RSP=RHOS(MNEJ,1)*FU1+RHOS(MNEJ+1,1)*FU2
      IF(RSP.LT.0.0)RSP=0.0
      THETRO= XLOC(1)*(1.-GAUS(NGP))+XLOC(2)*GAUS(NGP)
      THETRP= XLOC(2)-XLOC(1)
      DROF1=(1.-GAUS(NGP))*SIN(X(MNEJ))
      DROF2=GAUS(NGP)*SIN(X(MNEJ+1))
      DROFP1=-SIN(X(MNEJ))
      DROFP2=SIN(X(MNEJ+1))
      DZDFP1=-COS(X(MNEJ))
      DZDFP2=COS(X(MNEJ+1))
      DZDF1=(1.-GAUS(NGP))*COS(X(MNEJ))
      DZDF2=GAUS(NGP)*COS(X(MNEJ+1))
      DRMF1=0.0
      DRMF2=SIN(X(MNEL))
      DZMF1=0.0
      DZMF2=COS(X(MNEL))
      DFFDZ=ALPHA(2)-ALPHA(1)
      DFDO=ALPHA(1)*(1.-GAUS(NGP))
     1+ALPHA(2)*GAUS(NGP)
      FCR=RHOS(MNEJ+1,1)-RHOS(MNEJ,1)
      FCZ=ZS(MNEJ+1,1)-ZS(MNEJ,1)
      IF(MNEJ.GT.NE)GOTO 912
      DEDRZ1=(FCR**2+FCZ**2)**(-0.5)*(FCR*DROFP1
     1+FCZ*DZDFP1)
      DEDRZ2=(FCR**2+FCZ**2)**(-0.5)*(FCR*DROFP2
     1+FCZ*DZDFP2)
  912 ZBOT=(Z-ZSP)**2+(RHOP+RSP)**2
      NTTE=NE
      SIGMA=FU1*SIGM1+FU2*SIGM2
      VOLTA=VOLT(MNEJ)*FU1+VOLT(MNEJ+1)*FU2
      IF(MNEJ.GT.NTTE)GOTO 945
      S1=SIN(XLOC(1))
      S2=SIN(XLOC(2))
      CO1=COS(XLOC(1))
      CO2=COS(XLOC(2))
      DXDA=-4.*(RHOP*DROF1+RSP*DRMF1)/ZBOT
     1+8.*RHOP*RSP*
     1((Z-ZSP)*(DZMF1-DZDF1)+(RHOP+RSP)*(DRMF1+DROF1))/
     1ZBOT**2
      DXDA2=-4.*(RHOP*DROF2+RSP*DRMF2)/ZBOT
```

```
1+8.*RHOP*RSP*
1((Z-ZSP)*(DZMF2-DZDF2)+(RHOP+RSP)*(DRMF2+DROF2))/
1ZBOT**2
DZBOT=2.*((Z-ZSP)*(DZMF1-DZDF1)+(RHOP+RSP)
1*(DRMF1+DROF1))
DZBOT2=2.*((Z-ZSP)*(DZMF2-DZDF2)+(RHOP+RSP)
1*(DRMF2+DROF2))
ZK=4.*RHOP*RSP/ZBOT
ZKV=SQRT(4./ZBOT)
ZKE=-ZBOT**(-1.5)*DZBOT
ZKE2=-ZBOT**(-1.5)*DZBOT2
Z2=ZS(MNEJ+1,1)
Z1=ZS(MNEJ,1)
R2=RHOS(MNEJ+1,1)
R1=RHOS(MNEJ,1)
DXDSF1=-2*((R2-R1)*S1+(Z2-Z1)*CO1)/ZBOT-HQS(MNEJ)*
1DZBOT/ZBOT**2
DXDSF2=2*((R2-R1)*S2+(Z2-Z1)*CO2)/ZBOT-HQS(MNEJ)*
1DZBOT2/ZBOT**2
ZTOP=ZBOT/HQS(MNEJ)
Z2=ZS(MNEJ+1,1)
Z1=ZS(MNEJ,1)
R2=RHOS(MNEJ+1,1)
R1=RHOS(MNEJ,1)
S1=SIN(XLOC(1))
S2=SIN(XLOC(2))
CO1=COS(XLOC(1))
CO2=COS(XLOC(2))
DXDSF1=-2*((R2-R1)*S1+(Z2-Z1)*CO1)/ZBOT-HQS(MNEJ)*
1DZBOT/ZBOT**2
DXDSF2=2*((R2-R1)*S2+(Z2-Z1)*CO2)/ZBOT-HQS(MNEJ)*
1DZBOT2/ZBOT**2
ZTOP=ZBOT/HQS(MNEJ)
ZD=(Z-ZSP)
AQ=RHOP**2+ZD**2+RSP**2
BQ=2.*RHOP*RSP
REST=(LOG((R2-R1)**2+(Z2-Z1)**2)-LOG(AQ+BQ))
IF(MNEL.EQ.NE+NPL+1)REST=0.0
CALL VKR(ZK,FKE,DXDA,GKE,REST)
SIP11=FU1*(1./(4.*PI)*2.*
1WE(NGP)*(ZKE*RSP*FKE+
1DROF1
1*ZKV*FKE+ZKV*RSP*GKE)*SQRT(FCR**2+FCZ**2)+
11./(4.*PI)*2.0*
1WE(NGP)*ZKV*
```

```
1RSP*FKE*DEDRZ1)+SIP11
SIP12=FU2*(1./(4.*PI)*2.*
1WE(NGP)*(ZKE*RSP*FKE+
1DROF1
1*ZKV*FKE+ZKV*RSP*GKE)*SQRT(FCR**2+FCZ**2)+
11./(4.*PI)*2.0*
1WE(NGP)*ZKV*
1RSP*FKE*DEDRZ1)+SIP12
CALL VKR(ZK,FKE,DXDA2,GKE,REST)
SIP21=FU1*(1./(4.*PI)*2.*
1WE(NGP)*(ZKE2*RSP*FKE+
1DROF2
1*ZKV*FKE+ZKV*RSP*GKE)*SQRT(FCR**2+FCZ**2)+
1 1./(4.*PI)*2.0*
1WE(NGP)*ZKV*
1RSP*FKE*DEDRZ2)+SIP21
SIP22=FU2*(1./(4.*PI)*2.*
1WE(NGP)*(ZKE2*RSP*FKE+
1DROF2
1*ZKV*FKE+ZKV*RSP*GKE)*SQRT(FCR**2+FCZ**2)+
1 1./(4.*PI)*2.0*
1WE(NGP)*ZKV*
1RSP*FKE*DEDRZ2)+SIP22
ZD=-(Z-ZSP)
A=RHOP**2+RSP**2+ZD**2
B=2.*RSP*RHOP
DSQAB1=-1.*((DRMF1+DROF1)*(RHOP+RSP)+
1(DZMF1-DZDF1)*(Z-ZSP))/
1((A+B)**1.5)
DSQAB2=-1.*((DRMF2+DROF2)*(RHOP+RSP)+
1(DZMF2-DZDF2)*(Z-ZSP))/
1((A+B)**1.5)
R1=QQ(MNEJ)*SIN(XLOC(1))
R2=QQ(MNEJ+1)*SIN(XLOC(2))
Z1=QQ(MNEJ)*COS(XLOC(1))
Z2=QQ(MNEJ+1)*COS(XLOC(2))
RDEN=SQRT((R2-R1)**2+(Z2-Z1)**2)
S1=SIN(XLOC(1))
S2=SIN(XLOC(2))
CO1=COS(XLOC(1))
CO2=COS(XLOC(2))
ABH=SQRT(A+B)
DZNRF1=((Z2-Z1)/RDEN**3.0*((R2-R1)*S1+(Z2-Z1)*CO1)
1-CO1/RDEN)
DZNRF2=(-(Z2-Z1)/RDEN**3.0*((R2-R1)*S2+(Z2-Z1)*CO2)
```

```
1+CO2/RDEN)
DZNZF1=-((R2-R1)/RDEN**3.0*((R2-R1)*S1+(Z2-Z1)*CO1)
1-S1/RDEN)
DZNZF2=-(-(R2-R1)/RDEN**3.0*((R2-R1)*S2+(Z2-Z1)*CO2)
1+S2/RDEN)


DC1D1=2.*ZNR/RSP*DSQAB1+2.*DZNRF1/RSP/ABH-2.*ZNR
1 /RSP**2*DROF1/ABH
DC1D2=2.*ZNR/RSP*DSQAB2+2.*DZNRF2/RSP/ABH-2.*ZNR
1 /RSP**2*DROF2/ABH
C1=2.*ZNR/RSP/ABH
AMB=A-B
C2=4.*ZNR*(RSP-RHOP)/ABH/AMB
C3=4.*ZNZ*ZD/ABH/AMB
DABD1=-2.*((RHOP-RSP)*(DRMF1-DROF1)+(Z-ZSP)
1*(DZMF1-DZDF1))/
1AMB**2
DABD2=-2.*((RHOP-RSP)*(DRMF2-DROF2)+(Z-ZSP)
1*(DZMF2-DZDF2))/
1AMB**2
DC2D1=4.*(ZNR*((DROF1-DRMF1)/(ABH*AMB)+
1(RSP-RHOP)*(DSQAB1/
1AMB
1 +DABD1/ABH))+(RSP-RHOP)/AMB/ABH*DZNRF1)
DC2D2=4.*(ZNR*((DROF2-DRMF2)/(ABH*AMB)+
1(RSP-RHOP)*(DSQAB2/
1AMB
1 +DABD2/ABH))+(RSP-RHOP)/AMB/ABH*DZNRF2)
DC3D1=4.*(ZNZ*((DZDF1-DZMF1)/AMB/ABH+(DSQAB1/AMB
1 +DABD1/ABH)*ZD)+ZD/AMB/ABH*DZNZF1)
DC3D2=4.*(ZNZ*((DZDF2-DZMF2)/AMB/ABH+(DSQAB2/AMB
1 +DABD2/ABH)*ZD)+ZD/AMB/ABH*DZNZF2)

CALL VK2R(ZK,FKE2,DXDA,GKE2,REST)
DJOC=SQRT(FCZ**2+FCR**2)
SIPD1=((DC1D1*(FKE2-FKE)+C1*(GKE2-GKE)-(DC2D1
*FKE2+C2*GKE2)
1 -DC3D1*FKE2-C3*GKE2)*WE(NGP)*PIF*DJOC*RSP+
1 PIF*(2.*ZNR/(RSP*SQRT(A+B))*(FKE2-FKE)-
1 4.*(RSP-RHOP)*ZNR/(SQRT(A+B)*(A-B))*FKE2-
1 4.*ZNZ*ZD/((A-B)*SQRT(A+B))*FKE2)*WE(NGP)
1 *DEDRZ1*RSP+DROF1*PIF*WE(NGP)*
1 (C1*(FKE2-FKE)-C2*FKE2-C3*FKE2)*DJOC)*VOLTA+SIPD1
1 -((DC1D1*(FKE2-FKE)+C1*(GKE2-GKE)-(DC2D1*FKE2
1+C2*GKE2)
```

```
     1 -DC3D1*FKE2-C3*GKE2)*WE(NGP)*PIF*DJOC*RSP+
     1 PIF*(2.*ZNR/(RSP*SQRT(A+B))*(FKE2-FKE)-
     1 4.*(RSP-RHOP)*ZNR/(SQRT(A+B)*(A-B))*FKE2-
     1 4.*ZNZ*ZD/((A-B)*SQRT(A+B))*FKE2)*WE(NGP)
     1 *DEDRZ1*RSP+DROF1*PIF*WE(NGP)*
     1 (C1*(FKE2-FKE)-C2*FKE2-C3*FKE2)*DJOC)
     1*VOLT(MNEL)
     CALL VK2R(ZK,FKE2,DXDA2,GKE2,REST)
     SIPD2=((DC1D2*(FKE2-FKE)+C1*(GKE2-GKE)-(DC2D2
     1*FKE2+C2*GKE2)
     1 -DC3D2*FKE2-C3*GKE2)*WE(NGP)*PIF*DJOC*RSP+
     1 PIF*(2.*ZNR/(RSP*SQRT(A+B))*(FKE2-FKE)-
     1 4.*(RSP-RHOP)*ZNR/(SQRT(A+B)*(A-B))*FKE2-
     1 4.*ZNZ*ZD/((A-B)*SQRT(A+B))*FKE2)*WE(NGP)
     1 *DEDRZ2*RSP+DROF2*PIF*WE(NGP)*
     1 (C1*(FKE2-FKE)-C2*FKE2-C3*FKE2)*DJOC)*VOLTA+SIPD2
     1 -((DC1D2*(FKE2-FKE)+C1*(GKE2-GKE)-(DC2D2*FKE2
     1+C2*GKE2)
     1 -DC3D2*FKE2-C3*GKE2)*WE(NGP)*PIF*DJOC*RSP+
     1 PIF*(2.*ZNR/(RSP*SQRT(A+B))*(FKE2-FKE)-
     1 4.*(RSP-RHOP)*ZNR/(SQRT(A+B)*(A-B))*FKE2-
     1 4.*ZNZ*ZD/((A-B)*SQRT(A+B))*FKE2)*WE(NGP)
     1 *DEDRZ2*RSP+DROF2*PIF*WE(NGP)*
     1 (C1*(FKE2-FKE)-C2*FKE2-C3*FKE2)*DJOC)*VOLT(MNEL)
550  CONTINUE

     GIP1=1.-GSPEC(NGP)
     FU1=1.-GIP1
     FU2=1.-FU1
     TH=0.0
     F=0.0
     FCR=0.0
     FCZ=0.0
     THPSI=0.0
     THMM=X(MNEL)
     RHOP=RHOS(MNEL,1)
     IF(RHOP.LT.0.0)RHOP=0.0
     Z=ZS(MNEL,1)
     ZSP=ZS(MNEJ,1)*FU1+ZS(MNEJ+1,1)*FU2
     RSP=RHOS(MNEJ,1)*FU1+RHOS(MNEJ+1,1)*FU2
     IF(RSP.LT.0.0)RSP=0.0
     THETRO= XLOC(1)*(1.-GIP1)+XLOC(2)*GIP1
     THETRP= XLOC(2)-XLOC(1)
     DROF1=(1.-GIP1)*SIN(X(MNEJ))
     DROF2=GIP1*SIN(X(MNEJ+1))
```

```
      DROFP1=-SIN(X(MNEJ))
      DROFP2=SIN(X(MNEJ+1))
      DZDFP1=-COS(X(MNEJ))
      DZDFP2=COS(X(MNEJ+1))
      DZDF1=(1.-GIP1)*COS(X(MNEJ))
      DZDF2=GIP1*COS(X(MNEJ+1))
      DRMF1=0.0
      DRMF2=SIN(X(MNEL))
      DZMF1=0.0
      DZMF2=COS(X(MNEL))
      DFFDZ=ALPHA(2)-ALPHA(1)
      DFDO=ALPHA(1)*(1.-GIP1)
     1+ALPHA(2)*GIP1
      FCR=RHOS(MNEJ+1,1)-RHOS(MNEJ,1)
      FCZ=ZS(MNEJ+1,1)-ZS(MNEJ,1)
      IF(MNEJ.GT.NE)GOTO 1912
      DEDRZ1=(FCR**2+FCZ**2)**(-0.5)*(FCR*DROFP1
     1+FCZ*DZDFP1)
      DEDRZ2=(FCR**2+FCZ**2)**(-0.5)*(FCR*DROFP2
     1+FCZ*DZDFP2)
1912  ZBOT=(Z-ZSP)**2+(RHOP+RSP)**2
      NTTE=NE
      SIGMA=FU1*SIGM1+FU2*SIGM2
      VOLTA=VOLT(MNEJ)*FU1+VOLT(MNEJ+1)*FU2
      IF(MNEJ.GT.NTTE)GOTO 945
      S1=SIN(XLOC(1))
      S2=SIN(XLOC(2))
      CO1=COS(XLOC(1))
      CO2=COS(XLOC(2))
      DXDA=-4.*(RHOP*DROF1+RSP*DRMF1)/ZBOT
     1+8.*RHOP*RSP*
     1((Z-ZSP)*(DZMF1-DZDF1)+(RHOP+RSP)*(DRMF1+DROF1))/
     1ZBOT**2
      DXDA2=-4.*(RHOP*DROF2+RSP*DRMF2)/ZBOT+
     18.*RHOP*RSP*
     1((Z-ZSP)*(DZMF2-DZDF2)+(RHOP+RSP)*
     1(DRMF2+DROF2))/
     1ZBOT**2
      DZBOT=2.*((Z-ZSP)*(DZMF1-DZDF1)+(RHOP+RSP)*
     1(DRMF1+DROF1))
      DZBOT2=2.*((Z-ZSP)*(DZMF2-DZDF2)+(RHOP+RSP)
     1*(DRMF2+DROF2))
      ZK=4.*RHOP*RSP/ZBOT
      ZKV=SQRT(4./ZBOT)
      ZKE=-ZBOT**(-1.5)*DZBOT
```

```
ZKE2=-ZBOT**(-1.5)*DZBOT2
Z2=ZS(MNEJ+1,1)
Z1=ZS(MNEJ,1)
R2=RHOS(MNEJ+1,1)
R1=RHOS(MNEJ,1)
DXDSF1=-2*((R2-R1)*S1+(Z2-Z1)*CO1)/ZBOT-HQS(MNEJ)*
1DZBOT/ZBOT**2
DXDSF2=2*((R2-R1)*S2+(Z2-Z1)*CO2)/ZBOT-HQS(MNEJ)*
1DZBOT2/ZBOT**2
ZTOP=ZBOT/HQS(MNEJ)
CALL VKS(ZK,FKE,DXDA,GKE)
IF(MNEL.EQ.NE+NPL+1)THEN
FKE=0.0
GKE=0.0
ENDIF
SIP11=FU1*(1./(4.*PI)*2.*
1WSPEC(NGP)*(ZKE*RSP*FKE+
1DROF1
1*ZKV*FKE+ZKV*RSP*GKE)*SQRT(FCR**2+FCZ**2)+
11./(4.*PI)*2.0*
1WSPEC(NGP)*ZKV*
1RSP*FKE*DEDRZ1)+SIP11
SIP12=FU2*(1./(4.*PI)*2.*
1WSPEC(NGP)*(ZKE*RSP*FKE+
1DROF1
1*ZKV*FKE+ZKV*RSP*GKE)*SQRT(FCR**2+FCZ**2)+
11./(4.*PI)*2.0*
1WSPEC(NGP)*ZKV*
1RSP*FKE*DEDRZ1)+SIP12
CALL VKS(ZK,FKE,DXDA2,GKE)
IF(MNEL.EQ.NE+NPL+1)THEN
FKE=0.0
GKE=0.0
ENDIF
SIP21=FU1*(1./(4.*PI)*2.*
1WSPEC(NGP)*(ZKE2*RSP*FKE+
1DROF2
1*ZKV*FKE+ZKV*RSP*GKE)*SQRT(FCR**2+FCZ**2)+
1 1./(4.*PI)*2.0*
1WSPEC(NGP)*ZKV*
1RSP*FKE*DEDRZ2)+SIP21
SIP22=FU2*(1./(4.*PI)*2.*
1WSPEC(NGP)*(ZKE2*RSP*FKE+
1DROF2
1*ZKV*FKE+ZKV*RSP*GKE)*SQRT(FCR**2+FCZ**2)+
1 1./(4.*PI)*2.0*
```

```
1WSPEC(NGP)*ZKV*
1RSP*FKE*DEDRZ2)+SIP22
ZD=-(Z-ZSP)
A=RHOP**2+RSP**2+ZD**2
B=2.*RSP*RHOP
DSQAB1=-1.*((DRMF1+DROF1)*(RHOP+RSP)+
1(DZMF1-DZDF1)*(Z-ZSP))/
1((A+B)**1.5)
DSQAB2=-1.*((DRMF2+DROF2)*(RHOP+RSP)+
1(DZMF2-DZDF2)*(Z-ZSP))/
1((A+B)**1.5)
R1=QQ(MNEJ)*SIN(XLOC(1))
R2=QQ(MNEJ+1)*SIN(XLOC(2))
Z1=QQ(MNEJ)*COS(XLOC(1))
Z2=QQ(MNEJ+1)*COS(XLOC(2))
RDEN=SQRT((R2-R1)**2+(Z2-Z1)**2)
S1=SIN(XLOC(1))
S2=SIN(XLOC(2))
CO1=COS(XLOC(1))
CO2=COS(XLOC(2))
ABH=SQRT(A+B)
DZNRF1=((Z2-Z1)/RDEN**3.0*((R2-R1)*S1+(Z2-Z1)*CO1)
1-CO1/RDEN)
DZNRF2=(-(Z2-Z1)/RDEN**3.0*((R2-R1)*S2+(Z2-Z1)*CO2)
1+CO2/RDEN)
DZNZF1=-((R2-R1)/RDEN**3.0*((R2-R1)*S1+(Z2-Z1)*CO1)
1-S1/RDEN)
DZNZF2=-(-(R2-R1)/RDEN**3.0*((R2-R1)*S2+(Z2-Z1)*CO2)
1+S2/RDEN)


DC1D1=2.*ZNR/RSP*DSQAB1+2.*DZNRF1/RSP/ABH-2.*ZNR
1 /RSP**2*DROF1/ABH
DC1D2=2.*ZNR/RSP*DSQAB2+2.*DZNRF2/RSP/ABH-2.*ZNR
1 /RSP**2*DROF2/ABH
C1=2.*ZNR/RSP/ABH
AMB=A-B
C2=4.*ZNR*(RSP-RHOP)/ABH/AMB
C3=4.*ZNZ*ZD/ABH/AMB
DABD1=-2.*((RHOP-RSP)*(DRMF1-DROF1)+(Z-ZSP)
1*(DZMF1-DZDF1))/
1AMB**2
DABD2=-2.*((RHOP-RSP)*(DRMF2-DROF2)+(Z-ZSP)*
1(DZMF2-DZDF2))/
1AMB**2
```

```
DC2D1=4.*(ZNR*((DROF1-DRMF1)/(ABH*AMB)+(RSP-RHOP)
1*(DSQAB1/
1AMB
1 +DABD1/ABH))+(RSP-RHOP)/AMB/ABH*DZNRF1)
DC2D2=4.*(ZNR*((DROF2-DRMF2)/(ABH*AMB)+(RSP-RHOP)
1*(DSQAB2/
1AMB
1 +DABD2/ABH))+(RSP-RHOP)/AMB/ABH*DZNRF2)
DC3D1=4.*(ZNZ*((DZDF1-DZMF1)/AMB/ABH+(DSQAB1/AMB
1 +DABD1/ABH)*ZD)+ZD/AMB/ABH*DZNZF1)
DC3D2=4.*(ZNZ*((DZDF2-DZMF2)/AMB/ABH+(DSQAB2/AMB
1 +DABD2/ABH)*ZD)+ZD/AMB/ABH*DZNZF2)
CALL VK2S(ZK,FKE2,DXDA,GKE2)
IF(MNEL.EQ.NE+NPL+1)THEN
FKE2=0.0
GKE2=0.0
ENDIF
DJOC=SQRT(FCZ**2+FCR**2)
SIPD1=((DC1D1*(FKE2-FKE)+C1*(GKE2-GKE)-
1(DC2D1*FKE2+C2*GKE2)
1 -DC3D1*FKE2-C3*GKE2)*WSPEC(NGP)*PIF*DJOC*RSP+
1 PIF*(2.*ZNR/(RSP*SQRT(A+B))*(FKE2-FKE)-
1 4.*(RSP-RHOP)*ZNR/(SQRT(A+B)*(A-B))*FKE2-
1 4.*ZNZ*ZD/((A-B)*SQRT(A+B))*FKE2)*WSPEC(NGP)
1 *DEDRZ1*RSP+DROF1*PIF*WSPEC(NGP)*
1 (C1*(FKE2-FKE)-C2*FKE2-C3*FKE2)*DJOC)*VOLTA+SIPD1
1 -((DC1D1*(FKE2-FKE)+C1*(GKE2-GKE)-(DC2D1*FKE2
1+C2*GKE2)
1 -DC3D1*FKE2-C3*GKE2)*WSPEC(NGP)*PIF*DJOC*RSP+
1 PIF*(2.*ZNR/(RSP*SQRT(A+B))*(FKE2-FKE)-
1 4.*(RSP-RHOP)*ZNR/(SQRT(A+B)*(A-B))*FKE2-
1 4.*ZNZ*ZD/((A-B)*SQRT(A+B))*FKE2)*WSPEC(NGP)
1 *DEDRZ1*RSP+DROF1*PIF*WSPEC(NGP)*
1 (C1*(FKE2-FKE)-C2*FKE2-C3*FKE2)*DJOC)*VOLT(MNEL)
CALL VK2S(ZK,FKE2,DXDA2,GKE2)
IF(MNEL.EQ.NE+NPL+1)THEN
FKE2=0.0
GKE2=0.0
ENDIF
SIPD2=((DC1D2*(FKE2-FKE)+C1*(GKE2-GKE)-(DC2D2*FKE2
+C2*GKE2)
1 -DC3D2*FKE2-C3*GKE2)*WSPEC(NGP)*PIF*DJOC*RSP+
1 PIF*(2.*ZNR/(RSP*SQRT(A+B))*(FKE2-FKE)-
1 4.*(RSP-RHOP)*ZNR/(SQRT(A+B)*(A-B))*FKE2-
1 4.*ZNZ*ZD/((A-B)*SQRT(A+B))*FKE2)*WSPEC(NGP)
```

```
     1 *DEDRZ2*RSP+DROF2*PIF*WSPEC(NGP)*
     1 (C1*(FKE2-FKE)-C2*FKE2-C3*FKE2)*DJOC)*VOLTA+SIPD2
     1 -((DC1D2*(FKE2-FKE)+C1*(GKE2-GKE)-(DC2D2*FKE2
     1+C2*GKE2)
     1 -DC3D2*FKE2-C3*GKE2)*WSPEC(NGP)*PIF*DJOC*RSP+
     1 PIF*(2.*ZNR/(RSP*SQRT(A+B))*(FKE2-FKE)-
     1 4.*(RSP-RHOP)*ZNR/(SQRT(A+B)*(A-B))*FKE2-
     1 4.*ZNZ*ZD/((A-B)*SQRT(A+B))*FKE2)*WSPEC(NGP)
     1 *DEDRZ2*RSP+DROF2*PIF*WSPEC(NGP)*
     1 (C1*(FKE2-FKE)-C2*FKE2-C3*FKE2)*DJOC)*VOLT(MNEL)

150  CONTINUE


140  AMAT(MNEL+NE+3,MNEJ+1)=-SIGM1*SIP21+
     1AMAT(MNEL+NE+3,MNEJ+1)
     1-SIGM2*SIP22+SIPD2
     AMAT(MNEL+NE+3,MNEJ)=-SIGM1*SIP11
     1+AMAT(MNEL+NE+3,MNEJ)
     1-SIGM2*SIP12+SIPD1
     AMAT(MNEL+NE+3,MNEL)=-SIGM1*SIP31
     1+AMAT(MNEL+NE+3,MNEL)
     1-SIGM2*SIP32+SIPD3
     AMAT(MNEL+NE+3,MNEL+1)=-SIGM1*SIP41+
     1AMAT(MNEL+NE+3,MNEL+1)-SIGM2*SIP42+SIPD4
945  CONTINUE
     RETURN
     END


     SUBROUTINE ABFIN4(MNEL,MNEJ,SID,NTOT,SIDP,SIDW)
c    ************************************************
c    CALCULATES dR(L)/dSIGMA MATRIX
c    ************************************************
     IMPLICIT REAL*8(A-H,O-Z)
     COMMON / PRIP / RHOS(500,1),ZS(500,1),
     1HQS(500)
     COMMON/BOEL/SIGM(500)
     COMMON/WIR/ A, B
     COMMON / MON /NIPT,RFAC,NBLA,NPTP
     COMMON/BC/IBEG(500),IEND(500),BEG(500),EXIT(500)
     COMMON/FRON/NP,NE,NELL,NH,NPL,HNOZ,NNOZ
     COMMON/FE/QQ(600),QK(600),AMAT(600,600),RHS(600,2),
     1X(500),R(500),DETV(500),IDETV(500),DXOLD(500)
     COMMON/OTHER/EPSI,ITMAX,H,IDROP,NPARA,VOL,PI
```

```
      COMMON/GEL/G,HBP
      COMMON/INO/IN1
      COMMON/BOEL2/NT,NB,NBT,NRS,IEP,DBP,RDBP,ZKLL,
     1ZKLP,ZSUM
      COMMON/TET/THETA(500,1)
      COMMON/PHI2/PHI2(2),PHIX2(2),PHICE2(4,13)
      COMMON/MOOR/VOLT(500),FCODE(500)
      DIMENSION XLOC(2),ALPHA(2),RLOC(2),ESTIFM(2,2),
     1PSI(2),DPSI(2),GAUS(4),WE(4)
      GAUS(4)=0.930565
      GAUS(3)=0.669994
      GAUS(2)=0.33003
      GAUS(1)=0.069435
      WE(1)=0.34785/2.
      WE(2)=0.65214/2.
      WE(3)=WE(2)
      WE(4)=WE(1)

      PI=3.1415926535898
      PIF=1./(4.*PI)
      SID=0.
      SID11=0.0
      SID12=0.0
      SIP1=0.
      SIP2=0.0
      SIDP=0.0
      SIDW=0.0
      NELL=MNEJ
      ZNR=(ZS(MNEJ+1,1)-ZS(MNEJ,1))/HQS(MNEJ)
      ZNZ=(RHOS(MNEJ,1)-RHOS(MNEJ+1,1))/HQS(MNEJ)
      DO 10 I=1,2
      RLOC(I)=0.0
      DO 10 J=1,2
10    ESTIFM(I,J)=0.0
      DO 20 I=1,2
      LI=NELL-1+I
      XLOC(I)=X(LI)
20    ALPHA(I)=QQ(LI)
      DX=XLOC(2)-XLOC(1)
      ZNE=QQ(NP)
      HICC=0.0
      DO 150 NGP=1,4
      FU1=1.-GAUS(NGP)
      FU2=1.-FU1
      SIGM1=SIGM(MNEJ)
      SIGM2=SIGM(MNEJ+1)
```

```
      IF(FCODE(MNEJ).EQ.2.0)THEN
      SIGM1=0.0
      SIGM2=0.0
      ENDIF
      SIGMA=FU1*SIGM1+FU2*SIGM2
      VOLTA=FU1*VOLT(MNEJ)+FU2*VOLT(MNEJ+1)
      TH=0.0
      F=0.0
      FC=0.0
      DO 30 II=1,2
      TH=TH+PHICE2(II,NGP)*XLOC(II)
      F=F+PHICE2(II,NGP)*ALPHA(II)
30    FC=FC+PHICE2(II+2,NGP)*ALPHA(II)
      DO 35 II=1,2
35    PSI(II)=PHICE2(II,NGP)

      THETRO= XLOC(1)*(1.-GAUS(NGP))+XLOC(2)*GAUS(NGP)
      THETRP= XLOC(2)-XLOC(1)
      DFFDZ=ALPHA(2)-ALPHA(1)
      DFDO=ALPHA(1)*(1.-GAUS(NGP))
     1+ALPHA(2)*GAUS(NGP)
      FCR=RHOS(MNEJ+1,1)-RHOS(MNEJ,1)
      FCZ=ZS(MNEJ+1,1)-ZS(MNEJ,1)
      Z=ZS(MNEL,1)
      RHOP=RHOS(MNEL,1)
      IF(RHOP.LT.0.0)RHOP=0.0
      ZSP=ZS(MNEJ,1)*(1.-GAUS(NGP))+ZS(MNEJ+1,1)
     1*GAUS(NGP)
      RSP=RHOS(MNEJ,1)*(1.-GAUS(NGP))+RHOS(MNEJ+1,1)*
     1GAUS(NGP)
      IF(RSP.LT.0.0)RSP=0.0
      ZBOT=(Z-ZSP)**2+(RHOP+RSP)**2
      ZK=4.*RHOP*RSP/ZBOT
      ZKV=SQRT(4./ZBOT)
      CALL VK(ZK,FKE,DXDA,GKE)
      IF(MNEJ.LE.NE)GOTO 145
      SIP1=FU1*(1./(4.*PI)*2.0*WE(NGP)*HQS(MNEJ)*ZKV*
     1RSP*FKE)+SIP1
      SIP2=FU2*(1./(4.*PI)*2.0*WE(NGP)*HQS(MNEJ)*ZKV*
     1RSP*FKE)+SIP2
      SID=SIGMA*(1./(4.*PI)*2.0*WE(NGP)*HQS(MNEJ)*ZKV*
     1RSP*FKE)+SID
      CALL VK2(ZK,FKE2,DXDA2,GKE2)
      ZD=-(Z-ZSP)
      A=RHOP**2+RSP**2+ZD**2
      B=2.*RSP*RHOP
```

```
      SID11=FU1*RSP*PIF*(2.*ZNR/(RSP*SQRT(A+B))*(FKE2-FKE)
     1 4.*(RSP-RHOP)*ZNR/(SQRT(A+B)*(A-B))*FKE2-
     2 4.*ZNZ*ZD/((A-B)*SQRT(A+B))*FKE2)*WE(NGP)
     3 *HQS(MNEJ)+SID11
      SID12=FU2*RSP*PIF*(2.*ZNR/(RSP*SQRT(A+B))*(FKE2-FKE)
     1 4.*(RSP-RHOP)*ZNR/(SQRT(A+B)*(A-B))*FKE2-
     2 4.*ZNZ*ZD/((A-B)*SQRT(A+B))*FKE2)*WE(NGP)
     3 *HQS(MNEJ)+SID12
      IF(FCODE(MNEJ-1).EQ.1.0.AND.FCODE(MNEJ).EQ.2.)
     1SID11=0.0
      IF(FCODE(MNEJ).EQ.2.0.AND.FCODE(MNEJ+1).EQ.1.)
     1SID12=0.0

      SIDP=VOLTA*RSP*PIF*(2.*ZNR/(RSP*SQRT(A+B))
     1*(FKE2-FKE)-
     1 4.*(RSP-RHOP)*ZNR/(SQRT(A+B)*(A-B))*FKE2-
     2 4.*ZNZ*ZD/((A-B)*SQRT(A+B))*FKE2)*WE(NGP)
     3 *HQS(MNEJ)+SIDP
      SIDW=RSP*PIF*(2.*ZNR/(RSP*SQRT(A+B))*(FKE2-FKE)-
     1 4.*(RSP-RHOP)*ZNR/(SQRT(A+B)*(A-B))*FKE2-
     2 4.*ZNZ*ZD/((A-B)*SQRT(A+B))*FKE2)*WE(NGP)
     3 *HQS(MNEJ)+SIDW

      GOTO 150
  145 CONTINUE
      SIP1=FU1*(1./(4.*PI)*2.0*WE(NGP)*ZKV*
     1RSP*FKE*SQRT(FCR**2+FCZ**2))+SIP1
      SIP2=FU2*(1./(4.*PI)*2.0*WE(NGP)*ZKV*
     1RSP*FKE*SQRT(FCR**2+FCZ**2))+SIP2
      SID=SIGMA*(1./(4.*PI)*2.0*WE(NGP)*ZKV*
     1RSP*FKE*SQRT(FCR**2+FCZ**2))+SID
      CALL VK2(ZK,FKE2,DXDA2,GKE2)
      ZD=-(Z-ZSP)
      A=RHOP**2+RSP**2+ZD**2
      B=2.*RSP*RHOP
      SID11=FU1*RSP*PIF*(2.*ZNR/(RSP*SQRT(A+B))
     1*(FKE2-FKE)-
     1 4.*(RSP-RHOP)*ZNR/(SQRT(A+B)*(A-B))*FKE2-
     2 4.*ZNZ*ZD/((A-B)*SQRT(A+B))*FKE2)*WE(NGP)
     3 *SQRT(FCR**2+FCZ**2)+SID11
      SID12=FU2*RSP*PIF*(2.*ZNR/(RSP*SQRT(A+B))
     1*(FKE2-FKE)-
     1 4.*(RSP-RHOP)*ZNR/(SQRT(A+B)*(A-B))*FKE2-
     2 4.*ZNZ*ZD/((A-B)*SQRT(A+B))*FKE2)*WE(NGP)
     3 *SQRT(FCR**2+FCZ**2)+SID12
```

```
      IF(FCODE(MNEJ-1).EQ.1.0.AND.FCODE(MNEJ).EQ.2.)
     1SID11=0.0
      IF(FCODE(MNEJ).EQ.2.0.AND.FCODE(MNEJ+1).EQ.1.)
     1SID12=0.0

      SIDP=VOLTA*RSP*PIF*(2.*ZNR/(RSP*SQRT(A+B))
     1*(FKE2-FKE)-
     1 4.*(RSP-RHOP)*ZNR/(SQRT(A+B)*(A-B))*FKE2-
     2 4.*ZNZ*ZD/((A-B)*SQRT(A+B))*FKE2)*WE(NGP)
     3 *SQRT(FCR**2+FCZ**2)+SIDP
      SIDW=RSP*PIF*(2.*ZNR/(RSP*SQRT(A+B))*(FKE2-FKE)-
     1 4.*(RSP-RHOP)*ZNR/(SQRT(A+B)*(A-B))*FKE2-
     2 4.*ZNZ*ZD/((A-B)*SQRT(A+B))*FKE2)*WE(NGP)
     3 *SQRT(FCR**2+FCZ**2)+SIDW

150   CONTINUE

      IF(FCODE(MNEJ).EQ.1.)THEN
      AMAT(MNEL+NE+3,MNEJ+NE+3)=-SIP1+
     1AMAT(MNEL+NE+3,MNEJ+NE+3)
      AMAT(MNEL+NE+3,MNEJ+NE+3+1)=-SIP2
      ENDIF

      IF(FCODE(MNEJ).EQ.2)THEN
      AMAT(MNEL+NE+3,MNEJ+NE+3)=SID11+
     1AMAT(MNEL+NE+3,MNEJ+NE+3)
      AMAT(MNEL+NE+3,MNEJ+NE+3+1)=SID12
      ENDIF
      RETURN
      END

C     ************************************************************
C     APPXIMATION FOR ELIPTICAL INTEGRAL
C     ************************************************************
      SUBROUTINE VK(ZK,FKE,GX,GKE)
      IMPLICIT REAL*8(A-H,O-Z)

      A0=1.386294361
      A1=0.097932891
      A2=0.054544409
      A3=0.032024666
      B0=0.5
      B1=0.124750742
      B2=0.060118519
      B3=0.010944912
      ZNU=1.0-ZK
      IF(ZNU.EQ.0.)GOTO 30
```

```
      FKE=A0+A1*ZNU+A2*ZNU**2+A3*ZNU**3-(B0+B1*ZNU
     1+B2*ZNU**2+
     1 B3*ZNU**3)*LOG(ZNU)
      GKE=(A1+2.0*A2*ZNU+3.*A3*ZNU**2
     1 -(B1+2.*B2*ZNU+3.*ZNU**2*B3)*LOG(ZNU)-
     1 1./ZNU*(B0+B1*ZNU+B2*ZNU**2+B3*ZNU**3))*GX
      GOTO 40
30    FKE=A0
40    CONTINUE
      RETURN
      END


c     ************************************************
c     APPXIMATION FOR ELIPTICAL INTEGRAL OF
c     THE SECOND KIND
c     ************************************************
      SUBROUTINE VK2(ZK,FKE,GX,GKE)
      IMPLICIT REAL*8(A-H,O-Z)

      A0=1.000
      A1=0.44325141463
      A2=0.062606060122
      A3=0.04757483546
      A4=0.01746596451
      B1=0.24998368310
      B2=0.09200180037
      B3=0.04069697526
      B4=0.00426449639
      ZNU=1.0-ZK
      IF(ZNU.EQ.0.)GOTO 30
      FKE=A0+A1*ZNU+A2*ZNU**2+A3*ZNU**3+A4*ZNU**4-
     1 (B1*ZNU+B2*ZNU**2+B3*ZNU**3+B4*ZNU**4)*LOG(ZNU)
      GKE=(A1+2.0*A2*ZNU+3.*A3*ZNU**2+4.*A4*ZNU**3
     1 -(B1+2.*B2*ZNU+3.*B3*ZNU**2+4.*B4*ZNU**3)*LOG(ZNU)-
     1 (B1+B2*ZNU+B3*ZNU**2+B4*ZNU**3))*GX
      GOTO 40
30    FKE=A0
40    CONTINUE
      RETURN
      END


c     ***********************************************
c     APPXIMATION FOR ELIPTICAL INTEGRAL
c     OF THE SECOND KIND
c     ***********************************************
      SUBROUTINE VK2R(ZK,FKE,GX,GKE,REST)
```

```
      IMPLICIT REAL*8(A-H,O-Z)

      A0=1.000
      A1=0.44325141463
      A2=0.062606060122
      A3=0.04757483546
      A4=0.01746596451
      B1=0.24998368310
      B2=0.09200180037
      B3=0.04069697526
      B4=0.00426449639
      ZNU=1.0-ZK
      IF(ZNU.EQ.0.)GOTO 30
      FKE=A0+A1*ZNU+A2*ZNU**2+A3*ZNU**3+A4*ZNU**4-
     1 (B1*ZNU+B2*ZNU**2+B3*ZNU**3+B4*ZNU**4)*REST
      GKE=(A1+2.0*A2*ZNU+3.*A3*ZNU**2+4.*A4*ZNU**3
     1 -(B1+2.*B2*ZNU+3.*B3*ZNU**2+4.*B4*ZNU**3)*LOG(ZNU)-
     1 (B1+B2*ZNU+B3*ZNU**2+B4*ZNU**3))*GX
      GOTO 40
30    FKE=A0
40    CONTINUE
      RETURN
      END


c     ********************************************
c     APPXIMATION FOR ELIPTICAL INTEGRAL
c     OF THE SECOND KIND
c     ********************************************
      SUBROUTINE VK2S(ZK,FKE,GX,GKE)
      IMPLICIT REAL*8(A-H,O-Z)

      A0=1.000
      A1=0.44325141463
      A2=0.062606060122
      A3=0.04757483546
      A4=0.01746596451
      B1=0.24998368310
      B2=0.09200180037
      B3=0.04069697526
      B4=0.00426449639
      ZNU=1.0-ZK
      IF(ZNU.EQ.0.)GOTO 30
      FKE=-2.*(B1*ZNU+B2*ZNU**2+B3*ZNU**3+B4*ZNU**4)
      GKE=-2.*(B1+2.*B2*ZNU+3.*B3*ZNU**2+4.*B4*ZNU**3)*GX
      GKE=0.0
      GOTO 40
30    FKE=A0
```

```
40      CONTINUE
        RETURN
        END

c       ********************************************************
c       APPROXIMATION FOR REGULAR PART OF ELIPTICAL
c       INTEGRAL
c       ********************************************************
        SUBROUTINE VKR(ZK,FKE,GX,GKE,REST)
        IMPLICIT REAL*8(A-H,O-Z)

        A0=1.386294361
        A1=0.097932891
        A2=0.054544409
        A3=0.032024666
        B0=0.5
        B1=0.124750742
        B2=0.060118519
        B3=0.010944912
        ZNU=1.0-ZK
        IF(ZNU.EQ.0.)GOTO 30
        FKE=A0+A1*ZNU+A2*ZNU**2+A3*ZNU**3-(B0+B1*ZNU
     1+B2*ZNU**2+
     1 B3*ZNU**3)*REST
        GKE=((A1+2.0*A2*ZNU+3.*A3*ZNU**2)-
     1 1./ZNU*(B0+B1*ZNU+B2*ZNU**2+B3*ZNU**3)-
     1 (B1+2.*B2*ZNU+3.*B3*ZNU**2)*LOG(ZNU))*GX
        GOTO 40
30      FKE=A0
40      CONTINUE
        RETURN
        END


c       ********************************************************
c       APPROXIMATION FOR SINGULAR PART OF ELIPTICAL
c       INTEGRAL
c       ********************************************************
        SUBROUTINE VKS(ZK,FKE,GX,GKE)
        IMPLICIT REAL*8(A-H,O-Z)

        A0=1.386294361
        A1=0.097932891
        A2=0.054544409
        A3=0.032024666
        B0=0.5
        B1=0.124750742
        B2=0.060118519
```

```
      B3=0.010944912
      ZNU=1.0-ZK
      IF(ZNU.EQ.0.)GOTO 30
      FKE=-2.*(B0+B1*ZNU+B2*ZNU**2+
     1 B3*ZNU**3)
      GKE=-2.*(B1+2.*B2*ZNU+3.*ZNU**2*B3)*GX
      GKE=0.0
      GOTO 40
30    FKE=A0
40    CONTINUE
      RETURN
      END


      SUBROUTINE BODEPH
c     ******************************************************
c     Boundary Element Program - Conducting spheroid
c     by M. T. Harris - 8/11/89 - BODEPE.FOR
c     ******************************************************

      IMPLICIT REAL*8(A-H,O-Z)
      DIMENSION ALPA(300),BETTA(300)
      COMMON / PRIP / RHOS(500,1),ZS(500,1),
     1HQS(500)
      COMMON/BOEL/SIGM(500)
      COMMON/WIR/ A, B
      COMMON / MON /NIPT,RFAC,NBLA,NPTP
      COMMON/BC/IBEG(500),IEND(500),BEG(500),EXIT(500)
      COMMON/FRON/NP,NE,NELL,NH,NPL,HNOZ,NNOZ
      COMMON/FE/QQ(600),QK(600),AMAT(600,600),RHS(600,2),
     1X(500),R(500),DETV(500),IDETV(500),DXOLD(500)
      COMMON/OTHER/EPSI,ITMAX,H,IDROP,NPARA,VOL,PI
      COMMON/GEL/G,HBP
      COMMON/INO/IN1
      COMMON/BOEL2/NT,NB,NBT,NRS,IEP,DBP,RDBP,ZKLL,
     1ZKLP,ZSUM
      COMMON/TET/THETA(500,1)
      COMMON/MOOR/VOLT(500),FCODE(500)
      COMMON/LENGTH/IDBP,IHNOZ
      character*80 ifil1

      B=1.
      PI=3.1415926535898
      A=1.
      NLS=0
      RO=RDBP*DBP
      BESIG=1.
```

```
      NBT=0
      AESIG=0.
      ISP=0
      HSUM=0.
      DO 20 I=1,NE
      ZS(I,1)=QQ(I)*COS(X(I))
      RHOS(I,1)=QQ(I)*SIN(X(I))
      ZS(I+1,1)=QQ(I+1)*COS(X(I+1))
      RHOS(I+1,1)=QQ(I+1)*SIN(X(I+1))
      Z2=ZS(I+1,1)
      RHO2=RHOS(I+1,1)
      HQS(I)=SQRT((ZS(I,1)-Z2)**2+(RHOS(I,1)-RHO2)**2)
      HSUM=HSUM+HQS(I)
20    CONTINUE

      DO 59 I=1,NE
      FCODE(I)=1.
      VOLT(I)=1.
      SIGM(I)=QK(NE+3+I)
      QQ(NE+3+I)=QK(NE+3+I)
      Z2=ZS(I+1,1)
      RHO2=RHOS(I+1,1)
59    CONTINUE

      HSUM=ZSUM*HSUM
      HSUM=1.5707963
      IF(NBLA.EQ.0)HSUM=0.0
      DO 52 I=1,NE
      ALPA(I)=1.
52    BETTA(I)=0.
      NBLAB=NBLA
      B=QQ(NE+1)

c     *** DISCRETIZE NOZZLE ****

      IF(NNOZ.EQ.0.OR.HNOZ.EQ.0.0)GOTO 288
      HIC=0.
      NZTOT=NNOZ*(1+NNOZ)/2
      DO 27 I=NE+1,NE+NNOZ
      FCODE(I)=1.0
      VOLT(I)=1.0
      NNEW=NE+2+I
      IF(IDBP.EQ.1)NNEW=NE+3+I
      SIGM(I)=QK(NNEW)
      QQ(NE+3+I)=QK(NNEW)
      ALPA(I)=AESIG
      BETTA(I)=BESIG
```

```
      HQS(I)=(I-NE)*HNOZ/NZTOT
      RHOS(I,1)=QQ(NE+1)
      RHO2=QQ(NE+1)
      ZS(I,1)=-HIC
      HIC=HIC+HQS(I)
      Z2=-HQS(I)+ZS(I,1)
27    CONTINUE


288   continue


c     ****************************************
c     DISCRETIZE TOP PLATE NEAR DROP
c     ****************************************

      IF(NBLA.EQ.0)GOTO 942
      DO 24 I=NE+NNOZ+1,NE+NNOZ+NBLA
      FCODE(I)=1.0
      VOLT(I)=1.0
      NNEW=NE+2+I
      IF(IDBP.EQ.1)NNEW=NE+3+I
      SIGM(I)=QK(NNEW)
      QQ(NE+3+I)=QK(NNEW)
      ALPA(I)=1.
      BETTA(I)=0.
      HQS(I)=(HSUM)/NBLA
      RHOS(I,1)=B+(I-NE-NNOZ-1)*HQS(I)
      RHO2=RHOS(I,1)+HQS(I)
      Z2=-HNOZ
      ZS(I,1)=-HNOZ
24    CONTINUE


c     ****************************************************
c     DISCRETIZE THE REMAINDER OF TOP PLATE
c     ****************************************************

942   CONTINUE

      NTNT=NT*(NT+1)/2
      HIC=0.
      DO 22 I=NE+NNOZ+NBLA+1,NE+NNOZ+NT+NBLA
      FCODE(I)=1.0
      VOLT(I)=1.0
      NNEW=NE+2+I
      IF(IDBP.EQ.1)NNEW=NE+3+I
```

```
      SIGM(I)=QK(NNEW)
      QQ(NE+3+I)=QK(NNEW)
      ALPA(I)=1.
      BETTA(I)=0.
      HQS(I)=(I-NE-NNOZ-NBLA)*(RO-HSUM-B)/NTNT
      RHOS(I,1)=B+HSUM+HIC
      RHO2=RHOS(I,1)+HQS(I)
      HIC=HIC+HQS(I)
      Z2=-HNOZ
      ZS(I,1)=-HNOZ
22    CONTINUE


889   CONTINUE
      NTP=NE+NT+NBLA+NNOZ

c     ************************************************
c     DISCRETIZE RIGHT BOUNDARY
c     ************************************************

      IF(NRS.EQ.0)GOTO 298
      HIC=0.0
      DO 278 I=NTP+1,NTP+NRS
      SIGM(I)=0.0
      VOLT(I)=0.0

      FCODE(I)=2.0
      NNEW=NE+2+I
      IF(IDBP.EQ.1)NNEW=NE+3+I
      IF(FCODE(I).EQ.2.)VOLT(I)=QK(NNEW)
      IF(FCODE(I).EQ.1.)SIGM(I)=QK(NNEW)
      HQS(I)=DBP/NRS
      RHOS(I,1)=RO
      RHO2=RO
      ZS(I,1)=-HNOZ+(I-NTP-1)*HQS(I)
      Z2=HQS(I)+ZS(I,1)
      IF(FCODE(I).EQ.1.)VOLT(I)=1.0-(I-NTP-1)*HQS(I)/DBP
      RDEN=SQRT((Z2-ZS(I,1))**2+(RHO2-RHOS(I,1))**2)
      QQ(NE+3+I)=0.0
278   CONTINUE
298   CONTINUE
      VOLT(NTP+1)=1.0
      NNEW=NE+NTP+3+NRS
      IF(IDBP.EQ.1)NNEW=NE+NTP+4+NRS
      SIGM(NTP+1+NRS)=QK(NNEW)
      QQ(NE+3+NTP+1+NRS)=QK(NNEW)
      NTP=NTP+NRS
```

```
c       ****************************************************
c       DISCRETIZE THE REMAINDER OF BOTTOM PLATE
c       ****************************************************

        HIC=0.
        NTNB=NB*(NB+1)/2
        DO 23 I=NTP+1,NTP+NB
        FCODE(I)=1.0
        VOLT(I)=0.0
        NNEW=NE+2+I
        IF(IDBP.EQ.1)NNEW=NE+3+I
        SIGM(I)=QK(NNEW)
        QQ(NE+3+I)=QK(NNEW)
        ALPA(I)=1.
        BETTA(I)=0.
        HQS(I)=(NTP+NB+1-I)*(RO-HSUM)/NTNB
        RHOS(I,1)=RO-HIC
        HIC=HIC+HQS(I)
        RHO2=RHOS(I,1)-HQS(I)
        Z2=DBP-HNOZ
        ZS(I,1)=DBP-HNOZ
23      CONTINUE


28      continue
        NTP=NTP+NB
c       ****************************************************
c       DISCRETIZE THE REGION OF BOTTOM PLATE
c       NEAR DROPLET
c       ****************************************************
        IF(NBLA.EQ.0)GOTO 977
        HIC=0.0
        DO 26 I=NTP+1,NTP+NBLA
        FCODE(I)=1.0
        VOLT(I)=0.0
        NNEW=NE+2+I
        IF(IDBP.EQ.1)NNEW=NE+3+I
        SIGM(I)=QK(NNEW)
        QQ(NE+3+I)=QK(NNEW)
        ALPA(I)=1.
        BETTA(I)=0.
        HQS(I)=(HSUM+B)/NBLAB
        RHOS(I,1)=HSUM+B-HIC
        HIC=HIC+HQS(I)
        RHO2=RHOS(I,1)-HQS(I)
        Z2=DBP-HNOZ
```

```
      ZS(I,1)=DBP-HNOZ
26    CONTINUE


977   NTP=NTP+NBLA
      NNEW=NE+NTP+3
      IF(IDBP.EQ.1)NNEW=NE+NTP+4
      SIGM(NTP+1)=QK(NNEW)
      QQ(NE+3+NTP+1)=QK(NNEW)
      RHOS(NTP+1,1)=RHO2
      ZS(NTP+1,1)=Z2
      VOLT(NTP+1)=0.0
      FCODE(NTP+1)=1.0

      RETURN
      END

      SUBROUTINE SING3(MNEL,MNEJ,SID,NTOT)
c     ****************************************************
c     CALCULATES INTEGRALS WHEN I = J
c     ****************************************************
      IMPLICIT REAL*8(A-H,O-Z)
      COMMON / PRIP / RHOS(500,1),ZS(500,1),
     1HQS(500)
      COMMON/BOEL/SIGM(500)
      COMMON/WIR/ A, B
      COMMON / MON /NIPT,RFAC,NBLA,NPTP
      COMMON/BC/IBEG(500),IEND(500),BEG(500),EXIT(500)
      COMMON/FRON/NP,NE,NELL,NH,NPL,HNOZ,NNOZ
      COMMON/FE/QQ(600),QK(600),AMAT(600,600),RHS(600,2),
     1X(500),R(500),DETV(500),IDETV(500),DXOLD(500)
      COMMON/OTHER/EPSI,ITMAX,H,IDROP,NPARA,VOL,PI
      COMMON/GEL/G,HBP
      COMMON/INO/IN1
      COMMON/BOEL2/NT,NB,NBT,NRS,IEP,DBP,RDBP,ZKLL,
     1ZKLP,ZSUM
      COMMON/TET/THETA(500,1)
      COMMON/PHI2/PHI2(2),PHIX2(2),PHICE2(4,13)
      COMMON/MOOR/VOLT(500),FCODE(500)
      DIMENSION XLOC(2),ALPHA(2),RLOC(2),ESTIFM(2,2),
     1PSI(2),DPSI(2),GSPEC(8),WSPEC(8),GAUS(8),WE(8)

      PI=3.1415926535898
      SID=0.
      SIP=0.
      SIP1=0.0
```

```
      SIP2=0.0
      NELL=MNEJ
      SIGM1=SIGM(MNEJ)
      SIGM2=SIGM(MNEJ+1)
      IF(FCODE(MNEJ).EQ.2.)THEN
      SIGM1=0.0
      SIGM2=0.0
      ENDIF
      DO 10 I=1,2
      RLOC(I)=0.0
      DO 10 J=1,2
10    ESTIFM(I,J)=0.0
      DO 20 I=1,2
      LI=NELL-1+I
      XLOC(I)=X(LI)
20    ALPHA(I)=QQ(LI)
      DX=XLOC(2)-XLOC(1)
      ZNE=QQ(NP)
      GSPEC(1)=0.04144848
      GSPEC(2)=0.24527491
      GSPEC(3)=0.55616545
      GSPEC(4)=0.84898239
      WSPEC(1)=-0.3834641
      WSPEC(2)=-0.3868753
      WSPEC(3)=-0.1904351
      WSPEC(4)=-0.0392255
      GAUS(4)=0.930565
      GAUS(3)=0.669994
      GAUS(2)=0.33003
      GAUS(1)=0.069435
      WE(1)=0.34785/2.
      WE(2)=0.65214/2.
      WE(3)=WE(2)
      WE(4)=WE(1)
      DO 150 NGP=1,4
      TH=0.0
      F=0.0
      FC=0.0
      DO 30 II=1,2
      TH=TH+PHICE2(II,NGP)*XLOC(II)
      F=F+PHICE2(II,NGP)*ALPHA(II)
30    FC=FC+PHICE2(II+2,NGP)*ALPHA(II)
      DO 35 II=1,2
35    PSI(II)=PHICE2(II,NGP)

C
```

```
C
C       *** REGULAR NUMERICAL INTEGRALS FROM
C       0 TO 1.0 ***

        GIP1=GAUS(NGP)
        SIGMA=SIGM1*(1.-GIP1)+SIGM2*GIP1
        THETRO= XLOC(1)*(1.-GIP1)+XLOC(2)*GIP1
        THETRP= XLOC(2)-XLOC(1)
        DFFDZ=ALPHA(2)-ALPHA(1)
        DFDO=ALPHA(1)*(1.-GIP1)
        1+ALPHA(2)*GIP1
        FCR=RHOS(MNEJ+1,1)-RHOS(MNEJ,1)
        FCZ=ZS(MNEJ+1,1)-ZS(MNEJ,1)
        Z=ZS(MNEL,1)
        RHOP=RHOS(MNEL,1)
        IF(RHOP.LT.0.0)RHOP=0.0
        ZSP=ZS(MNEJ,1)*(1.-GIP1)+ZS(MNEJ+1,1)*GIP1
        RSP=RHOS(MNEJ,1)*(1.-GIP1)+RHOS(MNEJ+1,1)*GIP1
        IF(RSP.LT.0.0)RSP=0.0
        ZBOT=(Z-ZSP)**2+(RHOP+RSP)**2
        ZK=4.*RHOP*RSP/ZBOT
        ZKV=SQRT(4./ZBOT)
        Z2=ZS(MNEJ+1,1)
        Z1=ZS(MNEJ,1)
        R2=RHOS(MNEJ+1,1)
        R1=RHOS(MNEJ,1)
        ZD=(Z-ZSP)
        AQ=RHOP**2+ZD**2+RSP**2
        BQ=2.*RHOP*RSP
        REST=(LOG((R2-R1)**2+(Z2-Z1)**2)-LOG(AQ+BQ))
        IF(MNEL.EQ.1)REST=0.0
        CALL VKR(ZK,FKE,DXDA,GKE,REST)
        FU1=1.-GIP1
        FU2=GIP1
        IF(MNEJ.LE.NE)GOTO 145
        SIP1=FU1*(1./(4.*PI)*2.0*WE(NGP)*ZKV*
        1RSP*FKE*HQS(MNEJ))+SIP1
        SIP2=FU2*(1./(4.*PI)*2.0*WE(NGP)*ZKV*
        1RSP*FKE*HQS(MNEJ))+SIP2
        SID=1./(4.*PI)*2.0*SIGMA*WE(NGP)*ZKV*
        1RSP*FKE*HQS(MNEJ)+SID
        GOTO 160
145     CONTINUE
        SIP1=FU1*(1./(4.*PI)*2.0*WE(NGP)*ZKV*
        1RSP*FKE*SQRT(FCR**2+FCZ**2))+SIP1
```

```
      SIP2=FU2*(1./(4.*PI)*2.0*WE(NGP)*ZKV*
     1RSP*FKE*SQRT(FCR**2+FCZ**2))+SIP2
      SID=SIGMA*(1./(4.*PI)*2.0*WE(NGP)*ZKV*
     1RSP*FKE*SQRT(FCR**2+FCZ**2))+SID

c     *** SPECIAL NUMERICAL INTEGRATION FOR
c     LOGRITHMIC SINGULARITY **
c     *** (0 TO 1.0) ***

160   GIP1=GSPEC(NGP)
      SIGMA=SIGM1*(1.-GIP1)+SIGM2*GIP1
      THETRO= XLOC(1)*(1.-GIP1)+XLOC(2)*GIP1
      THETRP= XLOC(2)-XLOC(1)
      DFFDZ=ALPHA(2)-ALPHA(1)
      DFDO=ALPHA(1)*(1.-GIP1)
     1+ALPHA(2)*GIP1
      FCR=RHOS(MNEJ+1,1)-RHOS(MNEJ,1)
      FCZ=ZS(MNEJ+1,1)-ZS(MNEJ,1)
      Z=ZS(MNEL,1)
      RHOP=RHOS(MNEL,1)
      IF(RHOP.LT.0.0)RHOP=0.0
      ZSP=ZS(MNEJ,1)*(1.-GIP1)+ZS(MNEJ+1,1)*GIP1
      RSP=RHOS(MNEJ,1)*(1.-GIP1)+RHOS(MNEJ+1,1)*GIP1
      IF(RSP.LT.0.0)RSP=0.0
      ZBOT=(Z-ZSP)**2+(RHOP+RSP)**2
      ZK=4.*RHOP*RSP/ZBOT
      ZKV=SQRT(4./ZBOT)
      CALL VKS(ZK,FKE,DXDA,GKE)
      IF(MNEL.EQ.1)FKE=0.0
      FU1=(1.-GIP1)
      FU2=GIP1
      IF(MNEJ.LE.NE)GOTO 165
      SIP1=FU1*(1./(4.*PI)*2.0*WSPEC(NGP)*ZKV*
     1RSP*FKE*HQS(MNEJ))+SIP1
      SIP2=FU2*(1./(4.*PI)*2.0*WSPEC(NGP)*ZKV*
     1RSP*FKE*HQS(MNEJ))+SIP2
      SID=1./(4.*PI)*2.0*SIGMA*WSPEC(NGP)*ZKV*
     1RSP*FKE*HQS(MNEJ)+SID
      GOTO 150

165   SIP1=FU1*(1./(4.*PI)*2.0*WSPEC(NGP)*ZKV*
     1RSP*FKE*SQRT(FCR**2+FCZ**2))+SIP1
      SIP2=FU2*(1./(4.*PI)*2.0*WSPEC(NGP)*ZKV*
     1RSP*FKE*SQRT(FCR**2+FCZ**2))+SIP2
      SID=SIGMA*(1./(4.*PI)*2.0*WSPEC(NGP)*ZKV*
```

```
     1RSP*FKE*SQRT(FCR**2+FCZ**2))+SID

150  CONTINUE

     IF(FCODE(MNEJ).EQ.1.)THEN
     AMAT(MNEL+NE+3,MNEJ+NE+3)=-SIP1
     1+AMAT(MNEL+NE+3,MNEJ+NE+3)
     AMAT(MNEL+NE+3,MNEJ+NE+3+1)=-SIP2
     ENDIF



     RETURN
     END

     SUBROUTINE SING4(MNEL,MNEJ,SID,NTOT)
c    ****************************************************
c    CALCULATES INTEGRALS WHEN I = J+1
c    ****************************************************
     IMPLICIT REAL*8(A-H,O-Z)
     COMMON / PRIP / RHOS(500,1),ZS(500,1),
     1HQS(500)
     COMMON/BOEL/SIGM(500)
     COMMON/WIR/ A, B
     COMMON / MON /NIPT,RFAC,NBLA,NPTP
     COMMON/BC/IBEG(500),IEND(500),BEG(500),EXIT(500)
     COMMON/FRON/NP,NE,NELL,NH,NPL,HNOZ,NNOZ
     COMMON/FE/QQ(600),QK(600),AMAT(600,600),RHS(600,2),
     1X(500),R(500),DETV(500),IDETV(500),DXOLD(500)
     COMMON/OTHER/EPSI,ITMAX,H,IDROP,NPARA,VOL,PI
     COMMON/GEL/G,HBP
     COMMON/INO/IN1
     COMMON/BOEL2/NT,NB,NBT,NRS,IEP,DBP,RDBP,ZKLL,
     1ZKLP,ZSUM
     COMMON/TET/THETA(500,1)
     COMMON/PHI2/PHI2(2),PHIX2(2),PHICE2(4,13)
     COMMON/MOOR/VOLT(500),FCODE(500)
     DIMENSION XLOC(2),ALPHA(2),RLOC(2),ESTIFM(2,2),
     1PSI(2),DPSI(2),GSPEC(8),WSPEC(8),GAUS(8),WE(8)
     PI=3.1415926535898

     SID=0.
     SIP1=0.
     SIP2=0.
     SIP3=0.
     SIP4=0.
     NELL=MNEJ
```

```
      SIGM1=SIGM(MNEJ)
      SIGM2=SIGM(MNEJ+1)
      IF(FCODE(MNEJ).EQ.2.)THEN
      SIGM1=0.0
      SIGM2=0.0
      ENDIF
      DO 10 I=1,2
      RLOC(I)=0.0
      DO 10 J=1,2
10    ESTIFM(I,J)=0.0
      DO 20 I=1,2
      LI=NELL-1+I
      XLOC(I)=X(LI)
20    ALPHA(I)=QQ(LI)
      DX=XLOC(2)-XLOC(1)
      ZNE=QQ(NP)
      GSPEC(1)=0.04144848
      GSPEC(2)=0.24527491
      GSPEC(3)=0.55616545
      GSPEC(4)=0.84898239
      WSPEC(1)=-0.3834641
      WSPEC(2)=-0.3868753
      WSPEC(3)=-0.1904351
      WSPEC(4)=-0.0392255
      GAUS(4)=0.930565
      GAUS(3)=0.669994
      GAUS(2)=0.33003
      GAUS(1)=0.069435
      WE(1)=0.34785/2.
      WE(2)=0.65214/2.
      WE(3)=WE(2)
      WE(4)=WE(1)
      DO 150 NGP=1,4
      TH=0.0
      F=0.0
      FC=0.0
      DO 30 II=1,2
      TH=TH+PHICE2(II,NGP)*XLOC(II)
      F=F+PHICE2(II,NGP)*ALPHA(II)
30    FC=FC+PHICE2(II+2,NGP)*ALPHA(II)
      DO 35 II=1,2
35    PSI(II)=PHICE2(II,NGP)


c     *** REGULAR NUMERICAL INTEGRALS FROM 0
c     TO 1.0 ***
```

```
      GIP1=GAUS(NGP)
      SIGMA=SIGM1*(1.-GIP1)+SIGM2*GIP1
      THETRO= XLOC(1)*(1.-GIP1)+XLOC(2)*GIP1
      THETRP= XLOC(2)-XLOC(1)
      DFFDZ=ALPHA(2)-ALPHA(1)
      DFDO=ALPHA(1)*(1.-GIP1)
      1+ALPHA(2)*GIP1
      FCR=RHOS(MNEJ+1,1)-RHOS(MNEJ,1)
      FCZ=ZS(MNEJ+1,1)-ZS(MNEJ,1)
      Z=ZS(MNEL,1)
      RHOP=RHOS(MNEL,1)
      IF(RHOP.LT.0.0)RHOP=0.0
      ZSP=ZS(MNEJ,1)*(1.-GIP1)+ZS(MNEJ+1,1)*GIP1
      RSP=RHOS(MNEJ,1)*(1.-GIP1)+RHOS(MNEJ+1,1)*GIP1
      IF(RSP.LT.0.0)RSP=0.0
      ZBOT=(Z-ZSP)**2+(RHOP+RSP)**2
      ZK=4.*RHOP*RSP/ZBOT
      ZKV=SQRT(4./ZBOT)
      Z2=ZS(MNEJ+1,1)
      Z1=ZS(MNEJ,1)
      R2=RHOS(MNEJ+1,1)
      R1=RHOS(MNEJ,1)
      ZD=(Z-ZSP)
      AQ=RHOP**2+ZD**2+RSP**2
      BQ=2.*RHOP*RSP
      REST=(LOG((R2-R1)**2+(Z2-Z1)**2)-LOG(AQ+BQ))
      IF(MNEL.EQ.NE+NPL+1)REST=0.0
      CALL VKR(ZK,FKE,DXDA,GKE,REST)
      FU1=1.0-GIP1
      FU2=GIP1
      IF(MNEJ.LE.NE)GOTO 145
      SIP1=FU1*(1./(4.*PI)*2.0*WE(NGP)*ZKV*
      1RSP*FKE*HQS(MNEJ))+SIP1
      SIP2=FU2*(1./(4.*PI)*2.0*WE(NGP)*ZKV*
      1RSP*FKE*HQS(MNEJ))+SIP2
      SID=1./(4.*PI)*2.0*SIGMA*WE(NGP)*ZKV*
      1RSP*FKE*HQS(MNEJ)+SID
      GOTO 160
145   CONTINUE
      SIP1=FU1*(1./(4.*PI)*2.0*WE(NGP)*ZKV*
      1RSP*FKE*SQRT(FCR**2+FCZ**2))+SIP1
      SIP2=FU2*(1./(4.*PI)*2.0*WE(NGP)*ZKV*
      1RSP*FKE*SQRT(FCR**2+FCZ**2))+SIP2
      SID=SIGMA*(1./(4.*PI)*2.0*WE(NGP)*ZKV*
```

```
     1RSP*FKE*SQRT(FCR**2+FCZ**2))+SID

c    *** SPECIAL NUMERICAL INTEGRATION FOR
c    LOGRITHMIC SINGULARITY (0 TO 1.0) ***

160  GIP1=1.-GSPEC(NGP)
     SIGMA=SIGM1*(1.-GIP1)+SIGM2*GIP1
     THETRO= XLOC(1)*(1.-GIP1)+XLOC(2)*GIP1
     THETRP= XLOC(2)-XLOC(1)
     DFFDZ=ALPHA(2)-ALPHA(1)
     DFDO=ALPHA(1)*(1.-GIP1)
     1+ALPHA(2)*GIP1
     FCR=RHOS(MNEJ+1,1)-RHOS(MNEJ,1)
     FCZ=ZS(MNEJ+1,1)-ZS(MNEJ,1)
     Z=ZS(MNEL,1)
     RHOP=RHOS(MNEL,1)
     IF(RHOP.LT.0.0)RHOP=0.0
     ZSP=ZS(MNEJ,1)*(1.-GIP1)+ZS(MNEJ+1,1)*GIP1
     RSP=RHOS(MNEJ,1)*(1.-GIP1)+RHOS(MNEJ+1,1)*GIP1
     IF(RSP.LT.0.0)RSP=0.0
     ZBOT=(Z-ZSP)**2+(RHOP+RSP)**2
     ZK=4.*RHOP*RSP/ZBOT
     ZKV=SQRT(4./ZBOT)
     GP1=1.-GIP1
     CALL VKS(ZK,FKE,DXDA,GKE)
     IF(MNEL.EQ.NE+NPL+1)FKE=0.0
     FU1=1.-GIP1
     FU2=GIP1
     IF(MNEJ.LE.NE)GOTO 165
     SIP1=FU1*(1./(4.*PI)*2.0*WSPEC(NGP)*ZKV*
     1RSP*FKE*HQS(MNEJ))+SIP1
     SIP2=FU2*(1./(4.*PI)*2.0*WSPEC(NGP)*ZKV*
     1RSP*FKE*HQS(MNEJ))+SIP2
     SID=1./(4.*PI)*2.0*SIGMA*WSPEC(NGP)*ZKV*
     1RSP*FKE*HQS(MNEJ)+SID
     GOTO 150
165  SIP1=FU1*(1./(4.*PI)*2.0*WSPEC(NGP)*ZKV*
     1RSP*FKE*SQRT(FCR**2+FCZ**2))+SIP1
     SIP2=FU2*(1./(4.*PI)*2.0*WSPEC(NGP)*ZKV*
     1RSP*FKE*SQRT(FCR**2+FCZ**2))+SIP2
     SID=SIGMA*(1./(4.*PI)*2.0*WSPEC(NGP)*ZKV*
     1RSP*FKE*SQRT(FCR**2+FCZ**2))+SID

150  CONTINUE
```

```
      IF(FCODE(MNEJ).EQ.1.)THEN
      AMAT(MNEL+NE+3,MNEJ+NE+3)=-SIP1
     1+AMAT(MNEL+NE+3,MNEJ+NE+3)
      AMAT(MNEL+NE+3,MNEJ+NE+3+1)=-SIP2
      ENDIF


      RETURN
      END


      SUBROUTINE CONE(ACURV,CHARGE,FORCE)
      IMPLICIT REAL*8(A-H,O-Z)
      COMMON/FRON/NP,NE,NELL,NH,NPL,HNOZ,NNOZ
      COMMON/FE/QQ(600),QK(600),AMAT(600,600),RHS(600,2),
     1X(500),R(500),DETV(500),IDETV(500),DXOLD(500)
      COMMON/OTHER/EPSI,ITMAX,H,IDROP,NPARA,VOL,PI
      COMMON/PHI/PHI(2),PHIX(2),PHICE(4,3),W(3),GP(3)
      CHARGE=0.0
      FORCE=0.0
      SUMIT=0.0
      SUMAR=0.0
      DFDTET=(QQ(2)-QQ(1))/(X(2)-X(1))
      DTET=X(2)-X(1)
      DO 100 NGP=1,3
      F=QQ(2)*PHICE(2,NGP)+QQ(1)*PHICE(1,NGP)
      TET=X(2)*PHICE(2,NGP)+X(1)*PHICE(1,NGP)
      TERM1=F**2+DFDTET**2
      SUMAR=F**2*SIN(TET)*DTET*W(NGP)+SUMAR
100   SUMIT=(F**2+TERM1)*SIN(TET)*DTET*W(NGP
     1)/SQRT(TERM1)+SUMIT
      ACURV=QQ(2)*SIN(X(2))*DFDTET/SQRT(QQ(2)**2
     1+DFDTET**2)-SUMIT
      ACURV=ACURV/SUMAR
      DO 200 I=1,NE
      DFDTET=(QQ(I+1)-QQ(I))/(X(I+1)-X(I))
      DTET=X(I+1)-X(I)
      DO 210 NGP=1,3
      F=QQ(I+1)*PHICE(2,NGP)+QQ(I)*PHICE(1,NGP)
      TET=X(I+1)*PHICE(2,NGP)+X(I)*PHICE(1,NGP)
      TERM1=F**2+DFDTET**2
      TOP=F*COS(TET)+DFDTET*SIN(TET)
      SIGAR=QQ(NE+4+I)*PHICE(2,NGP)+QQ(NE+3+I)
     1*PHICE(1,NGP)
      CHARGE=2.*PI*SIGAR*F*SQRT(TERM1)*SIN(TET)
```

```
     1*DTET*W(NGP)+
     1CHARGE
     FORCE=2.*PI*SIGAR**2*TOP*QQ(NP)*SIN(TET)
     1*DTET*W(NGP)*F+
     1FORCE
210  CONTINUE
200  CONTINUE
     RETURN
     END
```

## A.2. Discretization of Boundary for Solving Electrohydrostatic Problem by Hybrid Finite Element-Boundary Element Method

Fig. A.1. illustrates the typical geometric discretization of the top and bottom plate. The droplet and nozzle are discetized in the same manner. Equally spaced elements are used on the side boundary.

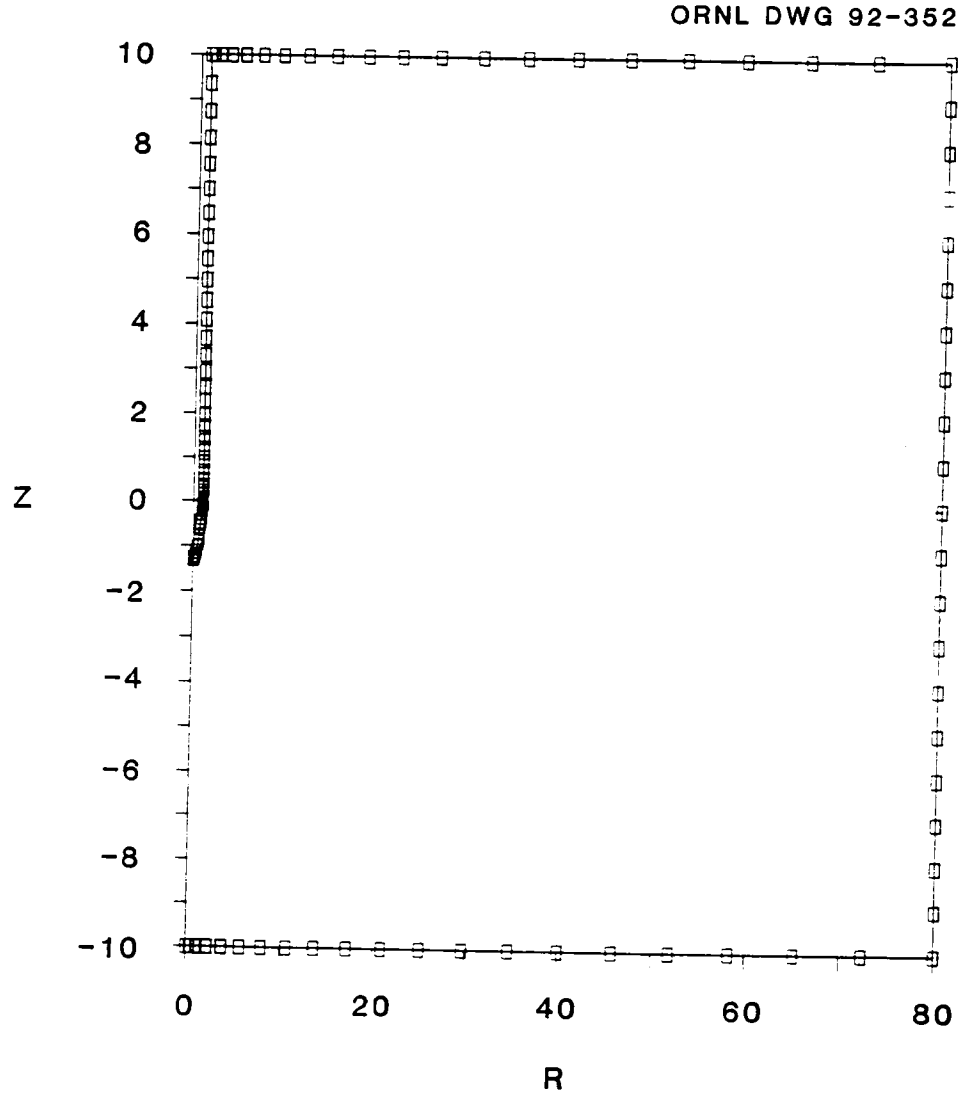



Fig. A.1. Discretization of boundary for solving electrohydrostatic problem by hydrid finite element-boundary element method.

# VITA

Michael Tyrone Harris was born in Mound Bayou, Mississippi on June 13, 1958. He graduated from John F. Kennedy High School in Mound Bayou, Mississippi in 1976, and entered Mississippi State University in the fall of the same year. He received a Bachelor of Science degree in Chemical Engineering in 1981, after participating in a cooperative education program that was offered by the university with the United States Environmental Protection Agency.

After graduation, he was employed by the Union Carbide Corporation at the Oak Ridge National Laboratory (ORNL) in Oak Ridge, Tennessee where he has conducted studies in the areas of municipal and industrial wastewater treatment, and is presently researching the synthesis of ultrafine metal hydrous oxide precusor powders for ceramic applications. During his employment at ORNL, he completed a Master of Science degree with a major in Chemical Engineering in the summer of 1987 and a Doctor of Philosophy degree with a major in Chemical Engineering.